Barry Nicolas

Ingénieur de l'Ecole Nationale Supérieure de Chimie de Rennes, France
Titulaire d'un Master de Chimie de l'Université de Rennes 1, France

Arene Ruthenium Assemblies for Biological Applications: From Carceplex to Host-Guest Metalla-Cages

Thèse présentée à la Faculté des Sciences,
Pour l'obtention du grade de Docteur ès Sciences

Membres du jury :

Prof. G. Süss-Fink	Co-directeur de thèse, Université de Neuchâtel
Dr. B. Therrien	Co-directeur de thèse, Université de Neuchâtel
Prof. F. Kessler	Rapporteur interne, Université de Neuchâtel
Prof. M. Pfeffer	Rapporteur externe, Université de Strasbourg

UNIVERSITÉ DE NEUCHÂTEL

Institut de Chimie de l'Université de Neuchâtel
Soutenue le 31 mars 2011

Université de Neuchâtel

FACULTE DES SCIENCES
Secrétariat-Décanat de la faculté
Rue Emile-Argand 11
CH-2000 Neuchâtel

IMPRIMATUR POUR LA THESE

Arene Ruthenium Assemblies for Biological Applications : From Carceplex to Host-Guest Metalla-Cages

Nicolas BARRY

UNIVERSITE DE NEUCHATEL

FACULTE DES SCIENCES

La Faculté des sciences de l'Université de Neuchâtel,
sur le rapport des membres du jury

MM. G. Süss-Fink (directeur de thèse), B. Therrien,
F. Kessler et M. Pfeffer (Strasbourg)

autorise l'impression de la présente thèse.

Neuchâtel, le 7 avril 2011

Le doyen :
P. Kropf

Remerciements

Les travaux reportés dans la présente thèse ont été effectués au sein du Laboratoire de Chimie Organométallique et de Catalyse Moléculaire de l'Université de Neuchâtel, sous la direction du Professeur Georg Süss-Fink et du Docteur Bruno Therrien.

Je tiens en premier lieu à remercier le Professeur Georg Süss-Fink pour m'avoir permis de réaliser ce doctorat au sein de son laboratoire. Je le remercie tout particulièrement pour les discussions qui ont accompagné la rédaction de cette thèse.

J'adresse mes remerciements les plus sincères au Docteur Bruno Therrien, avec qui j'ai travaillé au jour le jour au cours de ces années de doctorat. Bien plus qu'un encadrement, c'est véritablement un apprentissage du métier de chercheur qu'il m'a été donné de recevoir, tant au niveau scientifique, qu'au niveau rédactionnel ou humain. Je le remercie également pour les longues discussions sur mon avenir académique et les nombreux conseils donnés. Je ne saurais donc assez remercier le Docteur Bruno Therrien pour cette transmission sans réserve de ses connaissances et pour ces années que j'ai vécues comme un réel « compagnonnage ».

Je tiens également à remercier les Professeurs Félix Kessler et Michel Pfeffer pour avoir accepté de faire partie de mon jury de thèse. Je les remercie d'avoir pris connaissance de mon travail et d'y avoir porté un jugement.

Je remercie bien évidemment le Professeur Paul J. Dyson et le Docteur Olivier Zava pour les tests biologiques réalisés avec la grande majorité de mes produits. Je remercie particulièrement Olivier pour m'avoir initié avec pédagogie à l'art délicat des cultures de cellules cancéreuses et aux tests *in vitro*.

Je remercie le Docteur Ramón Vilar et le Professeur Jérôme Lacour pour l'accueil chaleureux que j'ai reçu dans leurs laboratoires respectifs. Je remercie également Nurul H. Abd Karim et Martina Austeri avec qui travailler lors de ces collaborations a été un réel plaisir.

Je remercie toutes les personnes qui ont participé de près à la réalisation de ce travail de doctorat et qui m'ont permis d'avancer rapidement dans de nombreux projets. Je pense particulièrement au Docteur Julien Furrer pour les nombreuses expériences RMN, parfois

complexes ou nouvelles. Je pense également à Anaïs sans laquelle toute la partie « dendrimères » de ce travail n'aurait pas pu être réalisée : merci pour avoir initié l'idée du projet et pour les grammes de dendrons synthétisés en un temps record.

Je remercie finalement les membres du laboratoire et de l'institut qui ont su faire régner une ambiance conviviale durant ces trois années.

Concernant ma famille, je resterai dans le contexte de mon doctorat, car résumer ce qui a contribué à faire l'essence même et la personnalité d'un homme en quelques phrases serait par définition incomplet et imparfait.

Je remercie donc mes parents pour m'avoir donné, d'une part, le goût des sciences et d'autre part, le goût des lettres, deux conditions nécessaires pour la réalisation et l'écriture d'une thèse de doctorat. Le Palais de la Découverte, l'Arboretum de Chèvreloup et les leçons de vocabulaire du lundi matin n'auront finalement pas été inutiles.

Paul, je te dédie la partie 4.2 de cette thèse. Les deux semaines passées dans votre foyer londonien lors des expériences décrites dans ce chapitre m'ont presque fait regretter d'avoir choisi les sciences plutôt que la finance. Je te remercie surtout pour avoir toujours été fier de mes réalisations, aussi petites soient-elles. Savoir que son frère est de tout cœur et en toute sincérité derrière soi est quelque chose d'absolument essentiel dans la construction d'un enfant, d'un adolescent, mais aussi dans le développement intellectuel d'un adulte.

Anaïs, je te dédie le reste de ma thèse. Même en restreignant les remerciements au doctorat, une page ne suffirait pas pour être exhaustif, pas plus qu'un chapitre ni même qu'une nouvelle thèse. Je ne t'écrirai donc qu'un mot : MERCI.

Résumé

Le développement depuis les années 1980 de la chimie supramoléculaire a permis la synthèse d'objets discrets toujours plus complexes. Le rôle des métaux a été prépondérant, grâce notamment à leur mode de coordination qui permet d'orienter de façon rationnelle l'organisation moléculaire au sein même de l'architecture supramoléculaire. Ainsi, les métalla-cages ont été au centre de l'attention des chimistes, de par leur facilité d'accès au niveau synthétique mais aussi de par leur large spectre d'utilisation.

Depuis la mise sur le marché et le succès clinique du cisplatine comme agent antitumoral, les métaux de transition sont également particulièrement étudiés dans une telle optique d'application. Parmi les plus prometteurs, les complexes mononucléaires arène-ruthénium ont démontré un fort potentiel antiprolifératif tout en étant moins toxiques que les complexes de platine.

Le but de cette thèse de doctorat était de combiner les propriétés d'assemblage des complexes arène-ruthénium en chimie supramoléculaire avec leurs propriétés antiprolifératives. Pour cela, plusieurs métalla-cages ont été construites ; leurs habilités à encapsuler de façon permanente ou réversible des molécules invitées ont été étudiées par différentes méthodes spectroscopiques, et les comportements antiprolifératifs des systèmes ainsi obtenus ont été établis *in vitro* envers différentes lignées de cellules cancéreuses.

Mots clés

Complexes organométalliques, complexes arène-ruthénium, chimie supramoléculaire, auto-assemblage, métalla-cycles, complexes dinucléaires, complexes tétranucléaires, complexes hexanucléaires, complexes octanucléaires, carceplex, host-guest, activité anti-cancéreuse, G-quadruplexe,

Summary

Since the development of supramolecular chemistry in the 1980s more and more discrete molecular objects have been synthesised. In this research area metals play a key role. Indeed, the coordination-driven self-assembly allows a directional-bonding approach that organises the different building blocks into supramolecular objects according to the coordination modes of the transition metal. Therefore, the versatility of metalla-cages and their application potential raised an increasing interest for this chemistry.

On the other hand, ever since the clinical success of cisplatin as an antitumour drug, transition metals have raised considerable expectations for the treatment of cancer. So far, mononuclear arene ruthenium complexes are of central interest due to established cytotoxicity towards cancer cells and low general toxicity.

The aim of this thesis was to combine the assembling properties of arene ruthenium complexes in supramolecular chemistry with their antiproliferative activity. Thus, different metalla-cages were synthesised, the permanent or reversible hosting ability of which was studied by various spectroscopic methods with different guest molecules. The antiproliferative behaviour of the resulting systems was established *in vitro* towards different cancer cell lines.

Keywords

Organometallic complexes, arene ruthenium complexes, supramolecular chemistry, self-assembly, metalla-cycles, dinuclear complexes, tetranuclear complexes, hexanuclear complexes, octanuclear complexes, carceplex, host-guest, anticancer activity, G-quadruplex.

Table of Contents

Chapter 1: Introduction

1.1 Arene Ruthenium Complexes

1.1.1 Ruthenium: The Element 44

Ruthenium is one of the six elements, Ru, Os; Rh, Ir; Pd, and Pt – commonly called "platinum metals" – which together with the lighter homologues Fe, Co, Ni form Group VIII of the periodic table. Karl Karlovitch Klaus discovered this transition metal in 1844 in ores from the Urals and named "the new body, in honor of [his] motherland" ruthenia, the latinised name for Russia.[1] Ruthenium is a rare element with a terrestrial abundance in the earth's crustal rocks estimated at around 0.0001 ppm, and was the last element of the platinum metals to be discovered. Ruthenium is found in the metallic state along with the other metals of Group VIII, in particular in the nickel-copper sulphide ores found in South Africa, Canada (Grand Sudbury) and in the river sands of the Urals. These ores are purified by treatment with *aqua regia*, in order to remove Pt, Pd and Au, and by treatment with hot nitric acid to remove Ag as its soluble nitrate. Fusing with $NaHSO_4$, and then with Na_2O_2, to eliminate Rh and Ir, finally leads to the extraction of ruthenium as a lustrous and silvery metal that crystallises in a hexagonal close-packed (hcp) structure.[2] Ruthenium is the element 44 of Mendeleev's periodic table, its molecular weight is 101.07 $g{\cdot}mol^{-1}$, its density is 12.41 $g{\cdot}cm^{-3}$ at 20°C, and seven isotopes are naturally occurring. The electronic configuration of ruthenium is Kr [$4d^7$] [$5s^1$]. The organometallic chemistry of ruthenium mainly revolves around the oxidation states (0), (II) and (IV), the latter being more stable in the presence of strongly donating ligands, such as cyclopentadienyl (Cp) or pentamethylcyclopentadienyl (Cp*).[3] Other formal oxidation states are known such as (I) in $[Ru(CO)_2Cp]_2$ or (III) in $[RuCl_2Cp^*]_n$.[4] In mononuclear complexes the ligands usually contribute 10 electrons to give the metal an 18-electron configuration, although sterically demanding ligands may stabilize electronically unsaturated derivatives, as in the triisopropylphosphine complex $[RuCl(PPr^i_3)Cp]$ (16 electrons).[5] Other complexes of ruthenium have a square-planar stereochemistry with a 16-electron configuration, due to the high level of energy of the orbital p_z that cannot be filled in this square-planar geometry. This type of complexes can react to give an 18-electron intermediate before eliminating a ligand, thus coming back to the stable 16-electron

configuration. This reactivity provides to these complexes remarkable catalytic properties.[6] The wide range of oxidation states, the different geometries associated along with an important variety of coordination numbers as well as the possible tuning of the complex by ligands are the basis of the rich chemistry of ruthenium and more generally of the transition metals. However, these are also limitations and drawbacks in this chemistry and for this reason chemists need to control the reactivity of the metal centre. In particular, the control of the metal oxidation state is crucial.

1.1.2 The Arene Ligand

Arenes or aromatic hydrocarbons are defined by the International Union of Pure and Applied Chemistry (IUPAC) as hydrocarbons with a conjugated cyclic molecular structure that is much more stable than the hypothetical localized structure.[7] Arenes are nowadays some of the most popular ligands in ruthenium(II) chemistry. This popularity is particularly due to its strong π-acceptor behaviour that enhances the stability of the transition metal's d orbitals. This stabilisation of the orbitals of the ruthenium leads to a great stability against oxidation, in particular from Ru(II) to Ru(III). Another consequence is that the metal centre shows a strong preference for π-donor ligands. The stabilisation of the transition metal's d orbitals can be explained by the theory of the molecular orbitals.[8] An arene is a L_3 ligand and consequently gives 3 electron pairs to the metal in a coaxial way from p orbitals to vacant d orbitals of the metal, but also receives lateral bonding in return from filled d orbitals of the metal to π* antibonding p orbitals of the ligand. This bonding mode is called back π-bonding (see Figure 1).

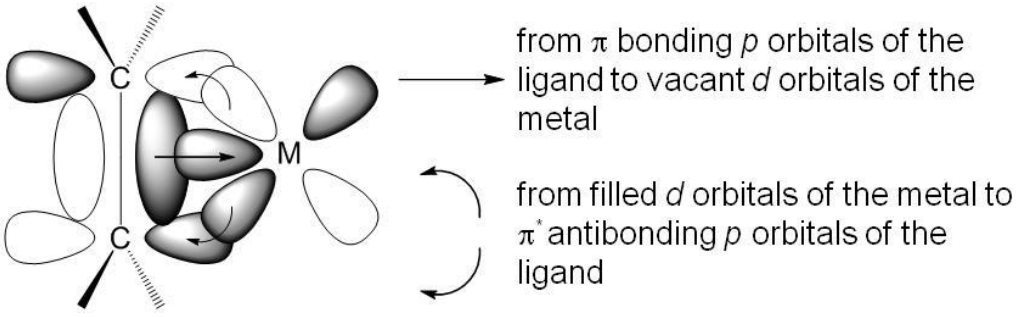

Figure 1. Bonding modes between transition metal and π-acceptor ligand

This high stabilisation of the transition metal's d orbitals by arene ligand *via* back π-bonding is described by molecular orbital diagrams. In the case of an octahedral or pseudo-octahedral complex ML_6, the simplified molecular orbital diagram – established without back π-bonding – (see Figure 2, A) shows that 3 d orbitals of the metal are nonbonding, molecular orbitals called t_{2g}. However, if the ligand L is a π-acceptor, like in the case of the arene ligand, these nonbonding d orbitals will be involved in the back π-bonding with the π* antibonding orbitals of L (see Figure 2, B). Therefore, these d orbitals will become bonding orbitals, and the 18-electron complex will be stabilised.[9]

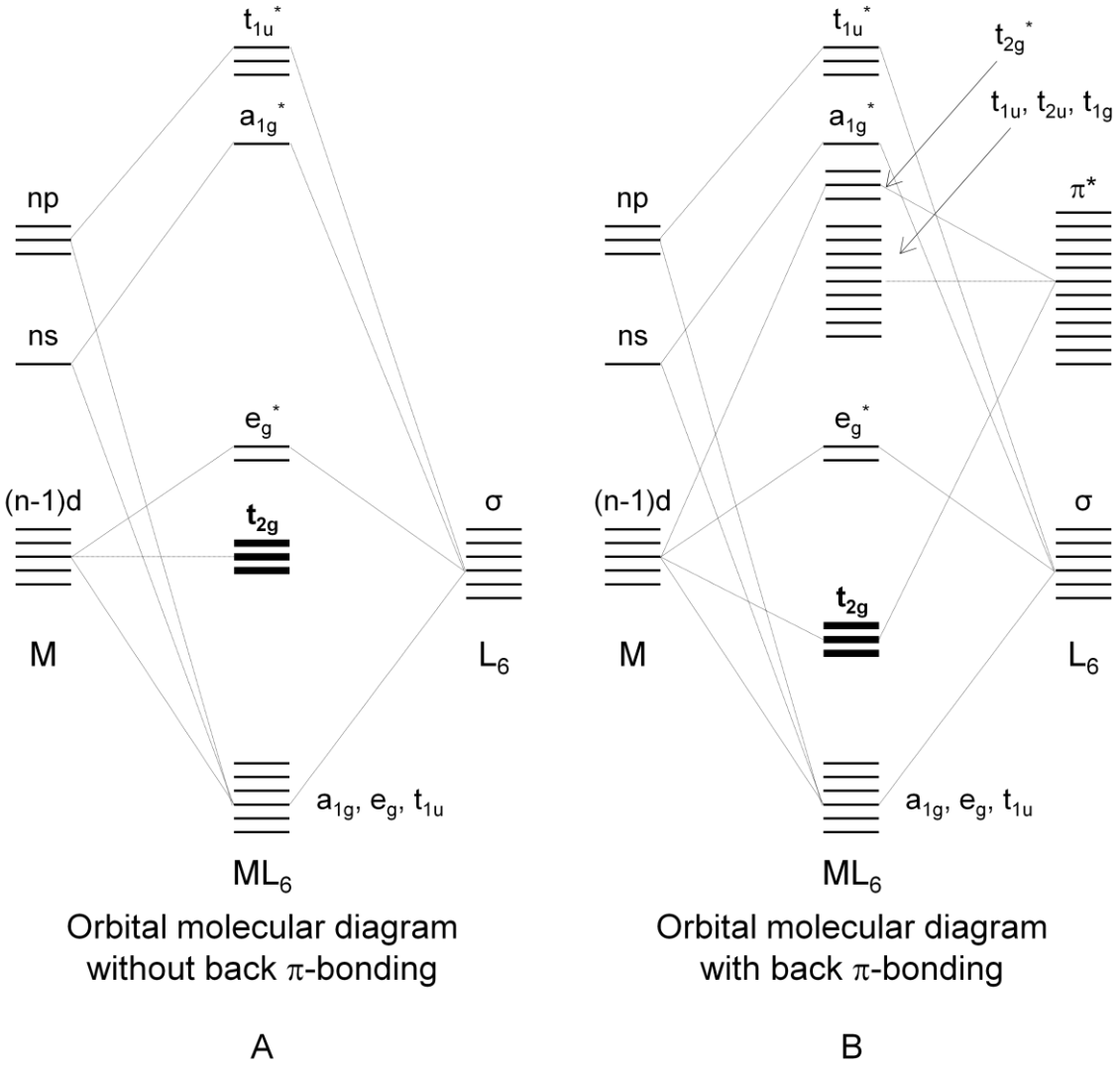

Figure 2. Molecular orbital diagram of an octahedral complex ML_6

In addition to this electronic protection of the oxidation state of the ruthenium centre, the arene ligands present other advantages. They are widely available and readily derivatised

by attaching different substituents on the benzene ring through electrophilic substitution.[10] Moreover, the structural occupation of three coordinating sites forces the arene ruthenium complex to adopt a pseudo-octahedral geometry. Finally, from a chemical reactivity point of view, the arene ligands are quite inert towards substitution reactions. It means that arene ruthenium units are relatively stable against a large variety of chemical reagents and reaction conditions.[11]

1.1.3 Dimeric Arene Ruthenium Chloro Complexes

The first arene ruthenium complex was prepared by Winkhaus and Singer in 1967 by reduction in ethanol of ruthenium tri-chloride hydrate ($RuCl_3 \cdot x\ H_2O$) in the presence of 1,3-cyclohexadiene (C_6H_8). This neutral diamagnetic complex was obtained as a brown precipitate, for which a polymeric structure with the formula $[RuCl_2(C_6H_6)]_n$ was proposed.[12]

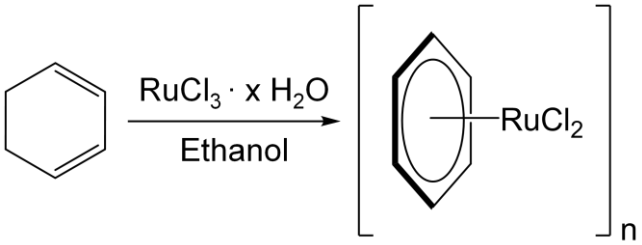

In 1972 Baird showed this polymeric formula to be erroneous and suggested a dimeric structure[13] by analogy with the complexes $[(\eta^5\text{-}C_5H_5)M(\mu_2\text{-}Cl)Cl]_2$ (M = Ir, Rh) published by Maitlis in 1969.[14] Eventually, in 1974, Bennett confirmed this dimeric structure $[(\eta^6\text{-}C_6H_6)Ru(\mu_2\text{-}Cl)Cl]_2$ in which each ruthenium atom is at the oxidation state II, and where the hapticity (η) of the arene is equal to 6. The two ruthenium centres are linked by two chloro bridges.[15]

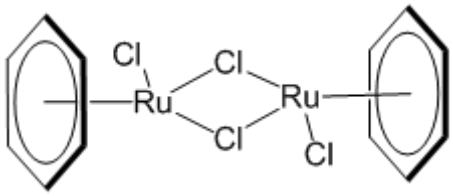

The recognition of the dimeric nature of these arene ruthenium complexes had marked the beginning of 40 years of arene-ruthenium-based chemistry. Thus, many different arene ruthenium dimers were synthesised and the method developed by Winkhaus and Singer is still

employed nowadays with electronically poor dienes. For instance, the dehydrogenation of (-)-(α)-phellandrene by ruthenium tri-chloride hydrate in ethanol leads to the formation of the well-used para-cymene (*p*-cym) dimer $[(\eta^6\text{-}p\text{-cym})Ru(\mu_2\text{-}Cl)Cl]_2$.[13]

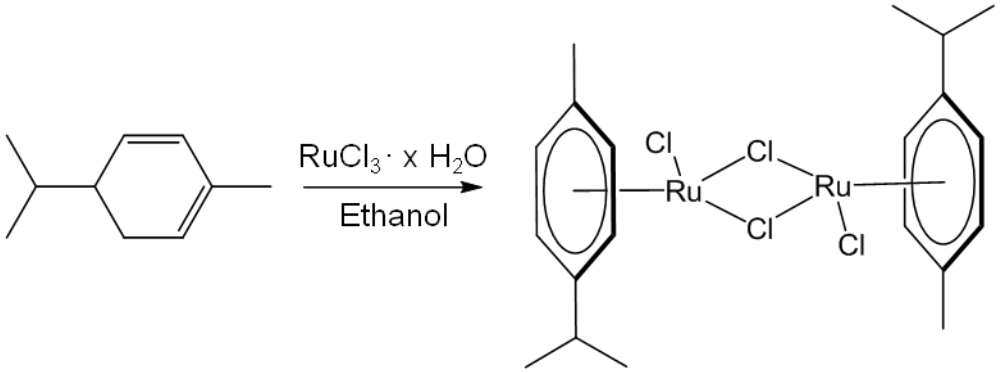

However, this method cannot be employed with the electronically rich arenes, such as hexamethylbenzene (hmb). In this case, the arene exchange method at elevated temperature can lead to the desired dimer. In 1982, following this method, Bennett succeeded in synthesising the hmb ruthenium dimer by exchange of the para-cymene ligand with the hexamethylbenzene arene at around 180°C.[16]

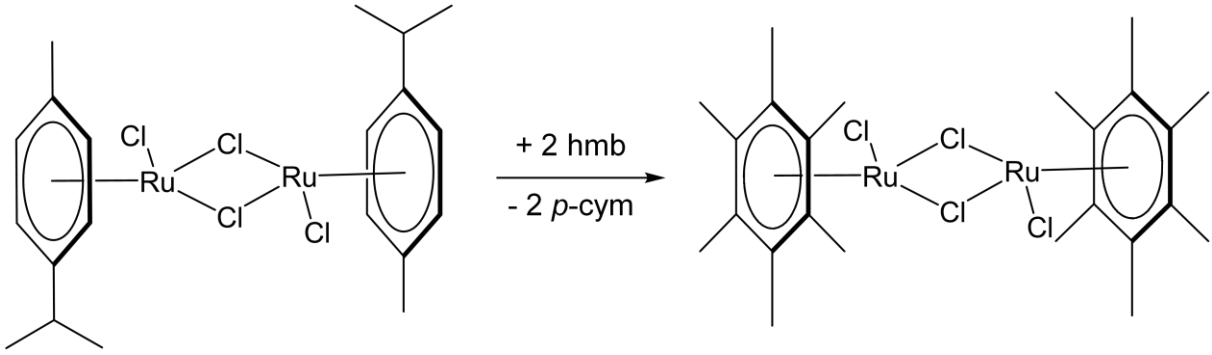

The enthusiasm for arene ruthenium dimers did not wane during the 1990s and found a revival with the emergence of functionalised arenes. These functionalisations are of interest because they are expected to combine the properties of the arene ruthenium unit with the properties of the grafted functions.[17]

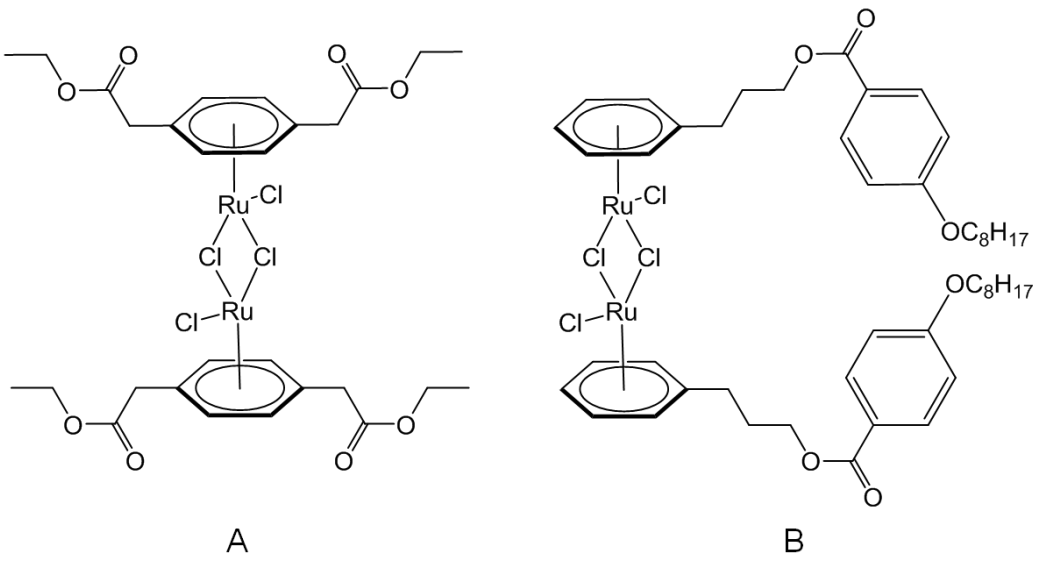

Figure 3. Examples of functionalised arenes in arene ruthenium dimers

A convenient method to introduce these functions is the preliminary functionalisation of an arene, followed by a Birch-type reduction[18] that converts the aromatic ring into a diene, which is then used as reagent for Winkhaus and Singer's method. For example, the dinuclear complexes $[(\eta^6\text{-}C_6H_5(CH_2)_3OCO\text{-}p\text{-}C_6H_4\text{-}OC_8H_{17})Ru(\mu_2\text{-}Cl)Cl]_2$ (A) and $[(\eta^6\text{-}p\text{-}C_6H_4(CH_2COOCH_2CH_3)_2)Ru(\mu_2\text{-}Cl)Cl]_2$ (B) were obtained in 2006 (see Figure 3).[19]

1.2 Supramolecular Chemistry of Host-Guest Systems

1.2.1 Coordination-Driven Self-Assembly and Molecular Recognition

Supramolecular chemistry has been defined by Jean-Marie Lehn as "the chemistry beyond the molecule".[20] This means that supramolecular chemistry is not focused on the synthesis of a single molecule constructed gradually *via* the formation of direct covalent linkages but deals with the assembly of a molecular object constituted by several single molecules held together by a variety of weak interactions, such as hydrogen bonds, hydrophobic and π-π interactions, and electrostatic effects.[21] These weak interactions are used by Nature to construct large and ordered molecular arrays with precise functions at the sub-cellular and cellular levels.[22] The most famous and telling example of supramolecular assembly created by Nature is the double helical structure of deoxyribonucleic acid (DNA), elucidated by Watson and Crick in 1953, in which two separate strands of nucleotides are connected through hydrogen bonds.[23] If the weak interactions have a predominant position in natural supramolecular assemblies, a considerable number of systems were however synthesised by chemists *via* metal-donor bonds – strictly covalent bonds – in order to assemble organic building blocks into molecular objects. Thus, supramolecular chemistry can be seen as an interface of organic chemistry – with the synthesis of the different building blocks – and inorganic chemistry – with the coordination of these organic building blocks to a transition metal. Furthermore, this meeting point also gathers physical chemistry – with the experimental and theoretical studies of interactions – and biochemistry – with the biological processes that start with substrate binding and recognition – together.[24]

The concept of supramolecular chemistry described by Lehn as "the designed chemistry of the intermolecular bond"[25] is based on a process by which a supramolecular species forms spontaneously from its components.[26] This process, called "self-assembly" is a simple convergent path giving rise to the assembled target in a straightforward manner, and this, for the majority of the synthetic systems.[27] However, it is important to notice that self-assembly is not confined to supramolecular systems, but on the contrary is ubiquitous throughout life chemistry. The growth of crystals,[28] the formation of liquid crystals,[29] the spontaneous generation of synthetic lipid bilayers,[30] and the alignment of molecules on existing surfaces[31] are some examples of self-assembly in chemical systems.

A very interesting subset of self-assembly, is the coordination-driven self-assembly,[32] which allows a directional-bonding approach that organises the different building blocks following the coordination modes of the transition metal.[33] Indeed, whereas many of the weaker noncovalent interactions are nondirectional – for example, hydrogen bonds, van der Waals, and hydrophobic interactions – covalent metal-ligand bonds, also called dative bonds, are highly directional and relatively strong. Consequently, coordination-driven self-assembly leads to the straightforward construction of large and rigid supramolecular objects with well-defined shapes, sizes, and geometries.[34] Over the last two decades, the groups of Fujita,[34] Stang,[35] Raymond,[36] Lehn,[25] or Mirkin[37] have pioneered the use of the directional-bonding coordination-driven approach to self-assembly. The idea of this approach is to combine rigid electron-poor metal centres and complementary, rigid electron-rich organic donors to provide a wide variety of discrete two dimensional (2D) and three dimensional (3D) polygonal and polyhedral coordination assemblies. It is important to notice that metal-ligand coordination bonds are kinetically labile, also being strong as compared to most other noncovalent interactions.

This lability is crucial since one important feature of supramolecular chemistry is that molecular assemblies are normally reversible. Therefore, the final product is in thermodynamic equilibrium with its components. In particular, this notion of reversibility is fundamental in the case of the systems assembled by molecular recognition. Like self-assembly, molecular recognition is a process that is widely found throughout both natural and synthetic systems. Molecular recognition is essential in a range of biological areas – for instance substrates-enzymes or proteins-DNA interactions – and is also of central importance in a number of chemical fields – sensors, separation science or catalysis for example –. In particular, molecular recognition is closely linked with host-guest chemistry.[38]

1.2.2 Host-Guest Systems and Carceplexes

Host-guest chemistry is a subset of supramolecular chemistry based on molecular recognition.[39] For many biological systems, as for substrate-enzyme systems, host-guest chemistry is the link between the nature of these biological systems and their functions. In other words, the structural adaptations of both enzyme and substrate in order to accommodate their shapes and to allow interactions and catalytic processes are the visible expressions of the

host-guest phenomenon. In that precise system, the enzyme can be seen as a host and the substrate as a guest of the host-guest system.

The place where the guest is accommodated by the host is called binding site. Furthermore, in a given supramolecular system the degree of electronic and steric complementary between host and guest dictates the magnitude of the molecular recognition occurring. In particular, the stoichiometry of a host-guest system is defined by the number of guest molecules that one molecule of host is able to accommodate.

It should be noted that host-guest chemistry is not only a natural and biological phenomenon, but is also widely used by chemists. Indeed, since D. J. Cram baptised this field of supramolecular chemistry in 1974,[40] many efforts have been invested on the design of numerous host-guest systems. In particular, a large array of synthetic hosts, capable of binding guest ions or molecules, has been developed. The field began with ionophores such as crown ethers[41] and cryptands,[25] (see Figure 4).

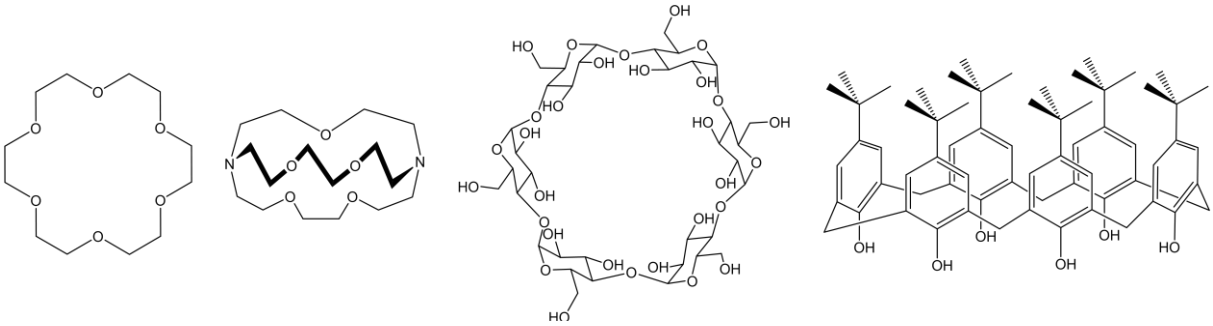

Figure 4. Some common host molecules

In the 1970s Cram began to develop cavitands,[42] and in the 1980s the first calixarenes were synthesised.[43] Cavitands have enforced cavities, and therefore they cannot collapse upon themselves. Such preorganisation optimises the van der Waals contacts between host and guest. Later, Cram synthesised a spheroid compound constituted by two hemispherical cavitands link together and able to entrap guests in such manner that the loss of the guest molecule is only possible *via* rupture of a covalent bond. Then, in 1983 Cram proposed the name of carceplex to define these host molecules that permanently incarcerate their guests.[44] Since this beginning of synthetic host-guest chemistry, host-guest systems and the limit case

of the carceplex molecules have been widely studied, with many different types of host and guest molecules.

1.2.3 Pyrene, the Guest of Honour

Among all the different guest molecules that have been encapsulated *via* host-guest chemistry since the 1970's, pyrene is one of the best studied. The success of pyrene as a guest molecule can be partially explained by the chemical nature of its structure. Pyrene is a highly symmetrical molecule (point group D_{2h}), and is the smallest peri-fused polycyclic aromatic hydrocarbon (PAHs) compound.[45] This planar structure confers to pyrene a very interesting sterical environment, which gives it the opportunity to fit into small host's cavity. This suggests that the design of host's small pockets can be ideal for pyrene.

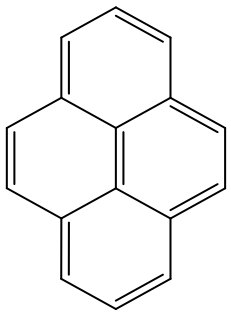

pyrene

Moreover, despite having 16 π electrons and consequently not following the Hückel's 4n + 2 π electrons rule, which states that cyclic planar molecules in which each atom has a p orbital are aromatic if they contain 4n + 2 π electrons, pyrene is an aromatic molecule, based on Clar sextet theory,[46] Platt's ring perimeter,[47] and the Randić-Herndon conjugated circuit models[48] commonly employed for qualitative characterisation of the aromaticity of polycyclic aromatic compounds.[49] This aromaticity is crucial for the use of pyrene as guest molecule. Indeed, as described in section 1.2.1, supramolecular chemistry in general, and host-guest chemistry in particular are mainly based on weak interactions such as hydrophobic or π - π stacking interactions. The presence of a rich π electronic environment is consequently susceptible to give strong intermolecular interactions, *via* π - π stacking, between an aromatic constituent of the host molecule and pyrene. This parallel π - π stacking can also be reinforced by T-shape interactions.[50]

Furthermore, the rich photochemistry and predictable substitution reactions of pyrene have important applications in organic chemistry, biochemistry, and materials science. For example, pyrene has been commonly used as a fluorescent probe because of its intense fluorescence,[51] its fluorescence lifetime reported to be very long (1.4 μs),[52] its excimeric formation,[53] and its fluorescence anisotropy.[54] In particular, fluorescence quenching of pyrene is routinely employed[55] for oxygen measurements in solution,[56] tissues,[57] and in living cells.[58] This wealth of potential applications of the pyrene properties is also an advantage for the use of pyrene as guest molecule in host-guest systems.

1.2.4 Metalla-Assemblies, Versatile Host Systems

If pyrene is a popular guest, metalla-assemblies are equally used as host molecules or carceplexes. This currency can be explained by the numerous advantages of the directional-bonding approach provided by coordination-driven self-assembly, see section 1.2.1. Indeed, the wide variety of possible structures that can be constructed *via* the use of either different building blocks or different metals affords a large array for the architectures of the cavities where the guest molecules will be encapsulated.

Concerning the different building blocks, the shapes of these building blocks are dominated by their turning angles. This type of angle is defined as the angle formed between the two coordinating sites of a ditopic ligand. For example, a linear ditopic ligand, such as 4,4'-bipyridine (bpy), will have its two sites of coordination oriented at 180° from each other while a ditopic building block such as 3,5-bis(pyridin-4-yl)-benzene (bpb) has a turning angle of 120° between its two pyridyl donor sites. By extension of this directional-bonding approach, the design of building blocks with more than two coordination sites allows the design of many possible angles, and consequently many possible geometries. For instance, the 2,4,6-tri(pyridin-4-yl)-1,3,5-triazine (tpt) ligand or the 5,10,15,20-tetra(pyridin-4-yl)porphyrin (tpp-2H) have an angle of respectively 120° and 90° between two neighbours pyridyl donor sites, (see Figure 5).

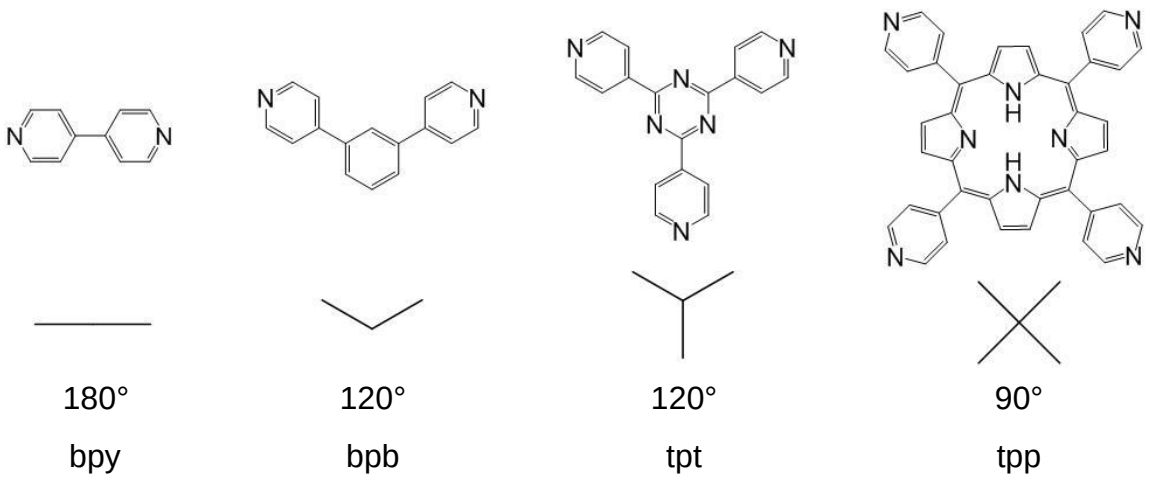

Figure 5. Representations of some ligands and their geometries

Concerning the different transition metals, the shapes of the final structure is dictated by the stereochemistry of the metal. This stereochemistry depends of the oxidation state, of the coordination number, of the ligands coordinated and of the metal itself. All these factors drastically influence the shapes of the metalla-assemblies and their hosting abilities and numerous examples can be found in the literature.

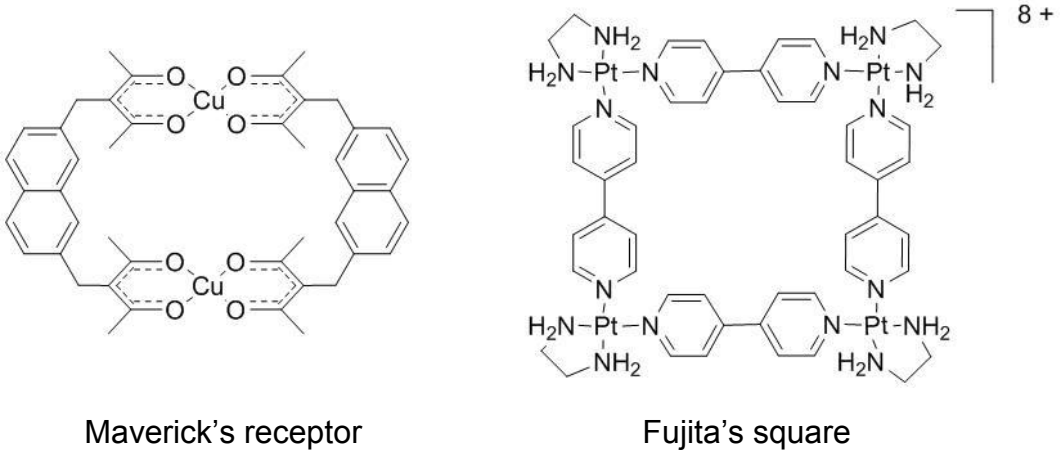

Figure 6. Examples of metalla-assemblies as host systems

A Cu(II)-linked macrocyclic receptor reported by Maverick ables to encapsulate guest molecule such as 1,4-diazabicyclo[2.2.2]octane (see Figure 6),[59] square planar and prismatic ethylenediamine Pd complexes of Fujita able to encapsulate guest molecules (1,3,5-trimethoxybenzene in solution in the square,[60] adamantane among others in the prism[61]) (see Figure 6), Fe- and Ga-containing M_4L_6 anionic cages reported by Raymond able to trap and

stabilize cation guests,[62] Re-containing squares reported by Hupp,[63] and of course all the host cages designed by Peter Stang, who is one of the first pioneers of the field together with Makoto Fujita.[32, 35, 64]

1.2.5 Arene Ruthenium Metalla-Assemblies as Host Systems

In the field of coordination-driven self-assembly, platinum, palladium and rhenium have been of central interest, but arene ruthenium complexes have also received considerable attention, in particular because they show a number of interesting characteristics.[65] First, the starting material is the easily accessible arene ruthenium dimer $[(\eta^6\text{-arene})Ru(\mu_2\text{-}Cl)Cl]_2$. Second, arene ruthenium complexes are robust and can be stored without a protecting inert atmosphere. These dimers are generally well soluble in standard organic solvents such as chloroform and interestingly, they are also soluble in water, monomeric aqua complexes being formed.[66] Finally, after abstraction of the halide ligands, three facial coordination sites are available for the coordination of neutral or anionic ligands (X, Y, Z). The corresponding complex has a so-called half-sandwich structure presenting a piano-stool geometry, (see Figure 7).

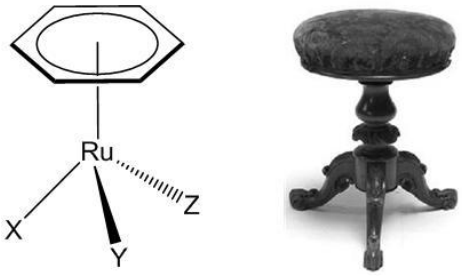

Figure 7. Typical piano-stool shape of half-sandwich arene ruthenium complexes

The three available coordination sites of arene ruthenium complexes can be used to construct metalla-macrocyclic complexes as well as coordination cages. One possibility to obtain those constructions is to combine the half-sandwich complexes with linear ligands such as bpy, or with trifunctional ligands, such as adenine-derivatives. Thus, over the last two decades, many metalla-cycles have been synthesised using half-sandwich arene ruthenium complexes with different ligands and used as host systems. Among them, we can quote for instance the metalla-macrocyclic complexes synthesised by the groups of Sheldrick[67] or Severin.[66, 68] The same strategy has been applied by Fish,[69] Rauchfuss,[70] and Yamanari[71] with

half-sandwich complexes of rhodium and iridium to construct metalla-cages able to encapsulate guest molecules.

Another method to synthesise arene ruthenium cages capable to host guest molecules is to use dinuclear metalla-clips. This strategy has been developed by our group and is based on the synthesis of an arene ruthenium dinuclear complex designed from arene ruthenium dimers and tetradentate ligand precursors such as 1,4-dihydroxy-benzoquinone derivatives. The synthesis is straightforward, since reaction of $[(\eta^6\text{-arene})Ru(\mu_2\text{-}Cl)Cl]_2$ with 1,4-benzoquinone derivatives (2,5-dihydroxy-1,4-benzoquinone (dhbq-H_2); 2,5-dichloro-1,4-benzoquinone (dClbq- H_2)) affords the corresponding dinuclear arene ruthenium metalla-clips $[(\eta^6\text{-arene})_2Ru_2(OO\cap OO)Cl_2]$ ($OO\cap OO$ = 2,5-dioxydo-1,4-benzoquinonato (dobq), 2,5-dichlorido-1,4-benzoquinonato (dClobq)) with a metal–metal distance of 7.9 Å, (see Figure 8 for the examples of two dinuclear clips **C₁**,[72] and **C₂**[73] with para-cymene as arene).

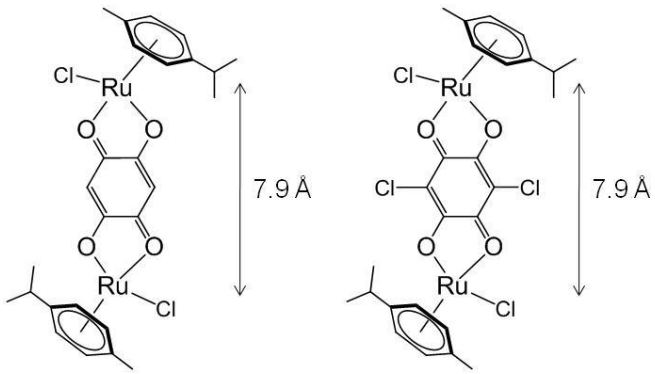

C₁ **C₂**

Figure 8. Dinuclear arene ruthenium metalla-clips **C₁** and **C₂**

These metalla-clips can then be used as building blocks to assemble cationic arene ruthenium metalla-prisms.[65] These hexanuclear cations consist of three dinuclear metalla-clips and two trigonal tpt panels. The synthesis is straightforward, since addition of a halide scavenger to the metalla-clip in the presence of tpt leads to the connection of the two panels by self-assembly (see Scheme 1 for a representation of the synthesis of arene ruthenium metalla-prisms and the example of $[Ru_6(p\text{-cym})_6(tpt)_2(dobq)_3]^{6+}$ ($[\mathbf{P_1}]^{6+}$) synthesis). The metalla-prisms are usually isolated as trifluoromethanesulfonate salts.[72]

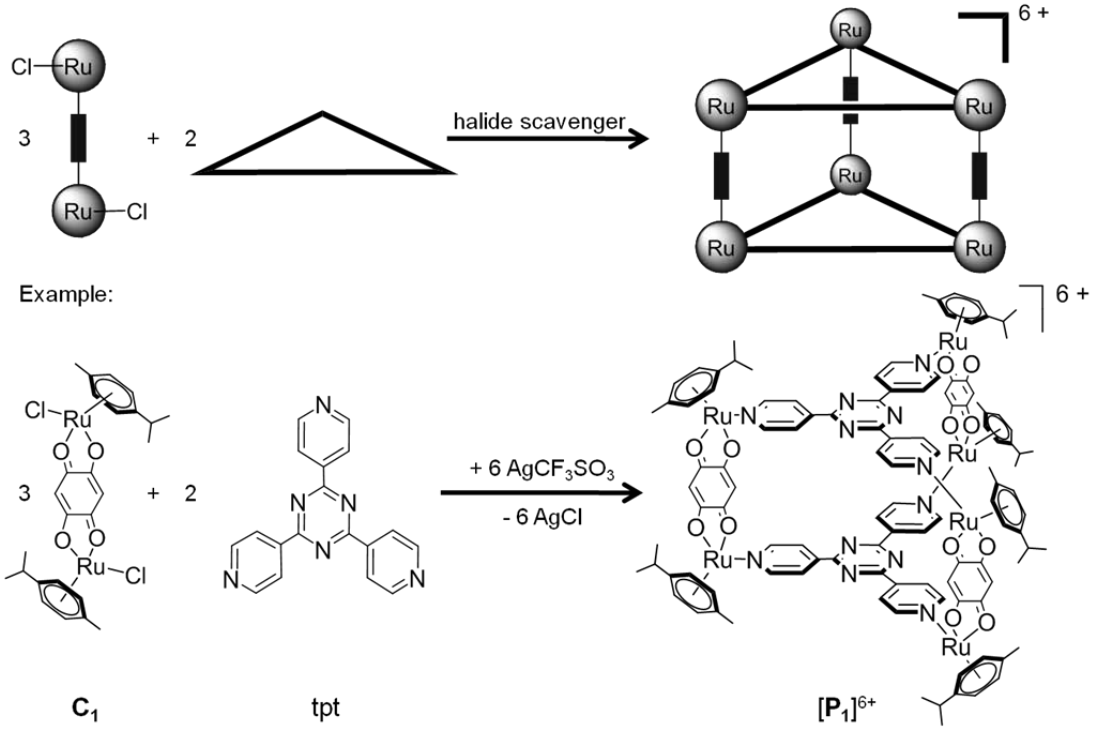

Scheme 1. Synthesis of arene ruthenium metalla-prisms

As shown in Scheme 1, those metalla-prisms contain a cavity and can permanently encapsulate a flat molecule such as pyrene ($C_{16}H_{10}$), fluoranthene ($C_{16}H_{10}$), triphenylene ($C_{18}H_{12}$), benzo[e]pyrene ($C_{20}H_{12}$), and coronene ($C_{24}H_{12}$). In this particular case, if the synthesis of the metalla-prism is carried out in the presence of such a flat aromatic molecule, a carceplex is found.[73] Permanent encapsulation of square-planar complexes $Pd(acac)_2$ and $Pt(acac)_2$ (acac = acetylacetonato) was also been observed giving the "complex-in-a-complex" cations $[Pd(acac)_2 \subset prism]^{6+}$ and $[Pt(acac)_2 \subset prism]^{6+}$, (see Figure 9).[72]

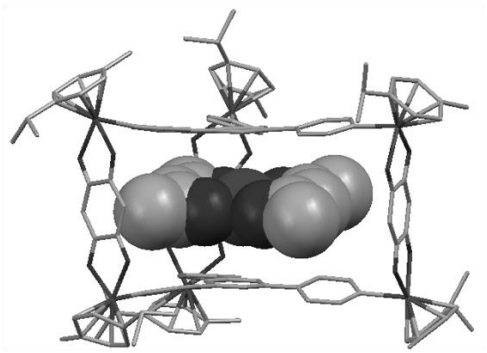

$[Pd(acac)_2 \subset \mathbf{P_1}]^{6+}$

Figure 9. Structure of $[Pd(acac)_2 \subset \mathbf{P_1}]^{6+}$, hydrogen atoms being omitted for clarity

1.3 Mononuclear Arene Ruthenium Complexes for Anticancer Treatment

1.3.1 Metals in Medicine

The beginnings of the use of metals in medicine were empiric. Gold was used to treat ulcers in ancient China more than four thousand years ago, and silver coins were added to containers for water storage in order to prevent intoxications due to silver's anti-bacterial property in ancient Rome, but the use of these metals was not based on real scientific knowledge.[74] Thus, in France during the 16th and 17th century, some physicians published several recipes of so-called "drinkable gold" made by distilling alcohol solutions with sulphuric acid and gold chloride. During this process diethyl ether is synthesised *in situ* and dissolves gold chloride, which forms a yellow coloured phase, *l'or potable*.[75] This solution was used as an *elixir de beauté* by Diane de Poitiers, who was a favourite of King Henri II, and recent findings suggest that this drinkable gold was the cause of a chronic intoxication leading to the death of Diane de Poitiers.[76] Nevertheless, disasters like this one did not discourage the cosmetic industry of the 21th century to use gold nanoparticles and other expensive and precious metals for modern *elixirs de beauté*.

More recently, in the early years of the 20th century, Paul Ehrlich discovered an arsenic drug against syphilis by screening a library of compounds and baptised it Salvarsan. Then, Ehrlich's laboratory developed a more water-soluble arsenical compound, called Neosalvarsan, which was easier to prepare and became available in 1912.[77] However, these arsenical compounds presented considerable side effects, and they were supplanted as treatments for syphilis in the 1940s by penicillin. After these only partial successes for metal-containing drugs, the pharmaceutical industry focused on the design of purely organic drugs and natural products, until the discovery by Barnett Rosenberg of the antiproliferative activity of the platinum complex cisplatin.[78]

The different geometries of the complexes, as well as the important variety of ligands that it is possible to coordinate onto different transition metals, allowed the syntheses of many kinds of molecules impossible to obtain *via* organic synthesis. However, despite the clinical success of cisplatin, this pool of complexes has only partially been explored by the pharmaceutical industry.

1.3.2 Cisplatin and other Platinum-Containing Anticancer Drugs

Cisplatin, or *cis*-diamminedichloroplatinum(II), is a square-planar Pt(II) complex (see Figure 12) and was the first metal-based drug to enter into worldwide clinical use for the treatment of cancer in 1978. Currently, cisplatin is used either by itself or in combination with other drugs for treating ovarian, lung, testicular, bladder, oesophageal, colon and prostate cancers. Moreover, this molecule is used as a benchmark for research in this area. For instance, the activities of platinum and non-platinum potential drugs are usually compared to cisplatin in most publications. More information concerning the chemical and physical properties of cisplatin, its biological mechanism of action or its clinical applications as well as many other topics can be found in the numerous articles, reviews and books of Rosenberg,[79] Lippard,[80] Reedijk,[81] Farrell,[82] Lippert,[83] Sadler,[84] or Schellens.[85]

Nevertheless, cisplatin presents major limitations, for example a strong nephrotoxicity, a phenomenon of resistance acquired by tumour cells, and other side effects such as bone marrow suppression.[86] Thus, in order to decrease these side effects, more than 4000 platinum compounds have been tested as potential anticancer drugs. Among them, about 1% has entered clinical trials, and the Food and Drug Administration (FDA) have approved only two complexes: carboplatin and oxaliplatin, (see Figure 10).

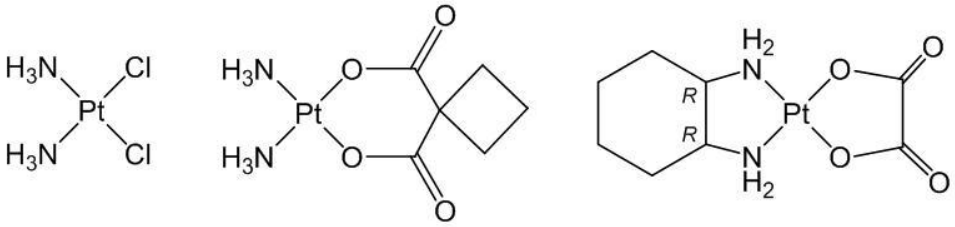

Figure 10. Structures of cisplatin, carboplatin and oxaliplatin

These new platinum anticancer drugs exhibit a better selectivity against cancer cells than cisplatin, but some of the limitations precisely due to the presence of platinum still reside. This is the reason why many researches are now focusing on metalla-drugs containing other metals as potential anticancer agents. Among them, ruthenium based-drugs are the most promising ones.

1.3.3 Ruthenium *versus* Platinum

Ruthenium complexes have raised considerable expectations for the treatment of cancer since the beginning of the 1990s.[87] Some of these molecules directly attack and kill cancer cells, while others present antimetastatic properties, preventing the tumour from releasing cancer cells that spread to other parts of the body. The structures and properties of these complexes range from traditional coordination compounds that lose their ligands by direct interaction with the biological targets, to organometallic compounds, which in addition to interact with the biological targets, can facilitate the generation of higher cytotoxic reactive oxygen species (ROS), such as singulet-oxygen. Finally, some ruthenium complexes are able to act as enzyme inhibitors which question the survival of the cell.[88] This large array of possible interactions is one of the advantages that ruthenium complexes possess over platinum complexes.

Another advantage for ruthenium complexes *versus* platinum complexes is the chemistry of ruthenium in the biological milieu. Among the numerous numbers of oxidation state of the ruthenium, only Ru(II) and Ru(III) have been incorporated into potential anticancer drugs. Since ruthenium is just bellow iron in the periodic table, most Ru(II) (S = ½) and Ru(III) (S = 0) complexes are low-spin, and the water exchange rate for aquated Ru(II) is about one order of magnitude faster than that of Pt(II), suggesting that complexes of Ru(II) may be better suited for reactions with biological targets in the body. This exchange rate for aquated Ru(II) is also an advantage for the elimination of ruthenium by the body. Consequently, the accumulation effect of platinum in the body of patients treated by platinum drugs might be not met with ruthenium drugs. Finally, studies show that the two oxidation states of the ruthenium Ru(II) and Ru(III) can be interconverted by substances in the body, which could explain the good elimination of Ru(III) complexes, despite of a slower water exchange rate than Ru(II) complexes.[89]

1.3.4 NAMI-A and KP1019: Promising Ruthenium(III) Anticancer Agents

Imidazolium-trans-dimethylsulfoxide-imidazole-tetrachlororuthenate (NAMI-A) and imidazolium-trans-bis(1H-indazole)-tetrachlororuthenate (KP1019) are two ruthenium agents that have successfully completed phase I clinical trials.[90] Despite their structural and chemical

similarities (see Figure 11), these two Ru(III) complexes show distinctly different antitumour behaviours.

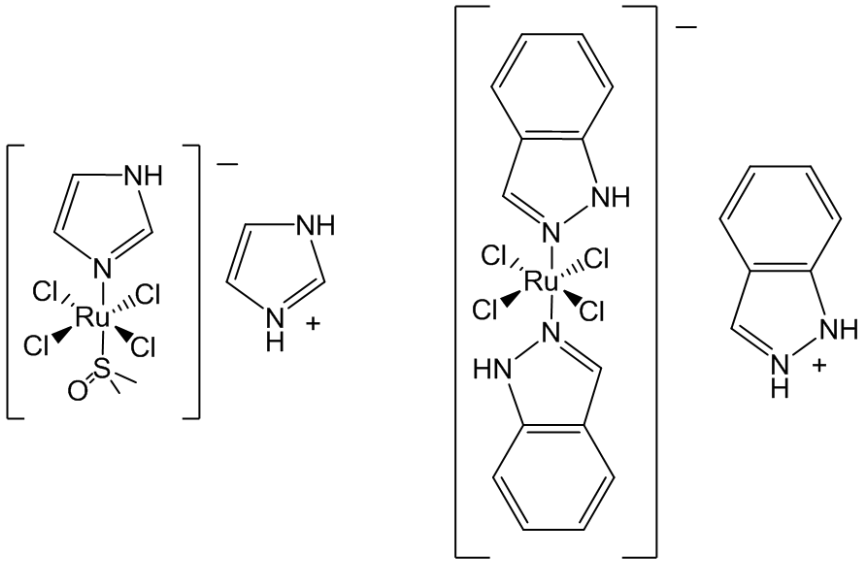

NAMI-A KP1019

Figure 11. Structures of NAMI-A and KP1019

In preclinical studies, NAMI-A has demonstrated inhibitory effects against the formation of cancer metastases in a variety of tumour animal models, but appears to have no direct cytotoxic effects on primary tumours.[91] Contemporary with the development of NAMI-A by Sava, Keppler discovered KP1019. KP1019 is more stable toward aquation and hydrolysis and is more readily taken up by cells than NAMI-A.[92] But more interestingly, KP1019 shows a remarkable activity against primary cisplatin-resistant colorectal tumours, but no pronounced anti-metastatic activities.[93]

Eventually, since both NAMI-A and KP1019 molecules react with biological reductants, as for example ascorbate or glutathione reductase, in protein-free model systems,[94] it was suggested that the reduction of Ru(III) pro-drugs to Ru(II) species may be required for their biological activity,[93] suggesting that the active species are Ru(II) complexes.

1.3.5 Mononuclear Arene Ruthenium(II) Complexes as Potential Anticancer Agents

The most common group of cytotoxic ruthenium compounds are arene ruthenium complexes where the ruthenium atom is in the oxidation state II. This type of air-stable and water-soluble anticancer agents was pioneered by Dyson[95] and Sadler.[96] In particular, Dyson's RAPTA-C complex[97] built from para-cymene ruthenium and 1,3,5-triaza-7-phosphaadamantane (pta) and Sadler's $[(\eta^6\text{-biphenyl})Ru(en)Cl]^+$ complex[98] built from biphenyl ruthenium and ethane-1,2-diamine (en) (see Figure 12) are two highly promising molecules that are currently in phase I of clinical trials.

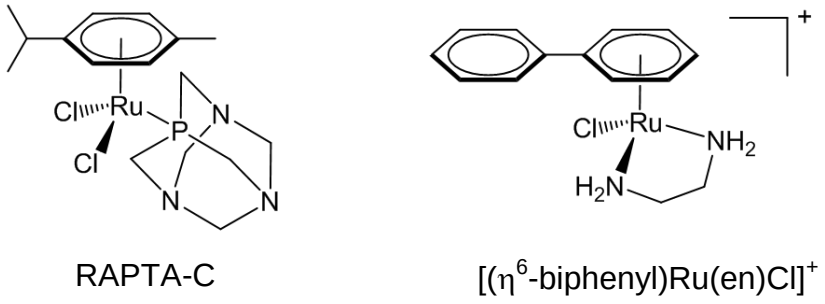

Figure 12. RAPTA-C and $[(\eta^6\text{-biphenyl})Ru(en)Cl]^+$ complexes

These arene ruthenium complexes possess chloro ligands that can dissociate as chloride anions, therefore theses complexes aquate and hydrolyse easily at physiological pH (~ 7.4) and low chloride concentration corresponding to intracellular conditions. However, in the case of a strong concentration of chloride, such as in blood plasma, this aquation equilibrium is decreasing and the rate of exchange is strongly inhibited.[98-99] This difference of aquation equilibrium between intra and extracellular milieu is essential in term of binding with biomolecules, and aquation seems to be the activating step in the cytotoxicity of arene ruthenium complexes. However, the mechanism of these complexes is still not completely understood.[100]

1.4 Arene Ruthenium Assemblies with Anticancer Properties

1.4.1 Drug Delivery and Enhanced Permeability and Retention Effect

So far only small molecules containing one metal atom, either platinum or ruthenium, have been discussed. This approach of small molecules as anticancer agents is the common strategy used by pharmaceutical industries to design new potential drugs. In 1997, to illustrate this widespread small molecule approach, Lipinski published five well known rules, based on the observation that most drugs are relatively small and lipophilic. According to these rules, the vast majority of the drugs approved by the FDA possess a molecular weight under 500 g · mol^{-1} and have not more than five hydrogen bond donors and not more than ten hydrogen bond acceptors.[101]

Nevertheless since the beginning of the 1980's, basic research in biochemistry increasingly studied large and high molecular weight molecules, in particular in the field of drug delivery. The idea of drug delivery is to hide the real drug into a larger molecule, called drug vector, which has different properties. For instance, this drug vector can protect the drug against the acidic pH of the stomach or of the basic pH of the bowels, but can also protect it against the metabolic action of the liver, or can increase the water-solubility of the drug. In fact, the aim is to modify the biodistribution and the clearance of the molecule without changing the structure of the drug.

Another interest of large and high molecular weight drugs is their potential selectivity for cancer cells. The discrimination of healthy with respect to cancer cells by a drug between normal and cancer cells is one of the major challenges of anticancer research. In the beginning of the 1980's, Maeda discovered a possible strategy to attain this selectivity by using large molecules called macromolecular drugs or nanomedicines. The concept behind this approach is the fact that cancer cells present a very important hypervasculature and a defective vascular architecture of the endothelial layer of blood vessels.[102] Moreover, in addition to this enhanced tumour vascular permeability, the lymphatic drainage system is substantially modified in cancer cells, and it appears that it does not operate efficiently.[103] Consequently, macromolecular drugs and large vectors are retained in the tumour interstitium for longer periods than in healthy tissues. Thus, the combination of poor tissue drainage with increased tumour vascular permeability results in a phenomenon called the enhanced permeability and

retention (EPR) effect. This effect is believed to play a major role in the selectivity of nanomedicines towards cancer cells with an intratumour drug delivery efficacy up to 100 fold greater than that observed in healthy cells.[104] Many types of nanomedicines exist, including antibodies and polymeric drugs, but also large drug delivery vectors such as micelles and nanoparticles. Indeed, an EPR effect has been observed for proteins,[105] micelles composed of block copolymers,[106] encapsulated drugs,[107] liposomes,[108] and even bacteria with diameters up to 12 μm.[109] These types of nanomedicines are fabricated by organic chemistry, organometallic chemistry or by biological techniques. Another and very useful way to design macromolecular drugs is supramolecular chemistry.

1.4.2 Arene Ruthenium Metalla-Rectangles Against Cancer

Supramolecular chemistry, and especially coordination-driven self-assembly, is a really simple and straightforward method to design large molecules able to target cancer cells *via* EPR effect, but surprisingly the application of supramolecular chemistry remains extremely scarce. As mentioned above, arene ruthenium complexes can be used either as building blocks for supramolecular chemistry, or as potential anticancer agents. Thus, this double face of these complexes allows the possibility to combine their versatile properties in only one object, and consequently, it becomes possible to associate the anticancer activity of these complexes into large structures precisely built from these arene ruthenium compounds.

This original approach has been developed by our group and different water-soluble arene ruthenium rectangles of general formula $[(\eta^6\text{-arene})_4Ru_4(OO\cap OO)_2(N\cap N)_2]^{4+}$ (arene = *p*-cym, hmb; $OO\cap OO$ = dobq, dClobq; $N\cap N$ = pyrazine (pyr), bpy, 1,2-bis(4-pyridyl)ethylene (bpe)) have been synthesised by our group[110] and by Jin's group.[111] We tested all these metalla-rectangles against cancer cell lines, (see Figure 13 and List of Structures).[110] The activities of these metalla-rectangles $\mathbf{R_1}$ – $\mathbf{R_{12}}$ against human ovarian cancer cell lines (A2780) were found to be moderate to excellent, depending of the size of the linker used as well as the nature of the arene (para-cymene *versus* hexamethylbenzene). Indeed, the IC_{50} values (IC_{50} being the drug concentration necessary for 50% inhibition of cell viability) of these metalla-rectangles were found in the range 4 – 66 μM. Later and following the same approach, Navarro and Barea's group published new arene ruthenium metalla-rectangles with antiproliferative activities.[112]

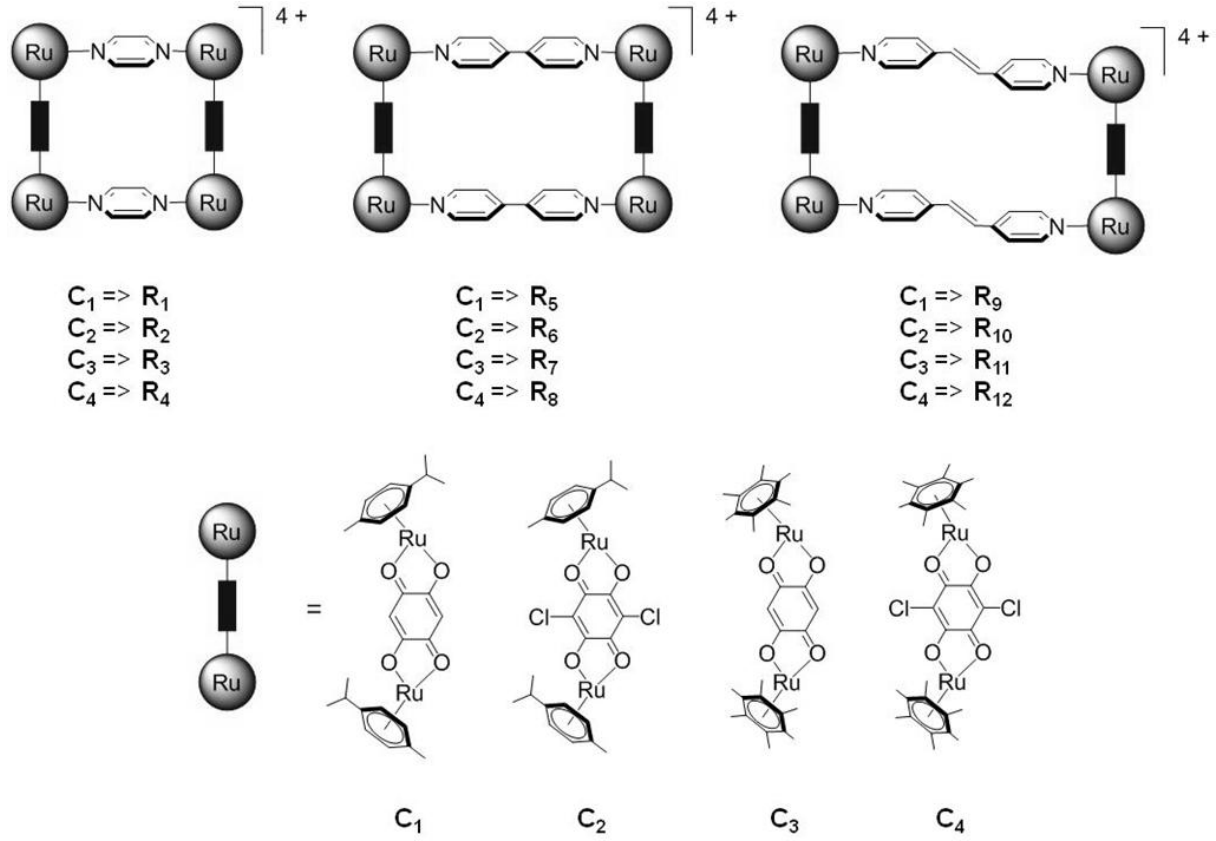

Figure 13. Schematic representation of metalla-rectangles $\mathbf{R_1}$ – $\mathbf{R_{12}}$

1.4.3 Trojan Horse Concept and Arene Ruthenium Metalla-Prisms

The molecular Trojan horse concept is based on the idea to encapsulate potential drugs that are not soluble in water and therefore that cannot enter the cells into the hydrophobic cavity of a water-soluble arene ruthenium prism. Thus, the metalla-prism becomes a drug vector that enhances the uptake of the hidden drug, by transporting it and releasing it into cancer cells, (see Figure 14). Moreover, as the prism is built by assembly of arene ruthenium units, it is also a potential anticancer agent. Finally, the size of the prism could allow the selective targeting of cancer cells *via* EPR effect.

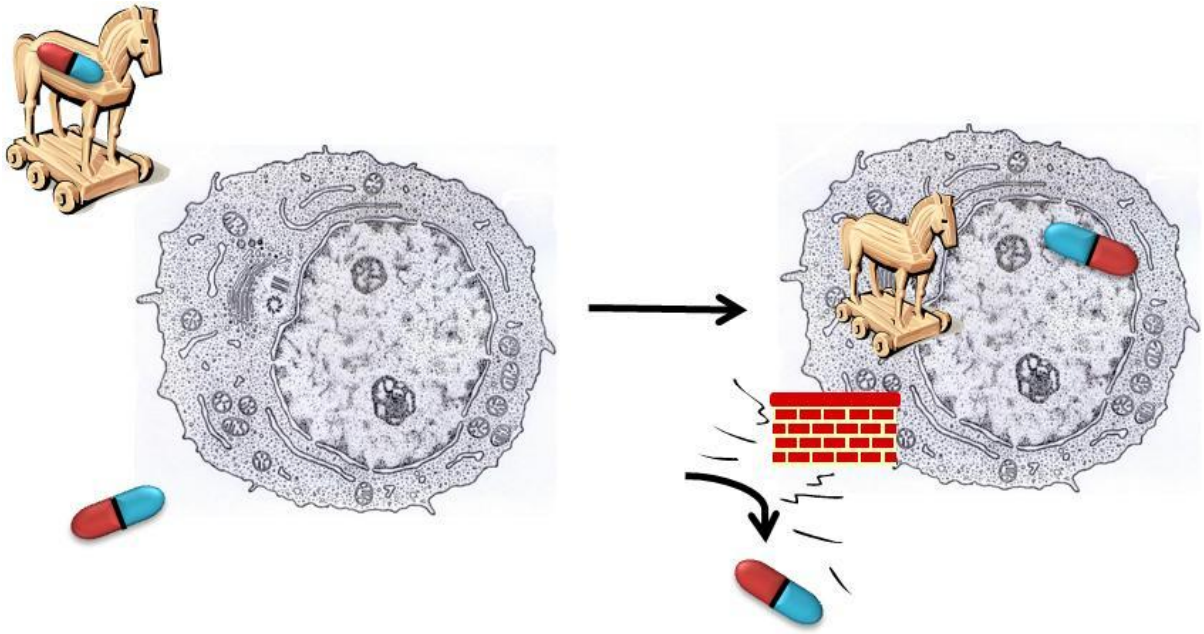

Figure 14. Molecular Trojan horse concept

As described earlier, arene ruthenium metalla-prisms able to permanently encapsulate small molecules have been synthesised by our group. This permanent encapsulation is due to the carceplex behaviour of the dobq and dClobq-bridged prisms and allows the transport and the release of these guest molecules into cancer cells.

The synthesis of such large and cytotoxic carceplex drug vectors is relatively new. Indeed, different arene ruthenium prisms have been synthesised so far by our group, but only the last generation has demonstrated carceplex abilities. In fact, the ability of the metalla-prism to encapsulate guest molecules depends on the size of the cavity, and therefore on the length of the bridge between the ruthenium atoms. This is the reason why our group has always tried to increase the length of the dinuclear clips, (see Figure 15).

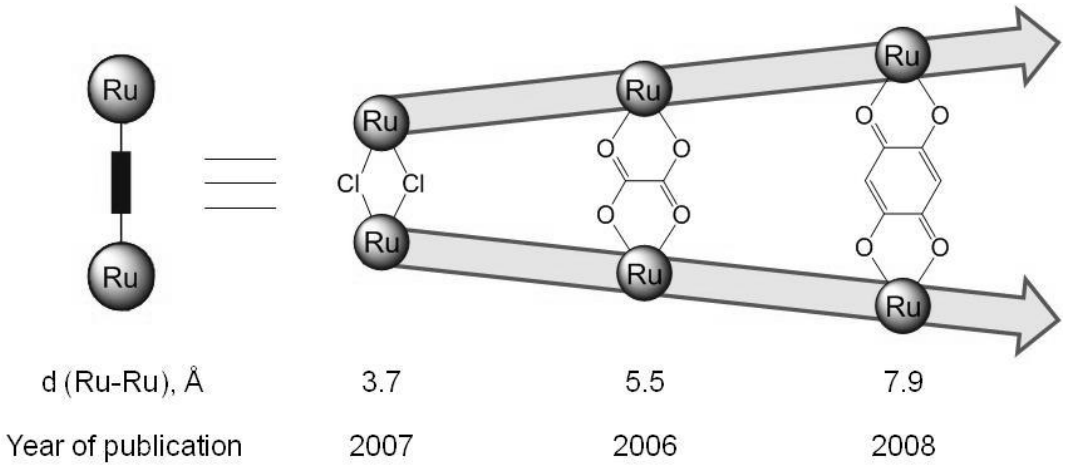

Figure 15. Length of the dinuclear clips used to synthesise metalla-prisms

The first metalla-prism synthesised in Neuchâtel was the para-cymene ruthenium chloro-bridged prism, (see Figure 16).[113] Since the discovery of these chloro-bridged prisms, our group synthesised other metalla-prisms built from arene ruthenium oxalato clips, (see Figure 16).[114]

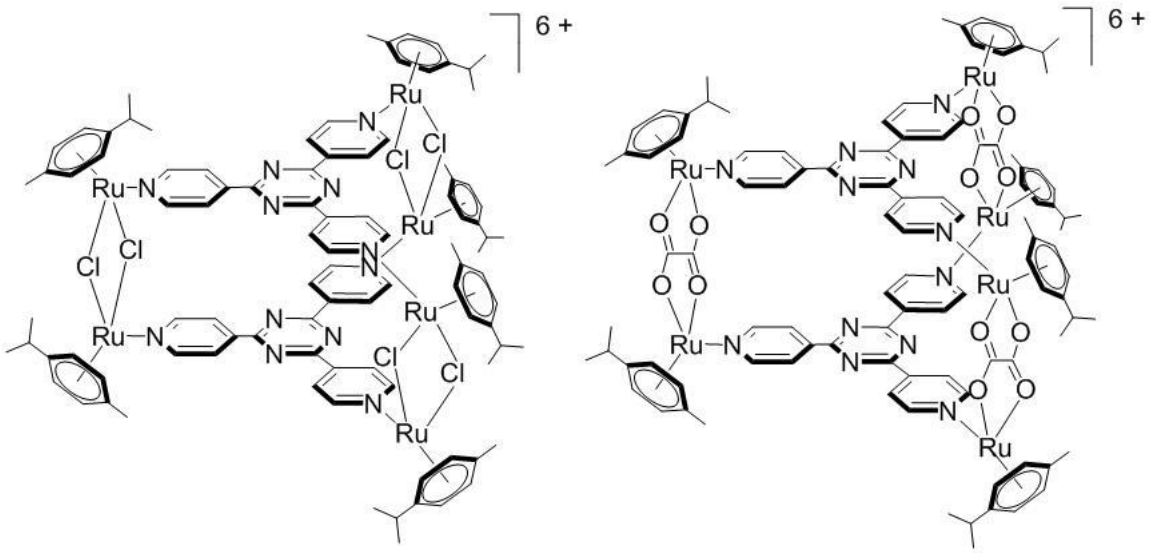

Figure 16. Para-cymene ruthenium chloro and oxalato-bridged prisms

In the cases of the chloro and oxalato-bridged prisms, the distance between the two ruthenium atoms, and thus between the two tpt panels does not allow the encapsulation of any molecules, and consequently these prisms cannot be used as anticancer molecular Trojan

horses. But in 2008, a major breakthrough was published by our group with the syntheses of dobq-bridged prisms that allow the permanent encapsulation of guest molecules.[72] Then, a series of different guest molecules have been encapsulated into prism **P$_1$** and the corresponding complexes have been tested against A2780 cancer cell lines, (see Scheme 2). As the metalla-prism **P$_1$** leads to a carceplex, the encapsulation of the guest molecules is performed during the synthesis of the prism. Moreover, once the guest is encapsulated, it cannot escape from the cavity of the host, unless if the cage molecule is destroyed.

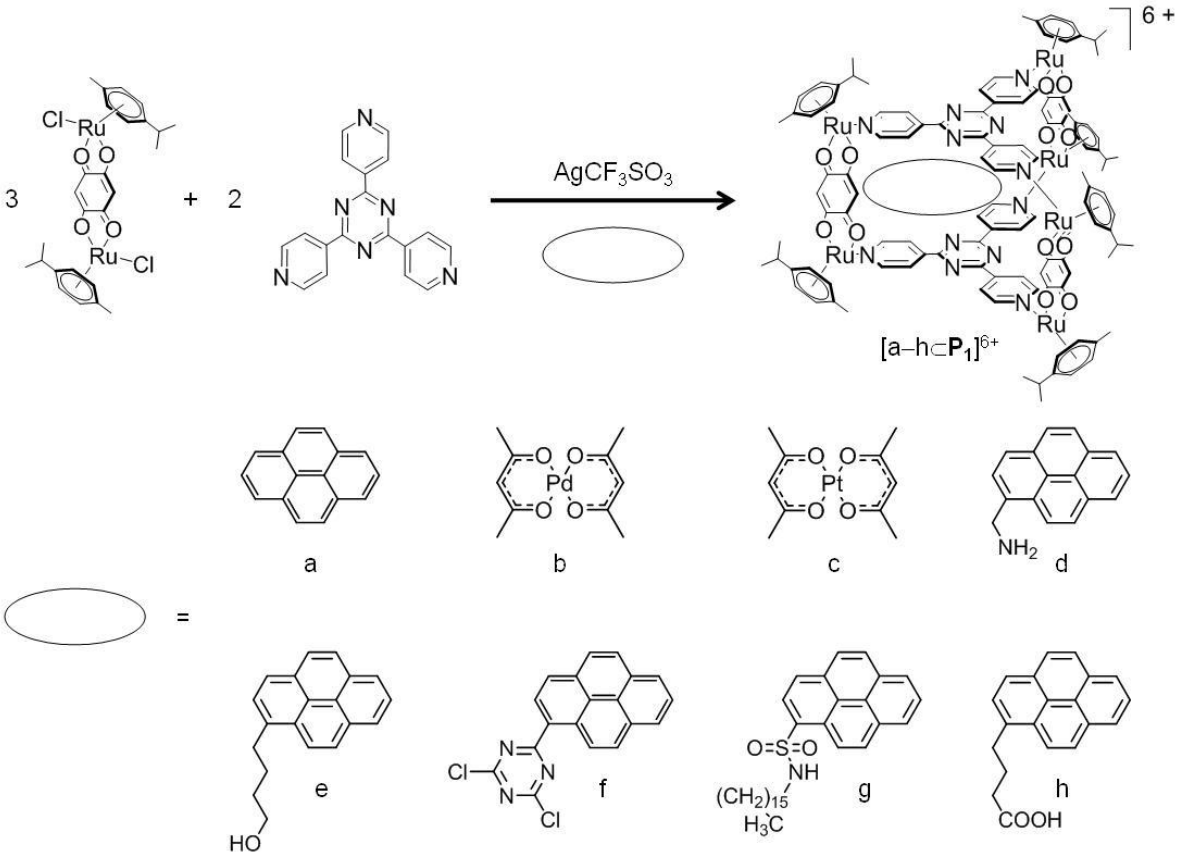

Scheme 2. Synthesis of trigonal-prismatic carceplexes [a-h⊂**P$_1$**]$^{6+}$ encapsulating a guest molecule

All these complexes show moderate to good cytotoxicities from 1 μM to 18 μM and the presence of guest molecule has either a negligible effect on the cytotoxicity (a, d, e and h) or significantly increases the cytotoxicity (b, c, f and g), with [b⊂**P$_1$**]$^{6+}$ (IC_{50}(A2780) = 1 μM),[72] and [g⊂**P$_1$**]$^{6+}$ (IC_{50}(A2780) = 2 μM)[115] being an order of magnitude more cytotoxic than the empty cage [**P$_1$**]$^{6+}$ (IC_{50}(A2780) = 23 μM). Indeed, the cytotoxicity of [b⊂**P$_1$**]$^{6+}$ and [g⊂**P$_1$**]$^{6+}$ is comparable to cisplatin. These differences could be due to the intrinsic cytotoxicities of the different pyrenyl derivatives, which due to the poor water solubility of

these compounds could not be evaluated, or to differences in the uptake and/or further intracellular release of these molecules.

Furthermore, using the highly fluorescent pyrene f as guest molecule, direct evidence for the efficient release of the hydrophobic guest molecule from the metalla-prism $\mathbf{P_1}$ into cancer cells has been provided.[116] Indeed, employing this fluorescent pyrene as a cargo and monitoring the fluorescence of the cells, it has been possible to follow the uptake and the accumulation of this molecule into cancer cells *via* microscopy and flow cytometry. The mechanism of the entry of the compound into the cells has been partly elucidated as being dependent on an assisted diffusion pathway. This mode of uptake has been described for cisplatin[117] and other platinum-based drugs,[118] for which potential transporters have been identified.[119] The existence of a facilitated mode of entry into cells implies a certain cell specificity, which offers a potential advantage for the use of such a delivery vehicle in medicinal applications.[119]

1.5 Aim of the Present Thesis

The systematic development of arene ruthenium cages by our group has led to the discovery of new metalla-rectangles as well as metalla-prisms. The idea behind this global project has been to combine the construction of metalla-cages assembled from arene ruthenium building blocks with the intrinsic biological and anticancer properties of these arene ruthenium complexes. The results of these attempts have been the syntheses of cytotoxic and antiproliferative complexes with high molecular weights, potentially able to target cancer cells *via* EPR effect.

Moreover, if we analyse the evolution of the molecules published by our group during the last years, we can clearly make out a trend towards the extension of the metalla-cage dimensions. The rise of the length of the dinuclear clips has led to the extension of the cavity size inside the cages. In 2008, the dimensions of the assemblies have been enough to permanently encapsulate some molecules, such as small PAHs or square planar complexes into metalla-prisms. This carceplex behaviour has allowed the use of the metalla-prisms as drug vectors and the transport and the release of the guest molecule into cancer cells have been proven. In the case of the metalla-rectangles, no encapsulation of molecules has been observed so far, but an important size effect for the cytotoxicity of the assemblies has been identified.

This thesis is neither the beginning nor the end but part of this project initiated in 2006 and a step forward in the evolution of the arene ruthenium assemblies as potential anticancer agents. In particular, during this thesis, the description of new and larger metalla-clips and the syntheses of the corresponding metalla-rectangles, metalla-prisms and metalla-cubes have been achieved. A very interesting feature of these new metalla-assemblies has been observed. Indeed, the rise of the metalla-clips has led to the extension of the size of the cavities of the corresponding metalla-assemblies to eventually allow host-guest properties between small aromatic molecules and metalla-prisms, but also between these guest molecules and metalla-rectangles. The thermodynamic equilibrium between free species and host-guest complexes has been studied and their antiproliferative comportments have been monitored by the group of Professeur Dyson at the Ecole Polytechnique Fédérale de Lausanne.

Chapter 2: Arene Ruthenium Metalla-Rectangles

2.1 Arene Ruthenium Metalla-Rectangles as Host Systems

2.1.1 Overview of Arene Ruthenium Metalla-Rectangles

The first arene ruthenium metalla-rectangle was reported in 1997.[120] The synthesis in methanol of this tetranuclear complex $[(\eta^6\text{-}p\text{-cym})_4Ru_4(ox)_2(bpy)_2]^{4+}$ in which two arene ruthenium oxalato dinuclear metalla-clips (arene = *p*-cym) **C_0** (see List of Structures) are bridged by two 4,4'-bipyridine linkers was straightforward and the metalla-rectangle was isolated as a trifluoromethanesulfonate salt in a very good yield. This first arene ruthenium metalla-rectangle was a key molecule for the development of the chemistry based on the use of arene ruthenium dinuclear metalla-clips. Despite the geometric simplicity of metalla-rectangles, this type of structure is more difficult to obtain than symmetrical polygons. Indeed, addition of two different connecting ligands with metal corners does not favour the formation of the desired rectangle but leads to the formation of molecular squares as well as trinuclear species due to a strong enthalpic driving force. However, the use of arene ruthenium oxalato dinuclear metalla-clips allowed the exclusive synthesis of the desired metalla-rectangle *via* a pre-organisation of the different building blocks after abstraction of the chloride ligands by a halide scavenger, (see Scheme 3).

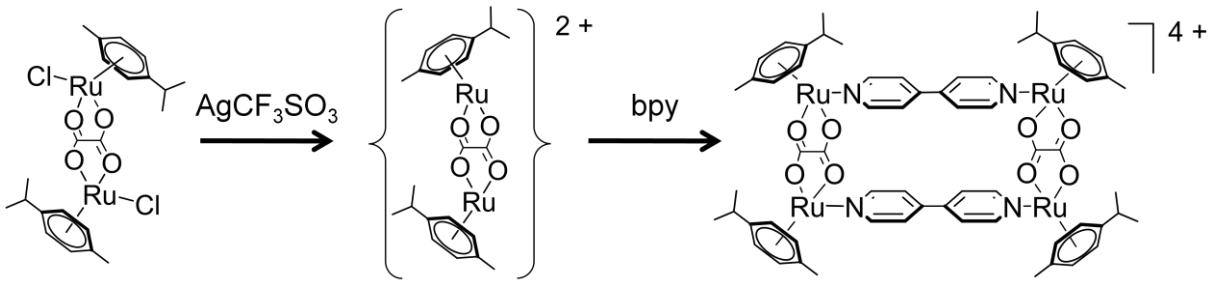

Scheme 3. Two-step synthesis of metalla-rectangle $[(\eta^6\text{-}p\text{-cym})_4Ru_4(ox)_2(bpy)_2]^{4+}$

This metalla-rectangle was too small to accommodate guest molecules between the two bpy units, but the same strategy was applied to generate larger metalla-rectangles of the general formula $[(\eta^6\text{-arene})_4Ru_4(OO\cap OO)_2(N\cap N)_2]^{4+}$ (arene = *p*-cym, hmb; $OO\cap OO$ = dobq, dClobq; $N\cap N$ = pyr, bpy, bpe) (**R_1** – **R_{12}**, see Table of Figures) have been synthesised in 2008

and 2009 by Jin's and our group.[110-111] X-ray structural analyses of $\mathbf{R_7}$ ([(η^6-hmb)$_4$Ru$_4$(dobq)$_2$(bpy)$_2$]$^{4+}$) and $\mathbf{R_{10}}$ ([(η^6-hmb)$_4$Ru$_4$(dClobq)$_2$(bpe)$_2$]$^{4+}$) have been performed and interestingly enough, an organisation in channels has been observed in the solid state for the metalla-rectangle $\mathbf{R_7}$, (see Figure 17).[110] This organisation in cationic nanotubes stabilised by trifluoromethanesulfonate anions between the rectangular channels allows the encapsulation of small molecules such as residual solvent molecules.

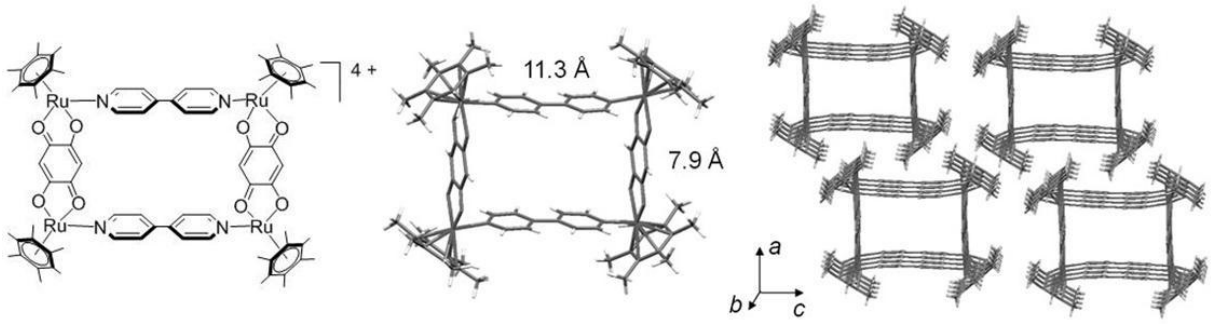

Figure 17. Molecular structure of cation $\mathbf{R_7}$ with a view of the molecular channels along the *b* axis

In the case of the metalla-rectangle $\mathbf{R_{10}}$, the linker being longer, the cavity is larger and upon crystallisation of this cation in a chloroform/diethyl ether mixture, two diethyl ether molecules have been encapsulated into the hydrophobic cavity of cation $\mathbf{R_{10}}$. Using the approach developed by our group, Jin synthesised in 2009 a new series of metalla-rectangles by the combination of arene ruthenium oxamide types dinuclear clips and bpy and bpe as linear bidentate pyridyl linkers to generate the corresponding metalla-rectangles.[121] Jin's group also proposed the construction of half-sandwich iridium metalla-rectangles *via* C–H activation to synthesize new metalla-clips.[122] Although this strategy seems interesting, it has not been yet applied with arene ruthenium. Finally, Navaro and Barea's group published in 2009 and 2010 new arene ruthenium metalla-rectangles built with different metalla-clips and bpy and 4,7-phenanthroline.[112, 123]

2.1.2 Arene Ruthenium Metalla-Rectangles and Host-Guest Chemistry

In large supramolecular assemblies, a cavity capable of accommodating guest molecules does not guarantee host-guest chemistry. Indeed, in a host-guest system an equilibrium between the unbound and bound states exists. This thermodynamic exchange

between free species and bound species makes the difference between the entrapment of a molecule into another molecule and a host-guest system. As a consequence, in the particular case of metalla-rectangles, the entrapment of small molecules such as anions or solvents in the solid state without exchange studies cannot be considered strictly speaking as host-guest chemistry.[124]

The access to the cavity is, however, essential for the host-guest process to take place. Therefore, in order to generate an efficient host-guest system, sufficient cavity size and portal size of the host are equally important, unless the cage possesses the ability to assemble-disassemble at will in solution by self-reparation for example. As described previously, the size of the cavity of the metalla-rectangle depends on the length of the dinuclear metalla-clip. Thus, in order to design arene ruthenium metalla-rectangles able to interact in a host-guest fashion with small aromatic molecules, the first step is to synthesise larger dinuclear metalla-clips.

2.1.3 Synthesis and Characterisation of Arene Ruthenium Metalla-Clips $C_5 - C_7$

In coordination and organometallic chemistry quinones are attracting a lot of interest.[125] Their numerous applications in organic chemistry,[126] physical chemistry[127] and biology[128] are well known, and moreover, these multifunctional ligands are becoming popular for the synthesis of complexes with arene ruthenium units.[129] In particular, the commercially available quinone derivatives, 5,8-dihydroxy-1,4-naphthoquinone (dhnq-H_2), 5,8-dihydroxy-1,4-anthraquinone (dhaq-H_2), and 6,11-dihydroxy-5,12-naphthacenedione (dhtq-H_2), have been used to form dinuclear species with ruthenium metals.[130]

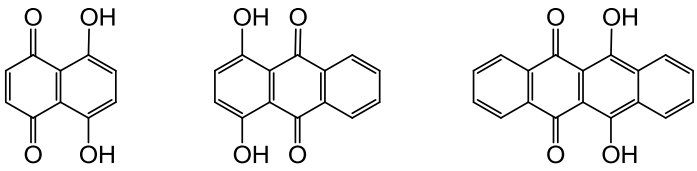

dhnq-H_2 dhaq-H_2 dhtq-H_2

However, the corresponding dinuclear complexes incorporating arene ruthenium units remain scarce in the literature and only [(η^6-*p*-cym)$_2$Ru$_2$(5,8-dioxydo-1,4-anthraquinonato(doaq))Cl$_2$] (**C_6**) has been synthesized so far.[131] Thus, using the same approach, we synthesised and characterised the new arene ruthenium metalla-clips [(η^6-*p*-

cym)$_2$Ru$_2$(*OO*∩*OO*)Cl$_2$] (*OO*∩*OO* = 5,8-dioxydo-1,4-naphthoquinonato (donq) and 6,11-dioxydo-5,12-naphthacenedionato (dotq)) (**C$_5$** and **C$_7$**), (see Figure 18).

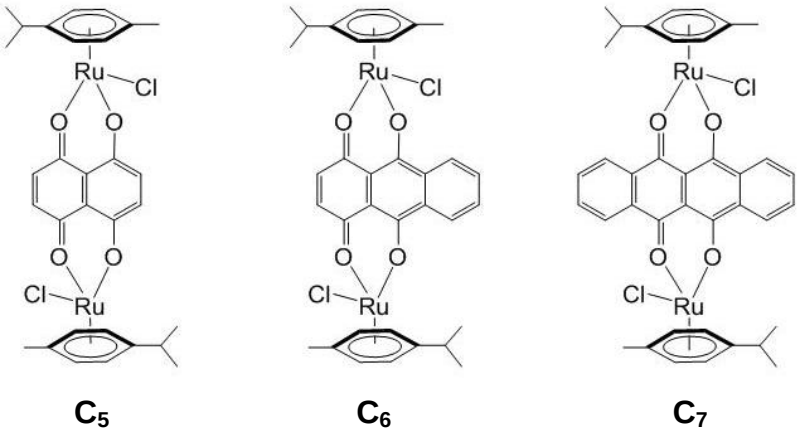

Figure 18. Dinuclear arene ruthenium metalla-clips **C$_5$**, **C$_6$** and **C$_7$**

The synthesis of these metalla-clips is easy and straightforward, since two equivalents of anhydrous sodium acetate, one equivalent of the quinone derivatives and one equivalent of chloro-bridged arene ruthenium dimer react in ethanol at 90°C for 12h. After filtration and several washings with ethanol, acetone and pentane, the dark green solids are collected in high yields. The three arene ruthenium metalla-clips are soluble in chloroform. As expected, the ^{1}H NMR spectra of **C$_5$** in $CDCl_3$ shows one singulet at δ = 6.98 ppm corresponding to the protons of the 5,8-dioxydo-1,4-naphthoquinonato bridging ligand along with the signals associated with the *p*-cym ligands while the ^{1}H NMR spectra of **C$_7$** in $CDCl_3$ shows two doublets at δ = 8.50 and 7.72 ppm corresponding to the protons of the 6,11-dioxydo-5,12-naphthacenedionato bridging ligand along with the signals associated with the *p*-cym ligands.

2.1.4 Synthesis of a Series of Arene Ruthenium Metalla-Rectangles (**R$_{13}$ – R$_{21}$**)

The three metalla-clips **C$_5$** – **C$_7$** possess a distance of 8.4 Å between the two ruthenium atoms, which is a significant increase of the span with respect to the arene ruthenium dinuclear metalla-clips previously reported. The rise of the span of these metalla-clips allows the syntheses of larger cationic arene ruthenium metalla-rectangles **R$_{13}$** – **R$_{21}$** of the general formula [(η^6-*p*-cym)$_4$Ru$_4$(*OO*∩*OO*)$_2$(*N*∩*N*)$_2$]$^{4+}$ (*OO*∩*OO* = donq (**R$_{13}$**, **R$_{16}$**, **R$_{19}$**),

doaq (**R_{14}**, **R_{17}**, **R_{20}**), dotq (**R_{15}**, **R_{18}**, **R_{21}**); *N*∩*N* = pyr (**R_{13}**, **R_{14}**, **R_{15}**), bpy (**R_{16}**, **R_{17}**, **R_{18}**), bpe (**R_{19}**, **R_{20}**, **R_{21}**)).

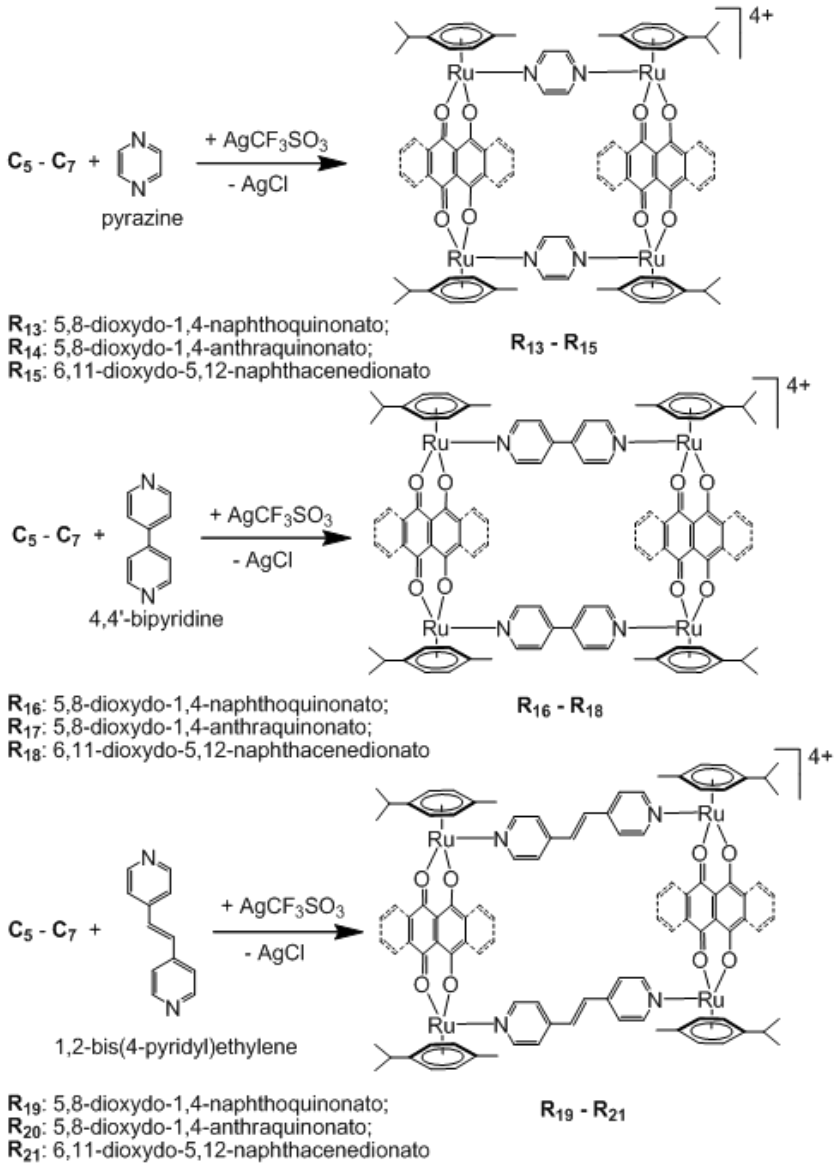

Scheme 4. Syntheses of arene ruthenium metalla-rectangles **R_{13}** – **R_{21}**

The synthesis of these metalla-rectangles is straightforward. Indeed, the arene ruthenium dinuclear complexes (**C_5** – **C_7**) react in methanol at room temperature in the presence of silver trifluoromethanesulfonate (halide scavenger) with different *N*∩*N* donor ligands (pyrazine, 4,4'-bipyridine, 1,2-bis(4-pyridyl)ethylene) to give the tetranuclear cations **R_{13}** – **R_{21}** isolated as trifluoromethanesulfonate salts, (see Scheme 4). The ^{1}H NMR spectra of **R_{13}** – **R_{15}** display a singulet due to the pyrazine protons. Unlike free pyrazine, where the proton signal is found at δ = 8.57 in CD_3CN, the signal in **R_{13}** – **R_{15}** appears slightly shifted

upfield at δ = 8.46 ppm. The ^{1}H NMR spectra of **R_{16}**, **R_{17}**, and **R_{18}** show two doublets due to the 4,4'-bipyridine protons with an upfield shift of about 0.2 ppm as compared with the free 4,4'-bipyridine in CD_3CN. The same upfield effect of about 0.2 ppm is observed with the protons of the 1,2-bis(4-pyridyl)ethylene linkers in complexes **R_{19}** − **R_{21}**. Upon formation of the cationic tetranuclear metalla-rectangles, the methyl and isopropyl signals of the *p*-cymene ligands in **R_{13}** − **R_{21}** remain almost unchanged as compared to complexes **C_5** – **C_7**, while the aromatic protons of the *p*-cymene ligands are slightly shifted downfield. Similarly, the proton signals of the 5,8-dioxydo-1,4-naphthoquinonato, 5,8-dioxydo-1,4-anthraquinonato and 6,11-dioxydo-5,12-naphthacenedionato bridging ligands in all metalla-rectangles **R_{13}** − **R_{21}** are shifted downfield as compared to their parent complexes **C_5** – **C_7**.

In the metalla-rectangles **R_{14}**, **R_{17}**, and **R_{20}** the asymmetry of the 5,8-dioxydo-1,4-anthraquinonato bridging ligand allows the formation of two isomers. Indeed, the presence of two isomers is quite obvious in the case of **R_{14}** in which two distinct sets of signals for the 5,8-dioxydo-1,4-anthraquinonato ligands are observed in the ^{1}H NMR spectrum (CD_3CN). However, the signals of the *p*-cym and pyrazine ligands remain equivalent despite the presence of these two isomers **R_{14}** and **R_{14}'**, (see Figure 19). In the case of **R_{17}** and **R_{20}**, in which the two 5,8-dioxydo-1,4-anthraquinonato bridges are far away from each other all signals show no sign of the presence of the two isomers and give rise to only one set of signals for both isomers at room temperature.

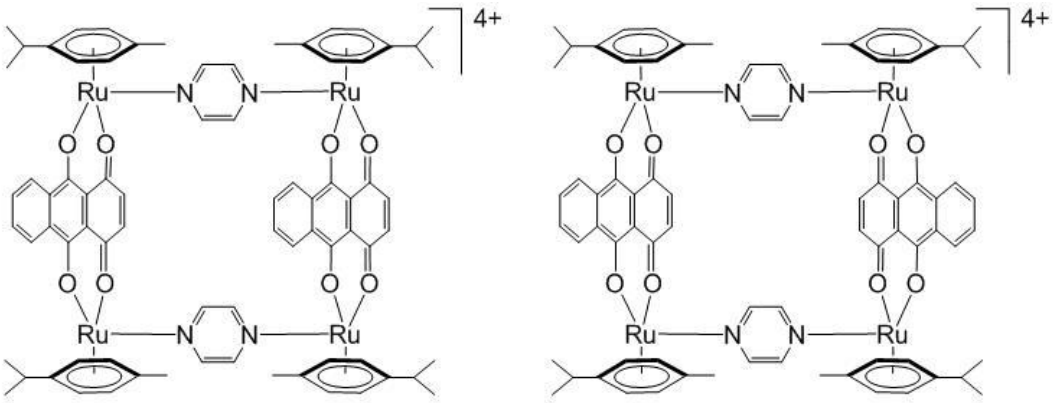

R_{14} **R_{14}'**

Figure 19. Schematic representation of the two isomers **R_{14}** and **R_{14}'**

The infrared spectra of **R_{13}** − **R_{21}** are dominated by absorptions of the coordinated *OO*∩*OO* and *N*∩*N* ligands, which are only slightly shifted as compared to the infrared

absorptions of the free ligands. In addition to the *N*∩*N* and *OO*∩*OO* signals, strong absorptions due to the stretching vibrations of the trifluoromethanesulfonate anions (1260(s), 1030(s), 638(m) cm^{-1}) are also observed in the infrared spectra of the salts [**R$_{13}$** – **R$_{21}$**][CF_3SO_3]$_4$.

The electronic absorption spectra of the metalla-rectangles **R$_{13}$** – **R$_{21}$** are characterised by an intense high-energy band centered at 320 nm, which is assigned to ligand–localized or intra-ligand $\pi \rightarrow \pi^*$ transition as well as broad low-energy bands associated to metal-to-ligand charge transfer (MLCT) transitions. In **C$_5$** – **C$_7$**, only one MLCT band is found (≈ 600 nm), while in metalla-rectangles **R$_{13}$** – **R$_{21}$** an additional band centered at around 400 nm is observed as well, (see Figure 20).

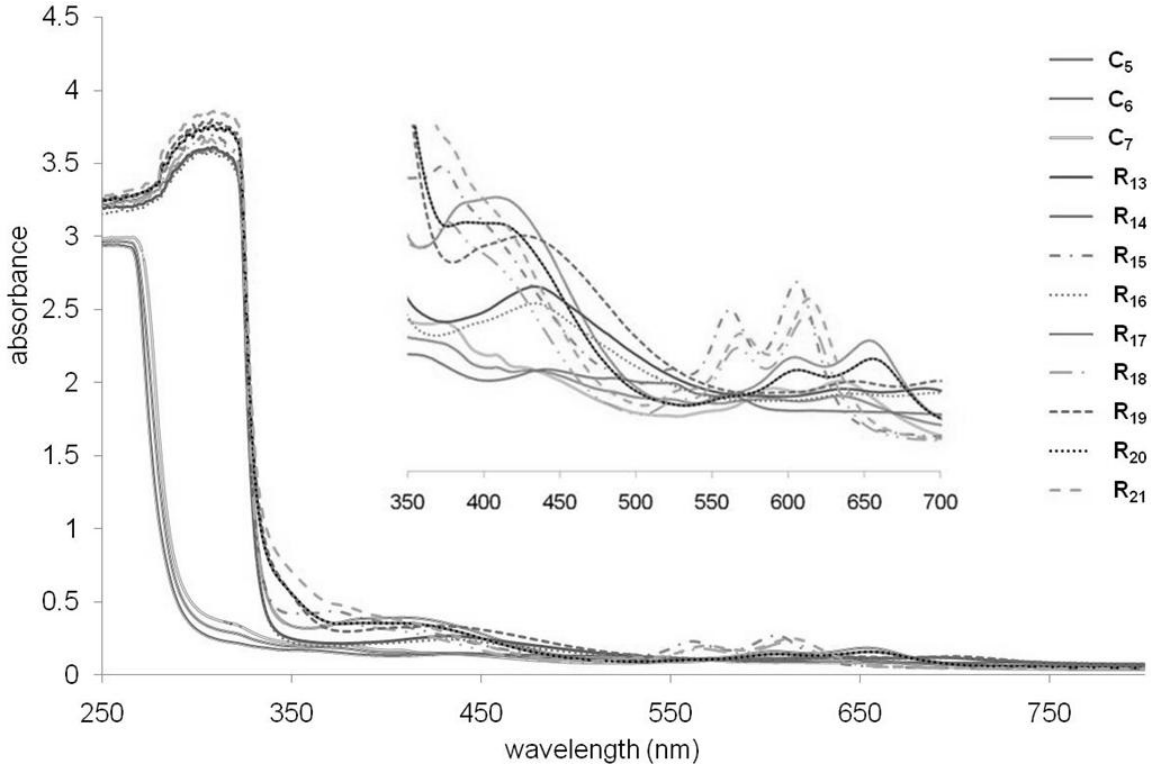

Figure 20. UV-visible spectra of **C$_5$** – **C$_7$** and **R$_{13}$** – **R$_{21}$** (10^{-5} M) in dichloromethane

In the absence of suitable crystals for X-ray measurements, the cavity sizes of the different metalla-rectangles were estimated by molecular modeling and from analogous structures incorporating the same bridging and connecting ligands. The pyrazine series possess a cavity of about ≈ 8.4 x 7.0 $Å^2$ (ruthenium-to-ruthenium edges), while the cavity

sizes of the 4,4'-bipyridine and 1,2-bis(4-pyridyl)ethylene series are expected to be approximately 8.4 x 11.2 and 8.4 x 13.6 $Å^2$, respectively, (see Figure 21).

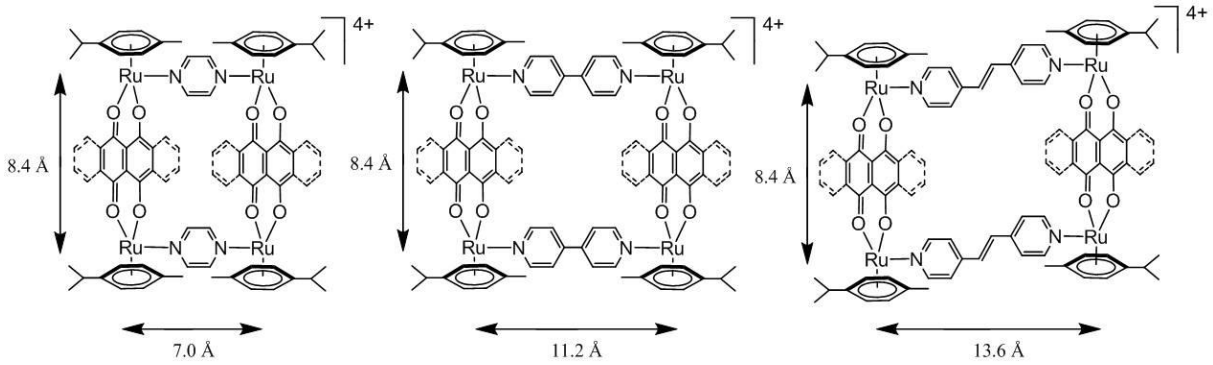

Figure 21. Estimated cavity size of the different metalla-rectangles

2.1.5 In- or Out-of-Cavity Interactions?

In order to study the ability of the hydrophobic cavity of the metalla-rectangles $\mathbf{R_{13}}$ – $\mathbf{R_{21}}$ to encapsulate guest molecules in solution, we performed various NMR experiments. ^{1}H NMR spectra of 1:1 mixtures of metalla-rectangles with planar aromatic molecules (pyrene, anthracene, perylene and coronene) were measured. In the case of the pyrazine-containing metalla-rectangles $\mathbf{R_{13}}$ – $\mathbf{R_{15}}$, no chemical shift for the protons of the host and of the aromatic molecule was observed in CD_3CN. The result is quite different with the larger metalla-rectangles $\mathbf{R_{16}}$ – $\mathbf{R_{21}}$, in which some protons of the metalla-rectangle and of the aromatic molecule are shifted as compared to their initial ^{1}H NMR spectra, (see Figure 22).

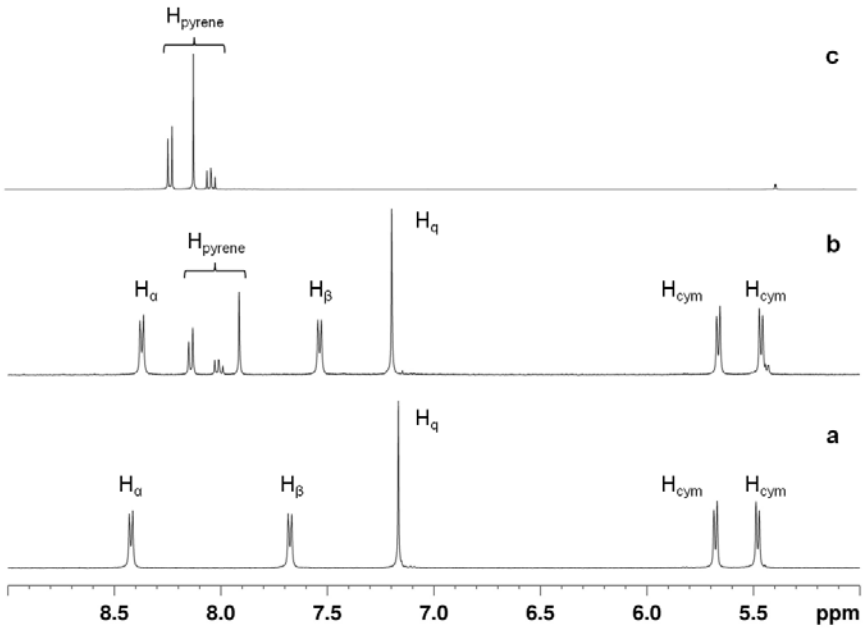

Figure 22. ^{1}H NMR spectra of **R_{16}** (a), pyrene + **R_{16}** (1:1 mixture) (b) and pyrene (c) (25 ºC, CD_3CN)

Consequently, these observations prompted us to further investigate the hosting potential of the metalla-rectangles **R_{16}** – **R_{21}** in solution by diffusion-ordered NMR spectroscopy (DOSY). DOSY measurement is a powerful tool for studying host-guest association in solution.[132] The diffusion coefficient depends on the shape and size of the molecules. Therefore, in a host-guest system in which the guest is perfectly encapsulated in the cavity of the host without significantly affecting the size and shape of the host, the diffusion coefficient of the guest⊂host adduct will be almost identical to the diffusion coefficient of the host alone. On the other hand, in a host-guest system in which the guest interacts with the host but not in a guest⊂host fashion, the host and the guest will keep their individual diffusion coefficients.

Room-temperature DOSY measurements of the 4,4'-bipyridine-containing metalla-rectangles **R_{16}** – **R_{18}** in the presence of anthracene, pyrene, perylene and coronene suggest out-of-cavity interactions between the different rectangles and the aromatic molecules. However, at -40 °C, the same DOSY experiment with anthracene and metalla-rectangle **R_{16}** clearly shows that anthracene diffuses at almost the same coefficient than the host, (see Figure 23), thus supporting an in-cavity location of anthracene. To confirm this assumption, a ROESY (Rotating Frame NOE SpectroscopY) measurement at -40 °C was performed, (see Figure 23). The ^{1}H ROESY shows that some protons of anthracene are in close proximity to

the protons of the 5,8-dioxydo-1,4-naphthoquinonato and 4,4'-bipyridine ligands which confirms together with the DOSY experiment at -40 ºC the presence of anthracene in the cavity of **R_{16}**. All other aromatic molecules (pyrene, perylene, coronene) do not show in-cavity interactions with metalla-rectangles **R_{16}** – **R_{18}**, even at low temperature, which fit with out-of-cavity interactions. In contrast, 1,2-bis(4-pyridyl)ethylene containing metalla-rectangles **R_{19}** – **R_{21}** show in-cavity interactions with these large planar aromatic molecules.

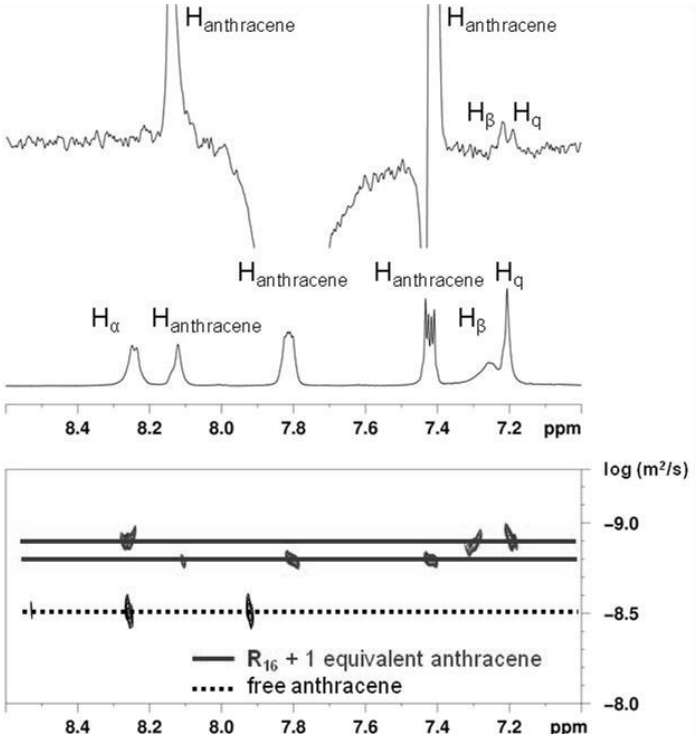

Figure 23. DOSY (bottom) and ROESY (top) NMR spectra of **R_{16}** + 1 equivalent of anthracene at -40°C (CD_3CN)

DOSY experiments of anthracene with metalla-rectangles **R_{19}** – **R_{21}** show both, in-cavity and out-of-cavity interactions at room temperature, as opposed to pyrene, perylene and coronene for which in-cavity interaction dominates. As an example, the DOSY spectra of coronene, metalla-rectangle **R_{19}** and a 1:1 mixture of coronene and **R_{19}** in CD_3CN at room temperature are presented in Figure 24. These experiments clearly show that at room temperature, coronene and **R_{19}** possess almost identical diffusion coefficients, which confirm the encapsulation of coronene in the hydrophobic cavity of **R_{19}** and the formation of a coronene⊂**R_{19}** adduct.

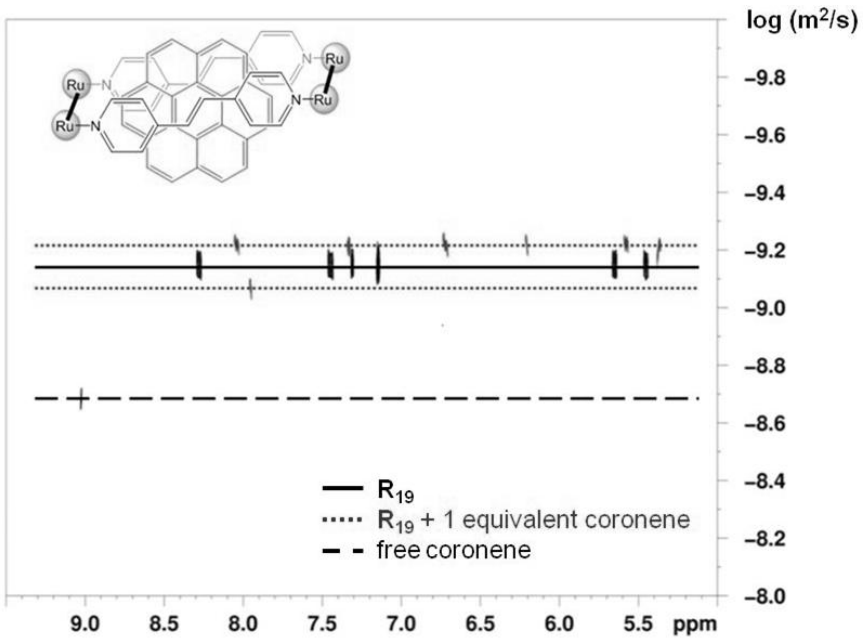

Figure 24. DOSY NMR spectra of coronene, **R_{19}** and **R_{19}** + 1 equivalent of coronene (25 ºC, CD_3CN)

In summary, ^{1}H, DOSY and ROESY NMR studies have revealed that no meaningful interaction occurs between the pyrazine containing metalla-rectangles **R_{13}** – **R_{15}** and planar aromatic molecules, while out-of-cavity interactions are prevailing in the case of the 4,4'-bipyridine containing metalla-rectangles **R_{16}** – **R_{18}**, with the exception of anthracene which can do both, in-cavity and out-of-cavity interactions with these metalla-rectangles. On the other hand, in-cavity interactions take place for the 1,2-bis(4-pyridyl)ethylene containing metalla-rectangles **R_{19}** – **R_{21}**, thus giving rise to guest⊂host systems. Therefore, to gain further insight in the hosting ability of **R_{19}** – **R_{21}** in solution, a series of ^{1}H NMR titration in CD_3CN solution with pyrene, perylene and coronene was performed.

2.1.6 Host-Guest Behaviour

The study of the host-guest properties of metalla-rectangles **R_{19}** – **R_{21}** was carried out in acetonitrile solution by using NMR spectroscopy and fluorescence emission titration. Upon gradual addition of guest molecule (0.0 – 20.0 equivalents of pyrene, perylene or coronene) to an CD_3CN solution of metalla-rectangles **R_{19}** – **R_{21}** (4.0 mM), ^{1}H NMR spectra were recorded. Then, the chemical shift changes ($\Delta\delta$) for one chosen signal of the metalla-

rectangles $\mathbf{R_{19}}$ – $\mathbf{R_{21}}$ (for example $H_{C=C}$) *versus* the molar ratio of the guest to the metalla-rectangle were plotted, (see Figure 25).

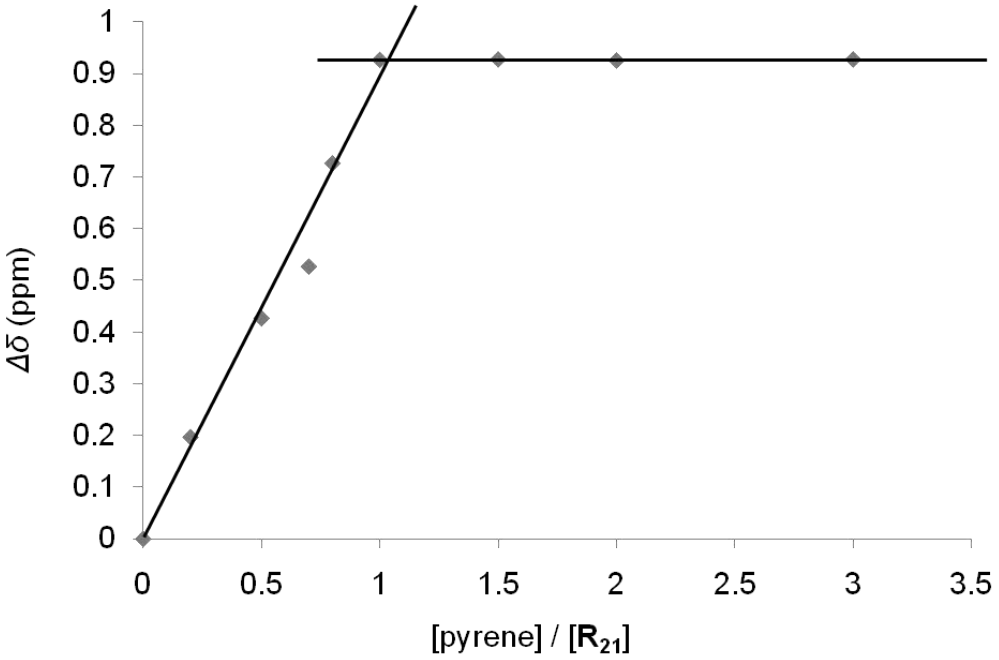

Figure 25. ^{1}H NMR chemical shift changes for the $H_{C=C}$ protons of the bpe ligands *versus* the molar ratio of pyrene to $\mathbf{R_{21}}$ (25 ºC, CD_3CN)

The plot of these chemical shift changes *versus* the molar ratio of the guest to the metalla-rectangle clearly indicates a stoichiometry 1:1 for the host-guest system,[133] which is in accordance with the DOSY experiments previously reported. Then using the $\Delta\delta$ value at known guest / host molar ratio with help of the nonlinear least-square fitting program winEQNMR2,[134] the stability constants of association (K_a) together with the free energies (ΔG^o) were estimated, (see Table 1).

Table 1. Stability constants (K_a) and free energies (ΔG^o) for the encapsulation of pyrene, perylene and coronene in metalla-rectangles **R_{19}** – **R_{21}** (CD_3CN at 25 °C, 4.0 mM of host)

guest⊂**host**	K_a (10^4 M^{-1})	ΔG^o (kcal · mol^{-1})
[pyrene⊂**R_{19}**]$^{4+}$	5.8 ± 0.9	-6.48 ± 0.05
[perylene⊂**R_{19}**]$^{4+}$	5.5 ± 0.4	-6.46 ± 0.02
[coronene⊂**R_{19}**]$^{4+}$	6.9 ± 0.6	-6.60 ± 0.02
[pyrene⊂**R_{20}**]$^{4+}$	6.8 ± 0.8	-6.59 ± 0.04
[perylene⊂**R_{20}**]$^{4+}$	5.7 ± 0.5	-6.47 ± 0.02
[coronene⊂**R_{20}**]$^{4+}$	5.6 ± 0.7	-6.47 ± 0.02
[pyrene⊂**R_{21}**]$^{4+}$	5.2 ± 0.9	-6.43 ± 0.02
[perylene⊂**R_{21}**]$^{4+}$	5.6 ± 0.4	-6.47 ± 0.02
[coronene⊂**R_{21}**]$^{4+}$	6.2 ± 0.7	-6.53 ± 0.04

The estimated stability constants are comprised between 52000 M^{-1} and 69000 M^{-1}, which imply a relatively strong affinity between the host and the guest – metalla-rectangle and aromatic molecules – which however suggest no selectivity or preference by the metalla-rectangle among these guests (pyrene, perylene and coronene). This non-specificity of the metalla-rectangles **R_{19} – R_{21}** for these planar aromatic molecules in acetonitrile was further confirmed by a competition experiment in which a 1:1:1:1 mixture of pyrene, perylene, coronene and **R_{19}** was performed. A DOSY experiment shows that the three potential guest molecules are competing equally for the hydrophobic cavity of **R_{19}**, which is not surprising with respect to their comparable stability constants.

To conclude these host-guest studies, we performed a fluorescence emission titration of perylene with metalla-rectangle **R_{19}**. Perylene has been intensively used as fluorescent probe and its basic fluorescence is well documented.[135] The fluorescent quenching of perylene *via* exciplex formation[136] or energy transfer[137] in solution has been also studied in detail and we propose here to see whether or not such quenching by encapsulation of perylene inside the cavity of metalla-rectangle **R_{19}** occurred. Thus the emission spectra of a dichloromethane solution of perylene (10^{-7} M, 350 nm as excitation wavelength) upon gradual addition of metalla-rectangle **R_{19}** (0.0 – 10 equivalents) were recorded, (see Figure 26).

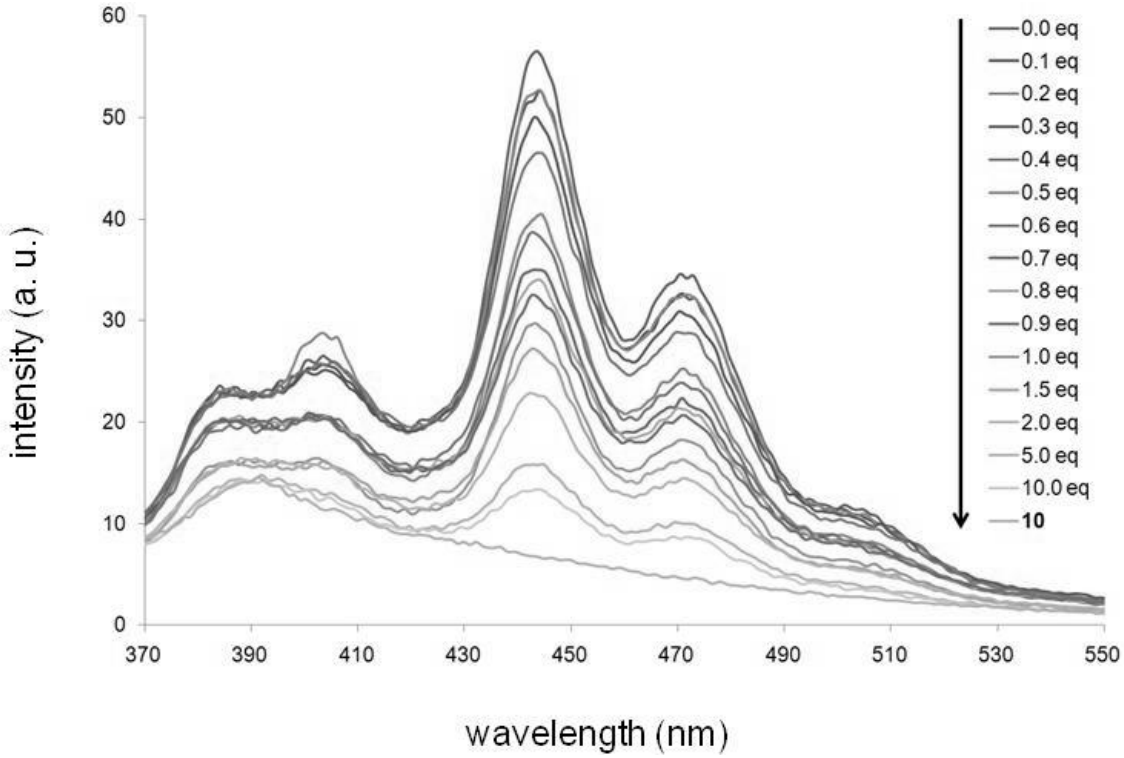

Figure 26. Fluorescence emission titration of perylene (10^{-7} M in dichloromethane) by metalla-rectangle $\mathbf{R_{19}}$ (excitation wavelength = 350 nm)

A quenching of the perylene fluorescence is clearly observed when $\mathbf{R_{19}}$ is added. This quench of the fluorescence of perylene can be explained by two effects. First, as the guest goes into the cavity of the metalla-rectangle $\mathbf{R_{19}}$, there is a loss of excitation energy received by the guest molecule: A part of the energy can be absorbed by the metalla-rectangle and consequently, the perylene molecule encapsulated in the metalla-rectangle is less excited and therefore cannot reemit the same energy as compared to its free state. Second, the quenching can result from energy transfer from perylene to metalla-rectangle $\mathbf{R_{19}}$. Indeed, due to a good spectral overlap of absorbance of metalla-rectangle $\mathbf{R_{19}}$ with the perylene emission, energy transfer can spontaneously take place, thus leading to a decrease in the emission energy of perylene and ultimately to fluorescence quenching, (see Figure 27).[138]

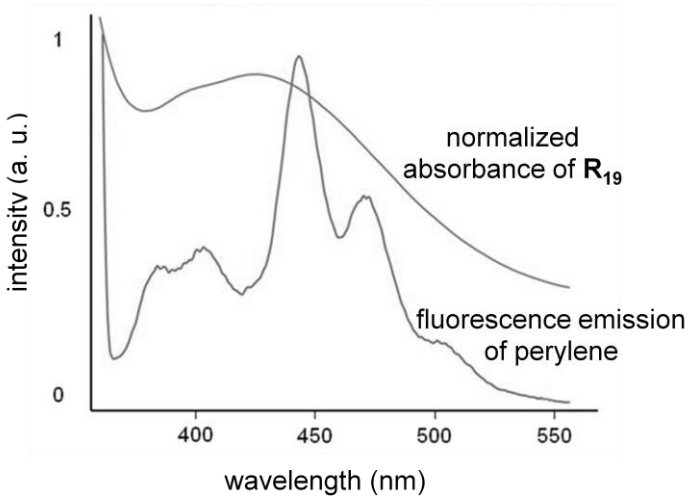

Figure 27. Overlap between normalized absorbance of **R_{19}** and fluorescence emission of perylene

This study[139] reveals that arene ruthenium metalla-rectangles containing new *OO*∩*OO*-bridges (5,8-dioxydo-1,4-anthraquinonato, 5,8-dioxydo-1,4-anthraquinonato, 6,11-dioxydo-5,12-naphthacenedionato) and *N*∩*N*-linkers (pyrazine, 4,4'-bipyridine, 1,2-bis(4-pyridyl)ethylene) can be designed to accommodate guest molecule outside and inside their cavity.[140] Various NMR experiments have shown that the small pyrazine containing metalla-rectangles **R_{13}** – **R_{15}** do not interact with planar aromatic molecules (anthracene, pyrene, perylene, coronene), while the more spacious 4,4'-bipyridine and 1,2-bis(4-pyridyl)ethylene containing metalla-rectangles **R_{16}** – **R_{21}** give both in-cavity and out-of-cavity interactions with these aromatic molecules. Encapsulation of perylene in the hydrophobic cavity of **R_{19}** strongly quenches the fluorescence of perylene in solution, which confirms the great potential of such metalla-rectangles for applications in host-guest chemistry.

2.2 Antiproliferative Activity of Arene Ruthenium Metalla-Rectangles

2.2.1 General

As described previously, arene ruthenium complexes have recently received considerable attention in the field of supramolecular chemistry.[65-66] The synthesis of new arene ruthenium metalla-rectangles able to interact with small aromatic molecules in a host-guest fashion is an example of the versatility of these metalla-assemblies.

On the other hand, arene ruthenium complexes have been widely studied as potential antitumoral and antimetastatic agents, in particular by Dyson and Sadler, who contributed to the emergence of arene ruthenium in bio-organometallic chemistry.[95b, 96a] Air-stable and water-soluble, arene ruthenium complexes have shown a low general toxicity and a high selectivity towards cancer cells.[95d, 141] Furthermore, the amphiphilic properties due to the hydrophobic arene ligand and the hydrophilic metal centre as well as the synthetic diversity of the arene ligand explain the flourishing design of arene ruthenium-based anticancer drugs.[142]

Since 2008, our group has pioneered the combination of the supramolecular chemistry of arene ruthenium building blocks with their antitumoural and antimetastatic activity.[72] It has been demonstrated that arene ruthenium metalla-assemblies are water-soluble and stable in biological medium, and also that they exhibit efficient antiproliferative activity. This approach has led to the syntheses of the metalla-rectangles $\mathbf{R_1} - \mathbf{R_{12}}$ (see Table of Figures), which have been tested against cancer cells. The activities of these metalla-rectangles against human ovarian cancer cell lines (A2780) were found to be moderate to excellent, depending on the size of the linker used as well as the nature of the arene (*p*-cym *vs* hmb), with IC_{50} values as low as 4 μM.[110]

To further study the impact on the antiproliferative activities of the building blocks used for the design of arene ruthenium metalla-rectangles, we proposed to investigate the role play by the nature of the *N*∩*N* linker as well as the role play by the length of the *OO*∩*OO* metalla-clip in the cytotoxicity of metalla-rectangles, (see Figure 28).

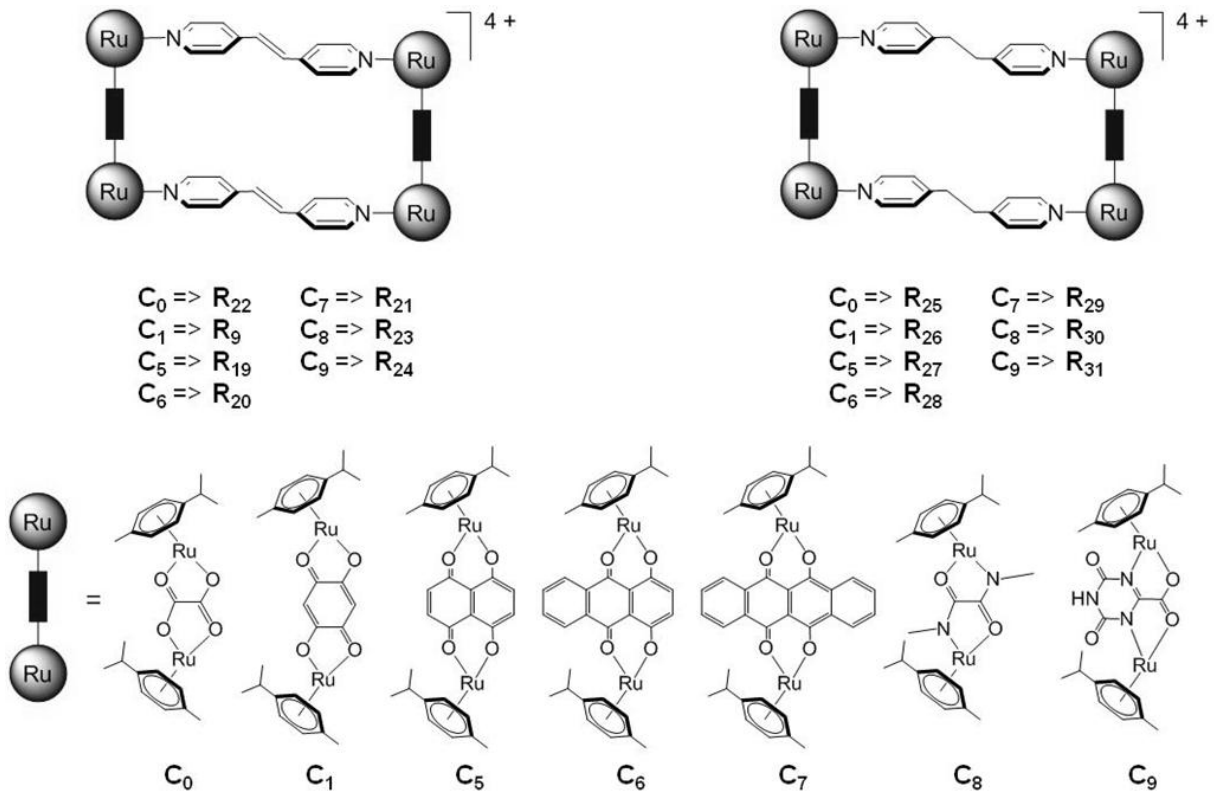

Figure 28. Arene ruthenium metalla-rectangles **R$_9$**, **R$_{19}$** − **R$_{31}$**

Thus, we described the syntheses, the characterisations and the antiproliferative properties of metalla-rectangles of general formula $[(\eta^6\text{-}p\text{-cym})_4Ru_4(OO{\cap}OO)_2(N{\cap}N)_2]^{4+}$ (*OO*∩*OO* = oxalato (ox), dobq, donq, doaq, dotq, oxamido (oxa), oxonico (oxo)); *N*∩*N* = bpe, 1,2-bis(4-pyridyl)ethane (bpa)) (**R$_9$**, **R$_{19}$** − **R$_{31}$**, see Table of Figures), prepared from the dinuclear complexes **C$_0$**, **C$_1$**, **C$_5$** − **C$_7$** and $[(\eta^6\text{-}p\text{-cym})_2Ru_2(OO{\cap}OO)Cl_2]$ (*OO*∩*OO* = oxa and oxo)) (**C$_8$** and **C$_9$**).

2.2.2 Synthesis of a Series of Arene Ruthenium Metalla-Rectangles (R$_9$, R$_{19}$ – R$_{31}$)

Metalla-rectangles **R$_{22}$** − **R$_{31}$** were synthesised following the procedure previously described for metalla-rectangles **R$_{13}$** − **R$_{21}$**. The infrared spectra of all the arene ruthenium metalla-cycles are dominated by absorptions of the coordinated *N*∩*N*, *OO*∩*OO* and *NO*∩*NO* ligands, which are only slightly shifted as compared to the infrared absorptions of the free ligands. In all metalla-clips as well as in all metalla-rectangles, a significant redshift of about 20 cm^{-1} is observed for the C=O vibration frequencies as compared to the frequencies of non-coordinated bridging ligands. This can be attributed to a decrease in the CO bond order upon

coordination with ruthenium atoms.[9] This decrease of the CO bond order leading to a redshift of the CO absorption is consistent with the X-ray data of the metalla-clip $\mathbf{C_5}(OH_2)_2$,[143] for which the lengths of the CO bounds are comprised between 1.27 Å and 1.32 Å, suggesting an intermediate bond order between single (~1.40 Å) and double (~1.20 Å).[63b] Furthermore, in metalla-rectangles $\mathbf{R_{23}}$ and $\mathbf{R_{24}}$ as well as in $\mathbf{R_{30}}$ and $\mathbf{R_{31}}$ strong absorptions due to the stretching vibrations of C=N oxonico bridging ligands are observed at around 1710 cm^{-1} alongside the absorptions of the stretching vibrations of the C=O bridging ligands at around 1600 cm^{-1}. In addition, to these CN and CO signals, strong absorptions due to the stretching vibrations of the trifluoromethanesulfonate anions (1260(s), 1030(s), 638(m) cm^{-1}) are observed in the infrared spectra of all the salts $[\mathbf{R_9}][CF_3SO_3]_4$ and $[\mathbf{R_{19}}][CF_3SO_3]_4$ – $[\mathbf{R_{31}}][CF_3SO_3]_4$.

The electronic absorption spectra of all the metalla-rectangles are characterised by an intense high-energy band centred at 270 nm, which can be attributed to ligand $\pi \rightarrow \pi^*$ transitions.[144] A broad, moderately intense absorption band in the visible region is tentatively assigned to mixed metal-to-ligand charge transfer (MLCT), intra-ligand charge transfer (ILCT) and ligand $\pi \rightarrow \pi^*$ transitions, where ILCT refers to intra-ligand charge transfer from the bpe or bpa *N*∩*N* linkers to the *OO*∩*OO* or *NO*∩*NO* bridging ligands.[145] Moreover, in the metalla-rectangles incorporating quinone derivatives ($\mathbf{R_{19}}$ – $\mathbf{R_{21}}$ and $\mathbf{R_{27}}$ – $\mathbf{R_{29}}$) several bands attributed to ILCT are observed in the visible region between 500 and 800 nm. Moreover bathochromic shifts are observed between the arene ruthenium metalla-rectangles incorporating the 1,2-bis(4-pyridyl)ethylene linkers and the metalla-rectangles incorporating the 1,2-bis(4-pyridyl)ethane linkers. This significant bathochromic shift of up to 13 nm of λ_{max} in the case of $\mathbf{R_{21}}$:$\mathbf{R_{29}}$ is presumably due to a lower contribution to intra-ligand charge transfer transitions from the bpa linkers to the *OO*∩*OO* bridging ligands as compared to the same ILCT from bpe linkers to the corresponding quinone bridging ligands.[146] The bathochromic shifts of absorption bands of metalla-rectangles $\mathbf{R_{19}}$:$\mathbf{R_{27}}$, $\mathbf{R_{20}}$:$\mathbf{R_{28}}$ and $\mathbf{R_{21}}$:$\mathbf{R_{29}}$ between 550 and 800 nm are depicted in Figure 29.

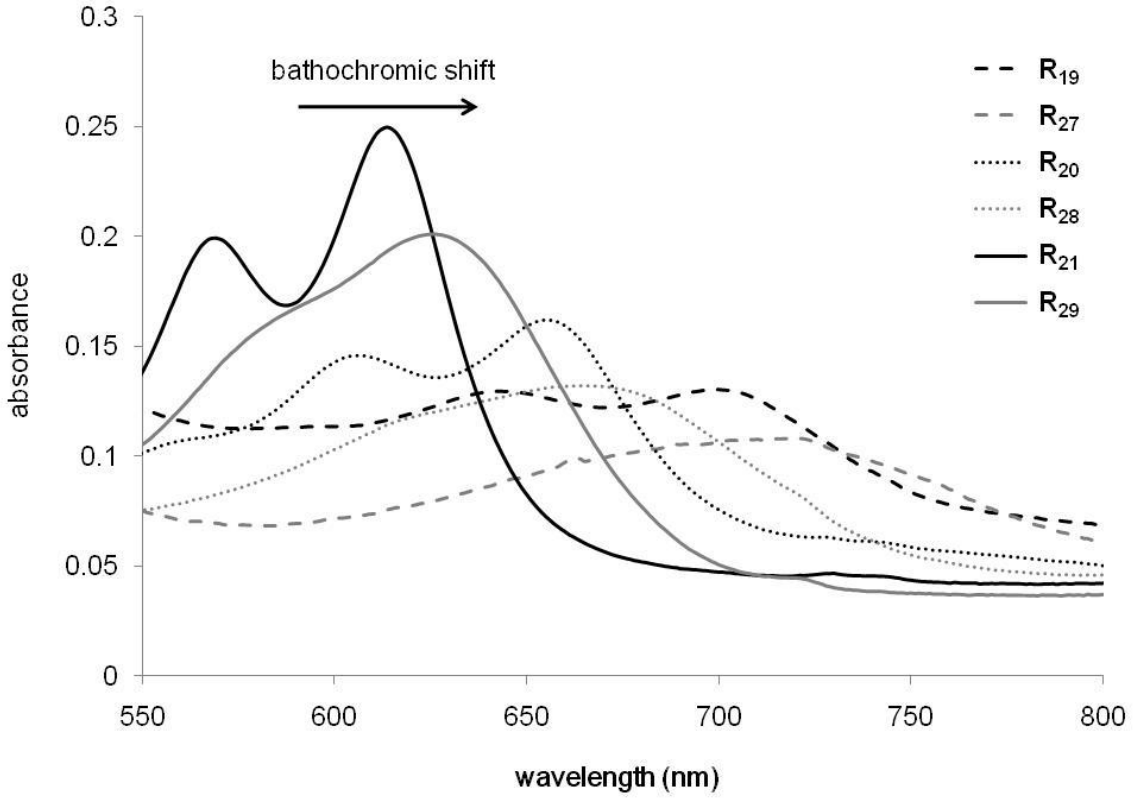

Figure 29. Bathochromic effect of metalla-rectangles **R19** – **R21** and **R27** – **R29**

The ^{1}H NMR spectra of **R25** and **R26** – **R29** display two doublets between 7.0 and 9.0 ppm due to the pyridyl protons of the bpa ligands. Unlike free bpa, where the signals of the pyridyl protons are found at δ = 8.54 (H_α) and 7.21 ppm (H_β) respectively (CD_3CN, 21 °C), the signal of H_α in **R25** and **R26** – **R29** appears slightly to strongly upfield shifted (up to 0.80 ppm in the case of **R25**), while the signal of H_β is either shifted upfield (**R25**, **R26**, **R27**) or downfield (**R28** and **R29**). The same behaviour is observed for the metalla-cycles incorporating the bpe linkers, where a significant upfield shift of the H_α signal (up to 0.75 ppm) and either an upfield or downfield shift of the H_β signal are monitored. Singulet associated of the ethane protons in all bpa-incorporating compounds (broad in the case of **R31**) is observed at around 3.30 ppm. This important upfield shift of about 0.40 ppm for this signal as compared to the chemical shift of the ethane signals in free bpa (2.92 ppm in CD_3CN, 21 °C) is characteristic of the formation of metalla-rectangles.[147] Indeed, this observation is in accordance with the chemical displacement of the ethylene protons observed in bpe-incorporating complexes where such an upfield shift (~ 0.30 ppm) is observed for the $H_{C=C}$ signals. Finally, the arene protons and the protons of the *OO*∩*OO* and *NO*∩*NO* bridging ligands are not strongly

influenced by the cyclisation and show almost the same chemical shifts in both the metalla-rectangles and the dinuclear metalla-clips.[139]

It is noteworthy that among the dinuclear arene ruthenium precursors, two are potentially chiral, **C_8** and **C_9** respectively. These dinuclear complexes possess the ability to form *racemic* and *meso* stereoisomers, if the coordination of the chlorido ligands is not sterically or electronically restricted to a particular position, (see Figure 30).

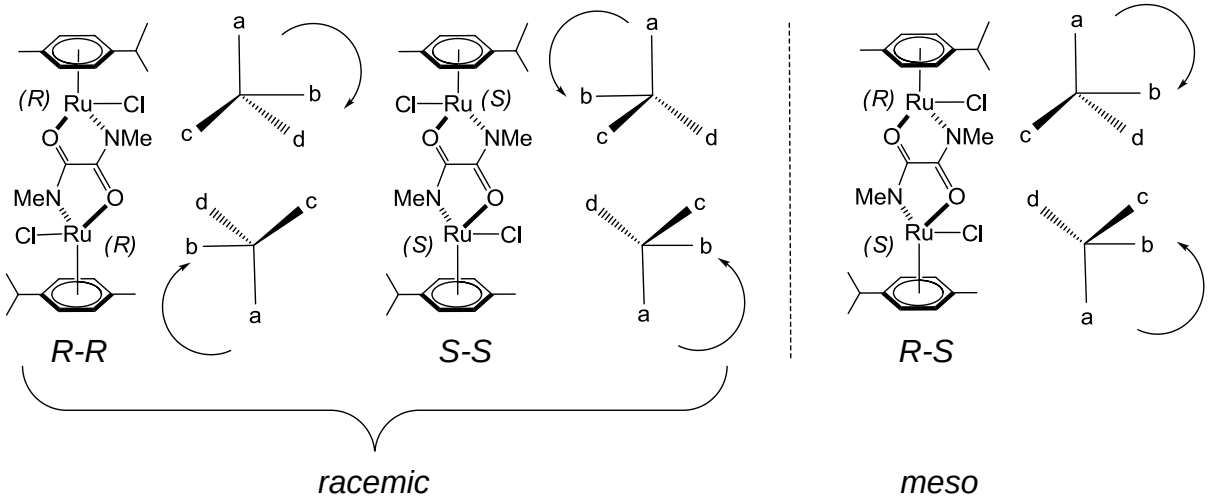

Figure 30. *Racemic* and *meso* stereoisomers of metalla-clip **C_8**

However, upon formation of the corresponding tetranuclear metalla-rectangles **R_{23}:R_{30}** and **R_{24}:R_{31}**, and despite the presence of four stereogenic ruthenium centers, only two diastereoisomers (S-R R-S and S-R S-R) are observed, (see Figure 31).

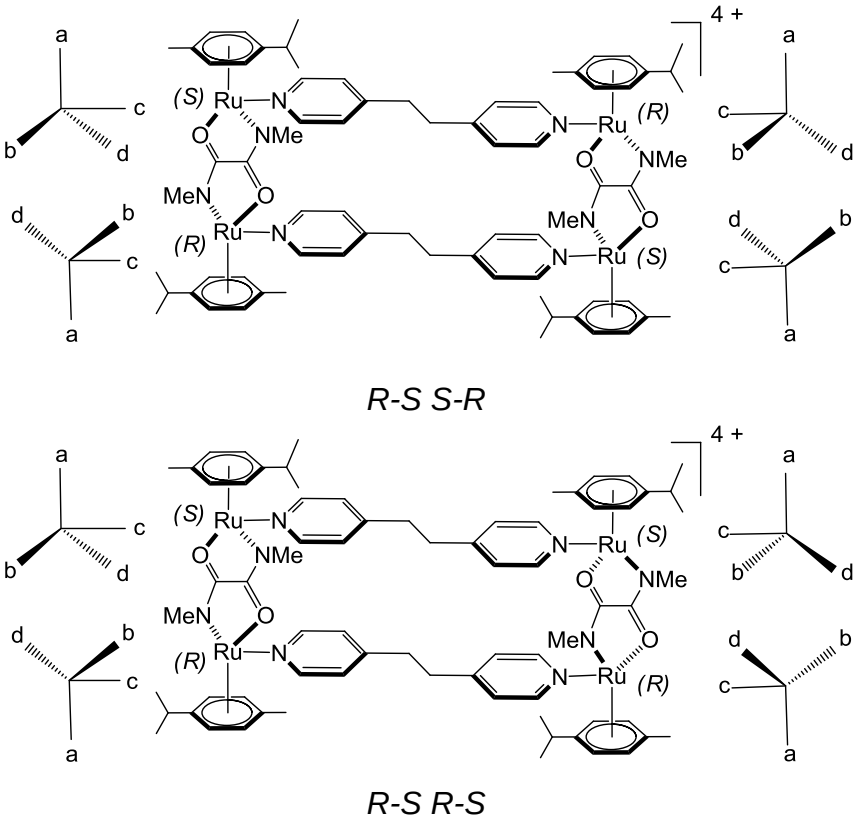

Figure 31. Schematic representation of the two isomers of **R_{30}**

Consequently, in the ^{1}H NMR spectra of metalla-rectangles **R_{23}:R_{30}** and **R_{24}:R_{31}** the presence of these two isomers leads to two distinct sets of signals for the pyridyl protons H_α and H_β (CD_3CN, 21 °C). Furthermore in metalla-rectangles **R_{23}:R_{24}** the two sets of signals are broad and present almost similar chemical shifts, while in **R_{30}:R_{31}** the two sets are less broaden and more separated. This different behaviour between bpe and bpa-incorporating metalla-rectangles could be explained by a difference of rigidity between bpe and bpa leading to different conformations of the metalla-rectangles **R_{23}:R_{24}** and **R_{30}:R_{31}**. Moreover a broadening of the singulet associated to the ethane and ethylene protons of the bpa and bpe linkers suggests non equivalent signals in these metalla-rectangles.

2.2.3 Antiproliferative Activity

The antiproliferative activity of the water-soluble compounds containing the ligands 1,2-bis(4-pyridyl)ethylene (**R_9**, and **R_{19}** – **R_{24}**) and 1,2-bis(4-pyridyl)ethane (**R_{25}** – **R_{31}**) was evaluated against the A2780 and A2780cisR ovarian cancer cell lines. All complexes exhibit

moderate to excellent activity with IC_{50} values (drug concentration necessary for 50% inhibition of cell viability) in the range 2 – 65 μM, except metalla-rectangle **R_{23}** for which the antiproliferative activity is not as good with an IC_{50} > 100 μM, (see Table 2). A remarkable trend in these biological results is the evolution of the Resistance Factor (RF = IC_{50}(A2780cisR) / IC_{50}(A2780)). Indeed, it is noteworthy that the activity of **R_{19}**, **R_{23}**, **R_{26}**, **R_{27}**, **R_{29}**, **R_{30}**, and **R_{31}** metalla-rectangle toward the A2780cisR cancer cell line with acquired resistance to cisplatin is significantly higher than the corresponding activity toward the A2780 cisplatin sensitive cancer cells. This phenomenon gives rise to unusually low Resistance Factors values.[148]

Table 2. Cytotoxicity of compounds towards A2780 cells and A2780cisR cells

compound	A2780 (IC_{50}, μM)	A2780cisR (IC_{50}, μM)	RF
[**R_9**][CF_3SO_3]$_4$	26.4 ± 1.0	112.7 ± 17.2	4.3
[**R_{19}**][CF_3SO_3]$_4$	35.5 ± 7.3	20.8 ± 5.3	0.6
[**R_{20}**][CF_3SO_3]$_4$	4.2 ± 0.9	10.3 ± 2.6	2.5
[**R_{21}**][CF_3SO_3]$_4$	65.8 ± 9.6	75.3 ± 9.8	1.1
[**R_{22}**][CF_3SO_3]$_4$	10.3 ± 1.2	23.3 ± 0.2	2.3
[**R_{23}**][CF_3SO_3]$_4$	144.7 ± 12.8	116.3 ± 9.2	0.8
[**R_{24}**][CF_3SO_3]$_4$	10.3 ± 5.4	13.3 ± 6.1	1.3
[**R_{25}**][CF_3SO_3]$_4$	2.4 ± 1.1	5.2 ± 0.7	2.1
[**R_{26}**][CF_3SO_3]$_4$	2.7 ± 1.0	2.5 ± 0.9	0.9
[**R_{27}**][CF_3SO_3]$_4$	2.6 ± 0.5	2.0 ± 0.3	0.7
[**R_{28}**][CF_3SO_3]$_4$	9.4 ± 0.8	13.8 ± 3.6	1.5
[**R_{29}**][CF_3SO_3]$_4$	8.3 ± 0.2	7.6 ± 2.1	0.9
[**R_{30}**][CF_3SO_3]$_4$	9.9 ± 1.8	8.5 ± 0.6	0.9
[**R_{31}**][CF_3SO_3]$_4$	17.5 ± 5.8	5.2 ± 1.4	0.3
cisplatin	0.7 ± 0.1	4.0 ± 0.5	5.6

2.3 Arene Ruthenium Metalla-Rectangles as Templates for [2 + 2] Cycloaddition

2.3.1 General

The supramolecular control of the solid-state reactivity is a relatively new topic.[149] The use of the solid state as a medium to synthesize molecules needs a pre-organisation of the starting materials in order to facilitate the reactions between functional groups.[150] For example, in the case of a photochemical [2 + 2] dimerisation, the proximity of the olefins is a crucial factor.[151] Indeed, these photochemical [2 + 2] cycloadditions of the olefinic double bonds are expected to occur with the minimal atomic and molecular movements when they are aligned parallel and within the range of 3.0 – 4.1 Å.[152] Among different solutions,[153] the use of a template molecule to assemble two olefins within a supramolecule represents a solution to gain a control of reactivity.[154]

This supramolecular control of reactivity of the olefinic double bonds was used by Jin's group to synthesise two organometallic rectangles of the general formula $[(\eta^5\text{-}Cp^*)_2M_2(ox)_2(bpe)_2]^{4+}$ incorporating half-sandwich complexes of Rh(III) and Ir(III) connected by oxalato and bpe ligands. In the solid state, upon UV irradiation of a crystal, the two olefinic double bonds which are positioned parallel to each other undergo intramolecular photochemical [2 + 2] cycloaddition, thus giving rise to the corresponding cyclobutane derivatives $[(\eta^5\text{-}Cp^*)_2M_2(ox)_2(tpcb)_2]^{4+}$ (tpcb = tetrakis(4-pyridyl)cyclobutane), (see Figure 29).[155]

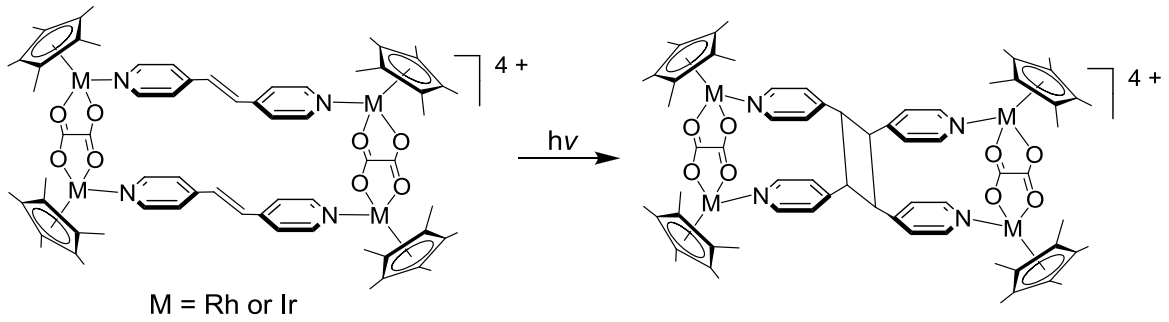

Scheme 5. Single-crystal-to-single-crystal [2 + 2] cycloaddition of $[\eta^5\text{-}Cp^*)_2M_2(ox)_2(bpe)_2]^{4+}$ to give $[(\eta^5\text{-}Cp^*)_2M_2(ox)_2(tpcb)_2]^{4+}$

Due to the Brownian motion, the stability of the pre-organisation of the olefinic double bonds observed in the solid state could not exist in solution. Therefore, we asked ourselves if the supramolecular control of reactivity of the olefins by the formation of an organometallic metalla-rectangle would be enough in solution to maintain a sufficient pre-organisation. In other words, the challenge was to see whether or not in the case of the arene ruthenium metalla-rectangle **R$_{22}$** $[(\eta^6\text{-}p\text{-cym})_4Ru_4(ox)_2(bpe)_2]^{4+}$, published in 1997 by our group, the two olefinic double bonds can react in a methanol solution and under UV irradiation, to afford the intramolecular [2 + 2] cycloaddition adduct, the metalla-rectangle **R$_{32}$** $[(\eta^6\text{-}p\text{-cym})_4Ru_4(ox)_2(tpcb)_2]^{4+}$, (see Table of Figures).

2.3.2 Intramolecular Cycloaddition of $[(\eta^6\text{-}p\text{-cym})_4Ru_4(ox)_2(bpe)_2]^{4+}$ (R_{22})

When a methanol solution of $[\mathbf{R_{22}}][CF_3SO_3]_4$ is irradiated for a period of 60 hours using a Hg lamp (180 W), a photochemical [2 + 2] cycloaddition reaction takes place, thus giving rise in excellent yield to the cationic cyclobutane derivative **R$_{32}$** $[(\eta^6\text{-}p\text{-cym})_4Ru_4(ox)_2(tpcb)_2]^{4+}$, (see Scheme 6). The rectangular cation $[\mathbf{R_{32}}]^{4+}$ is isolated and characterised as its trifluoromethanesulfonate salt ($[\mathbf{R_{32}}][CF_3SO_3]_4$).

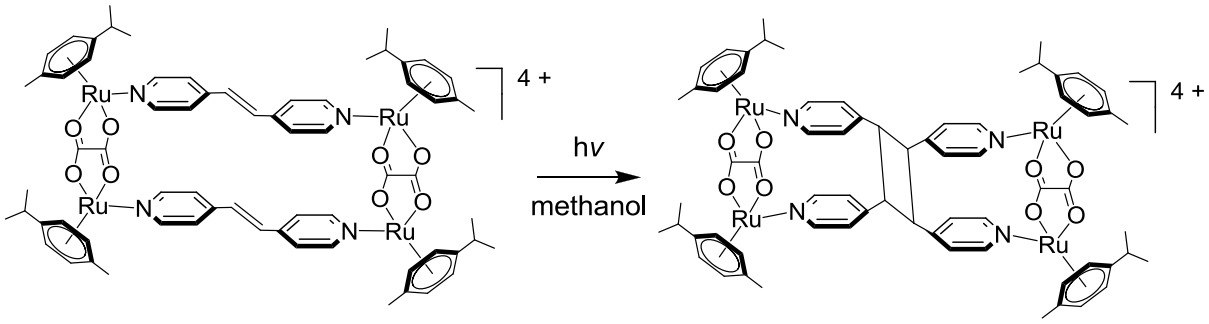

Scheme 6. [2 + 2] cycloaddition of **R$_{22}$** in methanol solution to give **R$_{32}$**

The photodimerisation of $[\mathbf{R_{22}}]^{4+}$ to give $[\mathbf{R_{32}}]^{4+}$ upon UV irradiation can be easily monitored by ^{1}H NMR spectroscopy, (see Figure 29). The [2 + 2] cycloaddition reaction of the olefinic double bonds is followed by the disappearance of the olefinic protons signal at δ = 7.49 ppm and with the emergence of a new signal at δ = 4.99 ppm which is assigned to the cyclobutane protons. Interestingly, upon formation of $[\mathbf{R_{32}}]^{4+}$ diastereotopic protons are observed for the pyridyl groups suggesting a non-equivalent environment. This is in accordance with the X-ray structure analysis of $[(\eta^5\text{-Cp*})_2Ir_2(ox)_2(tpcb)_2]^{4+}$ in which the *rctt*-

cyclobutane isomer (*rctt*-tetrakis(4-pyridyl)cyclobutane) is observed.[155] Consequently, based on the assumption that the same reactivity takes place in solution and using multiple one-dimensional and two-dimensional NMR experiments (ROESY, COSY, HSQC),[156] the complete assignment of the tpcb proton signals in cation $[\mathbf{R_{32}}]^{4+}$ has been determined, (see Figure 32).

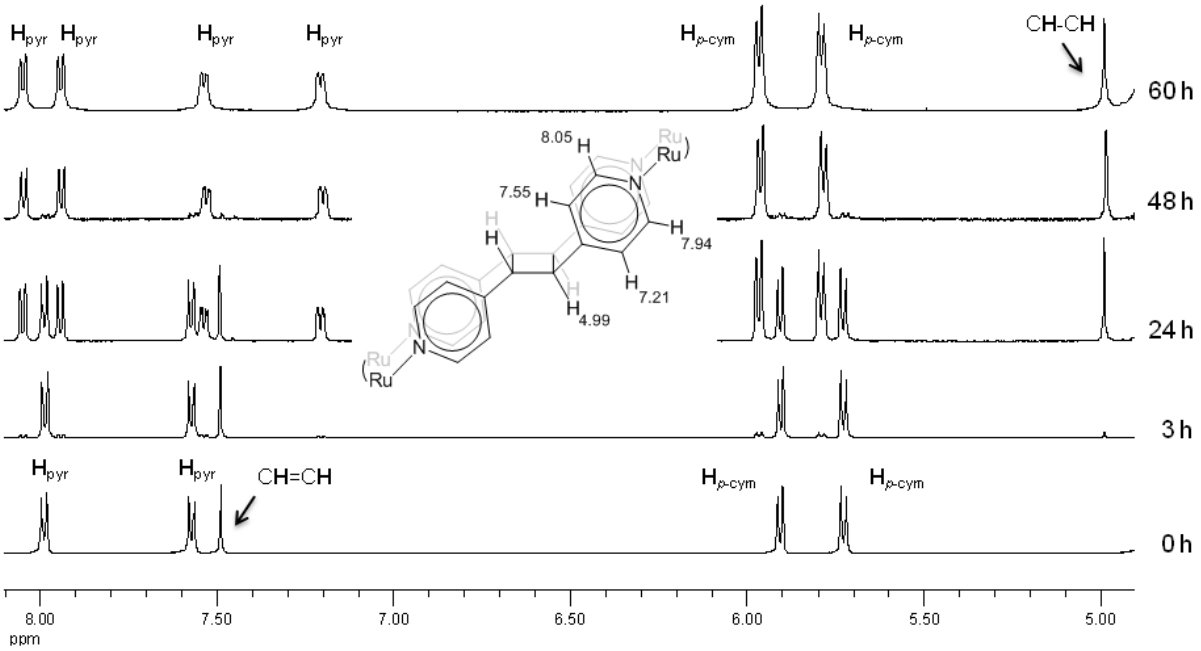

Figure 32. ^{1}H NMR spectra in CD_3OD of the photodimerisation reaction over a 60 h including the assignment of the *rctt*-tpcb protons

The infrared spectra of $[\mathbf{R_{22}}][CF_3SO_3]_4$ and $[\mathbf{R_{32}}][CF_3SO_3]_4$ are almost identical and they are dominated by absorptions of the *p*-cymene, pyridyl, and oxalato groups. In addition, strong absorptions attributed to the trifluoromethanesulfonate anions are observed in the infrared spectra at 1262(s), 1029 (s) and 638(s) cm^{-1}.[157] It is noteworthy to mention that the band corresponding to the stretching vibration of the bpe ethylene groups ($\nu_{CH=CH}$) in $[\mathbf{R_{22}}]^{4+}$, centred at 1595(s) cm^{-1} in free bpe[158] and observed as a shoulder in $[\mathbf{R_{22}}]^{4+}$, disappears during the formation of $[\mathbf{R_{32}}]^{4+}$, as showed in Figure 33. Moreover, the stretching vibration of the C=O oxalato moieties are observed at 1632 cm^{-1} and remains unchanged after the photochemical cycloaddition.

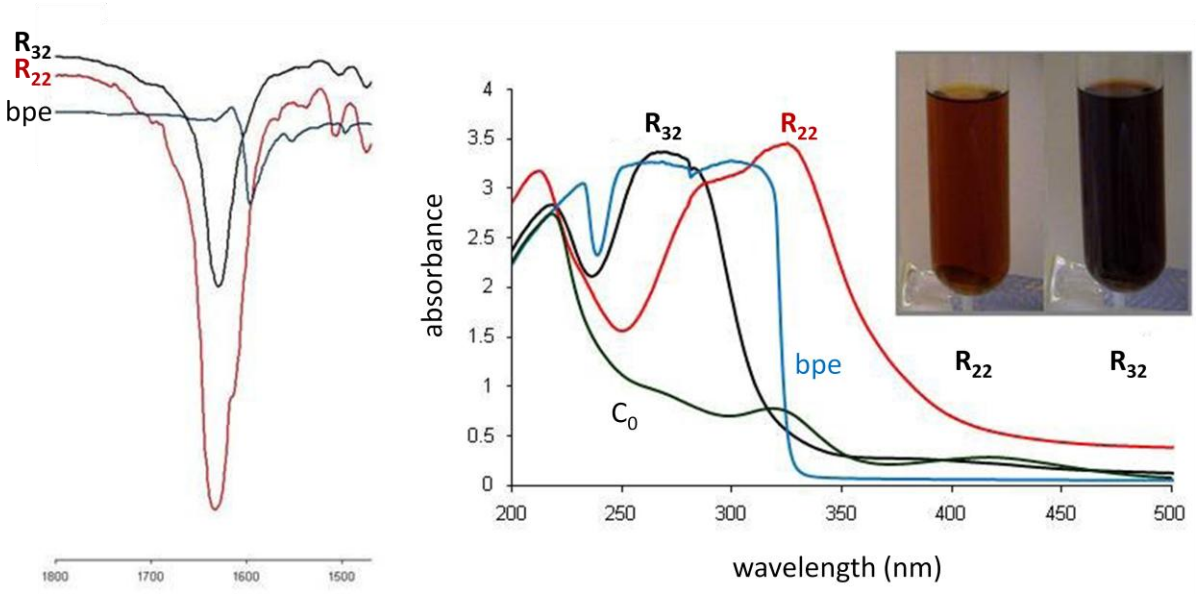

Figure 33. Infrared (KBr pellets) and UV-visible spectra (10^{-5} M, CH_3OH) of metalla-clip $\mathbf{C_0}$, bpe and metalla-rectangles $\mathbf{R_{22}}$ and $\mathbf{R_{32}}$

During the photochemical [2 + 2] cycloaddition reaction, the initial orange CH_3OH solution of $[\mathbf{R_{22}}]^{4+}$ turns dark red upon formation of $[\mathbf{R_{32}}]^{4+}$, see inset in Figure 30. The absorption spectra of $\mathbf{C_0}$, $[\mathbf{R_{22}}]^{4+}$, $[\mathbf{R_{32}}]^{4+}$ and uncoordinated bpe are presented in Figure 30. The absorbance in the electronic spectrum of $[\mathbf{R_{22}}]^{4+}$ exhibits two UV visible transitions which correspond to bpe ($\pi - \pi^*$) and $[(\eta^6\text{-}p\text{-cym})_2Ru_2(ox)Cl_2]$ (MLCT) transitions.[159] The extinction coefficient attributed to the clip transition increases significantly upon formation of rectangle $\mathbf{R_{22}}$. In $\mathbf{R_{32}}$ a hypsochromic shift of the MLCT transition is observed.

2.3.3 Isolation of the Free Organic Linker

It is well known that in coordinating solvents ligand exchange can easily occur in arene ruthenium complexes. In order to isolate the *rctt*-tetrakis(4-pyridyl)cyclobutane (tpcb) moiety, we heated an acetonitrile solution of $[\mathbf{R_{32}}]^{4+}$ for 24 hours in the presence of triphenylphosphine. [160] After this period the cleavage of the different connectors is observed and additional new set of signals observed. Among them, two doublets at δ = 8.4 and 7.5 ppm and a singulet at δ = 4.5 ppm which is assigned to free *rctt*-tpcb molecules: This assignment being in accordance with the ^{1}H NMR values reported for *rctt*-tpcb.[160]

In this study,[161] we have shown a simple and straightforward synthesis of oxalato-bridged arene ruthenium metalla-rectangle using bpe connectors. The parallel arrangement of the olefinic double bonds in this supramolecular assembly allows a facile photochemical [2 + 2] cycloaddition reaction to form the cyclobutane derivative in solution. These data are in agreement with those of the analogous compounds $[(\eta^5\text{-Cp*})_2M_2(ox)_2(bpe)_2][CF_3SO_3]_4$ and $[(\eta^5\text{-Cp*})_2M_2(ox)_2(tpcb)_2][CF_3SO_3]_4$ (M = Rh or Ir), for which the structures, before and after irradiation, were confirmed by single-crystal X-ray structure analysis. Moreover, if wanted, the *rctt*-tetrakis(4-pyridyl)cyclobutane can be recovered.

Chapter 3: Arene Ruthenium Metalla-Prisms

3.1 Arene Ruthenium Metalla-Prisms as Host Systems

3.1.1 From Carceplex to Host-Guest Chemistry

The host-guest chemistry previously described with metalla-rectangles is a part of the considerable attention that encapsulations of appropriately sized, shaped and functionalized guest molecules into self-assembling supramolecular capsules has recently received.[162] In particular, in the case of three-dimensional cages, a number of different models have been reported in the literature over the past few years. Peter Stang,[64a] Makoto Fujita,[34] or Kenneth Raymond[36] are some of the most important contributors to this area of supramolecular chemistry. For example, to illustrate the work of Stang and Fujita we can quote the nitrate encapsulation, both in the solid state and in solution, by a cationic trigonal prismatic host reported by Stang,[163] and the entrapment of sizable neutral molecules, including *o*-carborane and adamantane, by water-soluble truncated tetrahedral capsule described by Fujita.[164] The host ability of these three-dimensional self-assembled aggregates has been largely demonstrated and potential uses are still in development.[65]

The contribution of our group in the encapsulation of guest molecules in three-dimensional coordination cages begins in 2008. The ability of hexacationic metalla-prism **P_1** $[(p\text{-cym})_6Ru_6(dobq)_3(tpt)_2]^{6+}$ (tpt = 2,4,6-tri(pyridin-4-yl)-1,3,5-triazine) (see List of Structures) built from metalla-clip **C_1** and possessing a cavity of 7.8 × 11.7 × 11.7 $Å^3$, to permanently encapsulate square-planar complexes[72] and aromatic molecules was reported.[73] Nevertheless, in these structurally nonlabile systems the portal size was too small or too rigid to let the encapsulated compound escape. Moreover, all attempts at introducing a guest into the empty cavity of **P_1** failed, and therefore no host-guest properties were observed with these hexacationic metalla-prismatic cages. This type of metalla-prism seems to act only as a carceplex system since encapsulation of guest molecule during the synthesis of the metalla-cage is allowed, but after this synthesis the guest molecule cannot run away from the cavity of the host unless if the prism is destroyed.

However, the fabrication of larger arene ruthenium metalla-clips $[(\eta^6\text{-}p\text{-cym})_2Ru_2(OO\cap OO)Cl_2]$ ($OO\cap OO$ = donq, doaq, dotq) (**C₅** – **C₇**) allowed us to cross the border between carceplex and host-guest systems, with the synthesis of new arene ruthenium metalla-prisms $[(\eta^6\text{-}p\text{-cym})_6Ru_6(OO\cap OO)_3(tpt)_2]^{6+}$ ($OO\cap OO$ = donq, doaq, dotq) (**P₂** – **P₄**), (see Figure 34).

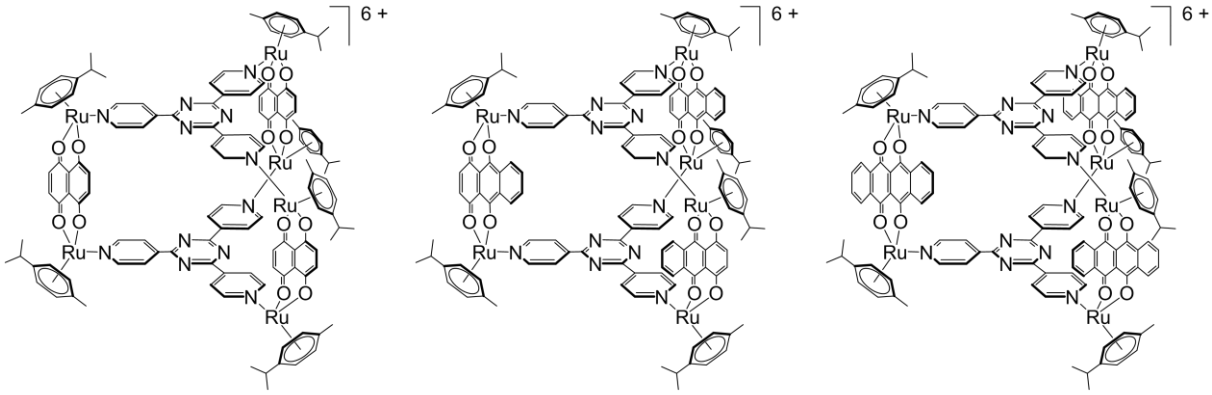

P₂ **P₃** **P₄**

Figure 34. Structures of metalla-prisms **P₂** – **P₄**

These metalla-prisms **P₂** – **P₄** were found to be capable to interact in a host-guest fashion with small aromatic molecules. Therefore, we described the synthesis, the characterisation and their ability to permanently encapsulate or to temporary host aromatic molecules (phenanthrene, pyrene, triphenylene and coronene) in solution. The corresponding binding constants of association for the host-guest systems were estimated.

3.1.2 Synthesis of a Series of Arene Ruthenium Metalla-Prisms (P₂ – P₄)

The hexacationic metalla-prisms **P₂** – **P₄** have been synthesized following a one-pot strategy. The corresponding dinuclear arene ruthenium complex $[Ru_2(\eta^6\text{-}p\text{-cym})_2(donq)Cl_2]$, $[Ru_2(\eta^6\text{-}p\text{-cym})_2(doaq)Cl_2]$ or $[Ru_2(p\text{-cym})_2(dotq)Cl_2]$ reacts in methanol at room temperature in the presence of silver trifluoromethanesulfonate (halide scavenger) with tpt (donor ligand) to give the metalla-hexanuclear cation $[\mathbf{P_2}]^{6+}$, $[\mathbf{P_3}]^{6+}$ or $[\mathbf{P_4}]^{6+}$ isolated as trifluoromethanesulfonate salt in good yield (≈ 80%), (see Scheme 7). The addition of one equivalent of phenanthrene, pyrene, triphenylene or coronene leads to the direct encapsulation

of the aromatic molecule in the metalla-prism, following the same procedure but with a slightly better yield (≈ 85%), possibly due to template effect, (see Scheme 7).

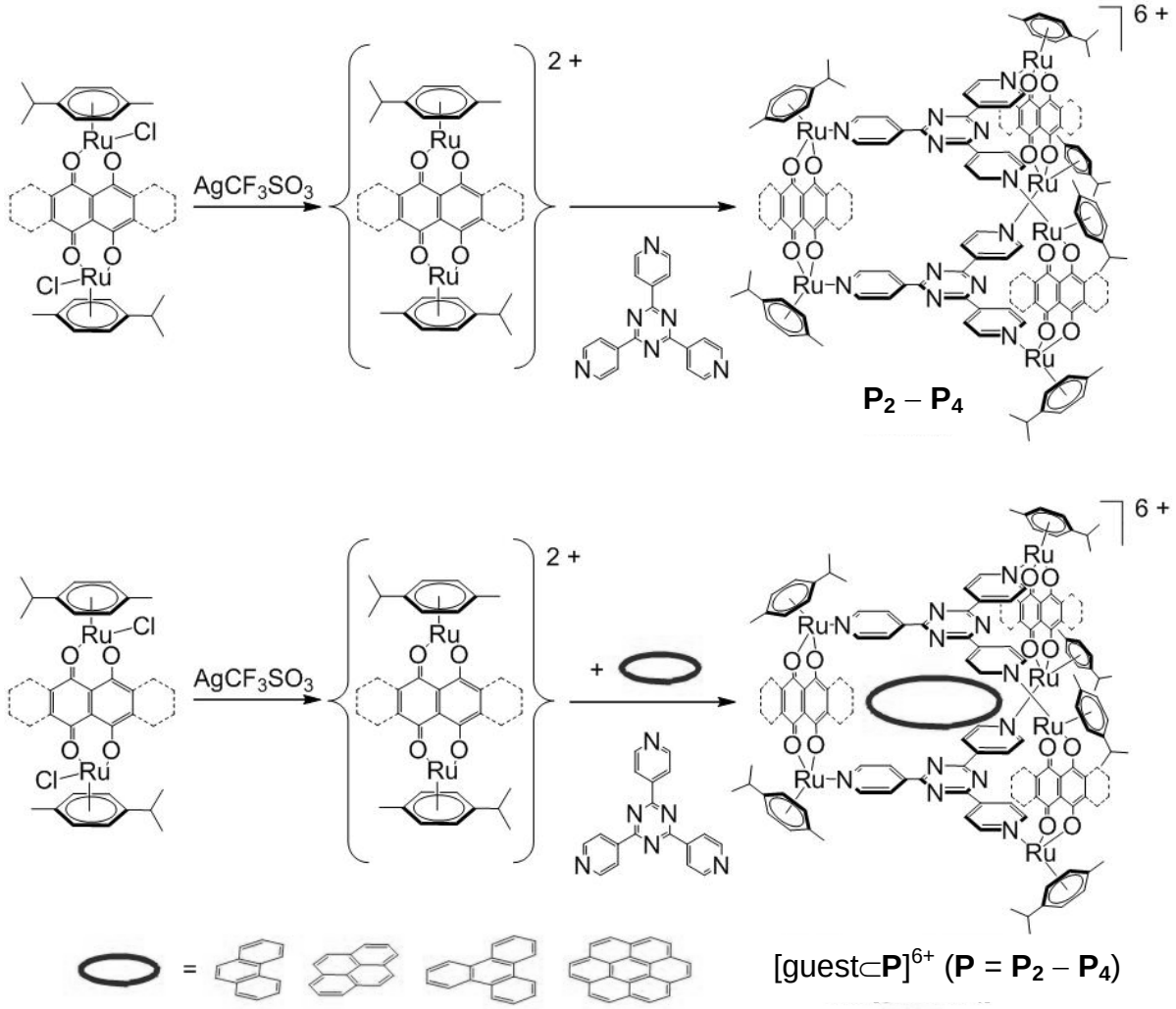

Scheme 7. Syntheses of $[\mathbf{P_2}]^{6+}$, $[\mathbf{P_3}]^{6+}$ and $[\mathbf{P_4}]^{6+}$ (top line) and of $[guest\subset\mathbf{P_2}]^{6+}$, $[guest\subset\mathbf{P_3}]^{6+}$ and $[guest\subset\mathbf{P_4}]^{6+}$ (bottom line)

The infrared spectra of $\mathbf{P_2}$ – $\mathbf{P_4}$ are dominated by absorptions of the coordinated quinonato ligands, which are only slightly shifted as compared to the infrared absorptions of the free ligands. In addition to these signals, strong absorptions due to the stretching vibrations of the trifluoromethanesulfonate anions (1260(s), 1030(s), 638(m) cm^{-1}) are also observed in the infrared spectra of the salts $[\mathbf{P_2}][CF_3SO_3]_6$ – $[\mathbf{P_4}][CF_3SO_3]_6$. In the cases of the $[guest\subset\mathbf{P}]^{6+}$ ($\mathbf{P}$ = $\mathbf{P_2}$ – $\mathbf{P_4}$) systems, additional absorptions due to the guest molecule are observed, and in particular signal at around 1500 cm^{-1} assigned to valence vibrations of aromatic Csp^2-Csp^2. The electronic absorption spectra of the metalla-prisms $\mathbf{P_2}$ – $\mathbf{P_4}$ are

characterised by an intense high-energy band centered at around 320 nm, which is assigned to ligand–localized or intra-ligand $\pi \rightarrow \pi^*$ transition as well as broad low-energy bands associated to metal-to-ligand charge transfer (MLCT) transitions. The ^{1}H NMR spectra of **P$_2$** – **P$_4$** show two doublets due to the tpt protons with an upfield shift of the signals as compared to the free tpt molecule in acetone-d_6. Similarly, the proton signals of the 5,8-dioxydo-1,4-naphthoquinonato, 5,8-dioxydo-1,4-anthraquinonato and 6,11-dioxydo-5,12-naphthacenedionato bridging ligands in metalla-prisms **P$_2$** – **P$_4$** are shifted downfield as compared to their parent complexes $[(\eta^6\text{-}p\text{-cym})_2Ru_2(donq)Cl_2]$, $[(\eta^6\text{-}p\text{-cym})_2Ru_2(doaq)Cl_2]$ and $[(\eta^6\text{-}p\text{-cym})_2Ru_2(dotq)Cl_2]$ while the methyl, isopropyl and phenyl signals of the *p*-cym ligands remain almost unchanged.

To further study the structural behaviour of cationic metalla-prisms **P$_2$** – **P$_4$** in solution, NMR enantiodifferentiation in acetone-d_6 was achieved in the presence of the NMR chiral solvating agent *Λ*-trisphat (trisphat = tris(tetrachlorobenzenediolato)-phosphate(V)).[165] Upon gradual addition of *Λ*-trisphat (0.1 – 5.0 equiv.) to an acetone-d_6 solution of metalla-prism **P$_2$** – **P$_4$**, a rapid and effective splitting of all signals of metalla-prisms is observed, (see baseline-to-baseline separation of *p*-cym proton signals of **2** in Figure 35). This NMR enantiodifferentiation confirms the expected helical chirality of metalla-prisms **P$_2$** – **P$_4$**, already observed with similar metalla-assemblies.[114, 166]

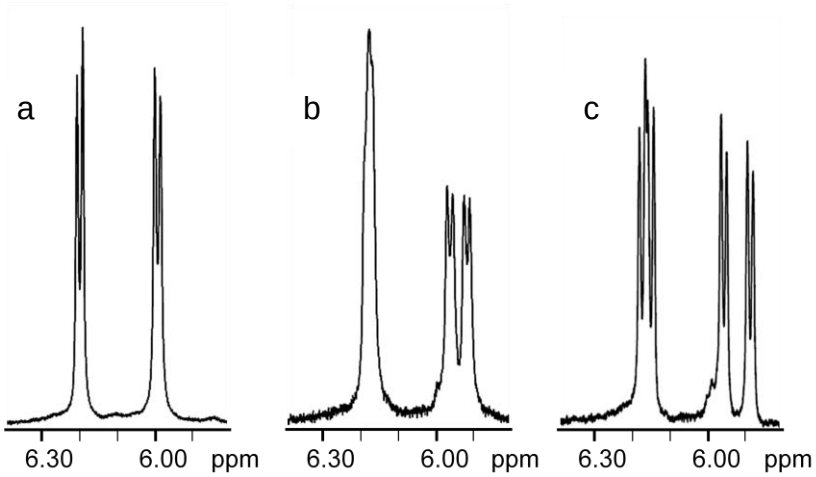

Figure 35. Splitting of *p*-cym proton signals of metalla-prism $[\mathbf{P_4}][CF_3SO_3]_6$ upon addition of *Λ*-trisphat in acetone-d_6 at 21°C; (a) $[\mathbf{P_4}]^{6+}$ (4.0 mM), (b) $[\mathbf{P_4}]^{6+}$ + 2.0 equiv. of *Λ*-trisphat, (c) $[\mathbf{P_4}]^{6+}$ + 5.0 equiv. of *Λ*-trisphat

3.1.3 Host-Guest Properties

The formation of [guest⊂**P**]$^{6+}$ (**P** = **P$_2$** – **P$_4$**) can be easily monitored by NMR spectroscopy. The signals of the different protons of the guest molecule as well as those of the pyridyl protons of the tpt panels are shifted upfield upon formation of the host-guest system, whereas the signals of the CH protons of the donq, doaq and dotq bridging ligands are shifted downfield. On the other hand, the signals of the protons of the *p*-cym ligands located at the periphery of the prisms are not significantly affected by the presence of a guest molecule in the cavities of [**P$_2$**]$^{6+}$ – [**P$_4$**]$^{6+}$, (see Figure 36).

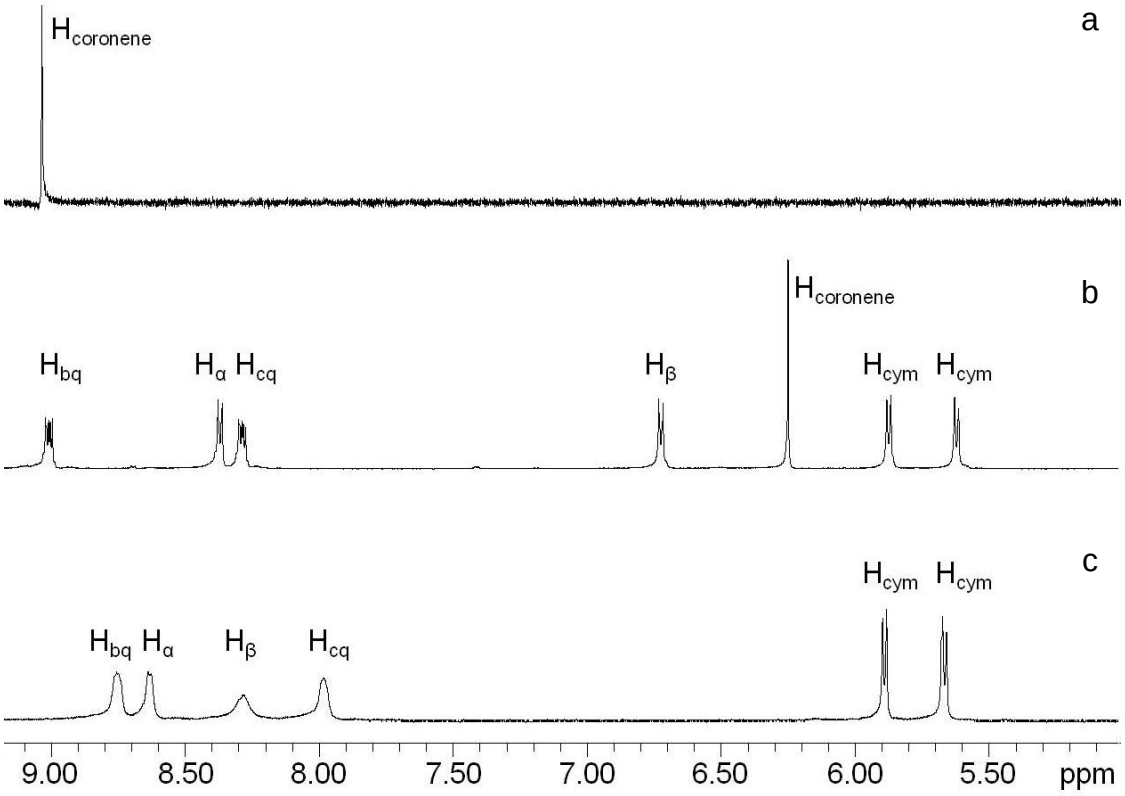

Figure 36. ^{1}H NMR spectra (21°C, CD_3CN) of (a) free coronene, (b) [coronene⊂**P$_4$**][CF_3SO_3]$_6$ and (c) [**P$_4$**][CF_3SO_3]$_6$

^{1}H ROESY experiments confirm the encapsulation of aromatic molecules (phenanthrene, pyrene, triphenylene and coronene) in metalla-prisms **P$_2$** – **P$_4$**. For example, the ^{1}H ROESY spectrum of [coronene⊂**P$_4$**]$^{6+}$ shows a strong nuclear overhauser effect between the irradiated coronene protons and tpt protons (H_{bq} and H_{cq}□). Moreover a weak

nuclear overhauser interaction with the protons of the quinonato bridges (H_{bq} and H_{cq}) is as well observed, (see Figure 37).

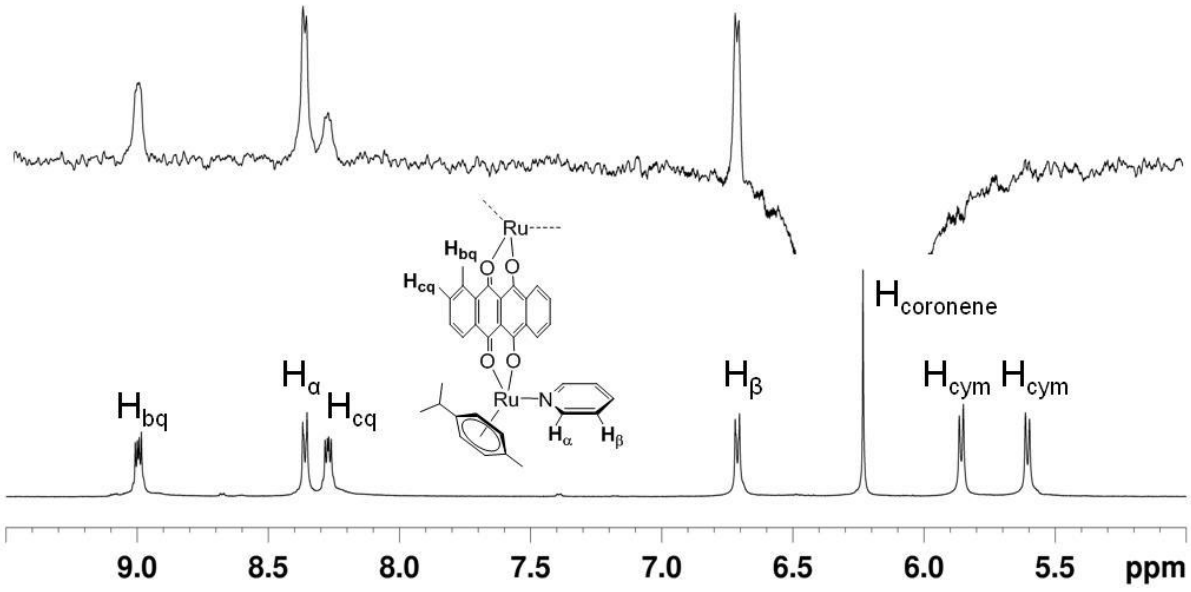

Figure 37. One-dimensional ^{1}H ROESY spectrum (21°C, CD_3CN) of [coronene⊂**P**$_4$][CF_3SO_3]$_6$. The ^{1}H NMR spectrum of [coronene⊂**P**$_4$][CF_3SO_3]$_6$ is given below

In order to evaluate these metalla-cages as potential host-guest systems, we first studied the stability of all systems in solution (water, toluene, acetonitrile) at room and elevated temperatures. Complexes [triphenylene⊂**P**]$^{6+}$ and [coronene⊂**P**]$^{6+}$ (**P** = **P**$_2$ – **P**$_4$) show no degradation of the cages or leaching of the guests in all solvents tested, even at reflux for 24 h. However, [phenanthrene⊂**P**]$^{6+}$ and [pyrene⊂**P**]$^{6+}$ (**P** = **P**$_2$ – **P**$_4$) show rapid loss of their guest molecules in toluene-d_8 at 80 °C, while these systems remain intact in acetonitrile and water. Therefore, we decided to further study the host-guest chemistry of the metalla-prisms [**P**$_2$]$^{6+}$ – [**P**$_4$]$^{6+}$ in CD_3CN solution by using NMR spectroscopy. Upon gradual addition of guest (either phenanthrene or pyrene) (0.1 – 3.0 equiv.) to an CD_3CN solution of metalla-prism ([**P**$_2$][CF_3SO_3]$_6$ – [**P**$_4$][CF_3SO_3]$_6$) (4.0 mM), the ^{1}H NMR spectra show chemical shifts of the signals for some protons of the host and of the guest. The broadening and chemical shifts of the signals clearly support a rapid inclusion of guest molecule in the hydrophobic cavity of metalla-prisms. Plots of these chemical shift changes ($\Delta\delta$) for the H_β proton of the tpt ligands *versus* the molar ratio of pyrene/[**P**]$^{6+}$ (**P** = **P**$_2$ – **P**$_4$) indicate the formations of 1:1 host-guest systems for which association constants are calculated by the nonlinear least-square fitting program winEQNMR2, (see Table 3).

Table 3. Stability constants (K_a) and free energies (ΔG^o) for the encapsulation of pyrene and phenanthrene in metalla-prisms **P_2** – **P_4** (21°C, CD_3CN, 4.0 mM of host)

guest⊂**host**	K_a (10^4 M^{-1})	ΔG^o (kcal · mol^{-1})
[pyrene⊂**P_2**]$^{6+}$	4.0 ± 1.7	-6.28 ± 0.33
[pyrene⊂**P_3**]$^{6+}$	2.0 ± 0.4	-5.87 ± 0.13
[pyrene⊂**P_4**]$^{6+}$	2.2 ± 0.5	-5.93 ± 0.63
[phenanthrene⊂**P_2**]$^{6+}$	2.9 ± 1.1	-6.08 ± 0.20
[phenanthrene⊂**P_3**]$^{6+}$	2.0 ± 0.7	-5.88 ± 0.22
[phenanthrene⊂**P_4**]$^{6+}$	2.9 ± 0.9	-6.08 ± 0.20

In this study,[167] we described three new cationic metalla-prisms with different portal sizes able to allow small aromatic molecules to enter and leave in solution the hydrophobic cavity.[168] However, for planar molecules capable of fitting into the cavity, but too large to exit the portal of the cage, permanent encapsulation was observed, thus giving rise to stable carceplex systems. More interestingly, the development of three new metalla-prisms **P_2** – **P_4** with different portal sizes and able to interact in a host-guest fashion with small aromatic molecules was a new way to explore the anticancer behaviour of our arene ruthenium metalla-systems.

3.2 Arene Ruthenium Metalla-Prisms as Water-Soluble Nano-Capsules

3.2.1 General

In recent years the use of host-guest systems to efficiently deliver drugs to cancer cells has attracted a lot of interest.[169] In such systems the physicochemical properties of the host-guest complex are generally superior to those of the guest leading to improvements in efficacy and biocompatibility.[170] It is not surprising that cisplatin,[98, 171] the most widely used metal-based drug in the treatment of cancer, has been encapsulated in various hosts in order to reduce the severe side effects associated with this drug.[172] Indeed, platinum-based drugs have been incorporated to hosts including carbon nanotubes,[173] proteins,[174] macrocycles[175] and dendrimers.[176] These large systems tend to accumulate preferentially in tumours due to enhanced permeability and retention (the EPR effect) of macromolecules in cancerous tissue.[102]

As explained previously, our group combined the medicinal properties of arene ruthenium complexes, a promising class of organometallic drugs,[142] with aspects of supramolecular chemistry,[65] to generate a new hybrid drug delivery system, $[(\eta^6\text{-}p\text{-cym})_6Ru_6(dobq)_3(tpt)_2]^{6+}$ (**P_1**), in which guest molecules were encapsulated in the cavity of the host.[177] This host was found to encapsulate planar aromatic compounds[115] as well as planar Pt and Pd acetylacetonato complexes.[72] The biological activity of these compounds was evaluated on human ovarian cancer cell lines, and the empty cage **P_1** was found to have an IC_{50} value of 23 μM with the carceplexes being at least an order of magnitude more cytotoxic (the guests were not cytotoxic on their own). The ability of this host to deliver guest molecules to cells was further confirmed by encapsulation of a fluorescent labelled pyrene-X derivative, 1-(4,6-dichloro-1,3,5-triazin-2-yl)pyrene.[116] Fluorescence experiments used to monitor the uptake of pyrene-X into cancer cells demonstrated one order of magnitude greater uptake of the carceplex [pyrene-X⊂**P_1**]$^{6+}$ over pyrene-X alone.

To compare the *in vitro* biological behaviour of the host-guest systems *versus* the [pyrene-X⊂**P_1**]$^{6+}$ carceplex systems, we encapsulated the same pyrene-X into the new metalla-prisms **P_2** – **P_4**. The binding constants of association of the host-guest systems involving pyrene-X, were studied in solution by NMR and fluorescence spectroscopy and the antiproliferative activity of the empty cages and of the host-guest systems were evaluated on

human ovarian cancer cell lines. The uptake and release of pyrene-X by the [pyrene-X⊂**P**]$^{6+}$ (**P** = **P$_2$** – **P$_4$**) systems were determined and correlated to the portal size of the host molecule. We also studied the uptake mechanism of [pyrene-X⊂**P$_2$**]$^{6+}$. Pd(acac)$_2$ was also encapsulated into these three arene ruthenium metalla-prisms.

3.2.2 Synthesis and Host-Guest Properties of [pyrene-X⊂P]$^{6+}$ (P = P$_2$ – P$_4$)

The syntheses of the empty arene ruthenium metalla-prisms [**P$_2$**]$^{6+}$, [**P$_3$**]$^{6+}$, and [**P$_4$**]$^{6+}$, have been previously described. The encapsulation of Pd(acac)$_2$ and pyrene-X in these cages follows the same pathway than the encapsulations of pyrene, phenanthrene, triphenylene and coronene previously reported. The formation of [guest⊂**P**]$^{6+}$ (**P** = **P$_2$** – **P$_4$**) was monitored by ^{1}H NMR spectroscopy. The resonances of the different protons of the guest molecule and the pyridyl protons of the tpt panels are shifted upfield upon formation of the encapsulated system, whereas the signals of the CH protons of the bridging ligands (donq, doaq, or dotq) are shifted downfield. In the ^{1}H NMR spectra of [Pd(acac)$_2$⊂**P**]$^{6+}$ (**P** = **P$_2$** – **P$_4$**) the CH and CH$_3$ signals of the acetylacetato ligands are shifted upfield by about 1.7 ppm compared to the free complex, and in the spectra of [pyrene-X⊂**P**]$^{6+}$ (**P** = **P$_2$** – **P$_4$**) the signals of the CH protons of the encapsulated aromatic guest are all shifted upfield relative to the free molecule, the frequencies being similar to those observed in [pyrene-X⊂**P$_1$**]$^{6+}$.[116] The electronic absorption spectra of the systems [guest⊂**P**]$^{6+}$ (**P** = **P$_2$** – **P$_4$**) (see Figure 38) are characterised by an intense high-energy band centred at around 300 nm, which is assigned to ligand-localised or intra-ligand $\pi \rightarrow \pi^*$ transition as well as broad low-energy bands associated to metal-to-ligand charge transfer (MLCT) transitions.

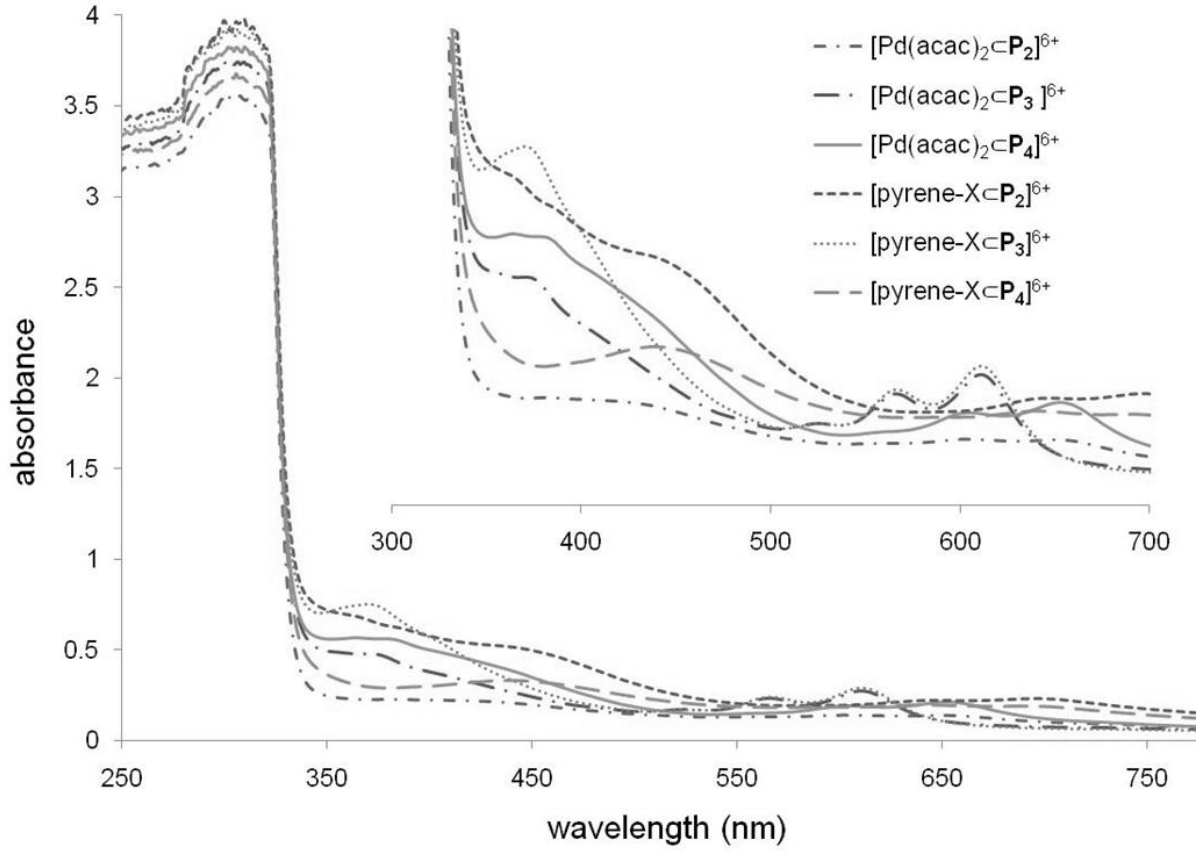

Figure 38. UV-visible spectra of [guest⊂**P**]$^{6+}$ (**P** = **P$_2$** – **P$_4$**) in CH_2Cl_2 (10^{-5} M)

The host-guest properties of the [guest⊂**P**]$^{6+}$ (**P** = **P$_2$** – **P$_4$**) systems were studied in solution, establishing their stability in water, toluene and acetonitrile, at room and elevated temperatures. The [Pd(acac)$_2$⊂**P**]$^{6+}$ (**P** = **P$_2$** – **P$_4$**) systems show no signs of degradation of the cage, or leaching of the guest, in all solvents tested, even at reflux for 24 hours. However, all [pyrene-X⊂**P**]$^{6+}$ (**P** = **P$_2$** – **P$_4$**) systems show rapid lost of the guest in toluene-d_8 at 80 ºC, but remain intact in acetonitrile and water. The host-guest interactions between pyrene-X and the metalla-prisms [**P$_2$**]$^{6+}$ **–** [**P$_4$**]$^{6+}$ were further studied by diffusion-ordered NMR spectroscopy (DOSY). As an example, the DOSY spectra of pyrene-X, [**P$_2$**]$^{6+}$ and pyrene-X + [**P$_2$**]$^{6+}$ in CD_3CN at room temperature are presented in Figure 39. These experiments clearly show that at room temperature, [**P$_2$**]$^{6+}$ and pyrene-X + [**P$_2$**]$^{6+}$ possess an almost identical diffusion coefficients, which confirm the encapsulation of pyrene-X in the hydrophobic cavity of [**P$_2$**]$^{6+}$.

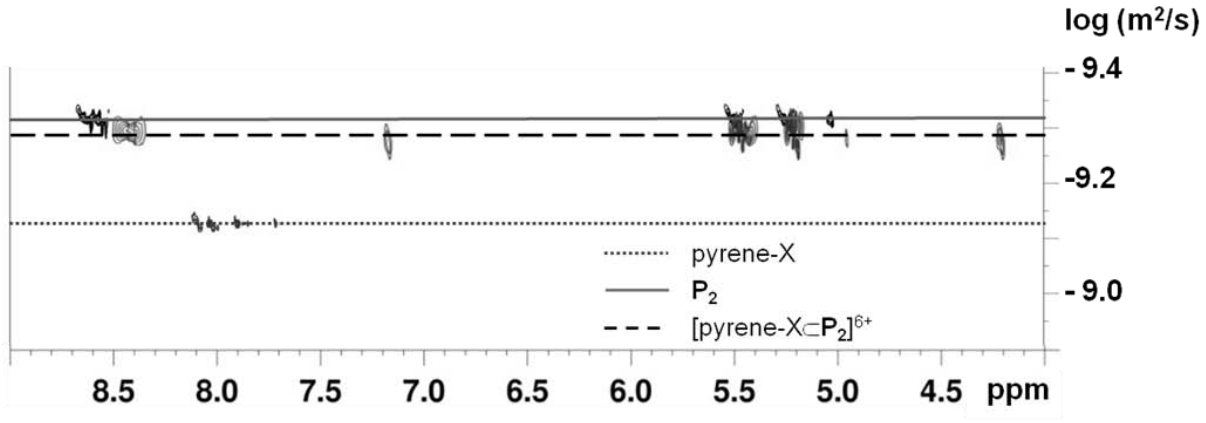

Figure 39. DOSY NMR spectra of pyrene-X, $[\mathbf{P_2}]^{6+}$ and $[\mathbf{P_2}]^{6+}$ + 1 eq. of pyrene-X in CD_3CN at 21°C

The host-guest properties of the [pyrene-X⊂**P**]$^{6+}$ (**P** = $\mathbf{P_2}$ – $\mathbf{P_4}$) systems were further studied in CD_3CN by ^{1}H NMR titrations. Upon gradual addition of pyrene-X (0.1 – 3.0 equivalents) to a CD_3CN solution of the host (4.0 mM), chemical shift changes for some protons are observed. ^{1}H NMR spectra obtained from the titration experiments with $[\mathbf{P_4}]^{6+}$ at 21 ºC in CD_3CN are shown in Figure 40. The broadening and chemical shifts of the signals are indicative of rapid inclusion of the pyrene-X into the hydrophobic cavity of $[\mathbf{P_4}]^{6+}$.

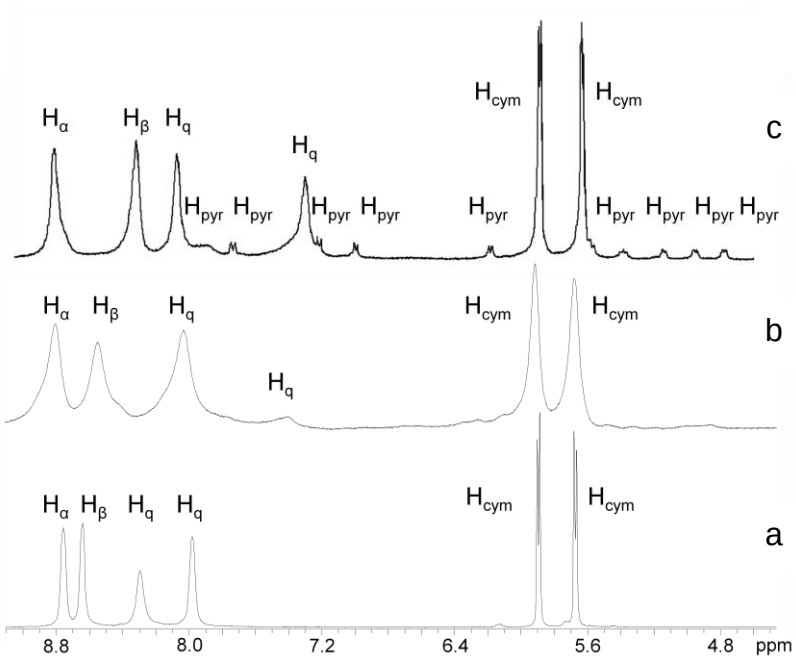

Figure 40. ^{1}H NMR titration of pyrene-X in a CD_3CN solution of $[\mathbf{P_4}][CF_3SO_3]_6$ at 21 °C, (a) $[\mathbf{P_4}]^{6+}$ (4.0 mM), (b) $[\mathbf{P_4}]^{6+}$ + 0.5 eq. of pyrene-X, and (c) $[\mathbf{P_4}]^{6+}$ + 1.0 eq. of pyrene-X

Plots of the chemical shift changes ($\Delta\delta$), for the H_β proton of the tpt ligands *versus* the molar ratio of pyrene-X to the prisms $[\mathbf{P_2}]^{6+}$ **–** $[\mathbf{P_4}]^{6+}$, indicate the formation of 1:1 stoichiometric host-guest systems (see Figure 41). From these plots, stability constants of association were estimated using the non-linear least square fitting program winEQNMR2 (see Table 4). The binding free energies (ΔG^o) for the [pyrene-X⊂**P**]$^{6+}$ (**P** = $\mathbf{P_2}$ – $\mathbf{P_4}$) systems were determined from the corresponding association constants obtained at 21 ºC in CD_3CN.

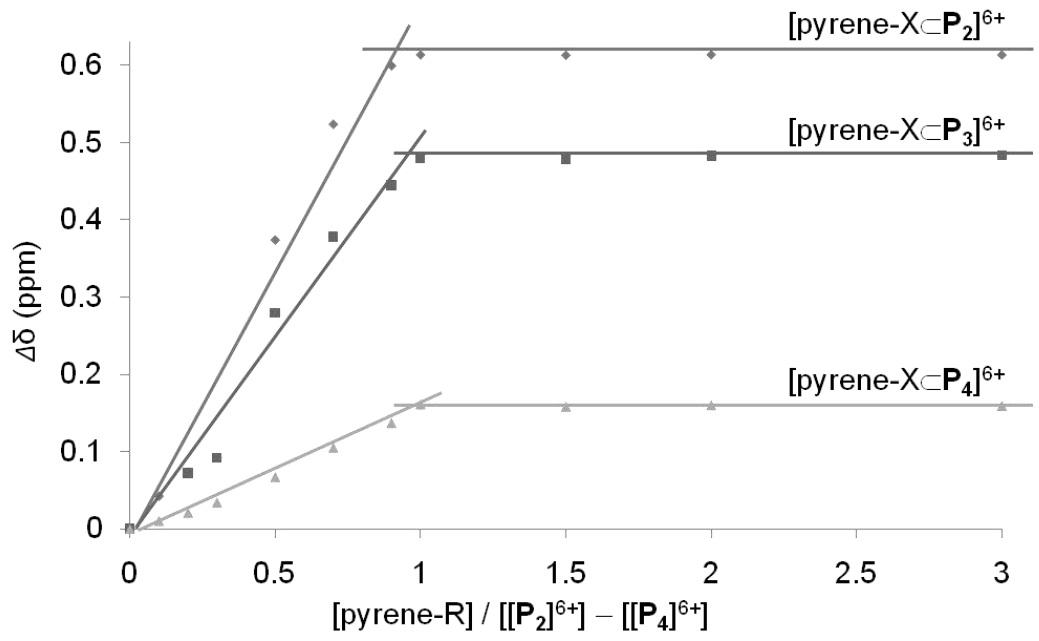

Figure 41. ^{1}H NMR chemical shift changes for the signal of the H_β protons of the tpt ligands *versus* the molar ratio of pyrene-X/$[\mathbf{P_2}]^{6+}$ **–** $[\mathbf{P_4}]^{6+}$ in CD_3CN at 21 °C

Table 4. Stability constants (K_a) and free energies (ΔG^o) for the encapsulation of pyrene-X in metalla-prisms $\mathbf{P_2 - P_4}$ (21°C, CD_3CN, 4.0 mM of host)

guest⊂**host**	K_a (10^4 M^{-1})	ΔG^o (kcal · mol^{-1})
[pyrene-X ⊂ $\mathbf{P_2}$]$^{6+}$	4.1 ± 0.6	-6.27 ± 0.42
[pyrene-X ⊂ $\mathbf{P_3}$]$^{6+}$	2.0 ± 0.3	-5.86 ± 0.12
[pyrene-X ⊂ $\mathbf{P_4}$]$^{6+}$	1.2 ± 0.7	-5.56 ± 0.58

As opposed to the carceplex system, [pyrene-X⊂$\mathbf{P_1}$]$^{6+}$, in which the fluorescence of the pyrene-X guest is totally quenched upon encapsulation, some fluorescence remains in the

host-guest systems [pyrene-X⊂**P**]$^{6+}$ (**P** = **P$_2$** – **P$_4$**) (see Figure 42). Indeed, the fluorescence of the pyrenyl part is quenched but the triazin-2-yl group does not entirely lose its fluorescent properties. Spectral overlap between the emission of the pyrenyl part and the absorbance of the metalla-prism is encountered for the fluorescence quenching of pyrene.

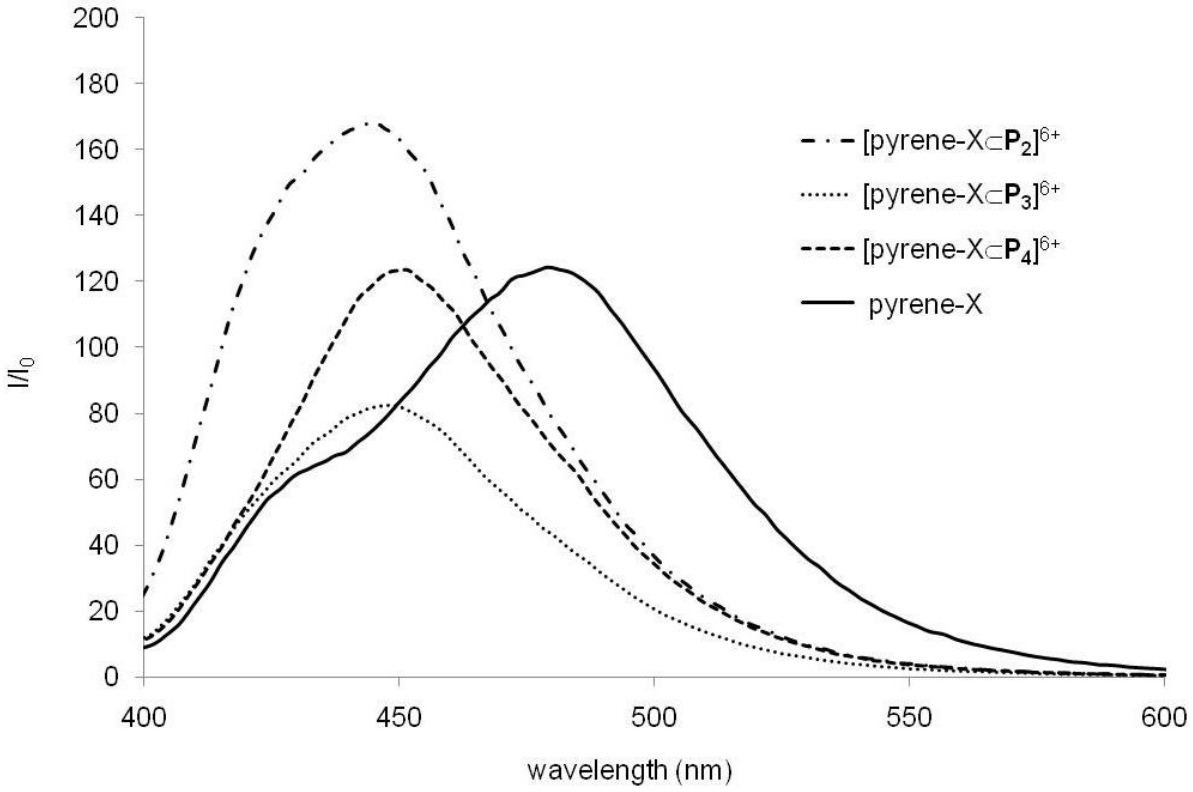

Figure 42. Fluorescence emission spectra of pyrene-X and [pyrene-X⊂**P**]$^{6+}$ (**P** = **P$_2$** – **P$_4$**) in H_2O:DMSO (99.5:0.5; V:V) solution (10^{-7} M) at 21 °C, excitation 350 nm

However, the fluorescence of the triazin-2-yl unit remains almost at the same energy state. This partial quench of the fluorescence of pyrene-X in metalla-prisms [**P$_2$**]$^{6+}$ **–** [**P$_4$**]$^{6+}$ is illustrated by emission spectra from fluorescence titrations. Upon gradual addition of [**P$_2$**][CF_3SO_3]$_6$ **–** [**P$_4$**][CF_3SO_3]$_6$ (0.1 – 6.0 equivalents) to a H_2O:DMSO (99.5:0.5; V:V) solution of pyrene-X (10^{-7} M), the emission spectra (excitation: 350 nm, 21 °C) show a strong quenching of the band associated to the pyrenyl part, while the band associated to the triazin-2-yl arm is not affected by addition of [**P$_2$**]$^{6+}$ **–** [**P$_4$**]$^{6+}$ (see Figure 43).

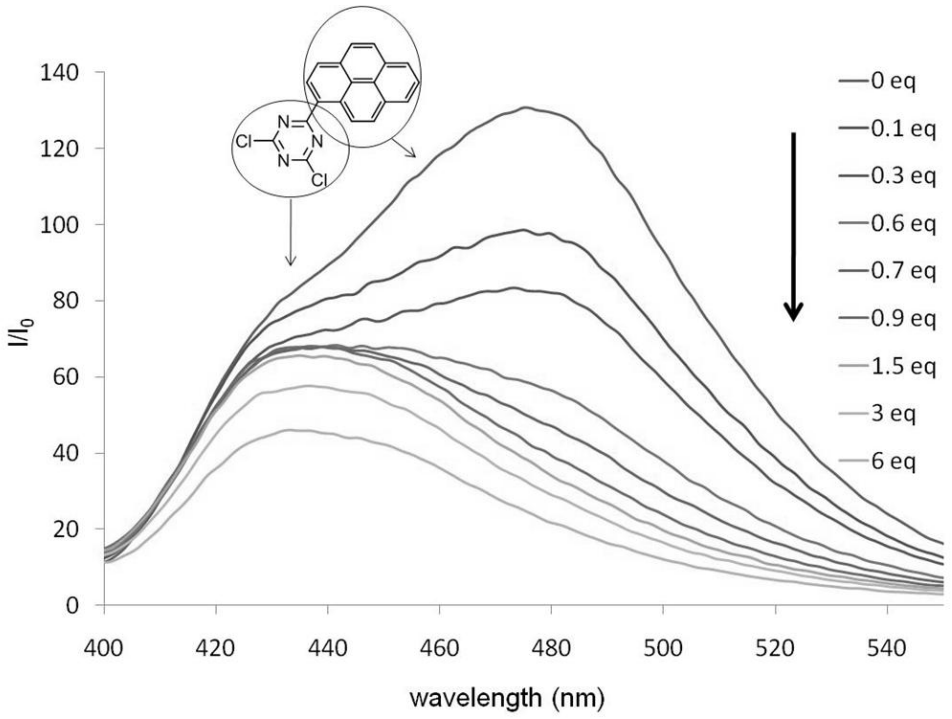

Figure 43. Fluorescence titration at 21 °C of $[\mathbf{P_3}][CF_3SO_3]_6$ (0.1 – 6.0 equivalents) in H_2O:DMSO (99.5:0.5; V:V) solution (10^{-7} M) containing pyrene-X (excitation 350 nm)

3.2.3 Antiproliferative Study

In order to determine the impact of the structure of the different metalla-prisms on the cytotoxicity of the host-guest systems, the portal size of these systems were evaluated. Indeed, the size of the cavity is equivalent in $\mathbf{P_2}$, $\mathbf{P_3}$ and $\mathbf{P_4}$. However, the use of different *OO*∩*OO* connectors controls the portal size of the systems, thus modulating the dynamic of the host-guest systems. Molecular modelling using HyperChem in the gas phase was applied to equilibrate each metalla-prism, and the output of the simulation was then minimized to full convergence.[178] This molecular dynamics simulation was performed to estimate the portal size of these cages in the gas phase (see Figure 44). The largest portal, estimated to be approximately 7.4 Å (height) by 10.2 Å (width), is found in [pyrene-X⊂$\mathbf{P_2}$]$^{6+}$ which shows highest fluorescence, *i.e.* most facile loss of the pyrene-X guest. Compound [pyrene-X⊂$\mathbf{P_3}$]$^{6+}$ which contains the smallest portal (7.4 x 7.8 Å^2) exhibits least fluorescence corresponding to a more stable host-guest system. Indeed, these results correlate very nicely with the association constants determined for the three systems.

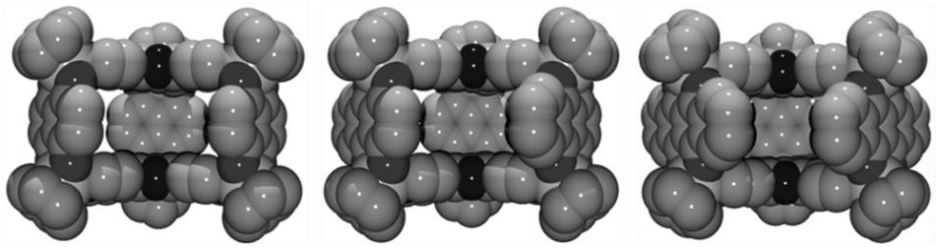

$[\mathbf{P_2}]^{6+}$ $[\mathbf{P_3}]^{6+}$ $[\mathbf{P_4}]^{6+}$

Figure 44. HyperChem simulations of metalla-prisms $[\mathbf{P_2}]^{6+}$ **–** $[\mathbf{P_4}]^{6+}$

The cytotoxicity of the compounds was established in the A2780 human ovarian cancer cell line, (see Table 5). The toxicity of the pyrene-X or $Pd(acac)_2$ inside the cage systems is systematically higher than that of the corresponding cages and pyrene-X or $Pd(acac)_2$ alone. Moreover, the $[Pd(acac)_2\subset\mathbf{P}]^{6+}$ (**P** = $\mathbf{P_2}$ – $\mathbf{P_4}$) systems are more cytotoxic than the corresponding $[\text{pyrene-X}\subset\mathbf{P}]^{6+}$ (**P** = $\mathbf{P_2}$ – $\mathbf{P_4}$) systems, which is consistent with previously published supramolecular systems.[116]

Table 5. Cytotoxicity of compounds towards A2780 cells

compound	IC_{50} (μM)	SD (μM)[a]
pyrene-X	ND	ND
$Pd(acac)_2$	ND	ND
$[\mathbf{P_2}][CF_3SO_3]_6$	3.2	1.1
$[\mathbf{P_3}][CF_3SO_3]_6$	13.1	1.1
$[\mathbf{P_4}][CF_3SO_3]_6$	4.1	0.1
$[\text{pyrene-X}\subset\mathbf{P_2}][CF_3SO_3]_6$	1.9	0.1
$[\text{pyrene-X}\subset\mathbf{P_3}][CF_3SO_3]_6$	2.3	0.6
$[\text{pyrene-X}\subset\mathbf{P_4}][CF_3SO_3]_6$	1.1	0.2
$[Pd(acac)_2\subset\mathbf{P_2}][CF_3SO_3]_6$	<0.3	ND
$[Pd(acac)_2\subset\mathbf{P_3}][CF_3SO_3]_6$	0.9	0.3
$[Pd(acac)_2\subset\mathbf{P_4}][CF_3SO_3]_6$	<0.3	ND

[a] Standard Deviation

Uptake of ruthenium into the cells was determined with the $[\text{pyrene-X}\subset\mathbf{P}]^{6+}$ (**P** = $\mathbf{P_2}$ – $\mathbf{P_4}$) systems by inductively coupled plasma mass spectroscopy (ICP-MS) which reveals that

all compounds enter the cells to essentially the same extent (see Figure 45), indicating a similar uptake mechanism for the three compounds. However, release of the pyrene-X guest following uptake is not constant and varies for the three systems. As previously reported, the fluorescence of pyrene-X is quenched inside the ruthenium cage,[116] and consequently fluorescence can be used to evaluate the release of free pyrene-X inside the A2780 cells. Flow cytometry was used to study the fluorescence of cells incubated with [pyrene-X⊂**P**]$^{6+}$ (**P** = **P$_2$** – **P$_4$**), (see Figure 45) and shows that the portal size of the host influences the release of pyrene-X. Cells were incubated with [**P$_2$**][CF_3SO_3]$_6$ and [pyrene-X⊂**P$_2$**][CF_3SO_3]$_6$ – [pyrene-X⊂**P$_4$**][CF_3SO_3]$_6$ at 2 μM for 24 hours.

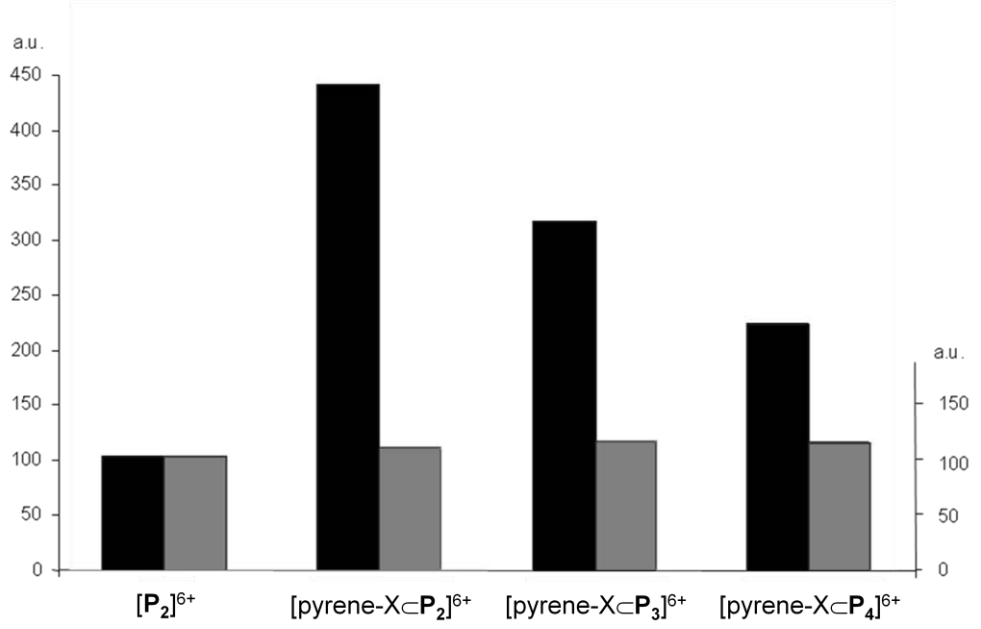

Figure 45. Fluorescence recorded by flow cytometry of [pyrene-X⊂**P**]$^{6+}$ (**P** = **P$_2$** – **P$_4$**) indicative of pyrene-X release from the host (black), ruthenium uptake determined by ICP-MS (grey)

The uptake mechanism of [pyrene-X⊂**P**]$^{6+}$ (**P** = **P$_2$** – **P$_4$**) was also studied, with uptake found to be both temperature and wortmannin-sensitive, (see Figure 46). Wortmannin blocks specific endocytic mechanisms and has been widely used to study intracellular transport mechanisms.[179] Combined, these data indicate that the uptake of [pyrene-X⊂**P$_2$**]$^{6+}$ involves endocytosis/macropinocytosis, rather than passive diffusion across the cell membrane.

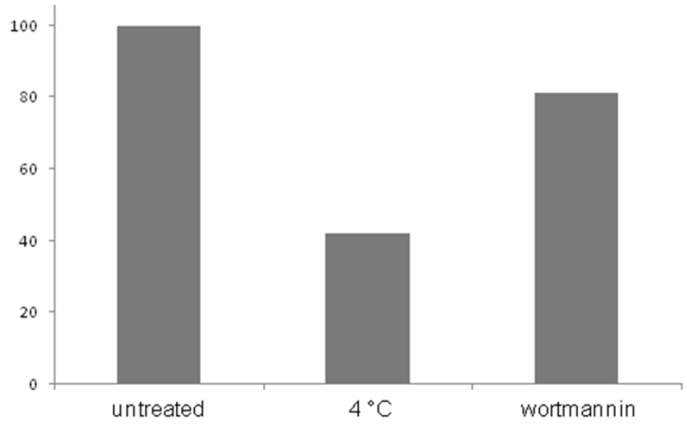

Figure 46. Intracellular fluorescence quantification by flow cytometry of A2780 incubated with [pyrene-X⊂**P$_2$**]$^{6+}$ either after 1 h pre-incubation in culture medium (untreated), or pre-incubated at 4 °C, or wortmannin. Results represent the percentage of fluorescence

Following release of pyrene-X from the host, confocal microscopy was used to show that the pyrene-X stains vesicle-like cytoplasmic organelles, and accumulates in the intracellular vesicle part of the cell endocytotic system.[180] In order to identify the organelles, their fluorescence pattern was compared to that of the lysosomal dye lysotracker Red and the fluid phase endocytosis marker FITC-dextran.[181] This study shows that the free pyrene-X does not enter lysosomal compartments and does not accumulate in the endocytic compartments that are enriched in FITC-dextran. Consequently, these data suggest that pyrene-X accumulates in endocytic compartments rather than lytic compartments.

In this study,[182] we described the synthesis, characterisation, host-guest properties and *in vitro* activity of a modular and adjustable supramolecular drug delivery system based on arene ruthenium metalla-prisms. The cellular uptake of the host-guest systems is likely to involve an active transport mechanism, and that following uptake into the cell, the rate of release of the guest molecule depends on the portal size of the host. This study paves the way for the rational design of host-guest systems that can function in a time-controlled manner.

3.3 Arene Ruthenium Metalla-Prisms and Dendrimers

3.3.1 General

Dendrimers are a polymeric class of compounds that can possess different shapes (spherical, ellipsoidal or cylindrical), different sizes and structures depending of the dendrimer generation, and different cores and peripheral groups.[183] This high number of possibilities in designing dendrimers has a strong impact on the physical and chemical properties of these molecules.[184] Moreover, since their development in the 1980s, many efforts have been made by chemists in order to facilitate the synthesis of these "cascade molecules". In particular Newkome,[185] Tomalia,[186] Fréchet,[187] have provided numerous new strategies to synthesise dendritic systems. The versatility and the accessibility of dendrimers have found several applications, in liquid-crystal chemistry,[188] in materials,[189] and also in biochemistry.[190] From antibacterial drugs by copper's polypropylenimine (PPI) dendrimers,[191] to antiviral drugs by Majoral's poly-(phosphor-hydrazone) dendrimers with terminal phosphonic acid and alkyl chain groups,[192] many examples of dendrimers used as biological agents can be found in the literature. Among others, we can cite Tomalia's polyamidoamine (PAMAM),[186] Denkewalter's poly-(L-lysine),[193] Newkome's polyamide,[189] Vögtle's polypropylenimine,[194] and Hult's poly-(2,2-bis(hydroxymethyl) propionic acid (bis-MPA)[195] dendrimers. The host-guest properties of some dendrimers have even allowed their successful utilisation as drug carriers,[196] while their combination with metallic atoms has led to the discovery of new possible anticancer agents with novel mechanisms of action.[176c]

On the other hand, the previously described modular and adjustable supramolecular drug delivery system based on arene ruthenium metalla-prisms led to the biological determination of the antiproliferative activities of different host-guest systems (see section 3-2).[197] In this study, the impact of the portal size of three different metalla-prisms ($\mathbf{P_2 - P_4}$) on the association constants was studied in the presence of one guest molecule pyrene-X and was correlated to the biological activities of the host-guest systems. Now we set out to study the impact of the size of the guest molecule, without modifying the structure of the host metalla-prism. Therefore, a series of large pyrenyl-containing dendrimers of different generations were prepared, *i.e.* 4'-cyanobiphenyl-4-yl-4-(10-(4-(pyren-1-yl)butanoyloxy)decyloxy)benzoate (pyrene-G_0), bis(10-(4-((4'-cyanobiphenyl-4-

yloxy)carbonyl)phenoxy)decyl)-5-(4-(pyren-1-yl)butanoyloxy)isophthalate (pyrene-G_1), and bis(di(10-(4-((4'-cyanobiphenyl-4-yloxy)carbonyl)phenoxy)decyl)5-hydroxyisophthalate)-5-(4-(10-(4-(pyren-1-yl)butanoyloxy)decyloxy)benzoyloxy)isophtalate (pyrene-G_2). The pyrenyl units were encapsulated in the hydrophobic cavity of the hexanuclear arene ruthenium metalla-prism $[(\eta^6\text{-}p\text{-cym})_6Ru_6(donq)_3(tpt)_2]^{6+}$ (**P_2**). The cytotoxicity of these resulting host-guest systems, [pyrene-G_0⊂**P_2**]$^{6+}$, [pyrene-G_1⊂**P_2**]$^{6+}$, and [pyrene-G_2⊂**P_2**]$^{6+}$, was evaluated and correlated to their size.

3.3.2 Encapsulation of Pyrenyl-Modified Dendrimers and Host-Guest Properties

The synthesis of the guest molecules pyrene-G_0, pyrene-G_1, and pyrene-G_2 involves different generations of cyanobiphenyl dendritic precursors, 4'-cyanobiphenyl-4-yl-4-(10-hydroxydecyloxy)benzoate (G_0), bis(10-(4-((4'-cyanobiphenyl-4-yloxy)carbonyl)phenoxy)decyl) 5-hydroxyisophthalate (G_1) and bis(di(10-(4-((4'-cyanobiphenyl-4-yloxy)carbonyl)phenoxy)decyl)-5-hydroxyisophthalate)-5-(4-(10-hydroxydecyloxy)benzoyloxy)isophtalate (G_2). The precursors G_0, G_1 and G_2 have been reported previously,[198] and pyrene-G_0, pyrene-G_1, and pyrene-G_2 were prepared by an esterification reaction between 1-pyrenebutyric acid and the different generations of cyanobiphenyl dendrimers, (see Scheme 8). In the case of G_2, an arm comprising an aliphatic $C_{10}H_{20}$ chain was included to provide flexibility to this large dendritic moiety and to increase the yield of the coupling reaction.

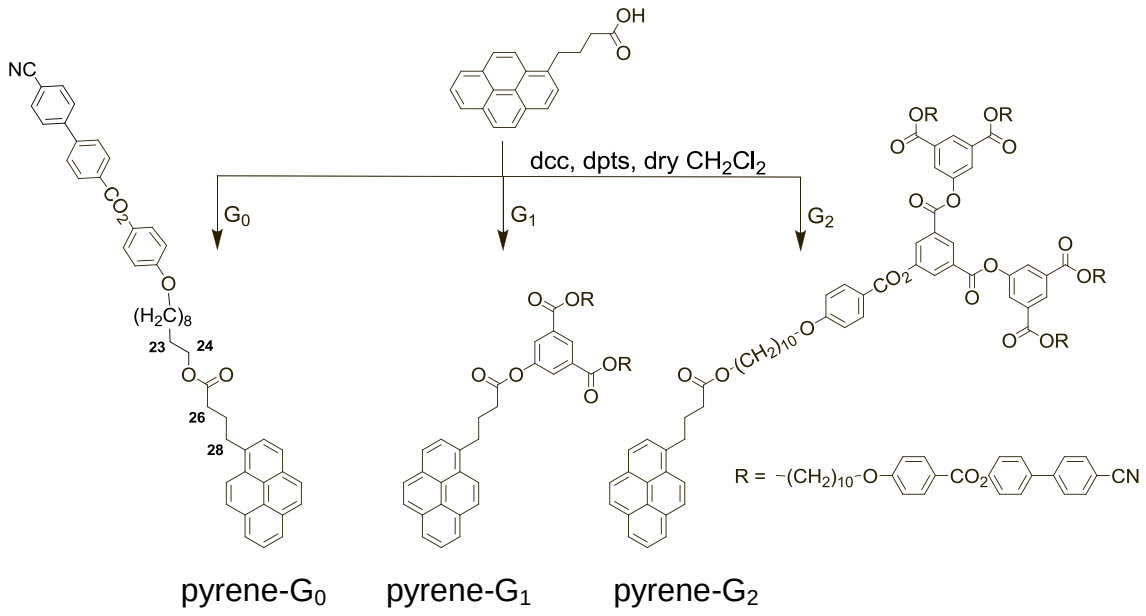

Scheme 8. Syntheses of pyrene-G_0, pyrene-G_1, and pyrene-G_2 (dcc = *N*,*N*'-dicyclohexylcarbodiimide, dpts = 4-(dimethylamino)pyrimidium para-toluenesulfonate)

The esterification reactions were monitored by NMR spectroscopy with signals of protons H_{26}, H_{27}, and H_{28} of the pyrenyl unit being shifted slightly upfield (by up to 0.05 ppm relative to 1-pyrenebutyric acid) after coupling (see Scheme 1 for assignment). Additionally, a strong modification of the chemical environment of protons H_{24} and H_{23} of the dendritic part leads to a significant upfield shift of 0.44 ppm of the resonance in the case of proton H_{24}, and by 0.05 ppm for H_{23}, confirming the formation of pyrene-G_0, pyrene-G_1, and pyrene-G_2.

Encapsulation of the pyrenyl moiety into metalla-prism $[\mathbf{P_2}]^{6+}$ is straightforward with P_0 and P_1; addition of silver trifluoromethanesulfonate to the dinuclear metalla-clip $[(\eta^6\text{-}p\text{-cym})_2Ru_2(donq)Cl_2]$ in the presence of tpt panels and the guest molecule leads to the formation of [pyrene-$G_0\subset\mathbf{P_2}$][CF_3SO_3]$_6$ and [pyrene-$G_1\subset\mathbf{P_2}$][CF_3SO_3]$_6$, respectively. In the case of pyrene-G_2, direct encapsulation requires 2 days and dichloromethane is needed to solubilise pyrene-G_2 and to afford the desired system [pyrene-$G_2\subset\mathbf{P_2}$][CF_3SO_3]$_6$. All the complexes were isolated as trifluoromethanesulfonate salts and are highly soluble in apolar solvents such as dichloromethane, but also in polar solvents and in particular in water. Molecular modelling was performed with HyperChem to estimate the shape and size of all these complexes in the gas phase, (see Figure 47).

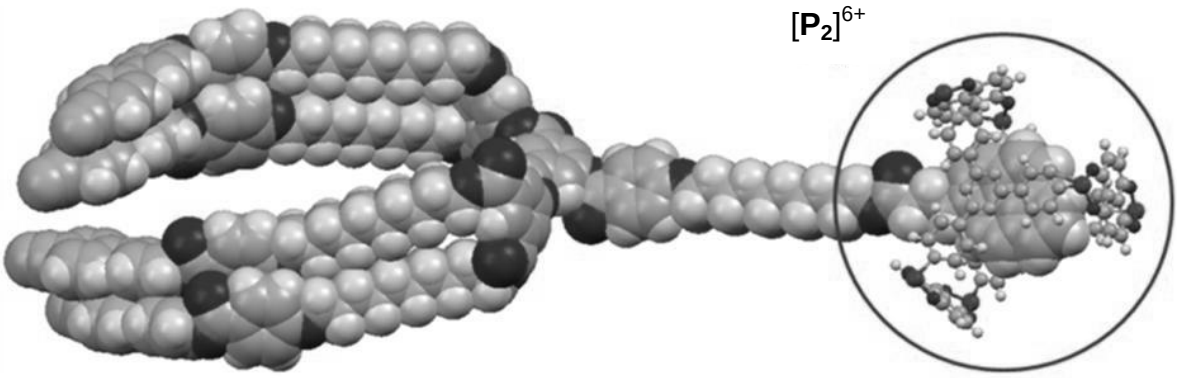

Figure 47. Hyperchem simulation of [pyrene-G_2⊂**P₂**]$^{6+}$, arene ligands omitted for clarity

The HyperChem simulations show, as expected, the dendritic arm extending from the cavity with the pyrene moiety encapsulated in the cavity of the prism. The complexes also possess two distinct regions, a hydrophilic head constituted by the hexacationic metalla-cage and a lipophilic tail formed by the dendritic part. Such amphiphilicity is highly relevant with respect to the biological properties of these compounds.[199]

The host-guest properties of the complexes were studied in solution by a combination of NMR, UV-visible and fluorescence spectroscopy. ^{1}H NMR titrations of pyrene-G_0, pyrene-G_1 in the presence of [**P₂**]$^{6+}$ were performed in CD_3CN at room temperature. In the case of pyrene-G_2 broadening of the signals precludes such an analysis.

Upon gradual addition of guest molecule pyrene-G_0 or pyrene-G_1 (0.1 – 3.0 equivalents) to a CD_3CN solution of [**P₂**][CF_3SO_3]$_6$ (4.0 mM), the ^{1}H NMR spectra show displacements of the chemical shifts of some of the protons of both the host and the guest. The broadening and chemical shifts of the signals support a rapid inclusion of the guest molecule into the cavity of [**P₂**]$^{6+}$. Plots of these chemical shift changes, $\Delta\delta$, for the H_β proton of the tpt ligands *versus* the molar ratio of pyrene-G_0 or pyrene-G_1 to the prism [**P₂**]$^{6+}$ indicate a 1:1 stoichiometry of the host-guest systems. From these plots, stability constants of association, K_a, were estimated by using the non-linear least square fitting program winEQNMR2 (see Table 6). The binding free energies, ΔG^o, for [pyrene-G_0⊂**P₂**]$^{6+}$ and [pyrene-G_1⊂**P₂**]$^{6+}$ were determined from the corresponding association constants obtained at 21 ºC in CD_3CN and in all cases ΔG^o is inferior to -5.80 kcal · mol^{-1}.

Table 6. Association constants (K_a) and free energies for the encapsulation of pyrene-G_0, pyrene-G_1 and pyrene-G_2 in $[\mathbf{P_2}]^{6+}$ determined by ^{1}H NMR titration (CD_3CN at 21°C, 4.0 mM concentration of $[\mathbf{P_2}]^{6+}$) and by UV–visible method (CH_2Cl_2 at 21°C)

guest ⊂ **host**	K_a (10^4 M^{-1})[a]	K_a (10^4 M^{-1})[b]	ΔG^o (kcal · mol^{-1})
pyrene-G_0⊂$\mathbf{P_2}$	4.1	7.8	-6.29
pyrene-G_1⊂$\mathbf{P_2}$	1.9	2.7	-5.83
pyrene-G_2⊂$\mathbf{P_2}$	ND	0.8	-5.36

[a] determined by NMR [b] determined by UV-visible

Since the association constant of [pyrene-G_2⊂$\mathbf{P_2}$]$^{6+}$ could not be determined by NMR titration due to broadening of the signals, this constant was estimated using UV–visible spectroscopy, employing a widely used method for the study of binding phenomena (particularly suited to 1:1 host-guest systems).[200] Aliquots of a CH_2Cl_2 solution of guest molecule pyrene-G_2 were added to a CH_2Cl_2 solution of $[\mathbf{P_2}][CF_3SO_3]_6$ ($[\mathbf{P_2}]$/[pyrene-G_2] = 0 to 2 eq), and the mixtures were analysed by UV–vis spectroscopy at 21 ºC. Based on changes to the absorbance (see Figure 48 for the UV–vis titration of $[\mathbf{P_2}]^{6+}$ with pyrene-G_2), and applying the Rose and Drago equation,[201] the association constant of [pyrene-G_0⊂$\mathbf{P_2}$]$^{6+}$, [pyrene-G_1⊂$\mathbf{P_2}$]$^{6+}$ and [pyrene-G_2⊂$\mathbf{P_2}$]$^{6+}$ was estimated (see Table 6). The K_a values for [pyrene-G_0⊂$\mathbf{P_2}$]$^{6+}$ and [pyrene-G_1⊂$\mathbf{P_2}$]$^{6+}$ obtained using UV–visible spectroscopy are consistent with the values estimated by ^{1}H NMR titrations.

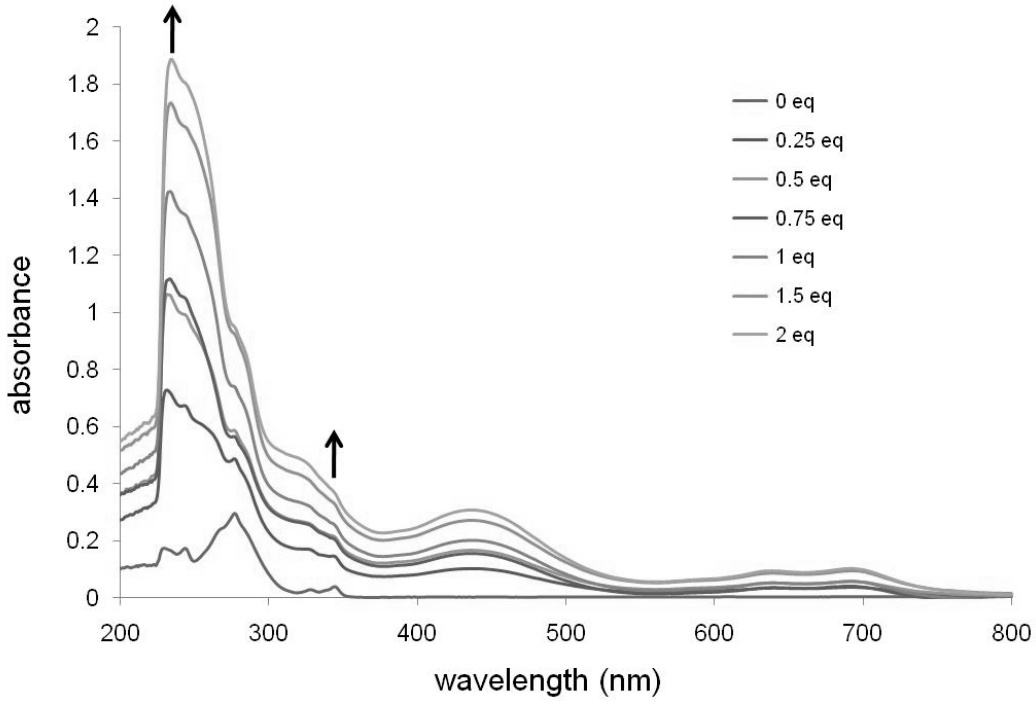

Figure 48. UV–vis titration of $[\mathbf{P_2}]^{6+}$ in a CH_2Cl_2 solution of pyrene-G_2 (10^{-5} M) at 21 °C

A decrease of the kinetics of encapsulation is observed with the increase of the generation of dendrimer precursors graft onto the pyrene moiety. This can be easily understood since the pyrenyl part of the molecule is less accessible for the encapsulation with a larger generation than with a shorter generation. The association constants are quite high and free energies ($\Delta G°$ up to -5.3 kcal · mol^{-1}) demonstrate a preference for the encapsulated systems over the dissociated systems.

3.3.3 Antiproliferative Study

The antiproliferative activity of the pyrenyl-containing dendrimers pyrene-G_0, pyrene-G_1, and pyrene-G_2, the complex $[\mathbf{P_2}][CF_3SO_3]_6$ and the host-guest systems $[\text{pyrene-}G_0\subset\mathbf{P_2}]^{6+}$, $[\text{pyrene-}G_1\subset\mathbf{P_2}]^{6+}$ and $[\text{pyrene-}G_2\subset\mathbf{P_2}]^{6+}$ were evaluated against the A2780 (cisplatin sensitive) and A2780cisR (cisplatin resistant) human ovarian cancer cell lines. Their cytotoxicities, in comparison to cisplatin, are presented in Table 7. The pyrenyl-containing dendrimers pyrene-G_0, pyrene-G_1, and pyrene-G_2 are inactive against both A2780 and A2780cisR cancer cells, probably due to poor water solubility resulting in their precipitation from the cell culture medium. The water-soluble metalla-prism $[\mathbf{P_2}]^{6+}$ is quite cytotoxic and

the host-guest systems are even more cytotoxic, in the case of [pyrene-G_0⊂**P_2**][CF_3SO_3]$_6$ the IC_{50} value (0.4 μM) is an order of magnitude more cytotoxic than the empty cage. The IC_{50} values of [pyrene-G_1⊂**P_2**][CF_3SO_3]$_6$ and [pyrene-G_2⊂**P_2**][CF_3SO_3]$_6$ are similar to the IC_{50} value of the empty cage alone [**P_2**][CF_3SO_3]$_6$. High generations of dendritic systems are known to be biocompatible, and tend to show different levels of cytotoxicity,[202] however due to the lipophilic nature of pyrene-G_n, their intrinsic cytotoxicity could not be established in this study. It is noteworthy that [**P_2**]$^{6+}$ and the host-guest compounds show similar cytotoxicities on both the cisplatin sensitive and the cisplatin resistant cancer cell lines, indicating that they do not share the same mechanism of action than the reference drug cisplatin.

Table 7. IC_{50} values of pyrenyl-containing dendrimers pyrene-G_0, pyrene-G_1, pyrene-G_2 and complexes [**P_2**][CF_3SO_3]$_6$ and [pyrene-G_0 − pyrene-G_2⊂**P_2**][CF_3SO_3]$_6$ on A2780 and A2780cisR cell lines

compound	A2780 (IC_{50}, μM)	A2780cisR (IC_{50}, μM)
pyrene-G_0	ND	ND
pyrene-G_1	ND	ND
pyrene-G_2	ND	ND
[**P_2**][CF_3SO_3]$_6$	3.1 ± 1.0	4.6 ± 0.5
[pyrene-G_0⊂**P_2**][CF_3SO_3]$_6$	0.4 ± 0.1	0.5 ± 0.4
[pyrene-G_1⊂**P_2**][CF_3SO_3]$_6$	2.2 ± 1.1	2.4 ± 0.8
[pyrene-G_2⊂**P_2**][CF_3SO_3]$_6$	2.6 ± 0.8	2.8 ± 1.0
cisplatin	1.6 ± 0.6	8.6 ± 0.6

The synthesis of three new pyrenyl-containing dendrimers and their encapsulation into a water-soluble arene-ruthenium metalla-prism was described.[197] The host-guest systems, [pyrene-G_n⊂**P_2**][CF_3SO_3]$_6$, are remarkably stable in solution as shown from NMR, UV−visible and fluorescence spectroscopic studies. The cytotoxicity of the host-guest systems have been evaluated on human ovarian A2780 and A2780cisR cancer cell lines and an increase by one order of magnitude in cytotoxicity was observed for [pyrene-G_0⊂**P_2**][CF_3SO_3]$_6$ compared to the empty metalla-prism. The cytotoxicity of the higher generations of encapsulated dendrimers, [pyrene-G_1⊂**P_2**][CF_3SO_3]$_6$ and [pyrene-

$G_2 \subset \mathbf{P_2}][CF_3SO_3]_6$, was found to be equivalent to that of the cage alone. Notably, for the first time, this study demonstrated that metalla-cage host systems are able to deliver hydrophobic guest molecules with extremely large appendages into cancer cells.

Chapter 4: Arene Ruthenium Metalla-Cubes

4.1 Antiproliferative Activity of Arene Ruthenium Metalla-Cubes

4.1.1 General

Most solid tumours possess a unique extracellular environment comprising a hypervasculature, a defective vascular architecture, and impaired lymphatic drainage. The resulting enhanced vascular permeability of solid tumours has become an effective way to target cancer cells. While the normal endothelial layer surrounding the blood vessels feeding healthy cells restricts the size of molecules that can diffuse from the blood, the endothelial layer of blood vessels in diseased tissues is more porous towards large molecules providing access to the surrounding cancer cells. Moreover, diseased tissue does not usually have a lymphatic drainage system, so once large molecules have entered the tumour environment they are more likely to be retained. This passive targeting of tumours by large molecules is referred to as the "enhanced permeability and retention" (EPR) effect.[102]

On the other hand, due to the clinical success of platinum-based cancer drugs, macromolecular derivatives have been evaluated in an attempt to target tumours more effectively to reduce the severe toxic side effects and to overcome resistance associated with platinum agents.[203] In particular, in recent years ruthenium compounds have been shown to exhibit promising anticancer activity, since ruthenium complexes are believed to bind with large biomolecules[204] in the plasma and consequently could take advantages of the EPR effect. However, larger multinuclear ruthenium complexes could potentially use the EPR effect without having to bind to biomolecules.

The deve lopment of arene ruthenium metalla-rectangles and arene ruthenium metalla-prisms led to the synthesis of large structures that show a pronounced size effect and that are possibly able to selectively target cancer cells *via* the EPR effect. The cytotoxicity of these metalla-assemblies being promising we decided to synthesize larger metalla-assemblies. Thus, we synthesised a series of octanuclear metalla-cubes **Q_1** – **Q_8**, of general formula $[(\eta^6\text{-arene})_8Ru_8(OO\cap OO)_4(NN\cap NN)_2]^{8+}$ (arene = *p*-cym (**Q_1** – **Q_6**), indane (**Q_7**), nonylbenzene (**Q_8**); *OO*∩*OO* = ox (**Q_1** – **Q_3**), dobq (**Q_4** – **Q_8**); *NN*∩*NN* = 5,10,15,20-tetra(4-

pyridyl)porphyrin (tpp-2H) (**Q$_1$**, **Q$_4$**, **Q$_7$** and **Q$_8$**), 5,10,15,20-tetra(4-pyridyl)porphyrin-Ni(II) (tpp-Ni) (**Q$_2$** and **Q$_5$**), 5,10,15,20-tetra(4-pyridyl)porphyrin-Zn(II) (tpp-Zn) (**Q$_3$** and **Q$_6$**), (see Figure 49). Thus, two new arene ruthenium dinuclear metalla-clips (**C$_0$**, **C$_1$**, [(η^6-indane)$_2$Ru$_2$(dobq)Cl$_2$] (**C$_{10}$**), [(η^6-nonylbenzene)$_2$Ru$_2$(dobq)Cl$_2$] (**C$_{11}$**)) were also synthesised, (see List of Structures).

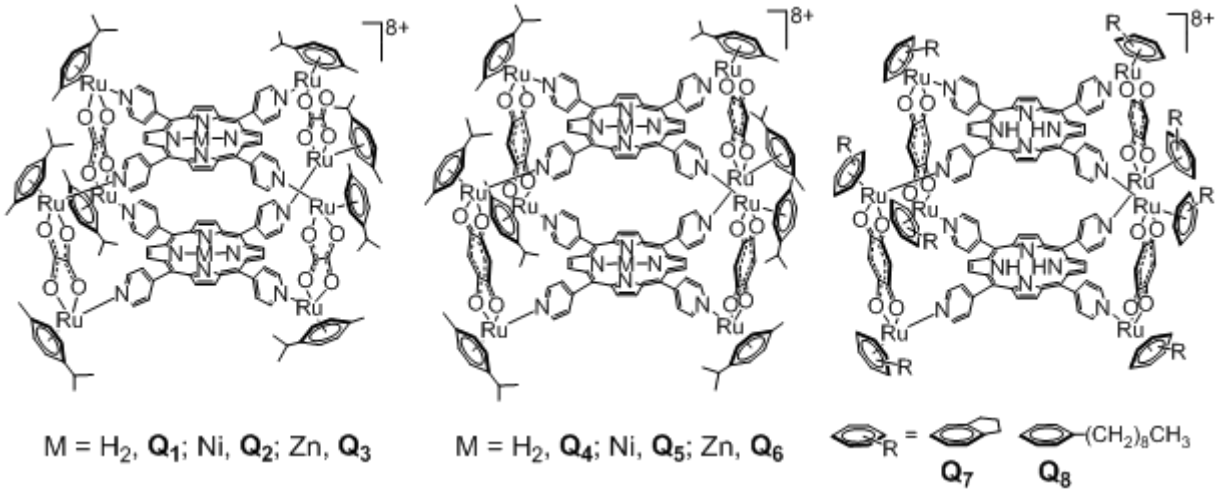

Figure 49. Metalla-cubes **Q$_1$** – **Q$_8$**

The antiproliferative activity of these metalla-cubes was established *in vitro* on human ovarian cancer cell lines. We also studied the formation of unsymmetrical metalla-cubes constructed from mixtures of different porphyrin panels during the synthesis of the cubes.

4.1.2 Synthesis and Characterisation of Arene Ruthenium Metalla-Cubes (Q$_1$ – Q$_8$)

As shown previously, the synthesis of arene ruthenium metalla-cubes **Q$_1$ – Q$_8$** is straightforward. Addition of silver trifluoromethanesulfonate to the dinuclear metalla-clips **C$_0$**, **C$_1$**, **C$_{10}$** and **C$_{11}$** in the presence of tpp-2H, tpp-Ni and tpp-Zn leads in good yield to the formation of **Q$_1$ – Q$_8$**, (see Scheme 9).[205] All the metalla-cubes were isolated as their trifluoromethanesulfonate salts and characterised by IR, NMR, ESI-MS and by elemental analysis (see below and Experimental). The metalla-cubes are quite soluble in dichloromethane, acetonitrile, acetone and DMSO and slightly soluble in methanol and water. The stability of the metalla-cubes in D_2O:DMSO-d_6 (90:10) was monitored by ^{1}H NMR spectroscopy and following 48 hours of heating at 60°C no degradation was observed.

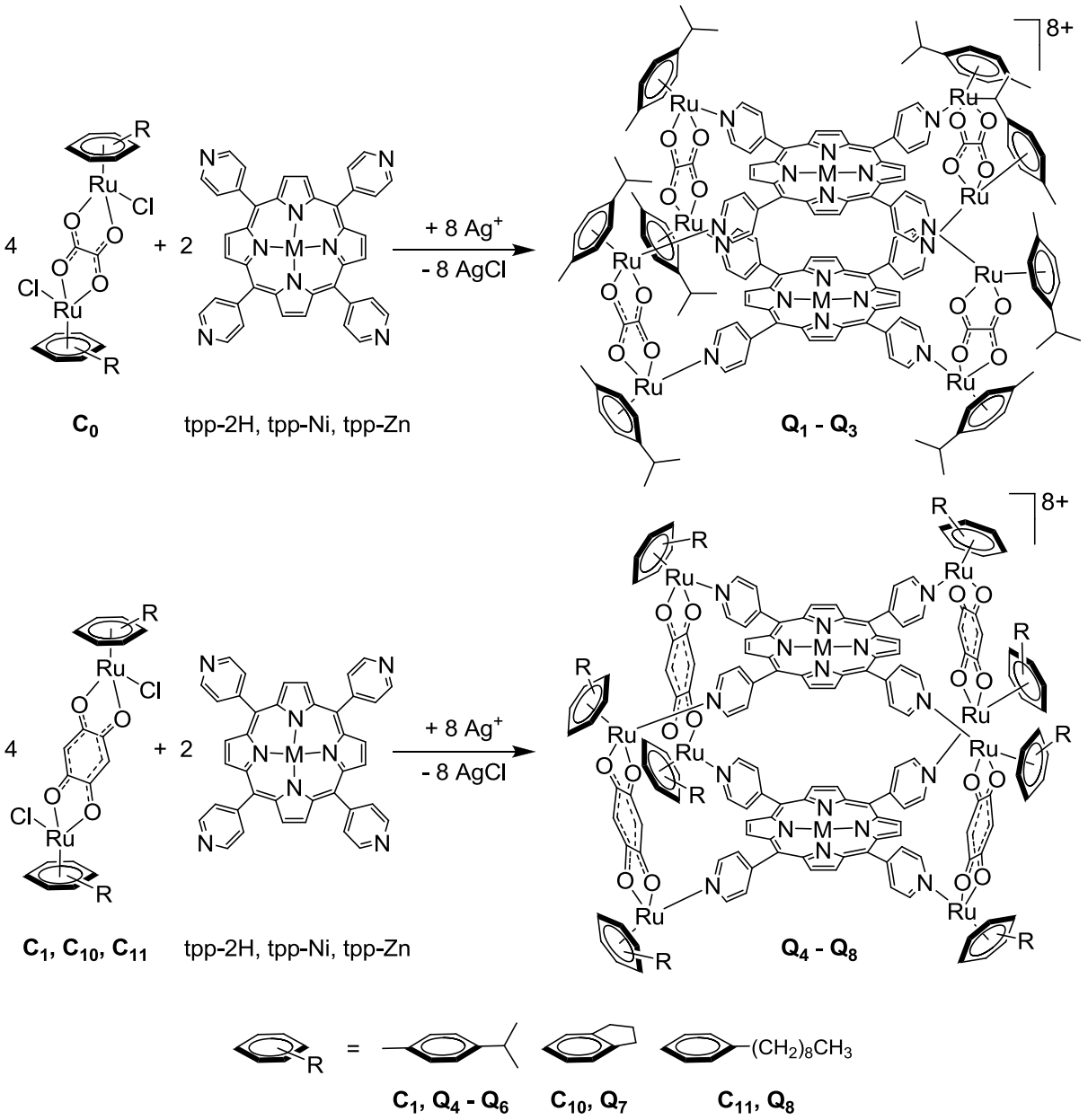

Scheme 9. Synthesis of metalla-cubes **Q_1 – Q_8** from metalla-clips **C_0**, **C_1**, **C_{10}** and **C_{11}**

The ^{1}H NMR spectra (in CD_3CN or CD_2Cl_2) of **Q_1 – Q_8** display a similar signal pattern to the corresponding porphyrin (tpp-2H, tpp-Ni or tpp-Zn) and arene protons. In the case of metalla-cubes **Q_1 – Q_8** (arene = *p*-cym) four doublets are observed in the region 6.2 – 5.9 ppm for the arene protons, whereas in **Q_7** (arene = indane) two doublets and two triplets and in **Q_8** (arene = nonylbenzene) one doublet of doublets, two doublets and one triplet are observed in the same region. In **Q_1**, **Q_4**, **Q_7** and **Q_8**, an additional signal at $\delta \sim$ -6.96 ppm corresponding to the N-H protons of the tpp-2H porphyrin panels are observed, while in **Q_4 – Q_8** the benzoquinonato singulet is observed at around 6.2 ppm. Moreover, the tpp panels give

between 9.5 and 7.0 ppm a total of six multiplets corresponding to four pyridyl and two pyrrole protons, (see Figure 50 for a COSY spectrum (7.3 ppm – 9.0 ppm) of **Q_4**).

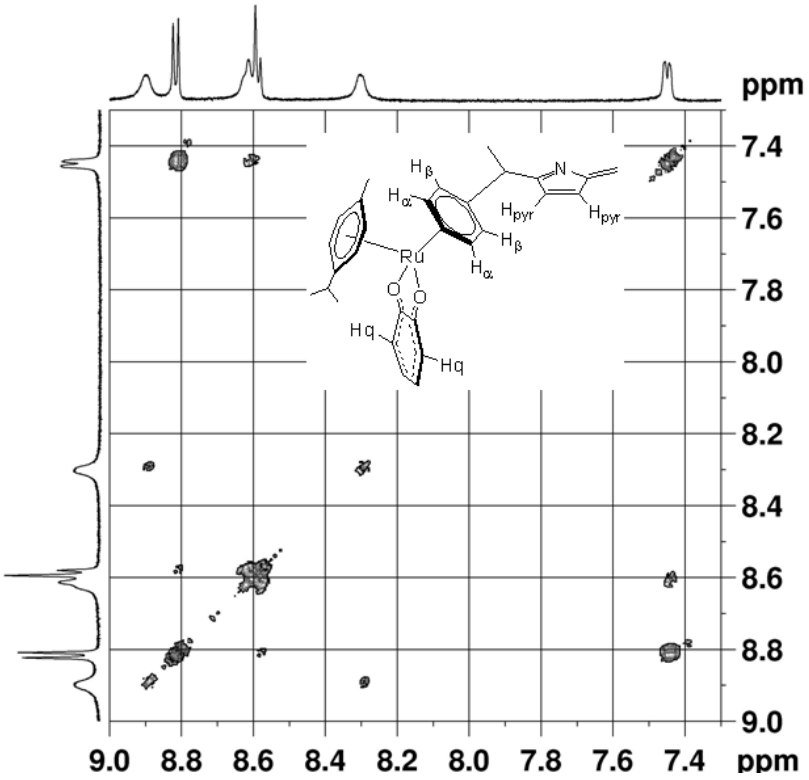

Figure 50. COSY spectrum (7.3 ppm – 9.0 ppm) of **Q_4**

The non-equivalence of the inner and outer pyridyl protons can be surprising, but it is explained by helical chirality, (see Scheme 10).[206] Indeed, the presence of diastereotopic protons is attributed to a tilt of the dinuclear metalla-clips and a twist of the two porphyrins panels, thus leading to a $P \leftrightarrow M$ helical conversion in "double rosette"-type architecture.[207]

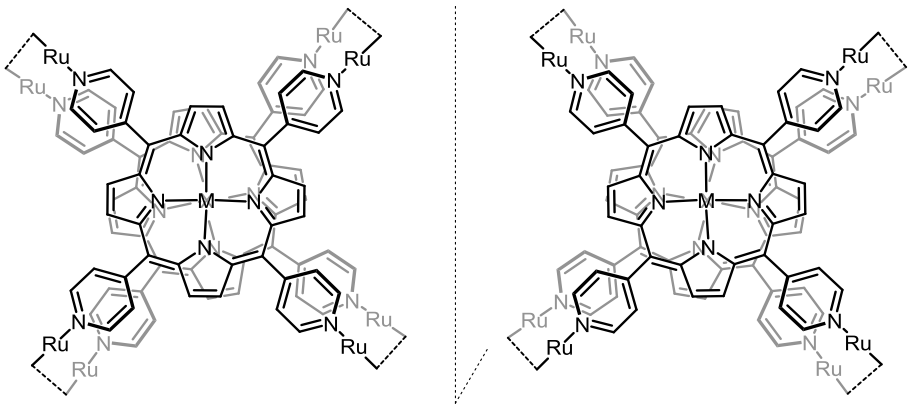

Scheme 10. Chiral conformation of metalla-cubes **$Q_1 - Q_8$**

Under the conditions of electrospray mass spectrometry (ESI-MS), all the metalla-cubes $\mathbf{Q_1}$ – $\mathbf{Q_8}$ are remarkably stable. The ESI-MS spectra of $\mathbf{Q_2}$ – $\mathbf{Q_8}$ show peaks corresponding to $[\mathbf{Q_2} + (CF_3SO_3)_4]^{4+}$, $[\mathbf{Q_3} + (CF_3SO_3)_4]^{4+}$, $[\mathbf{Q_4} + (CF_3SO_3)_4]^{4+}$, $[\mathbf{Q_5} + (CF_3SO_3)_4]^{4+}$, $[\mathbf{Q_6} + (CF_3SO_3)_4]^{4+}$, $[\mathbf{Q_7} + (CF_3SO_3)_4]^{4+}$ and $[\mathbf{Q_8} + (CF_3SO_3)_4]^{4+}$, at m/z 1045.0, 1048.7, 1067.3, 1095.5, 1099.3, 1035.5 and 1207.8, respectively, which are assigned unambiguously on the basis of their characteristic Ru_8 isotope pattern. Figure 51 shows the ESI-MS spectrum of $[\mathbf{Q_7}][CF_3SO_3]_8$ in acetonitrile.

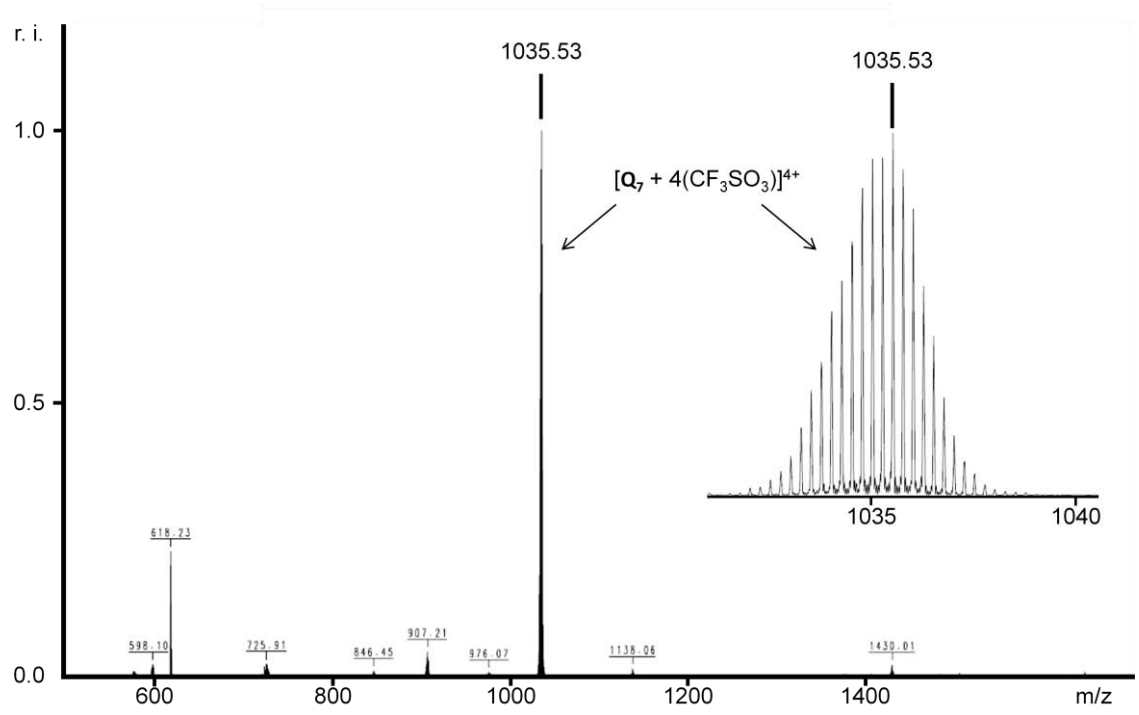

Figure 51. ESI-MS spectrum of $[\mathbf{Q_7}][CF_3SO_3]_8$

Electronic absorption spectra of $\mathbf{Q_1}$ – $\mathbf{Q_8}$ as well as the porphyrin panels (tpp-2H, tpp-Ni and tpp-Zn) were acquired in dichloromethane at 10^{-5} M concentration in the range 250–800 nm. The UV-visible spectra of all compounds are characterised by intense absorptions due to the porphyrin panels, including the Soret Band at around 400 nm and a series of Q bands between 500 and 700 nm. In all complexes, as compared to the free porphyrins, the Soret band is blue shifted and the full width at half-maximum ($\Delta\nu$) increased. In the case of metalla-cube $\mathbf{Q_7}$, the full width at half-maximum ($\Delta\nu$ = 1471 cm^{-1}) is 33% larger than the width of tpp-2H (1106 cm^{-1}). In all metalla-cubes a weak hypsochromic shift of the Soret band and a strong bathochromic shift of the Q bands are observed with respect to the free porphyrins. These photophysical changes in the UV-visible spectra of the metalla-cubes are

characteristic of sandwich-type porphyrin dimers.[208] UV-visible spectra in dichloromethane at 10^{-5} M of metalla-cubes **Q_2**, **Q_5**, **Q_7** and **Q_8** as well as tpp-2H and tpp-Ni are shown as example in Figure 52.

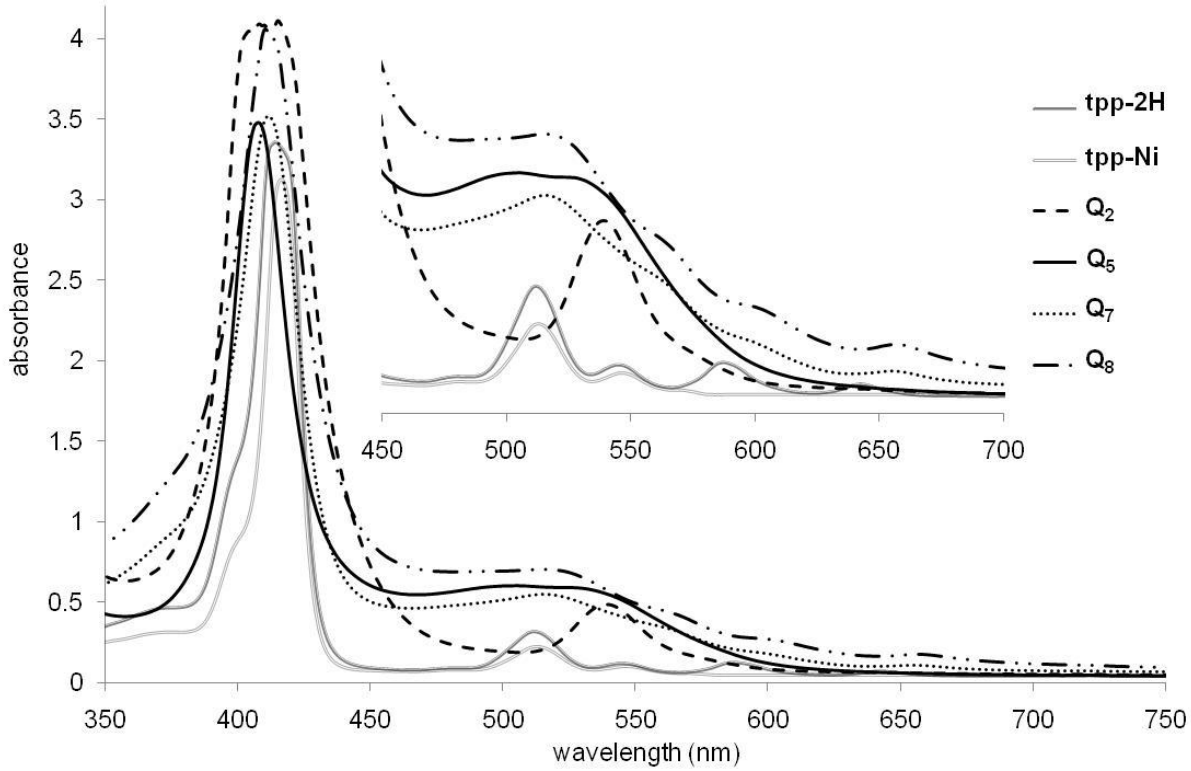

Figure 52. UV-visible spectra of tpp-2H, tpp-Ni and metalla-cubes **Q_2**, **Q_5**, **Q_7** and **Q_8** in CH_2Cl_2 (10^{-5} M)

4.1.3 **Unsymmetrical Metalla-Cubes ($Q_9 - Q_{11}$)**

As mentioned above, arene ruthenium metalla-cubes **$Q_1 - Q_8$** are particularly stable under the conditions of ESI-MS. For this reason, we used this technique to investigate the formation of unsymmetrical metalla-cubes, *i.e.* the formation of metalla-cubes built from two different porphyrin panels. Consequently, a stock solution of the dinuclear metalla-clip [(η^6-*p*-cym)$_2$Ru$_2$(dobq)Cl$_2$] with silver trifluoromethanesulfonate was freshly prepared in methanol. Next, mixtures containing equimolar amount of porphyrin panels (Mx$_1$: tpp-2H + tpp-Ni; Mx$_2$: tpp-2H + tpp-Zn; Mx$_3$: tpp-Ni + tpp-Zn; Mx$_4$: tpp-2H + tpp-Ni + tpp-Zn) were added to four fractions of the stock solution and heated at reflux for 48 hours leading to the formation of statistical mixtures of symmetrical and unsymmetrical metalla-cubes (in Mx$_1$: **Q_4** + **Q_5** + **Q_9**; Mx$_2$: **Q_4** + **Q_6** + **Q_{10}**; Mx$_3$: **Q_5** + **Q_6** + **Q_{11}**; Mx$_4$: **Q_4** + **Q_5** + **Q_6** + **Q_9** + **Q_{10}** + **Q_{11}**). The

precipitates obtained were directly analysed by ESI-MS without further purification or separation. All attempts to separate the metalla-cubes were unsuccessful. The proposed structures of the unsymmetrical metalla-cubes **Q$_9$**, **Q$_{10}$** and **Q$_{11}$** are presented in Figure 53.

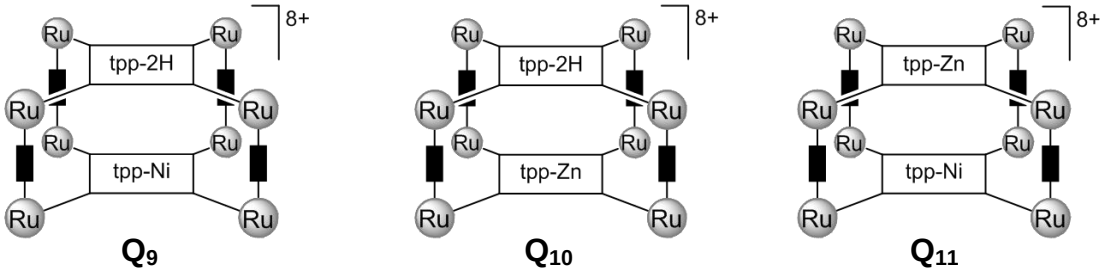

Figure 53. The unsymmetrical metalla-cubes **Q$_9$** − **Q$_{11}$**

The ESI-MS spectrum of a solution of Mx_1 shows the formation of the expected metalla-cubes [**Q$_4$**]$^{8+}$ and [**Q$_5$**]$^{8+}$ as well as the formation of the unsymmetrical metalla-cube [(η^6-*p*-cym)$_8$Ru$_8$(dobq)$_4$(tpp-2H)(tpp-Ni)]$^{8+}$ ([**Q$_9$**]$^{8+}$). In the same way, the formations of [(η^6-*p*-cym)$_8$Ru$_8$(dobq)$_4$(tpp-2H)(tpp-Zn)]$^{8+}$ ([**Q$_{10}$**]$^{8+}$) and [(η^6-*p*-cym)$_8$Ru$_8$(dobq)$_4$(tpp-Zn)(tpp-Ni)]$^{8+}$ ([**Q$_{11}$**]$^{8+}$) are observed in mixtures Mx_2 and Mx_3, respectively. Finally, in Mx_4, the formation of all unsymmetrical and symmetrical metalla-cubes can be observed by ESI-MS, (see Figure 54).

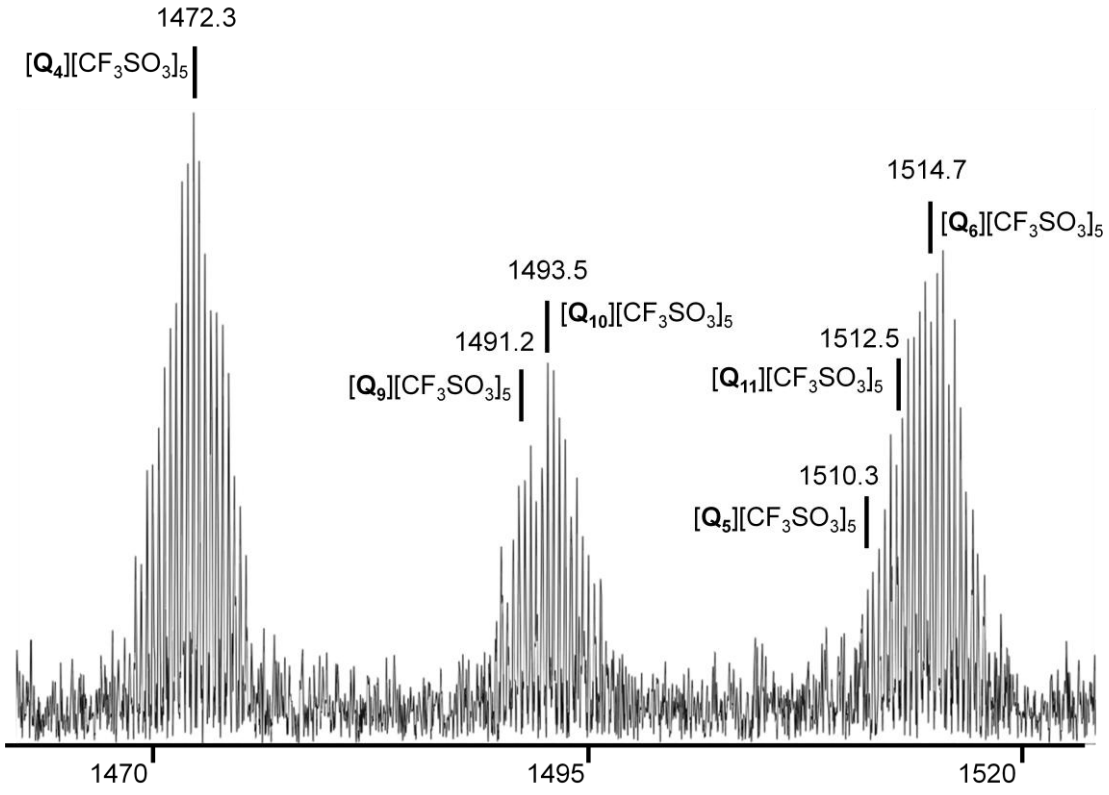

Figure 54. ESI-MS of Mx_4 showing the presence of **Q_4**, **Q_5**, **Q_6**, **Q_9**, **Q_{10}** and **Q_{11}**

4.1.4 Antiproliferative Study

The antiproliferative activity of the isolated metalla-cubes **$Q_1 - Q_8$**, the stoichiometric mixtures of metalla-cubes **$Q_4 - Q_6$** (entries 13 to 16) and the mixtures $Mx_1 - Mx_4$ containing the unsymmetrical metalla-cubes (entries 9 to 12) were evaluated against the A2780 (cisplatin sensitive) and A2780cisR (cisplatin resistant) human ovarian cancer cell lines. Their cytotoxicities, in comparison to cisplatin, are presented in Table 8. All compounds show similar cytotoxicities towards both cisplatin sensitive and cisplatin resistant cancer cell lines, suggesting that they do not share the same mechanisms of action than the reference drug, *i.e.* cisplatin. Moreover, among the compounds tested, additional trends can be drawn from these results: The oxalato containing metalla-cubes **$Q_1 - Q_3$** are at least an order of magnitude less cytotoxic than the 2,5-dioxydo-1,4-benzoquinonato analogues **$Q_4 - Q_6$**, indicating that the nature of the *OO*∩*OO* connecting spacer plays a crucial role. Similarly, the nature of the arene ligand can influence the cytotoxicity of the metalla-cubes. Indeed, the indane and nonylbenzene derivatives, **Q_7** and **Q_8** respectively, are significantly less cytotoxic than the

corresponding *p*-cym analogue **Q_4**. In contrast, metallation of the porphyrin core with the Zn^{2+} ion (metalla-cube **Q_6**) does not modify the activity while metallation with Ni^{2+} (metalla-cube **Q_5**) slightly reduces the cytotoxicity of the compound.

Table 8. IC50 values of complexes **Q_1 – Q_8**, Mx_1 – Mx_4 and stoichiometric mixtures of **Q_4 – Q_6** in A2780 and A2780cisR cell lines

	compound	A2780 (IC_{50}, μM)	A2780cisR (IC_{50}, μM)
1	**Q_1**	57.6 ± 1.9	44.2 ± 5.6
2	**Q_2**	41.5 ± 5.8	49.5 ± 8.9
3	**Q_3**	34.5 ± 7.5	35.7 ± 8.0
4	**Q_4**	8.0 ± 4.5	7.0 ± 4.5
5	**Q_5**	15.5 ± 4.5	14.8 ± 4.5
6	**Q_6**	7.6 ± 0.6	9.8 ± 0.4
7	**Q_7**	19.4 ± 4.5	21.5 ± 3.8
8	**Q_8**	21.2 ± 2.5	24.1 ± 5.2
9	Mx_1 (**Q_4** + **Q_5** + **Q_9**)	3.3 ± 1.1	2.2 ± 0.9
10	Mx_2 (**Q_4** + **Q_6** + **Q_{10}**)	2.8 ± 0.1	2.0 ± 0.5
11	Mx_3 (**Q_5** + **Q_6** + **Q_{11}**)	5.4 ± 1.3	4.3 ± 0.3
12	Mx_4 (**Q_4** + **Q_5** + **Q_6** + **Q_9** + **Q_{10}** + **Q_{11}**)	3.2 ± 0.4	2.5 ± 0.3
13	**Q_4** + **Q_5**	14 ± 3.9	16.2 ± 5.0
14	**Q_4** + **Q_6**	7.1 ± 1.5	9.2 ± 0.5
15	**Q_5** + **Q_6**	13.8 ± 5.2	16.4 ± 4.3
16	**Q_4** + **Q_5** + **Q_6**	12.4 ± 1.4	16.5 ± 1.3
17	cisplatin	2.2 ± 0.8	12.2 ± 1.2

Interestingly, the mixtures Mx_1 – Mx_4 containing the unsymmetrical metalla-cubes (entries 9 to 12) are the most cytotoxic, with activities comparable to cisplatin or superior to cisplatin in the resistant cancer cell line A2780cisR. This distinctive activity is most probably due to the presence of the unsymmetrical metalla-cubes **Q_9**, **Q_{10}** and **Q_{11}** but not due to an additive effect of the metalla-cubes as the stoichiometric mixtures of the symmetrical metalla-cubes (entries 13 to 16) clearly show, as expected, a cytotoxicity averaging the activity of the parent complexes **Q_4 – Q_6** (entries 4 to 6). It is not clear at the moment the reason for such a

different activity of the unsymmetrical metalla-cubes compared to their symmetrical counterparts, but it could be linked to a better internalisation of the products, to a different mode of interaction in the cell, or to a greater or lesser overall stability in the cellular environment. Nevertheless, these results are quite unexpected and further studies will be needed to provide an explanation for this difference in cytotoxicity between symmetrical and unsymmetrical metalla-cubes.

The synthesis of water-soluble metalla-cubes and of their *in vitro* anticancer activity against the A2780 and A2780cisR ovarian cancer cell lines showed that the larger assemblies were found to be highly active and equally potent on both cell lines.[209] It is likely that these large complexes would be taken up more efficiently by tumours due to the enhance permeability and retention effect of cancer cells, thus providing a degree of selectivity and ultimately giving a better efficacy. Further studies will be done to delineate the surprisingly low IC_{50} values observed for the unsymmetrical metalla-cubes.

4.2 Arene Ruthenium Metalla-Cubes as G-Quadruplex Binders

4.2.1 Background to G-Quadruplexes

Since the Nobel Prize in Physiology or Medicine 2009 was awarded jointly to Elizabeth H. Blackburn, Carol W. Greider and Jack W. Szostak "for the discovery of how chromosomes are protected by telomeres and the enzyme telomerase",[210] more than 5500 articles have been dedicated to the nature and the biological role of G-quadruplex, G-quadruplex stabilisers or telomerase. To understand the importance of this area of research, a definition of a G-quadruplex structure and the potential utilisation of such structure in medicine is needed.

Self-association of guanosine has been observed in solution already in the 19th century by the ready formation of polycrystalline gels. In the 1960's Gellert showed by crystallographic methods that this association of guanine bases is a tetrameric arrangement and Gellert described it as a G-quartet arrangement.[211] More precisely, the four guanine bases form a co-planar square where each base is both a hydrogen bond donor and a hydrogen bond acceptor. Utilisation of both the N_1 and N_2 of one face with the O_6 and N_7 of the second face on guanosine yields eight hydrogen bonds per planar G-quartet, giving to the structure a remarkable stability, (see Figure 55). Additional interactions stabilise this structure and the presence of a small cation like potassium or sodium is crucial.

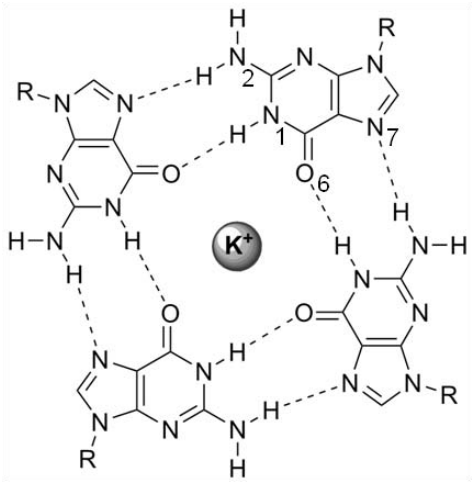

Figure 55. A guanine quartet with hydrogen bonds, including the central potassium cation. Deoxyribose sugars are removed for clarity

More interestingly, at millimolar concentrations of guanines in solution, a stacking of these quartets is observed. The driving force between the tetrads is the π – π stacking, and an energetic equilibrium is found when three quartets are stack on top of each other. This structure of three quartets of four guanines is called a G-quadruplex structure, (see Figure 56).[212]

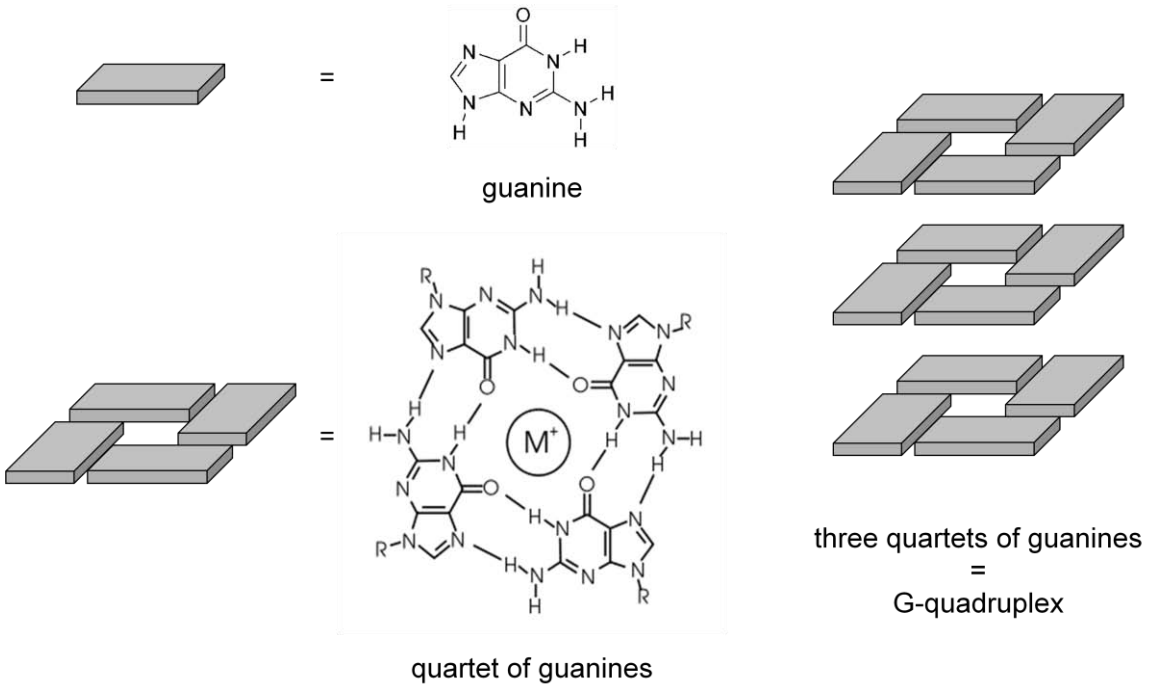

Figure 56. Schematic representation of a G-quadruplex

In reality, G-quadruplex structures are not simple arrangements of three quartets of four guanines. Indeed, these stacked tetrads align themselves with a regular rise and twist between the tetrad planes. This shape of the stacking leads to the generation of a right-handed helical twist. In this case the phosphate backbones, linking the nucleosides together, generate four grooves of variable width instead of two. This motif is called G-quadruplex DNA motif and possesses a similar appearance to that of duplex DNA, (see Figure 57).

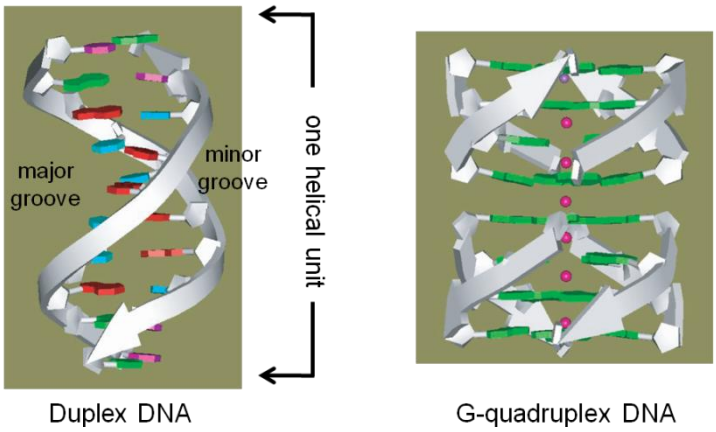

Figure 57. Duplex DNA and G-quadruplex DNA

A major breakthrough was made in the early 1990's by the chemist Blackburn with the discovery of guanine-rich repetitive sequences located at the end of chromosomes (telomeres), and the identification of a protein, with a reverse transcriptase activity, involved in their maintenance.[213] Then, it was quickly realised that these guanine-rich repetitive telomeric DNA sequences could form higher ordered structures, such as G-quadruplex, and they are likely to be involved in chromosomal maintenance. From this major discovery to nowadays, many studies have revealed several topologies for G-quadruplex DNA, depending on various factors such as the DNA sequence and the templating metal cation. For example, a very nice structure of G-quadruplex established by X-ray crystallography was published by Neidle in 2002, (see Figure 58).[214]

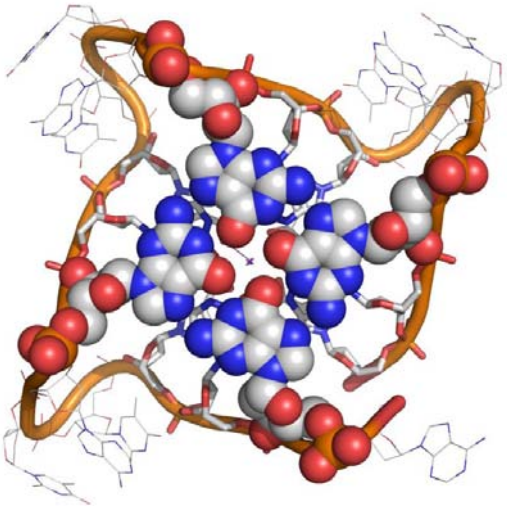

Figure 58. G-quadruplex structure

4.2.2 Biological Relevance of G-quadruplex DNA

Recent bio-informatic studies have shown that in the human genome there are approximately 350 000 guanine-rich sequences that can potentially form G-quadruplex DNA structures.[215] Some of these sequences have been identified as potential anticancer drug targets. For example, the formation of G-quadruplexes in human telomeric DNA has been shown to inhibit telomerase – an enzyme over-expressed in 85-90% of cancer cells, which plays an important role in cancer cell immortalization.[216] On the other hand, formation of G-quadruplex DNA structures in the promoter region of certain oncogenes (*e.g.* c-myc and c-kit) has been shown to control transcription of these genes and as a consequence their expression.[217]

An ongoing challenge in this area is to develop molecules that can interact strongly with G-quadruplex DNA but weakly with duplex DNA. Achieving this selectivity is essential to realise the potential advantages of G-quadruplex-targeting anticancer drugs. Most G-quadruplex DNA stabilisers reported to date are based on planar poly-aromatic compounds that interact with guanine quartets *via* $\pi - \pi$ stacking.[218] In addition, these molecules are often substituted with positively charged groups (*e.g.* protonated amines) to increase their solubility and also electrostatic interaction with the loops and grooves of DNA. However, often planar poly-aromatic molecules not only stack on top of the guanine quartet of G-quadruplexes, but also intercalate in between base-pairs of duplex DNA, thus reducing their selectivity for G-quadruplex *versus* duplex DNA.

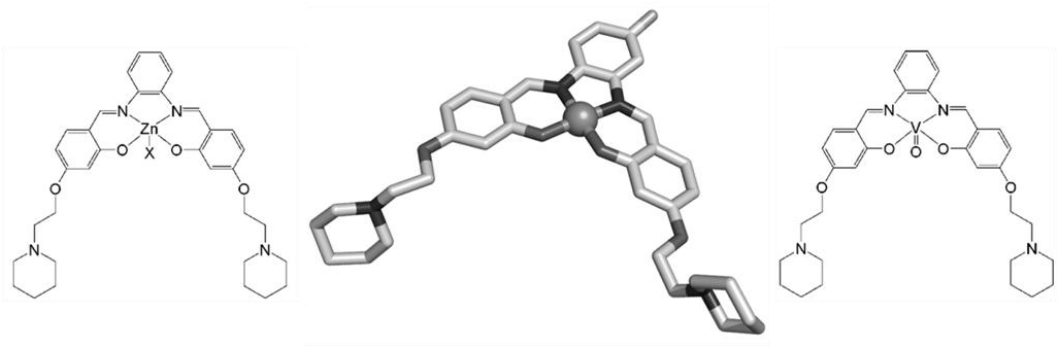

Figure 59. Metal salphen complexes as G-quadruplex DNA stabilisers

With the aim of reducing the undesired interactions between G-quadruplex-binding molecules and duplex DNA, square-based pyramidal metal complexes have been recently

reported as G-quadruplex DNA stabilisers, (see Figure 59).[219] The axial ligand in these complexes is proposed to reduce their ability to intercalate in between base pairs of duplex DNA. Polymetallic complexes where the metals are positioned outside the guanine quartet have also been recently reported to increase G-quadruplex DNA affinity and selectivity.[220] Cationic porphyrin derivatives have also attracted a great interest as G-quadruplex DNA stabilisers.[221] This interest is particularly due to a large surface for potential π stacking interactions with tetrads of guanines.[222] Finally, complexes from supramolecular chemistry have also been studied as G-quadruplex binders, in particular the palladium metalla-rectangle [Pt(ethylenediamine)(4,4′-bipyridyl)]$_4$ synthesised by Fujita.[223]

4.2.3 Synthesis of Arene Ruthenium Metalla-Cubes Q_{12} and Q_{13}

The arene ruthenium metalla-cubes previously described **Q_1 – Q_8** are built from porphyrin derivatives (tpp-2H, tpp-Ni and tpp-Zn). Porphyrins are known to bind strongly to G-quadruplex DNA, but their selectivity is usually poor since they also bind strongly to duplex DNA. We hypothesised that by linking two porphyrin rings *via* coordination bonds, their quadruplex binding ability would be retained, but their ability to intercalate in between bases of duplex DNA would be greatly reduced. Moreover, the arene ruthenium metalla-boxes are octoacationic and are water-soluble. Therefore we synthesised two new toluene ruthenium metalla-cubes **Q_{12}** and **Q_{13}** of general formula [(η^6-toluene)$_8$Ru$_8$(dobq)$_4$(*NN*∩*NN*)$_2$]$^{6+}$ (*NN*∩*NN* = tpp-2H (**Q_{12}**), tpp-Zn (**Q_{13}**)), (see Figure 60).

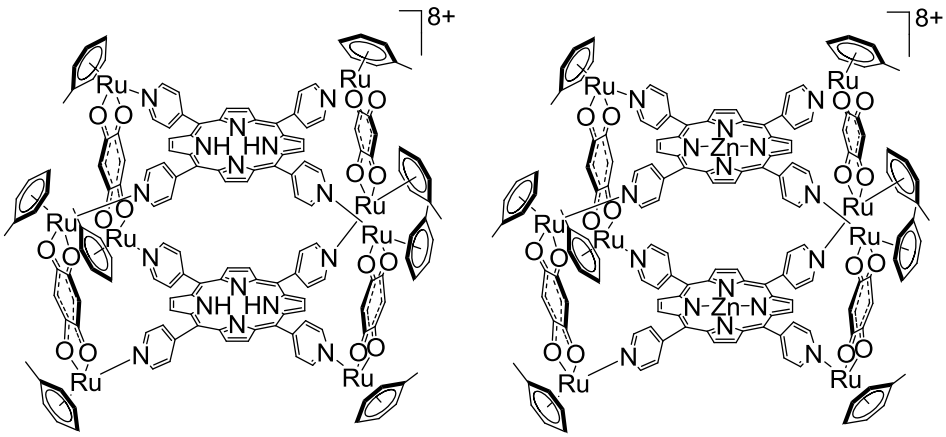

Q_{12} **Q_{13}**

Figure 60. Arene ruthenium metalla-cubes **Q_{12}** and **Q_{13}**

The synthesis of these two arene ruthenium metalla-cubes involves the reaction of four equivalents of new arene ruthenium dinuclear metalla-clip **C_{12}** of formula $[(\eta^6\text{-toluene})_2Ru_2(dobq)(Cl)_2]$ with eight equivalents of halide scavenger in the presence of two equivalents of porphyrin panel (either tpp-2H or tpp-Zn), (see Scheme 11).

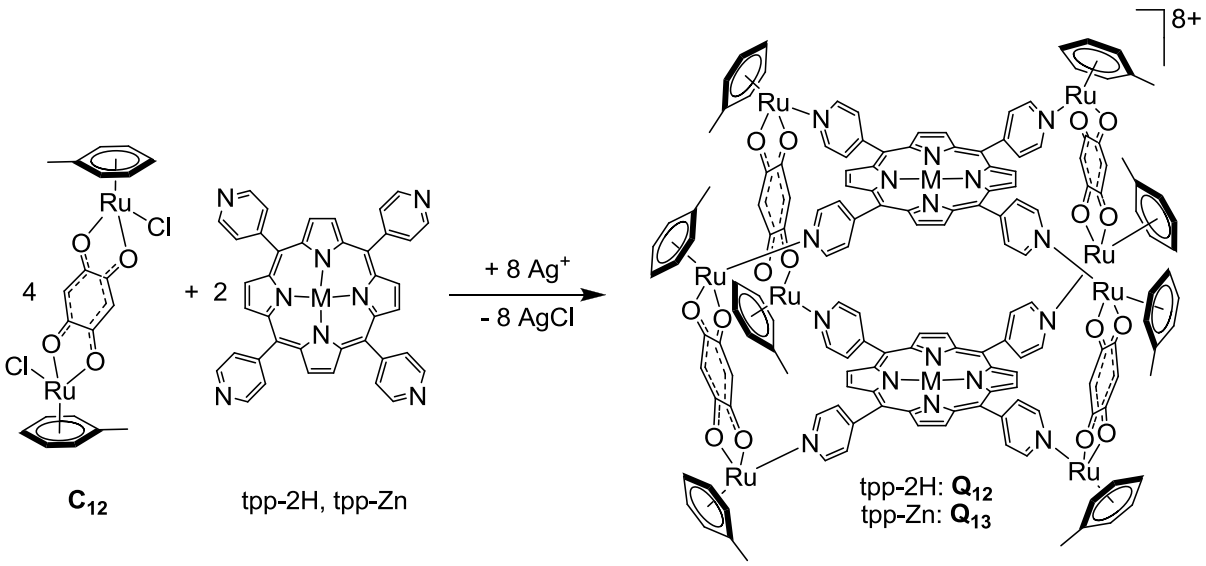

Scheme 11. Synthesis of arene ruthenium metalla-cubes **Q_{12}** and **Q_{13}**

The ^{1}H NMR spectra of **Q_{12}** and **Q_{13}** display signals of diastereotopic protons suggesting the same helical-type chirality previously observed with arene ruthenium metalla-cubes **$Q_1 - Q_8$**. Under conditions of electro-spray mass spectrometry, the cationic cubes **Q_{12}** and **Q_{13}** show a remarkable stability (see Figure 61): the ESI-MS spectra show peaks corresponding to $[\mathbf{Q_{12}} + (CF_3SO_3)_4]^{4+}$ and $[\mathbf{Q_{13}} + (CF_3SO_3)_4]^{4+}$ at m/z 983.0 and 1014.7, respectively. These peaks can be assigned unambiguously on the basis of their characteristic Ru_8 and Ru_8Zn_2 isotope patterns. Furthermore, in the ESI-MS spectra of $[\mathbf{Q_{12}}][CF_3SO_3]_8$ and $[\mathbf{Q_{13}}][CF_3SO_3]_8$ the second major peak corresponding to $[\mathbf{Q_{12}}][CF_3SO_3]_8$ and $[\mathbf{Q_{13}} + (CF_3SO_3)_5]^{3+}$ is observed at m/z 1359.3 and 1402.6, respectively.

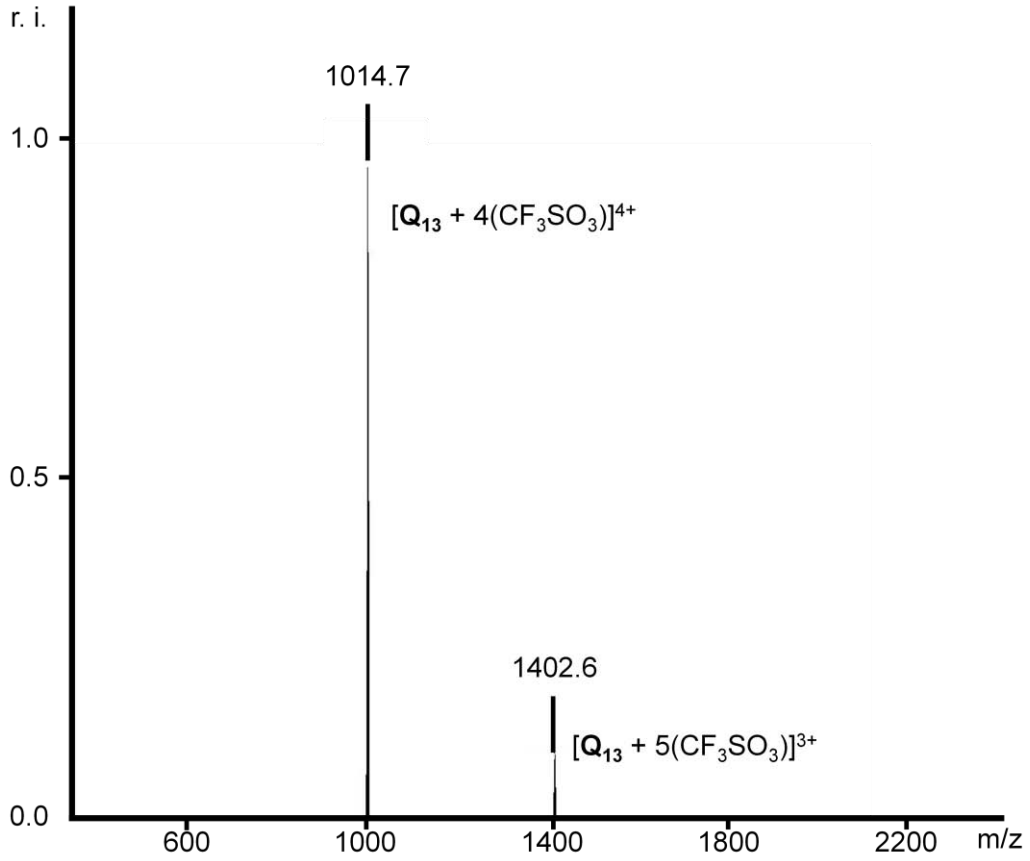

Figure 61. ESI-MS spectrum of $[\mathbf{Q_{13}}][CF_3SO_3]_8$

4.2.4 Interactions of some Arene Ruthenium Metalla-Cubes with DNA

In order to evaluate the ability of toluene ruthenium complexes $\mathbf{Q_{12}}$ and $\mathbf{Q_{13}}$ to interact with G-quadruplex and duplex DNA, fluorescence intercalation displacement (FID) assays were carried out.[224] Moreover, in order to compare the influence of the peripheric arene ligand on these interactions, corresponding para-cymene ruthenium metalla-cubes $\mathbf{Q_4}$ and $\mathbf{Q_6}$ were also tested.

In this recently reported assay thiazole orange (TO) is mixed with G-quadruplex DNA with which it interacts in a single-site manner and with high affinity. The fluorescence of this dye is quenched in solution, however, upon interaction with G-quadruplex DNA, it displays up to a 3000-fold increase in its emission. Therefore, displacement of TO by another molecule provides a measure of the affinity of the compound for G-quadruplex or duplex DNA, (see Figure 62).

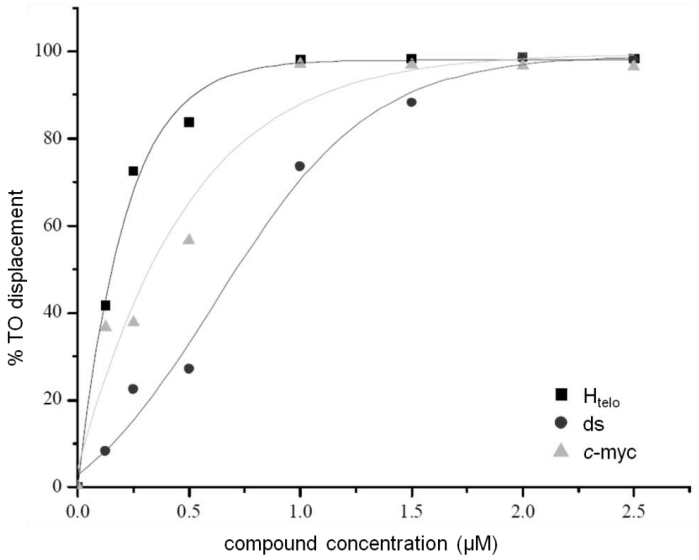

Figure 62. Representation of the TO displacement from H_{telo} (■), *c*-myc (▲) G-quadruplex DNA and ds (●) duplex DNA upon increasing concentration of **Q_4** (0.125–2.5 μM)

In order to quantify the displacement, the compound's concentration at which TO fluorescence decreases by 50% (assumed to be 50% displacement of TO), is calculated ($^{G4}DC_{50}$). Table 9 summarises the DC_{50} values obtained by FID for the interactions of complexes **Q_4**, **Q_6**, **Q_{12}** and **Q_{13}** with two different G-quadruplex DNA sequences (H_{telo} and *c*-myc) and one duplex DNA sequence (ds). From these DC_{50} values it is possible to conclude that the octanuclear arene ruthenium metalla-cubes are able to displace TO at very low concentrations (μM), which suggests that they interact strongly with G-quadruplex DNA (both telomeric and *c*-myc). In addition, complexes **Q_4**, **Q_6**, **Q_{12}** and **Q_{13}** show good selectivity for G-quadruplex *versus* duplex DNA binding.

Table 9. $^{H_{telo}}DC_{50}$, $^{c\text{-myc}}DC_{50}$ and $^{ds}DC_{50}$ values (μM) determined using FID assays for **Q_4**, **Q_6**, **Q_{12}** and **Q_{13}**

	TO displacement			selectivity		
compound	$^{H_{telo}}DC_{50}$ (μM)	$^{c\text{-myc}}DC_{50}$ (μM)	$^{ds}DC_{50}$ (μM)	$^{ds}DC_{50}$ / $^{H_{telo}}DC_{50}$	$^{ds}DC_{50}$ / $^{c\text{-myc}}DC_{50}$	$^{c\text{-myc}}DC_{50}$ / $^{H_{telo}}DC_{50}$
Q_4	0.15	0.32	0.72	4.8	2.3	2.1
Q_6	0.22	0.27	0.94	4.3	3.5	1.2
Q_{12}	0.33	0.70	1.25	3.8	1.8	2.1
Q_{13}	0.20	0.37	0.65	3.3	1.8	1.9

Among the four complexes, **Q_4** shows the highest binding and selectivity towards G-quadruplex DNA. No discrimination between toluene and para-cymene metalla-cubes can be observed, suggesting that the influence of the arene ligand on the binding is minor. In the same way, the difference of binding and selectivity between metalla-cubes built from tpp-2H and tpp-Zn is also not observable. Finally, the results also suggest that all the metalla-cubes are equipotent for the two G-quadruplex sequences under study (H_{telo} and *c*-myc). However, the main point of this study[225] is the selectivity observed between the binding of G-quadruplex and duplex DNA by arene ruthenium metalla-cubes. This selectivity (up to four) confirms the starting hypothesis that stated that by linking two porphyrin rings *via* coordination bonds, their G-quadruplex binding ability would be retained but their ability to intercalate in-between bases of duplex DNA would be greatly reduced.

4.3 Open Arene Ruthenium Metalla-Cubes

4.3.1 General

Arene ruthenium metalla-cubes showed great interest for biological applications. Their antiproliferative properties and their ability to bind strongly G-quadruplex DNA are two potential applications for this type of octanuclear complexes. Moreover, these water-soluble metalla-cages are robust, easy to synthesise and stable in biological medium. By using different porphyrin panels, arene and *OO*∩*OO* linkers it is even possible to modify their chemical structure and consequently their physical and chemical properties, without any difficulties. Furthermore, these complexes can target cancer cells *via* EPR effect thanks to their high molecular weight.

In order to modify charge and rigidity of these arene ruthenium metalla-cubes, we extended the strategy to new arene ruthenium metalla-assemblies incorporating poly-pyridylporphyrin panels, 5,15-bis(4-pyridyl)-10,20-diphenylporphyrin (bpp) and 5,10,15-tris(4-pyridyl)-20-phenylporphyrin (tpp). These open arene ruthenium metalla-cubes were connected by the arene ruthenium dinuclear metalla-clips **C_0** and **C_1** to afford the tetracationic $[(\eta^6\text{-}p\text{-cym})_4Ru_4(OO\cap OO)_2(bpp)_2]^{6+}$ (*OO*∩*OO* = ox (**Q_{14}**), dobq (**Q_{15}**)) and the hexacationic $[(\eta^6\text{-}p\text{-cym})_4Ru_4(OO\cap OO)_2(tpp)_2]^{6+}$ (*OO*∩*OO* = ox (**Q_{16}**), dobq (**Q_{17}**)) metalla-assemblies, (see Figure 60).

4.3.2 Synthesis of a Series of Arene Ruthenium Metalla-Cubes Q_{14} – Q_{17}

The tetranuclear arene ruthenium metalla-assemblies $[(\eta^6\text{-}p\text{-cym})_4Ru_4(OO\cap OO)_2(bpp)_2]^{6+}$ (*OO*∩*OO* = ox (**Q_{14}**), dobq (**Q_{15}**)) (see Figure 63) are readily prepared from the dinuclear complexes $[(\eta^6\text{-}p\text{-cym})_2Ru_2(ox)Cl_2]$ (**C_0**) and $[(\eta^6\text{-}p\text{-cym})_2Ru_2(dobq)Cl_2]$ (**C_1**) and the commercially available porphyrin derivative 5,15-bis(4-pyridyl)-10,20-diphenylporphyrin (bpp). The coordinatively unsaturated intermediates, $[(\eta^6\text{-}p\text{-cym})_2Ru_2(ox)]^{2+}$ and $[(\eta^6\text{-}p\text{-cym})_2Ru_2(dobq)]^{2+}$, formed upon addition of silver trifluoromethanesulfonate, react at room temperature in the presence of the bpp ligands to give the corresponding tetranuclear cations **Q_{14}** and **Q_{15}**. These open metalla-assemblies are isolated as trifluoromethanesulfonate salts, *i.e.* $[(\eta^6\text{-}p\text{-cym})_4Ru_4(OO\cap OO)_2(bpp)_2][CF_3SO_3]_4$

(*OO*∩*OO* = ox (**Q14**), dobq (**Q15**)). Despite a molecular weight of 2946.9 g·mol^{-1} for [**Q14**][CF_3SO_3]$_4$ and 3047.0 g·mol^{-1} for [**Q15**][CF_3SO_3]$_4$, and their relatively high charge, these two tetranuclear metalla-assemblies are quite soluble in $(CH_3)_2CO$, CH_3CN and DMSO and sparingly soluble in CH_2Cl_2, $CHCl_3$ and H_2O.

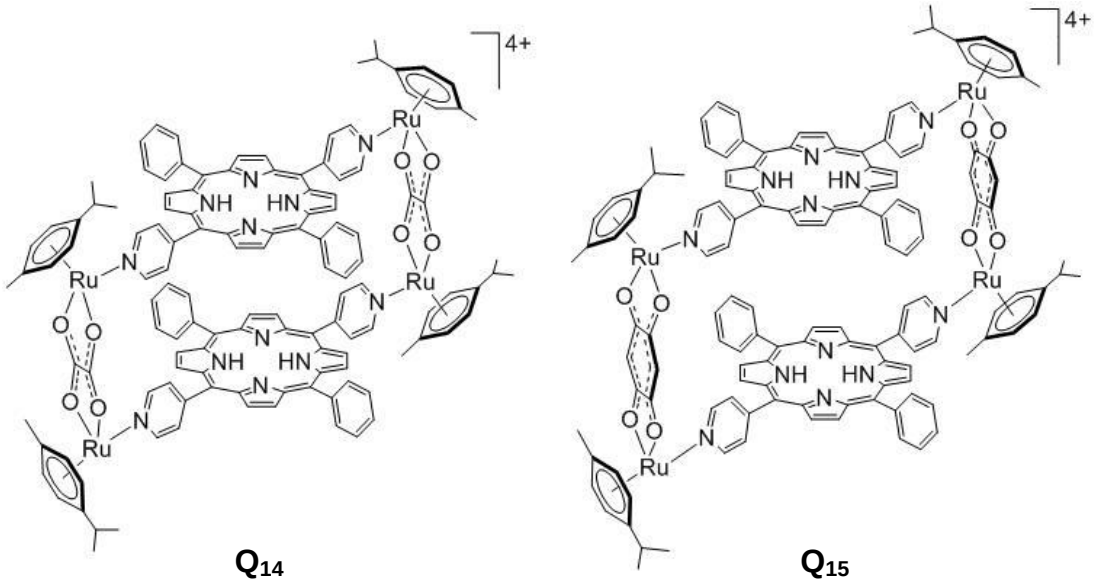

Figure 63. Open arene ruthenium metalla-cubes **Q14** and **Q15**

The hexanuclear derivatives **Q16** and **Q17** are obtained following the same strategy, but using the tridentate porphyrin panels, 5,10,15-tris(4-pyridyl)-20-phenylporphyrin (tpp). Cations **Q16** and **Q17** are also isolated as trifluoromethanesulfonate salts, *i.e.* [(η^6-*p*-cym)$_6$Ru$_6$(*OO*∩*OO*)$_3$(bpp)$_2$][CF_3SO_3]$_6$ (*OO*∩*OO* = ox (**Q16**), dobq (**Q17**)), (see Figure 64). Despite their higher charge, **Q16** and **Q17** possess a similar solubility to **Q14** and **Q15**, with the molecular weight of the salts being 3803.6 and 3953.8 g·mol^{-1} for [**Q16**][CF_3SO_3]$_6$ and [**Q17**][CF_3SO_3]$_6$, respectively.

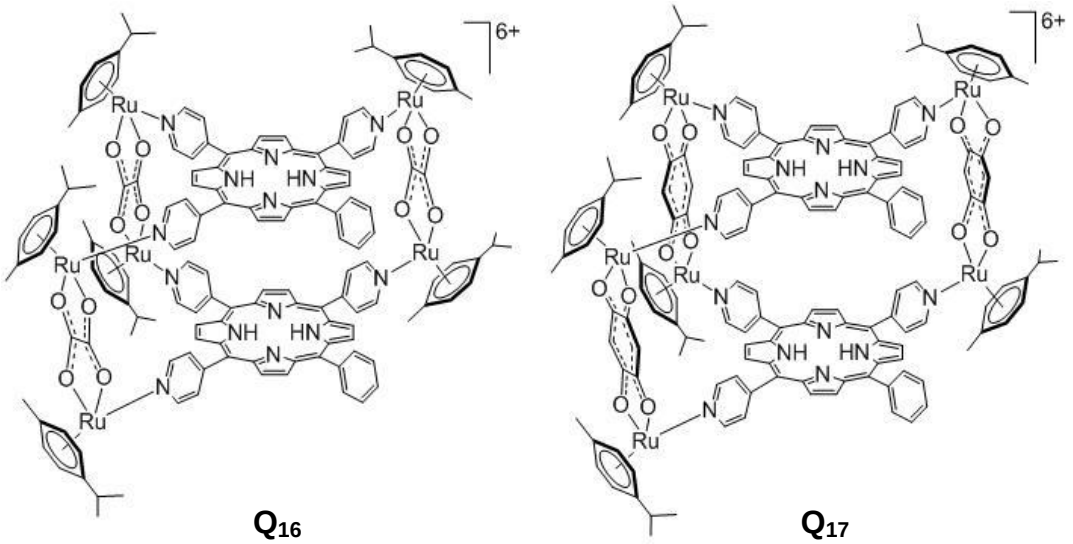

Q16 **Q17**

Figure 64. Open arene ruthenium metalla-cubes **Q16** and **Q17**

The IR spectra of [**Q14** – **Q15**][CF_3SO_3]$_4$ and [**Q16** – **Q17**][CF_3SO_3]$_6$ are dominated by absorptions of the coordinated poly-pyridylporphyrin panels with, in particular, the in-plane N–H deformation around 1220 cm^{-1},[226] and the bands assigned to the C=C and C=N skeletal modes of the porphyrins located between 1620 and 1400 cm^{-1}.[227] Moreover, the bands associated to the *OO*∩*OO* bridges, including the strong C=O stretching vibration (≈ 1630 cm^{-1}), are only slightly shifted as compared to the dinuclear complexes **C0** and **C1**. In addition to the porphyrin and *OO*∩*OO* absorptions, strong stretching vibrations due to the trifluoromethanesulfonate anions (1260(s), 1030(s), 638(m) cm^{-1}) are also observed in the IR spectra of the salts [**Q14** – **Q15**][CF_3SO_3]$_4$ and [**Q16** – **Q17**][CF_3SO_3]$_6$.

The metalla-assemblies **Q14** – **Q17** are stable in water at 60°C for 48 h, in which no degradation was observed by NMR spectroscopy. The ^{1}H NMR spectra of **Q14** and **Q15** show a similar chemical shift pattern for the protons of the bpp and *p*-cym ligands despite the different length of the bridging *OO*∩*OO* ligands. In the tetranuclear complexes **Q14** and **Q15**, large and broad signals are observed for the pyridyl and pyrrole protons of the porphyrin panels as well as for the signal of the N-H protons. In addition, the aromatic protons of the *p*-cym ligands appear as four superimposed doublets in the region 6.5 to 6.0 ppm. In **Q15**, an additional singulet is observed at δ = 6.17 ppm corresponding to the dobq protons. The ^{1}H NMR spectra of **Q16** – **Q17** are somewhat more complicated, not only due to the presence of diastereotopic protons in solution, which is in agreement with a chiral conformation as

previously observed in related metalla-assemblies, but as well due to the lost of a symmetry element present in **Q_{14}** and **Q_{15}**.

Indeed, each proton of **Q_{16}** and **Q_{17}** resonates at a distinct chemical shift, and accordingly the ^{1}H NMR spectrum of **Q_{17}** contains 142 distinct resonances. Due to their chiral conformation the chemical shift patterns for the protons of the bpp and *p*-cym ligands, as well as for the pyridyl and pyrrole protons of the porphyrin panels cannot be compared to the patterns observed in the case of the tetranuclear complexes **Q_{14}** and **Q_{15}**. Rather than attempting a partial attribution of some resonances, several 10-ppm HSQC experiments were recorded in order to improve the spectral resolution and determine the number of carbon signals at a given proton chemical shift. In usual heteronuclear ^{1}H–^{13}C NMR experiments, recorded with the full spectral width, the signals possess a typical width as large as 1 ppm in the ^{13}C dimension, making it impossible to distinguish between close signals. The use of 10-ppm experiments resolves the overlap problem and allows the determination of the correct ^{13}C chemical shifts, which is straightforward in these types of aliased spectra.[228] For instance, Figure 65 shows an excerpt of a 10-ppm HSQC recorded on **Q_{17}** displaying the region of the H_{α} of the pyridyl groups. In the Figure, the difficulty to distinguish between closed ^{13}C signals in a standard ^{1}H-^{13}C HSQC experiment is readily demonstrated (top), in which only ten distinct cross peaks are identified. Moreover, the 10-ppm HSQC experiment increases the resolution in the ^{13}C dimension by a factor of about 25, thus enabling all resonances to be separated, and the twelve independent signals of the H_{α} of the pyridyl groups could be resolved. The other resonances present in the 10-ppm spectrum arise from signals that are back-folded into the smaller window. Therefore, the discrimination of the resonances and the determination of the chemical shifts in a 10-ppm spectrum become straightforward.

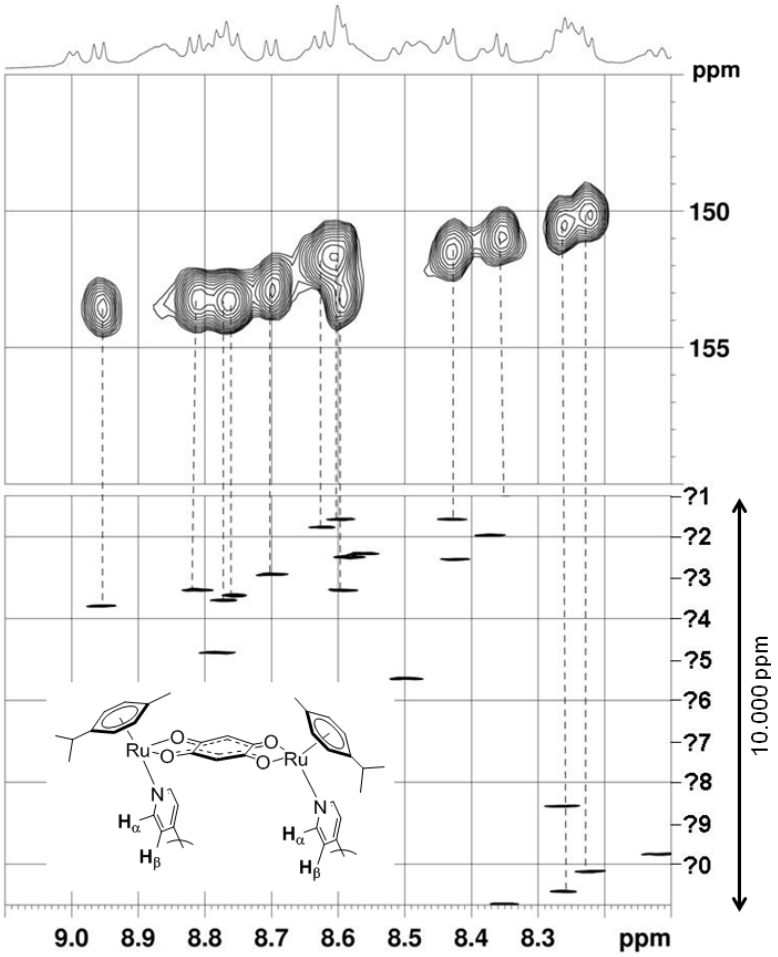

Figure 65. Excerpts of the full-width HSQC (top) and 10-ppm HSQC (bottom) NMR spectra in CD_3CN of the metalla-assembly [**Q$_{17}$**][CF_3SO_3]$_6$, showing the twelve independent signals of the H_α of the pyridyl groups (the question marks indicate unknown values)

Another example demonstrating the usefulness of the 10-ppm HSQC approach is presented in Figure 66. This Figure shows an excerpt of a 10-ppm HSQC recorded on [**Q$_{17}$**][CF_3SO_3]$_6$ displaying the region of the dobq bridging and *p*-cym ligands together with an excerpt of a usual HSQC recorded with the full spectral width. In the 10-ppm HSQC spectrum, the six independent cross peaks of the dobq bridging ligands, labelled 1 – 6, may be readily assigned. In the standard HSQC experiment, on the other hand, the signals possess a typical width of about 1 ppm in the ^{13}C dimension, making it impossible to distinguish between the six close signals.

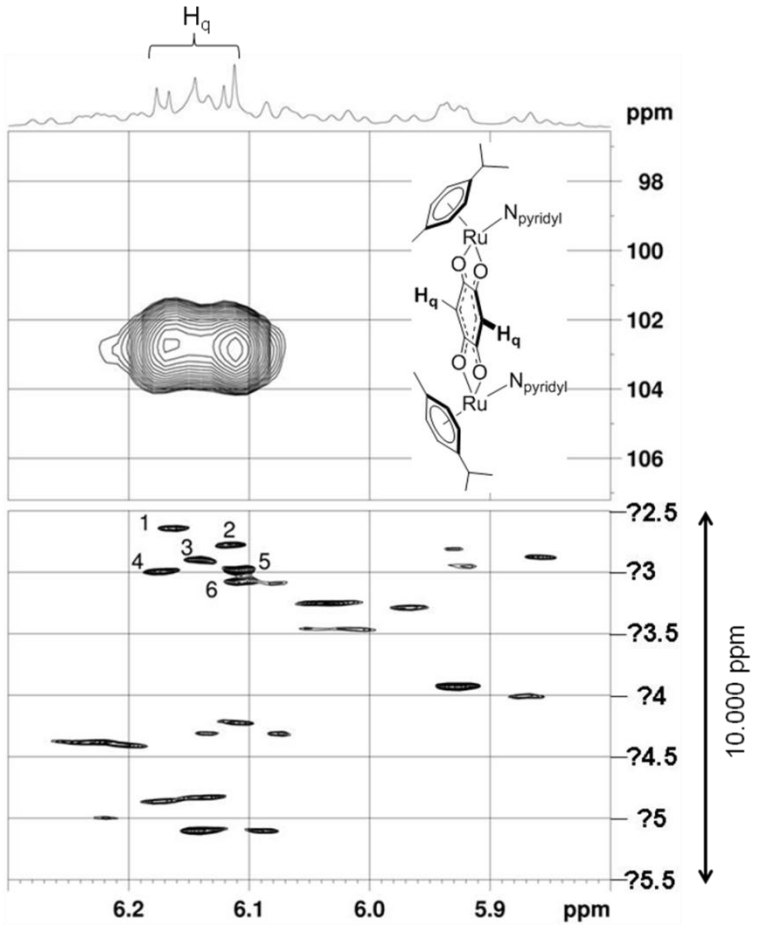

Figure 66. 10-ppm HSQC NMR spectrum in CD_3CN of the metalla-assembly $[\mathbf{Q_{17}}][CF_3SO_3]_6$, showing the six independent signals of the dobq (H_q) bridging ligands

Electronic absorption spectra of the multinuclear metalla-assemblies $\mathbf{Q_{14}}$ – $\mathbf{Q_{17}}$ as well as the poly-pyridylporphyrin panels (bpp and tpp) were acquired in acetone at 10^{-5} M concentration in the range 250 – 800 nm, (see Figure 67). The UV-visible spectra of all compounds are characterised by intense absorptions due to the porphyrin panels, including the Soret Band at around 400 nm and a series of Q bands between 500 and 700 nm. In complexes $\mathbf{Q_{14}}$ – $\mathbf{Q_{17}}$, as compared to the free porphyrins bpp and tpp, the Soret band is blue shifted and the full width at half-maximum ($\Delta\nu$) increases. In the case of metalla-assembly $\mathbf{Q_{17}}$, the full width at half-maximum ($\Delta\nu$ = 1870 cm^{-1}) is twice the width of bpp (865 cm^{-1}) and the Soret band is blue shifted by 712 cm^{-1}. Moreover, a clear red shift of the Q bands is observed in the metalla-assemblies $\mathbf{Q_{14}}$ – $\mathbf{Q_{17}}$. These photophysical changes in the UV-visible spectra of $\mathbf{Q_{14}}$ – $\mathbf{Q_{17}}$ are characteristic of sandwich-type dimeric structure of porphyrins,[208] which is consistent with the proposed structures.

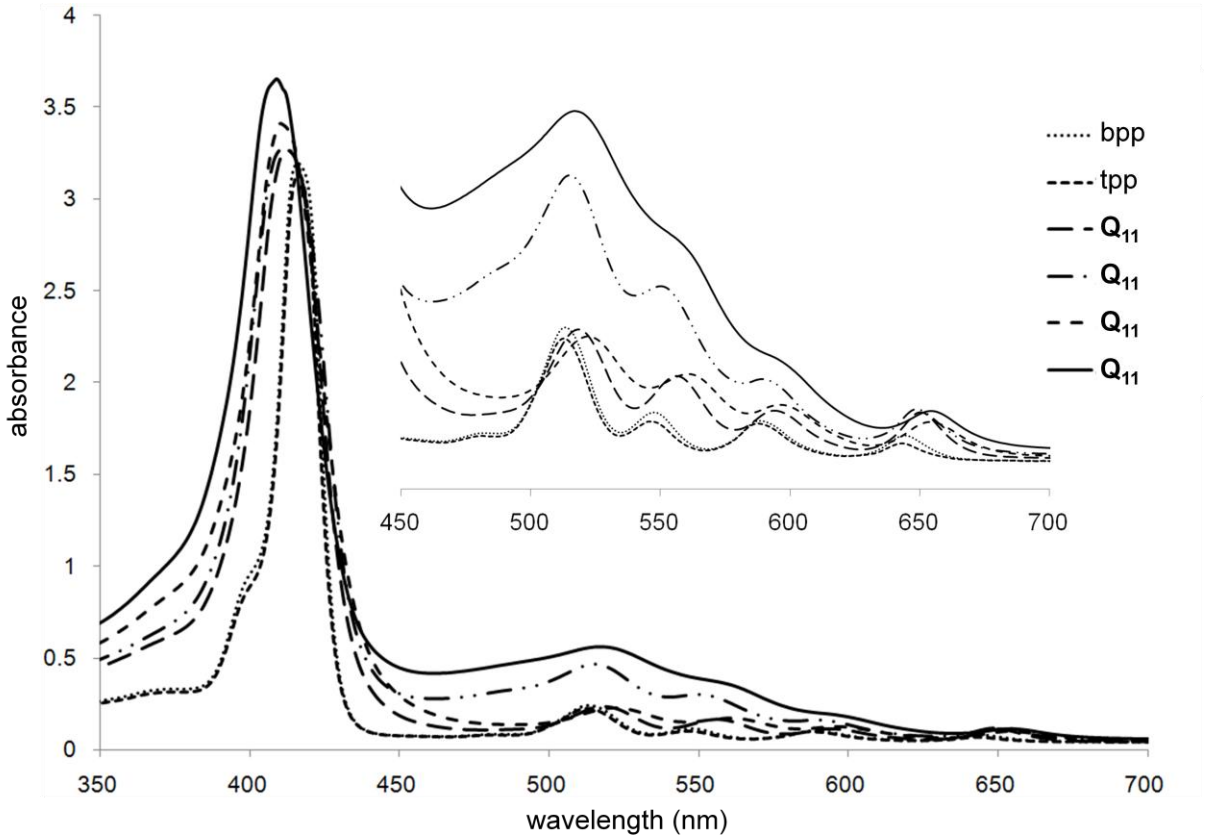

Figure 67. UV-visible spectra of bpp, tpp and the metalla-assemblies **Q14** – **Q17** in acetone (10^{-5} M)

Furthermore, the metalla-assemblies **Q14** – **Q17** were characterised by electrospray mass spectrometry with the four metalla-assemblies showing remarkable stability. The ESI-MS spectra show among others, peaks corresponding to $[\mathbf{Q_{14}}]^{4+}$, $[\mathbf{Q_{14}} + CF_3SO_3]^{3+}$, $[\mathbf{Q_{15}}]^{4+}$, $[\mathbf{Q_{15}} + CF_3SO_3]^{3+}$, $[\mathbf{Q_{16}} + (CF_3SO_3)_2]^{4+}$, $[\mathbf{Q_{16}} + (CF_3SO_3)_3]^{3+}$, $[\mathbf{Q_{17}} + (CF_3SO_3)_2]^{4+}$ and $[\mathbf{Q_{17}} + (CF_3SO_3)_3]^{3+}$ at m/z 587.9, 833.5, 612.8, 866.8, 802.3, 1119.8, 839.9 and 1169.5, respectively, (see Figure 68). These peaks are assigned unambiguously on the basis of their characteristic Ru_4 and Ru_6 isotope patterns.

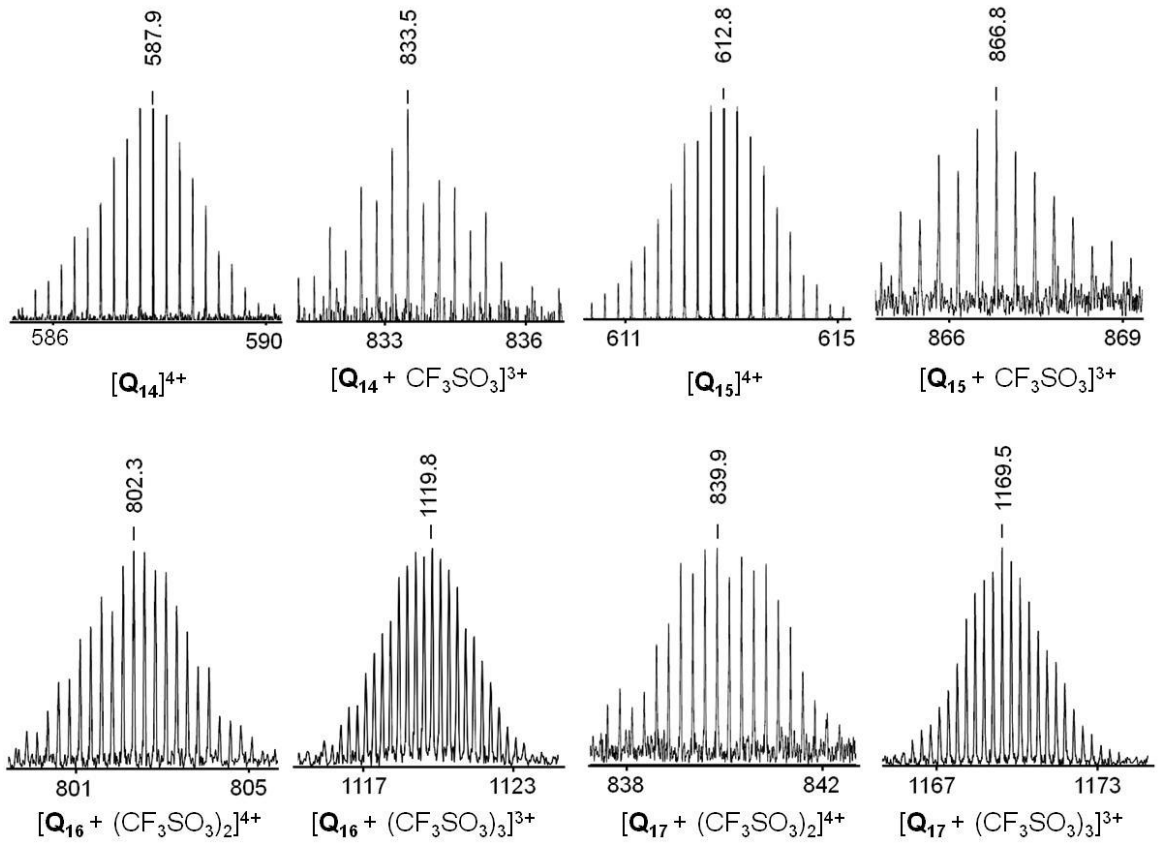

Figure 68. Selected peaks from the ESI-MS spectra of $[\mathbf{Q_{14}}][CF_3SO_3]_4$ – $[\mathbf{Q_{17}}][CF_3SO_3]_4$

4.3.3 Antiproliferative Study

The putative antitumour activity of compounds $[\mathbf{Q_{14}} - \mathbf{Q_{15}}][CF_3SO_3]_4$ and $[\mathbf{Q_{16}} - \mathbf{Q_{17}}][CF_3SO_3]_6$ was evaluated on A2780 (cisplatin sensitive) and A2780cisR (cisplatin resistant) human ovarian cancer cells. Although these compounds are highly charged, it has been shown that highly charged metal complexes cannot only traverse cell membranes, but some of them do it more effectively that neutral complexes or cations with low charges.[229] The cytotoxicities of the tetranuclear complexes $\mathbf{Q_{14}}$ and $\mathbf{Q_{15}}$ and the hexanuclear arene ruthenium complexes $\mathbf{Q_{16}}$ and $\mathbf{Q_{17}}$ are presented in Table 10. All compounds display good cytotoxicity towards both the sensitive and resistant cell lines with quite similar IC_{50} values. It is noteworthy, however, that the hexanuclear complexes $\mathbf{Q_{16}}$ and $\mathbf{Q_{17}}$ are slightly more cytotoxic than their tetranuclear counterparts $\mathbf{Q_{14}}$ and $\mathbf{Q_{15}}$, which is consistent with the number of ruthenium centres per metalla-assemblies. In general, for arene ruthenium complexes an additive effect is observed as the number of ruthenium centres increases.[176c] However, an additive effect is not always observed, for example, binuclear arene ruthenium

complexes (connected *via* pyridone-based chelators) were found to be highly active in a colorectal carcinoma cell line in the absence of any activity for the mononuclear counterparts.[230] Complexes **Q_{15}** and **Q_{17}** that contain the dobq ligand are more cytotoxic than the oxalato derivatives **Q_{14}** and **Q_{16}**, indicating that the length of the spacer is a relevant parameter in the design of these types of compounds.

Table 10. IC_{50} values of **Q_{14}** – **Q_{17}** in A2780 and A2780cisR cell lines

compound	A2780 (IC_{50}, μM)	A2780cisR (IC_{50}, μM)
Q_{14}	11.0 ± 0.2	12.7 ± 3.0
Q_{15}	5.6 ± 0.4	10.1 ± 1.2
Q_{16}	3.1 ± 1.0	10.7 ± 2.6
Q_{17}	2.1 ± 0.3	3.8 ± 0.8
cisplatin	1.6	8.6

This study[231] shows a series of cationic open metalla-cubes based on arene ruthenium dinuclear clips and poly-pyridylporphyrin panels. The compounds are stable, and based on promising results obtained for analogous ruthenium compounds, were evaluated for *in vitro* anticancer activity. Large compounds such as these could potentially exploit the EPR effect for tumour targeting but as yet an *in vivo* study has not been performed to gauge this possibility. From the *in vitro* study, however, it was found that the number of ruthenium centres and the type of spacer used influence the cytotoxicity of these metalla-assemblies.

Chapter 5: General Conclusion and Perspectives

5.1 Arene Ruthenium Metalla-Rectangles

The synthesis of arene ruthenium metalla-clips of the general formula $[(\eta^6\text{-}p\text{-cym})_2Ru_2(OO\cap OO)Cl_2]$ ($OO\cap OO$ = 5,8-dioxydo-1,4-naphthoquinonato (donq), 5,8-dioxydo-1,4-anthraquinonato (doaq), and 6,11-dioxydo-5,12-naphthacenedionato (dotq)) (**C_5**, **C_6** and **C_7**) allowed the development of a new generation of arene ruthenium metalla-rectangles **R_{13}** – **R_{21}** $[(\eta^6\text{-}p\text{-cym})_4Ru_4(OO\cap OO)_2(N\cap N)_2]^{4+}$ ($OO\cap OO$ = donq (**R_{13}**, **R_{16}**, **R_{19}**), doaq (**R_{14}**, **R_{17}**, **R_{20}**), dotq (**R_{15}**, **R_{18}**, **R_{21}**); $N\cap N$ = pyr (**R_{13}**, **R_{14}**, **R_{15}**), bpy (**R_{16}**, **R_{17}**, **R_{18}**), bpe (**R_{19}**, **R_{20}**, **R_{21}**)). The potential of such metalla-rectangles for applications in host-guest chemistry was studied with a series of planar aromatic molecules (anthracene, pyrene, perylene, coronene) and results clearly underlined the great interest of these metalla-rectangles for host-guest chemistry.

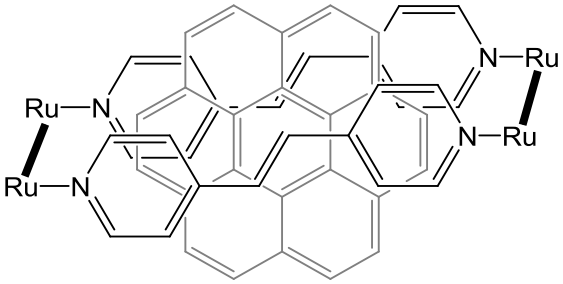

in-cavity

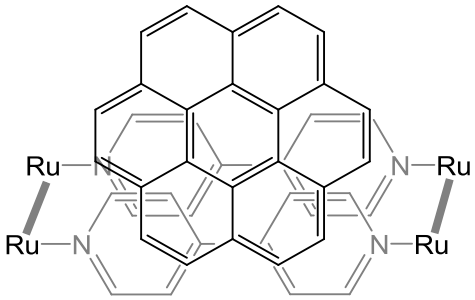

out-of-cavity

Moreover, this type of arene ruthenium metalla-rectangles can be easily designed to accommodate guest molecule outside and inside their cavities as it was determined by various NMR experiments, UV-visible and fluorescence spectroscopy. For a future project, extension of the length of the $N\cap N$ linker as well as a modification of its flexibility or rigidity could strongly modify the properties of arene ruthenium metalla-rectangles as host systems. In the same way, the synthesis of new arene ruthenium dinuclear metalla-clips could also modify the hosting ability of these tetranuclear metalla-assemblies.

On the other hand, the water-solubility, the robustness in biological media as well as a facile and straightforward synthetic pathway are some of the numerous properties of arene ruthenium metalla-rectangles. These characteristics allowed the antiproliferative testing of a

series of metalla-rectangles $[(\eta^6\text{-}p\text{-cym})_4Ru_4(OO\cap OO)_2(N\cap N)_2]^{4+}$ ($OO\cap OO$ = oxalato (ox), dobq, donq, doaq, dotq, oxamido (oxa), oxonico (oxo)); $N\cap N$ = bpe, 1,2-bis(4-pyridyl)ethane (bpa)) (**R$_9$**, **R$_{19}$** – **R$_{31}$**). The cytotoxicity of the compounds was established on A2780 and A2780cisR human ovarian cancer cell lines by the group of Prof. Dyson (EPFL). The activity of all complexes was found to be moderate to excellent, depending of the nature of the linker as well as the nature of the length of the metalla-clip. Interestingly enough, some metalla-rectangles were found to be more active for cisplatin resistant cancer cells A2780cisR than on A2780 cancer cells. This result suggests that the biological mechanism involved in the anticancer activity of metalla-rectangles differs from the biological mechanism of cisplatin. Furthermore, this selectivity toward cisplatin resistant cancer cells of certain arene ruthenium metalla-rectangles is unusual and highly promising.

Finally, arene ruthenium metalla-rectangles were also used to pre-organise two olefinic double bonds with a parallel arrangement that allowed a facile photochemical [2 + 2] cycloaddition reaction. This photoreaction in solution led to the synthesis of *rctt*-tetrakis(4-pyridyl)cyclobutane compound.

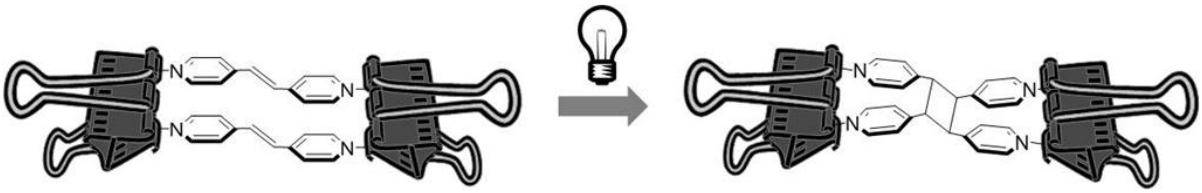

In conclusion, host-guest chemistry, anticancer therapy and supramolecular control of reactivity are some examples developed in this thesis for potential applications for arene ruthenium metalla-rectangles.

5.2 Arene Ruthenium Metalla-Prisms

The versatility of metalla-rectangles allowed very different applications for this type of complexes. In the case of arene ruthenium metalla-prisms, this versatility is well illustrated by the Trojan horse concept. The association of six arene ruthenium units in a large water-soluble metalla-cage (**P_1**) potentially able to target tumours *via* EPR effect with a non water-soluble drug encapsulated into the hydrophobic cavity of this carceplex metalla-prism was developed by our group before this thesis. The ability of the host **P_1** to deliver guest molecules to cells was further confirmed by encapsulation of a fluorescent labelled pyrene-X derivative, 1-(4,6-dichloro-1,3,5-triazin-2-yl)pyrene and fluorescence experiments were used to monitor the uptake of pyrene-X into cancer cells. This uptake was found to be one order of magnitude greater for the carceplex system over pyrene-X alone.

The present work developed this approach and the synthesis of new arene ruthenium metalla-prisms $[(\eta^6\text{-}p\text{-cym})_6Ru_6(OO\cap OO)_3(tpt)_2]^{6+}$ ($OO\cap OO$ = donq, doaq, dotq) (**P_2** – **P_4**) strongly modified the host ability of the prisms. Indeed these metalla-prisms allowed the encapsulation of small aromatic molecules either in a carceplex way or in a host-guest fashion. More precisely, these cationic metalla-prisms possess different portal sizes able to allow small aromatic molecules to enter and leave in solution the hydrophobic cavity, with different rate of release of the guest molecule depending on the portal size of the host. However, for planar molecules capable of fitting into the cavity, but too large to exit the portal of the cage, permanent encapsulation was observed, thus giving rise to stable carceplex systems. But maybe more interestingly, the development of these metalla-prisms **P_2** – **P_4** with different portal sizes and able to interact in a host-guest fashion with small aromatic molecules was a new way to explore the anticancer behaviour of our arene ruthenium metalla-systems.

In particular, the *in vitro* characterisation of this modular and adjustable supramolecular drug delivery system based on these three arene ruthenium metalla-prisms was described. The antiproliferative effect on A2780 and A2780cisR cancer cells of the empty metalla-cages was found to be efficient while the host-guest and the carceplex systems exhibited excellent IC_{50}, some of them being in the nanomolar scale. The cellular uptake of the host-guest systems was also studied and seems to involve an active transport mechanism,

and the rate of release of the guest molecule was found to depend on the portal size of the host.

Finally, the impact of the size of the guest molecule on the cytotoxicity of the host-guest systems was studied. A series of large pyrenyl-containing dendrimers of different generations (pyrene-G_0, pyrene-G_1, and pyrene-G_2) were prepared, and after encapsulation of the pyrenyl units in the hydrophobic cavity of the hexanuclear arene ruthenium metalla-prism **P_2**, the cytotoxicity of these resulting host-guest systems, [pyrene-G_0⊂**P_2**]$^{6+}$, [pyrene-G_1⊂**P_2**]$^{6+}$, and [pyrene-G_2⊂**P_2**]$^{6+}$, was evaluated and correlated to their size.

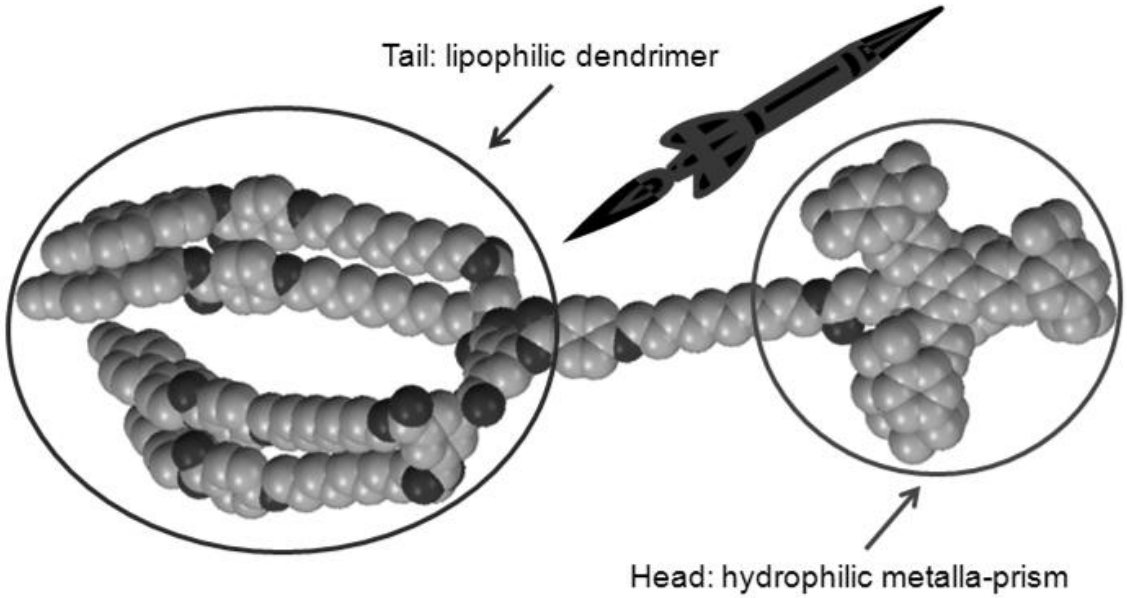

Results indicated that metalla-cage host systems are able to deliver hydrophobic guest molecules with extremely large appendages into cancer cells. Moreover, this study suggested that the most cytotoxic system was [pyrene-G_0⊂**P_2**]$^{6+}$, thus indicating the absence of a size effect of the guest molecule on the antiproliferative effect of the host-guest system. Nevertheless, [pyrene-G_1⊂**P_2**]$^{6+}$, and [pyrene-G_2⊂**P_2**]$^{6+}$ have higher molecular weights than [pyrene-G_0⊂**P_2**]$^{6+}$, and therefore could have a better selectivity for cancer cells than for healthy cells thanks to the EPR effect. This hypothesis needs to be confirmed by *in vivo* studies.

5.3 Arene Ruthenium Metalla-Cubes

Arene ruthenium metalla-rectangles and arene ruthenium metalla-prisms are possibly able to selectively target cancer cells *via* the EPR effect. In order to extend this strategy to larger metalla-assemblies we developed arene ruthenium metalla-cubes of the general formula $[(\eta^6\text{-arene})_8Ru_8(OO\cap OO)_4(NN\cap NN)_2]^{6+}$ where *NN*∩*NN* is a tetra-pyridylprophyrin derivative (tpp-2H, tpp-Ni or tpp-Zn). The antiproliferative activity of these metalla-cubes was established *in vitro* on human ovarian cancer cell lines.

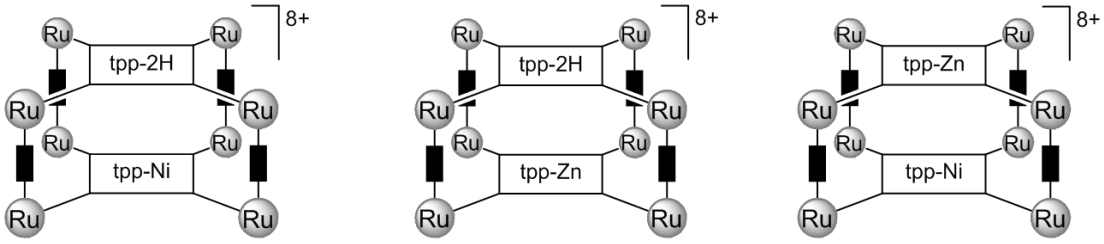

We also studied the formation of unsymmetrical metalla-cubes constructed from mixtures of different porphyrin panels during the synthesis of the cubes. All compounds showed similar cytotoxicities towards both cisplatin sensitive and cisplatin resistant cancer cell lines, suggesting that they do not share the same mechanisms of action than the reference drug, *i.e.* cisplatin. Moreover, among the compounds tested, additional trends were drawn from these results. In particular, the mixtures containing the unsymmetrical metalla-cubes are the most cytotoxic, with activities comparable to cisplatin or superior to cisplatin in the resistant cancer cell line A2780cisR. Further studies will be needed to provide an explanation for this difference in cytotoxicity between symmetrical and unsymmetrical metalla-cubes.

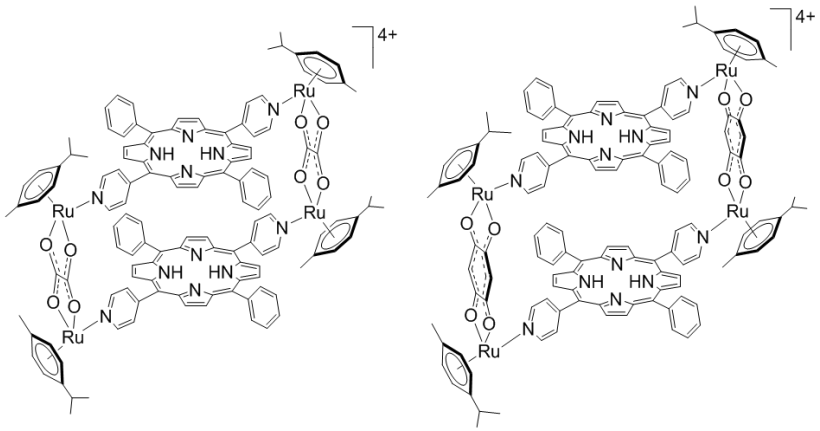

We also modified charge and rigidity of these arene ruthenium metalla-cubes, with the synthesis of open arene ruthenium metalla-assemblies incorporating bis-pyridylporphyrin and tris-pyridylporphyrin panels. These tetracationic and hexacationic open arene ruthenium metalla-cubes were evaluated for *in vitro* anticancer activity. It was found that the number of ruthenium centres and the type of spacer used influence the cytotoxicity of these metalla-assemblies, but in all cases, the complexes were found to be stable in biological medium suggesting a great potential for the tuning of such molecules.

Finally, as porphyrins are known to bind strongly to G-quadruplex DNA but with an usually poor selectivity since they also bind strongly to duplex DNA, we hypothesised that by linking two porphyrin rings *via* coordination bonds, their G-quadruplex binding ability would be retained but their ability to intercalate in-between bases of duplex DNA would be greatly reduced. In order to confirm or rule out this hypothesis we tested four arene ruthenium metalla-cubes as potential G-quadruplex DNA binders, in collaboration with the group of Dr. Vilar (Imperial College of London).

A noticeable selectivity was indeed observed between the binding of G-quadruplex and duplex DNA by arene ruthenium metalla-cubes. This selectivity (up to four) confirms the starting hypothesis that stated that by linking two porphyrin rings *via* coordination bonds, their G-quadruplex binding ability would be retained but their ability to intercalate in-between bases of duplex DNA would be reduced.

5.4 Perspectives

The development of host-guest chemistry with arene ruthenium metalla-assemblies and small aromatic molecules presented in this thesis opened a new chapter in the research of our group. The construction of new systems in thermodynamic exchanges, the characterisation of the equilibrium state and the potential application of such systems in medicinal chemistry were some of the features investigated in this work. In other words, the passage from carceplex to host-guest metalla-cages was certainly the main contribution of this thesis to the general project initiated in 2006 by our group.

As a consequence, a possible perspective is the development of this host-guest chemistry with new and larger arene ruthenium metalla-cages built either from new dinuclear metalla-clips or from new linkers. This natural perspective is already in progress,[146] and the increase of the cavity size of the host molecule could then allow the encapsulation of different guest molecules, such as non-planar, non-aromatic or even non-hydrophobic molecules. Using the same concept, we could imagine an enantiodifferentiation of chiral guest molecules with the construction of metalla-cages designed with chiral and enantiopure panels. We could also develop reactions between two guest molecules inside the cavity of the water-soluble metalla-cages. This could be interesting for the synthesis of non-water-soluble molecules in water, and therefore find applications in green chemistry. Concerning the medicinal applications, encapsulations of drugs or biological relevant molecules would also beneficiate from the development of new arene ruthenium metalla-cages. As a recent example, encapsulations of photosensitisers, such as porphyrins or phthalocyanines were achieved by our group.[232] The study of the antiproliferative behaviour of the systems as well as their potential utilisation as photodynamic therapy agents is under investigation. Thus, the development of the hosting ability of arene ruthenium metalla-cages could find applications as sensors, storage molecules, water-soluble reactors, but also as separator for *racemic* mixture of organic compounds or cargo for the delivery of biological relevant guest molecules into cancer cells.

Another possibility would be the utilisation of other transition metals than ruthenium for the construction of metalla-assemblies. In particular, osmium complexes are currently actively explored as novel chemotherapeutic agents.[233] Therefore it could be interesting to synthesise arene osmium metalla-assemblies and to evaluate their antiproliferative ability as

well as their hosting potential. An initiation of this project was realised during this thesis with the synthesis of arene osmium metalla-rectangles.[234]

If the replacement of ruthenium by osmium, or by other transition metals is relatively easy and imaginable, the construction of hetero-metallic dinuclear metalla-clips (Ru-Os, Ru-Ir, Ru-Rh for examples) would be a very interested progress. Indeed, the mix of different transition metals inside a unique structure could give rise to surprising chemical and physical properties, but also biological properties.

Finally, the metalla-cages and the corresponding host-guest systems developed by our group are synthesised *via* coordination-driven self-assembly and weak intermolecular interactions such as $\pi - \pi$ stacking and hydrophobic interactions, and therefore are part of the vast family of the supramolecular objects. A potential direction could be then the synthesis of nano-objects as for example organic-organometallic catenanes. These mechanically-interlocked molecular architectures consisting of two or more interlocked organic macrocycles and arene ruthenium metalla-cycles could find applications as molecular electronic devices or molecular sensors. We could also imagine organic-organometallic rotaxanes or different nano-objects where an organic macrocycle could be replaced by an organometallic metalla-cycle.

Eventually, the great adaptability of arene ruthenium metalla-assemblies, the versatility of their properties and their unique physical and chemical behaviours allow numerous possible developments for the kind of host-guest systems presented in this thesis.

Chapter 6: Experimental

6.1 General Remarks

6.1.1 Solvents, Lamp and Products

Solvents of analytical grade purchased from Acros organics or VWR International S.A.S were used for synthesis and not degassed prior to use. The photoreactions upon UV irradiation were performed with a Hg lamp (180 W). The silica used for column chromatography (32-63, 60Å) was purchased from Brunshwig AG. 2,4,6-tris(4-pyridyl)-1,3,5-triazine (tpt)[235] was synthesized according to published method. All organic starting materials were purchased from Acros organics, Sigma-Aldrich, Fluka, Alfa Aesar, Strem or TCI-Europe and used as received. The porphyrin derivatives were commercially available (Sigma-Aldrich, TriPorTech GmbH or Frontier Scientific) and used as received. $RuCl_3$ hydrate was a generous loan from Johnson-Matthey. The dimeric complexes $[(\eta^6\text{-}p\text{-cym})RuCl_2]_2$,[16] $[(\eta^6\text{-hmb})RuCl_2]_2$,[16] $[(\eta^6\text{-toluene})RuCl_2]_2$,[236] and $[(\eta^6\text{-indane})RuCl_2]_2$[237] were synthesized according to published methods. $[(\eta^6\text{-nonylbenzene})RuCl_2]_2$ was prepared by a Birch-type reduction[18] of the commercially available (Sigma-Aldrich) nonylbenzene. Addition of $RuCl_3 \cdot n\ H_2O$ in ethanol to the non-isolated 3-nonylcylohexa-1,4-diene using standard reaction and purification conditions afforded the dimer. ^{1}H NMR (400 MHz, $CDCl_3$): δ (ppm) = 5.66 (dd, 4 H, H_{phenyl}), 5.56 (t, 2 H, H_{phenyl}), 5.36 (d, 4 H, H_{phenyl}), 2.52 (t, 4 H, $CH_{2\alpha}$), 1.53 (m, 4 H, $CH_{2\beta}$), 1.27 (m, 24 H, CH_2), 0.86 (t, 6 H, CH_3). $^{13}C(^1H)$ NMR (100 MHz, $CDCl_3$): δ (ppm) = 102.8 (C_{phenyl}), 80.4 (CH_{phenyl}), 79.9 (CH_{phenyl}), 78.4 (CH_{phenyl}), 33.8 ($CH_{2\alpha}$), 32.6 ($CH_{2\beta}$), 30.2 (CH_2), 30.1 (CH_2), 30.0 (CH_2), 30.0 (CH_2), 23.4 (CH_2), 14.4 (CH_3). Pyrene-G_0, pyrene-G_1, and pyrene-G_2 were synthesised by co-worker.[197] The arene ruthenium metalla-clips $\mathbf{C_0}$,[120] $\mathbf{C_1}$,[72] $\mathbf{C_2}$,[73] $\mathbf{C_3}$,[73] $\mathbf{C_4}$,[73] $\mathbf{C_6}$,[131] and $\mathbf{C_9}$[112] were synthesized according to published methods. The arene ruthenium metalla-rectangles $\mathbf{R_1}$ – $\mathbf{R_{12}}$,[110-111] and $\mathbf{R_{22}}$[120] were synthesized according to published methods. The arene ruthenium metalla-cube $\mathbf{Q_1}$ was synthesized according to published method.[205a]

6.1.2 NMR Experiments

The ^{1}H, ^{13}C, $^{13}C(^{1}H)$, COSY, HSQC, 10-ppm HSQC, ROESY and DOSY NMR spectra were recorded on a Bruker AvanceII 400 spectrometer using the residual protonated solvent as internal standard. For all DOSY experiments, the temperature was regulated at 298 or 233 K, the airflow was increased to 670 L × min^{-1}, and the NMR tube was spun. The diffusion NMR experiments were performed with a standard pulsed-gradient stimulated echo (LED-PFGSTE) sequence and a bipolar gradient.[132] DOSY Spectra were generated by using the TopSpin 2.0 software package (Bruker). Experimental parameters were Δ = 50.0 ms (diffusion delay), and τ = 1.0 ms (gradient recovery delay), and *Te* = 5.0 ms (eddy current recovery delay). For each data set, 4096 complex points were collected, and the gradient dimension was sampled using 16 experiments in which the gradient strength was exponentially incremented from 1.0 to 50.8 G × cm^{-1}. The gradient duration $\delta/2$ was adjusted to observe a near complete signal loss at 50.8 G × cm^{-1}. Typically, the $\delta/2$ delay was chosen in the 1.2 - 2.0 ms range. A 1.0 s recycle delay was used between scans for data shown. For each data set, the spectral axis was processed with an exponential function (3 – 5 Hz line broadening), and Fourier transform was applied in order to obtain 4096 real points. The DOSY reconstruction was realised with 256 points in the diffusion dimension. The number of scans ranged from 8 to 64 and was adapted to each sample. The experimental time ranged from 4 to 30 min.

For the ROESY experiments, the temperature was regulated at 233 K, and the NMR tube was not spun. The ROESY NMR experiment was performed using a gradient selected ROESY experiment[238] using the Tr-ROESY scheme for efficient TOCSY transfer suppression. Experimental parameters were τ_m = 200 ms (mixing time), δ = 500 μs (gradient length), G_0 = 1.0 G × cm^{-1}, G_1 = 3.0 G × cm^{-1}, G_2 = 6.0 G × cm^{-1} (gradient strength) and τ_p = 100 ms (selective pulse, Seduce[-1]). 8192 complex points were collected. A 3 s recycle delay was used. The spectral axis was processed with an exponential function (3 Hz line broadening), and Fourier transform was applied in order to obtain 8192 real points. The number of scans was 1024 and the experimental time approximately 90 min.

6.1.3 Analytical Instruments

Infrared spectra were recorded as KBr pellets on a Perkin-Elmer FTIR 1720-X spectrometer. UV-visible absorption spectra were recorded on an Uvikon 930 spectrophotometer using precision cells made of quartz (1 cm). Fluorescence spectra were recorded on a Perkin-Elmer-LS50B luminescence spectrometer using precision cells made of quartz (1 cm). Electrospray ionization mass spectrometry conditions were recorded on a Bruker APEX II 9.4-tesra FT-ICR-MS equipped with an Apollo II electrospray ion source: sample condition 10-50 μmol/l in methanol at 30ºC, end plate voltage 3500v, and capillary voltage. Elemental analyses were done by Laboratoire de chimie pharmaceutique de l'Université de Genève (Switzerland) or by Mikroelementar-analytisches Laboratorium de ETH Zürich (Switzerland).

6.1.4 Biological Studies

All the biological studies were performed by the group of Professor Dyson (EPFL).

Culture and Inhibition of Cell Growth. Human A2780 ovarian carcinoma cells were obtained from the European Centre of Cell Cultures (ECACC, Salisbury, UK) and maintained in culture as described by the provider. The cells were routinely grown in RPMI 1640 medium containing 10% foetal calf serum (FCS) and antibiotics at 37°C and 5% CO_2. For the evaluation of growth inhibition tests, the cells were seeded in 96-well plates (25000 cells per well) and grown for 24 h in complete medium. Compounds were added to the required concentration and added to the cell culture for 72 h incubation. Solutions of the compounds were applied by diluting a freshly prepared stock solution of the corresponding compound in DMSO, with the final concentration of 0.05 % in the medium. The 3-(4,5-dimethylthiazol-2-yl)-2,5-diphenyltetrazolium bromide (MTT) test was performed in the last 2 h without changing the culture medium. Following drug exposure, MTT (from Sigma) was added to the cells at a final concentration of 0.2 mg/ml and incubated for 2 h, then the culture medium was aspirated and the violet formazan precipitate dissolved in DMSO. The optical density was quantified at 540 nm using a multiwell plate reader (iEMS Reader MF, Labsystems, USA), and the percentage of surviving cells was calculated from the ratio of absorbance of treated to untreated cells. The IC_{50} values for the inhibition of cell growth were determined by fitting

the plot of the percentage of surviving cells against the drug concentration using a sigmoidal function (Origin v7.5).

Microscopy Experiments. Cells were grown for 24 h on chambered coverglass (Lab-Tek, NUNC) slides in complete medium at a density of 1.10^4 and later exposed to the appropriate compound at 37°C in the dark. Cells were stained with lysotracker Red DND-99 (Invitrogen, Molecular Probes) and 10 kDa FITC-dextran (Invitrogen, Molecular Probes) for 30 min at 37°C. Excess complex was washed away with PBS, fixed with 4% formaldehyde in PBS for 30 min in the dark and rinsed twice with PBS before observation. Cells were mounted in PBS before being observed by confocal microscopy using a Zeiss LSM 700 inverted microscope equipped with a 40X oil immersion objective. Filters used for excitation and detection of fluorescent guest molecule were 405 nm and 492 nm respectively, 488 nm and 559 nm for detection of FITC-dextran, 555 nm and 587 nm for detection of lysotracker Red DND-99. Fluorescence signal intensities were evaluated using Zen© software (Carl Zeiss MicroImaging GmbH).

Flow Cytometry. Cells were detached from culture with EDTA (0.48 mM in PBS) and incubated at 1×10^6 cells/mL with complex salts (added from a concentrated DMSO stock) under conditions described above and then placed on ice. The fluorescence of ~20000 cells was measured using a BD LSR II analyser, exciting with the 355 nm laser for fluorescent guest molecule. Emission was observed at 450±40 nm. Fluorescence data were analysed using the FlowJo 8 software.

Inhibition of Endocytosis. Wortmannin (Applichem GmbH) was dissolved in DMSO and diluted to 500 nM in the culture medium. Cells were pre-incubated for 30 min either at 4 °C or with wortmannin at 37 °C before adding complex salts for 4 hours.

6.1.5 DNA Interactions

FID studies were performed by the group of Dr. Vilar (Imperial College of London).

Stock solution preparation. Complexes $\mathbf{Q_4}$ and $\mathbf{Q_6}$ were dissolved in acetone to give 10 mM stock solutions. Complexes $\mathbf{Q_9}$ and $\mathbf{Q_{10}}$ were dissolved in acetone to give 1 mM stock solutions. Thiazole Orange (TO, Sigma-Aldrich) was prepared as a 10 mM stock solution in DMSO. These stock solutions were freshly prepared prior to use and were further diluted to

final concentrations using 60 mM potassium cacodylate buffer (pH 7.4) (the potassium cacodylate buffer also contains 50 mM KCl).

Fluorescence Intercalator Displacement (FID) assay. The FID assays were performed on a Varian Cary Eclipse Spectrometer following a reported procedure.[224] The oligonucleotides 22 AG human telomeric DNA, 5'-AGGG TTA GGG TTA GGG TTA GGG-3'; 17bp duplex-DNA: [5'-CCAGTTCGTAGTAACCC-3']/[5'-GGGTTACTACGAACTGG- 3']; and 21bp c-myc: 5'-GGG-GAG-GGT-GGG-GAG-GGT-GGG-3' were purchased from Eurogentec and used without any further purification. The corresponding oligonucleotides were dissolved in MilliQ water to yield 20 μM stock solutions. These were diluted to yield 500 nM solutions using a 60 mM potassium cacodylate buffer (pH 7.4) and annealed to 90^{o} C for 5 min and then allowed to cool at room temperature overnight. An increasing concentration of the metal complex (ligand) (from 0.125 μM to 2.5 μM which correspond to 0.5 to 10 equivalent) was added onto a mixture of pre-folded G-quadruplex DNA (0.25 μM of either H_{telo} or *c*-myc) or duplex DNA (17bp, 0.25 μM) and thiazole orange (0.50 μM), in a 60 mM potassium cacodylate (pH 7.4). After 3 minutes equilibration time, the corresponding emission spectrum (between 510 and 750 nm) with an excitation wavelength of 501 nm was recorded. The fluorescence area (FA, 510-750 nm) of each spectrum obtained was converted to percentage of displacement in which % TO displacement = 100 – [(fluorescence area upon ligand addition /fluorescence area of standard) × 100], where fluorescence area of standard being fluorescence area before addition of ligand. The FA was plotted against the concentration of added ligand, from which the ability of ligand to induce TO displacement is expressed as DC_{50} ($^{Htelo}DC_{50}$ for H_{telo} DNA, $^{ds}DC_{50}$ for duplex DNA and $^{c\text{-}myc}DC_{50}$ for *c*-myc DNA) value which is the required concentration to displace 50% of TO from the DNA (either H_{telo}, *c*-myc or duplex DNA). The selectivities for H_{telo}- and *c*-myc-DNA over duplex-DNA are expressed by $^{ds}DC_{50}$ /$^{Htelo}DC_{50}$ value and $^{ds}DC_{50}$ /$^{c\text{-}myc}DC_{50}$ value, respectively.

6.2 Syntheses and Characterisations

6.2.1 Arene Ruthenium Metalla-Clips C_5, C_7, C_9, C_{10}, C_{11}, and C_{12}

General procedure for metalla-clips **C_5** and **C_7**: A mixture of $[(\eta^6\text{-}p\text{-cym})RuCl_2]_2$ (145.0 mg, 0.23 mmol), anhydrous sodium acetate (38.4 mg, 0.46 mmol) and quinone derivative (**C_5**: 5,8-dihydroxy-1,4-naphthoquinone (43.7 mg, 0.23 mmol); **C_7**: 6,11-dihydroxy-5,12-naphtacenedione (66.8 mg, 0.23 mmol) in ethanol (25 mL) is stirred at reflux for 12 h, then the precipitate is filtered and washed with ethanol, water, acetone, diethyl ether and pentane to afford green (**C_5**) and blue (**C_7**) solids.

C_5: Yield 154 mg (92 %): UV-vis (1.0×10^{-5} M, $CHCl_3$): λ_{max} 354 nm ($\varepsilon = 1.17 \times 10^4$ $M^{-1}\cdot cm^{-1}$), λ_{max} 439 nm ($\varepsilon = 1.50 \times 10^4$ $M^{-1}\cdot cm^{-1}$), λ_{max} 483 nm ($\varepsilon = 1.30 \times 10^4$ $M^{-1}\cdot cm^{-1}$), λ_{max} 520 nm ($\varepsilon = 1.30 \times 10^4$ $M^{-1}\cdot cm^{-1}$), λ_{max} 719 nm ($\varepsilon = 0.80 \times 10^4$ $M^{-1}\cdot cm^{-1}$). IR (KBr, cm^{-1}): 3071 (w, CH_{aryl}), 1535 (s, C=O). ^{1}H NMR (400 MHz, $CDCl_3$): δ = 6.98 (s, 4 H, H_q), 5.50 (d, 4 H, H_{cym}), 5.23 (d, 4 H, H_{cym}), 2.87 (sept, 2 H, C*H*$(CH_3)_2$), 2.16 (s, 6 H, CH_3), 1.58 (d, 12 H, CH(C*H*$_3)_2$) ppm. ^{13}C(^{1}H) NMR (100 MHz, $CDCl_3$): δ = 170.9 (CO), 137.0 (CH_q), 111.9 (C_q), 100.3 (C_{cym}), 98.0 (C_{cym}), 82.8 (CH_{cym}), 79.6 (CH_{cym}), 30.7 (*C*H$(CH_3)_2$), 22.4 (CH(*C*H$_3)_2$), 17.9 (CH_3) ppm. Anal. Calc. for $C_{30}H_{32}Cl_2O_4Ru_2$ (729.6): C 49.38, H 4.42; Found: C 49.39, H 4.37.

C_7: Yield 177 mg (93 %): UV-vis (1.0×10^{-5} M, $CHCl_3$): λ_{max} 326 nm ($\varepsilon = 3.06 \times 10^4$ $M^{-1}\cdot cm^{-1}$), λ_{max} 384 nm ($\varepsilon = 2.04 \times 10^4$ $M^{-1}\cdot cm^{-1}$), λ_{max} 416 nm ($\varepsilon = 1.02 \times 10^4$ $M^{-1}\cdot cm^{-1}$), λ_{max} 594 nm ($\varepsilon = 1.19 \times 10^4$ $M^{-1}\cdot cm^{-1}$), λ_{max} 648 nm ($\varepsilon = 0.16 \times 10^4$ $M^{-1}\cdot cm^{-1}$). IR (KBr, cm^{-1}): 3055 (w, CH_{aryl}), 1546 (s, C=O). ^{1}H NMR (400 MHz, $CDCl_3$): δ (ppm) = 8.50 (d, 4 H, H_q), 7.72 (d, 4 H, H_q), 5.68 (d, 4 H, H_{cym}), 5.33 (d, 4 H, H_{cym}), 3.06 (sept, 2 H, C*H*$(CH_3)_2$), 2.42 (s, 6 H, CH_3), 1.57 (d, 12 H, CH(C*H*$_3)_2$). ^{13}C(^{1}H) NMR (100 MHz, $CDCl_3$): δ (ppm) = 169.4 (CO), 134.5 (CH_q), 131.1 (CH_q), 126.8 (C_q), 99.8 (C_{cym}), 97.4 (C_{cym}), 83.1 (CH_{cym}), 79.3 (CH_{cym}), 30.9 (*C*H$(CH_3)_2$), 23.0 (CH(*C*H$_3)_2$), 18.0 (CH_3). Anal. Calc. for $C_{38}H_{36}Cl_2O_4Ru_2$ (829.7): C 55.01, H 4.37; Found: C 55.98, H 4.98.

Procedure for metalla-clip **C_9**: n-BuLi (0.30 mL, 0.48 mmol) is added to a solution of *N*,*N*′-dimethyloxamide (27.9 mg, 0.24 mmol) in THF (15 mL) at -78°C. The reaction mixture is stirred and warmed to room temperature (2 h). Then the mixture is added to a solution of $[(\eta^6$-

p-cym)$RuCl_2]_2$ (146.9 mg, 0.24 mmol) in THF (5 mL), and stirred overnight. The solvent is evaporated and the product is washed with water and pentane.

C_9: Yield 96 mg (61 %). UV-vis (1.0×10^{-5} M, CH_2Cl_2): λ_{max} 306 nm ($\varepsilon = 2.96 \times 10^5$ $M^{-1} \cdot cm^{-1}$). IR (KBr, cm^{-1}): 3060 (w, CH_{aryl}), 1609 (s, C=O). ^{1}H NMR (400 MHz, CD_2Cl_2): δ (ppm) = 5.35 (d, 2 H, H_{cym}), 5.32 (d, 2 H, H_{cym}), 5.26 (d, 2 H, H_{cym}), 5.06 (d, 2 H, H_{cym}), 3.27 (s, 6 H, CH_3), 2.71 (sept, 2 H, C*H*$(CH_3)_2$), 2.12 (s, 6 H, CH_3), 1.21 (d, 6 H, CH(C*H*$_3)_2$), 1.19 (d, 6 H, CH(C*H*$_3)_2$). ^{13}C(^{1}H) NMR (100 MHz, CD_2Cl_2): δ (ppm) = 170.3 (CO), 100.8 (C_{cym}), 95.8 (C_{cym}), 81.9 (CH_{cym}), 81.3 (CH_{cym}), 80.9 (CH_{cym}), 79.6 (CH_{cym}), 38.0 (CH_3), 31.5 (*C*H$(CH_3)_2$), 22.6 (CH(*C*H$_3)_2$), 22.5 (CH(*C*H$_3)_2$), 18.7 (CH_3). Anal. Calc. for $C_{24}H_{34}Cl_2N_2O_2Ru_2$ (655.6): C 43.97, H 5.23, N 4.27; Found: C 43.86, H 5.22, N 4.27.

General procedure for metalla-clips **C_{10}** and **C_{11}**: A mixture of [(η^6-arene)$RuCl_2]_2$ (**C_{10}**: indane, 500 mg, 0.86 mmol; **C_{11}**: nonylbenzene, 647 mg, 0.86 mmol) and 2,5-dihydroxy-1,4-benzoquinone (120 mg, 0.86 mmol) in ethanol (100 mL) was stirred at reflux for 24 h, then filtered. The black precipitate was washed with cold ethanol, pentane, and dried under vacuum.

C_{10}: Yield 528 mg (95 %). UV-vis (1.0×10^{-5} M, CH_2Cl_2): λ_{max} 268 nm ($\varepsilon = 2.83 \times 10^4$ $M^{-1} \cdot cm^{-1}$). IR (KBr, cm^{-1}): 3070 (w, CH_{aryl}), 1629 (s, C=O). ^{1}H NMR (400 MHz, $CDCl_3$): δ (ppm) = 6.31 (d, 8 H, H_{indane}), 6.22 (d, 8 H, H_{indane}), 6.15 (s, 8 H, H_q), 6.12 (t, 8 H, H_{indane}), 6.05 (t, 8 H, H_{indane}), 3.06 (m, 16 H, $CH_{2indane}$), 2.95 (m, 8 H, $CH_{2indane}$). ^{13}C(^{1}H) NMR (100 MHz, $CDCl_3$): δ (ppm) = 184.0 (CO), 104.2 (C_{indane}), 103.7 (C_{indane}), 102.0 (CH_q), 83.0 (CH_{indane}), 82.7 (CH_{indane}), 82.5 (CH_{indane}), 82.4 (CH_{indane}), 30.3 ($CH_{2indane}$), 23.4 ($CH_{2indane}$). Anal. Calc. for $C_{24}H_{22}Cl_2O_4Ru_2$ (647.5): C 44.52, H 3.42; Found: C 44.46, H 3.32.

C_{11}: Yield 690 mg (98 %). UV-vis (1.0×10^{-5} M, (CH_2Cl_2): λ_{max} 275 nm ($\varepsilon = 2.81 \times 10^4$ $M^{-1} \cdot cm^{-1}$). IR (KBr, cm^{-1}): 3068 (w, CH_{aryl}), 1630 (s, C=O). ^{1}H NMR (400 MHz, $CDCl_3$): δ (ppm) = 5.65 (dd, 4 H, H_{phenyl}), 5.56 (t, 2 H, H_{phenyl}), 5.37 (d, 4 H, H_{phenyl}), 2.51 (t, 4 H, $CH_{2\alpha}$), 1.53 (m, 4 H, $CH_{2\beta}$), 1.27 (m, 24 H, CH_2), 0.85 (t, 6 H, CH_3). ^{13}C(^{1}H) NMR (100 MHz, $CDCl_3$): δ (ppm) = 184.2 (CO), 102.5 (C_{phenyl}), 80.5 (CH_{phenyl}), 79.9 (CH_{phenyl}), 78.4 (CH_{phenyl}), 33.8 ($CH_{2\alpha}$), 32.8 ($CH_{2\beta}$), 30.2 (CH_2), 30.1 (CH_2), 30.0 (CH_2), 29.9 (CH_2), 23.4 (CH_2), 14.5 (CH_3). Anal. Calc. for $C_{36}H_{50}Cl_2O_4Ru_2$ (819.8): C 52.74, H 6.15; Found: C 52.66, H 5.97.

Procedure for metalla-clip **C_{12}**: A mixture of $[Ru(\eta^6\text{-}C_6H_5Me)_2Cl_2]_2$ (500 mg, 0.95 mmol) and 2,5-dihydroxy-1,4-benzoquinone (133 mg, 0.95 mmol) in MeOH (100 mL) is stirred at room temperature for 2 h, then filtered. The blood-red precipitate is filtered, washed with diethyl ether, and dried under vacuum.

C_{12}: Yield 452 mg (80 %). UV-vis (1.0×10^{-5} M, (CH_2Cl_2)): λ_{max} 280 nm ($\varepsilon = 3.1 \times 10^4$ $M^{-1}\cdot cm^{-1}$). IR (KBr, cm^{-1}): 3054 (w, CH_{aryl}), 1506 (s, C=O), 1269 (s, CH_3). ^1H NMR (400 MHz, $(CD_3)_2SO$): δ (ppm) = 7.20 (m, 2 H, H_q), 6.14 (m, 2 H, H_{tol}), 5.70 (m, 3 H, H_{tol}), 2.13 (s, 6 H, CH_3). $^{13}C(^1H)$ NMR (100 MHz, $(CD_3)_2SO$): δ (ppm) = 175.5 (CO), 175.2 (CO), 128.7 (CH_q), 95.5 (CCH_3), 89.4 (CH_{tol}), 84.8 (CH_{tol}), 82.2 (CH_{tol}), 16.1 (CH_3). Anal. Calc. for $C_{20}H_{18}Cl_2O_4Ru_2$ (595.4): C 40.34, H 3.02; Found: C 40.57, H 3.32.

6.2.2 Arene Ruthenium Metalla-Rectangles R_{13} – R_{32}

General procedure for metalla-rectangles **R_{13}** – **R_{21}**: A mixture of one equivalent of **C_5** – **C_7** (0.21 mmol), two equivalents of silver trifluoromethanesulfonate (0.43 mmol) and one equivalent of the corresponding *N*∩*N* linker (0.21 mmol) in methanol (40 mL) is stirred at 60°C for 24 hours and then the solution is filtered to remove silver chloride. The solvent is removed under vacuum and the residue is taken up in dichloromethane (3 mL) and diethyl ether is added to precipitate the products as green or blue solids.

R_{13}: Yield 191 mg (85 %): UV-vis (1.0×10^{-5} M, $(CH_3)_2CO$): λ_{max} 306 nm ($\varepsilon = 3.60 \times 10^5$ $M^{-1}.cm^{-1}$), λ_{max} 434 nm ($\varepsilon = 0.27 \times 10^5$ $M^{-1}.cm^{-1}$), λ_{max} 633 nm ($\varepsilon = 0.12 \times 10^5$ $M^{-1}.cm^{-1}$), λ_{max} 692 nm ($\varepsilon = 0.12 \times 10^5$ $M^{-1}.cm^{-1}$). IR (KBr, cm^{-1}): 3066 (w, CH_{aryl}), 1538 (s, C=O), 1263 (s, CF_3). ^1H NMR (400 MHz, CD_3CN): δ (ppm) = 8.56 (s, 8 H, $H_{pyrazine}$), 7.17 (s, 8 H, H_q), 5.77 (d, 8 H, H_{cym}), 5.72 (d, 8 H, H_{cym}), 2.85 (sept, 2 H, $CH(CH_3)_2$), 2.14 (s, 12 H, CH_3), 1.47 (d, 24 H, $CH(CH_3)_2$). $^{13}C(^1H)$ NMR (100 MHz, CD_3CN): δ (ppm) = 171.0 (CO), 148.8 ($CH_{pyrazine}$), 137.4 (CH_q), 111.5 (C_q), 105.3 (C_{cym}), 100.0 (C_{cym}), 84.1 (CH_{cym}), 84.0 (CH_{cym}), 30.8 ($CH(CH_3)_2$), 21.9 ($CH(CH_3)_2$), 16.8 (CH_3). Anal. Calc. for $C_{72}H_{72}F_{12}N_4O_{20}Ru_4S_4$ (2073.8): C 41.70, H 3.49, N 2.70; Found: C 41.02, H 3.16, N, 2.38.

R_{14}: Yield 169 mg (74 %): UV-vis (1.0×10^{-5} M, $(CH_3)_2CO$): λ_{max} 304 nm ($\varepsilon = 3.52 \times 10^5$ $M^{-1}\cdot cm^{-1}$), λ_{max} 442 nm ($\varepsilon = 0.25 \times 10^5$ $M^{-1}\cdot cm^{-1}$), λ_{max} 625 nm ($\varepsilon = 0.12 \times 10^5$ $M^{-1}\cdot cm^{-1}$), λ_{max} 696 nm ($\varepsilon = 0.11 \times 10^5$ $M^{-1}\cdot cm^{-1}$). IR (KBr, cm^{-1}): 3055 (w, CH_{aryl}), 1546 (s, C=O), 1261 (s,

CF_3). ^1H NMR (400 MHz, CD_3CN): δ (ppm) = 8.82 (d, 2 H, H_q), 8.59 (d, 2 H, $H_{q'}$), 8.58 (s, 8 H, $H_{pyrazine}$), 7.93 (d, 2 H, H_q), 7.82 (d, 2 H, $H_{q'}$), 7.17 (s, 2 H, H_q), 7.05 (s, 2 H, $H_{q'}$), 5.91 (d, 4 H, H_{cym}), 5.86 (d, 4 H, H_{cym}), 5.82 (m, 8 H, H_{cym}), 2.82 (sept, 4 H, C*H*$(CH_3)_2$), 2.13 (s, 12 H, CH_3), 1.45 (d, 24 H, CH(C*H*$_3)_2$). $^{13}C(^1H)$ NMR (100 MHz, CD_3CN): δ (ppm) = 172.3 (CO), 171.2 (CO), 145.7 ($CH_{pyrazine}$), 139.2 (CH_q), 132.7 (CH_q), 133.3 (C_q), 133.0 (C_q), 128.1 (CH_q), 104.2 (C_{cym}), 100.1 (C_{cym}), 85.9 (CH_{cym}), 85.1 (CH_{cym}), 83.2 (CH_{cym}), 83.8 (CH_{cym}), 31.5 (*C*H$(CH_3)_2$), 22.7 (CH(*C*$H_3)_2$), 17.6 (CH_3). Anal. calc. for $C_{80}H_{76}F_{12}N_4O_{20}Ru_4S_4$ (2173.4): C 44.21, H 3.52, N 2.58; Found: C 43.05, H 3.22, N, 2.41.

R_{15}: Yield 178 mg (73 %): UV-vis (1.0×10^{-5} M, $(CH_3)_2CO$): λ_{max} 312 nm ($\varepsilon = 3.68 \times 10^5$ $M^{-1}\cdot cm^{-1}$), λ_{max} 380 nm ($\varepsilon = 0.42 \times 10^5$ $M^{-1}\cdot cm^{-1}$), λ_{max} 530 nm ($\varepsilon = 0.14 \times 10^5$ $M^{-1}\cdot cm^{-1}$), λ_{max} 568 nm ($\varepsilon = 0.21 \times 10^5$ $M^{-1}\cdot cm^{-1}$), λ_{max} 613 nm ($\varepsilon = 0.24 \times 10^5$ $M^{-1}\cdot cm^{-1}$). IR (KBr, cm^{-1}): 3060 (w, CH_{aryl}), 1542 (s, C=O), 1260 (s, CF_3). ^1H NMR (400 MHz, CD_3CN): δ (ppm) = 8.57 (d, 8 H, H_q), 8.47 (s, 8 H, $H_{pyrazine}$), 7.82 (d, 8 H, H_q), 5.90 (d, 8 H, H_{cym}), 5.76 (d, 8 H, H_{cym}), 2.93 (sept, 4 H, C*H*$(CH_3)_2$), 2.16 (s, 12 H, CH_3), 1.29 (d, 24 H, CH(C*H*$_3)_2$). $^{13}C(^1H)$ NMR (100 MHz, CD_3CN): δ (ppm) = 169.9 (CO), 149.4 ($CH_{pyrazine}$), 134.2 (CH_q), 128.4 (CH_q), 107.8 (C_q), 107.8 (C_{cym}), 106.1 (C_{cym}), 100.7 (C_q), 84.6 (CH_{cym}), 84.5 (CH_{cym}), 31.3 (*C*H$(CH_3)_2$), 22.4 (CH(*C*$H_3)_2$), 17.8 (CH_3). Anal. calc. for $C_{88}H_{80}F_{12}N_4O_{20}Ru_4S_4$ (2273.50): C 46.49, H 3.52, N 2.46; Found: C 47.65, H 3.78, N 2.80.

R_{16}: Yield 180 mg (77 %): UV-vis (1.0×10^{-5} M, $(CH_3)_2CO$): λ_{max} 306 nm ($\varepsilon = 3.58 \times 10^5$ $M^{-1}.cm^{-1}$), λ_{max} 434 nm ($\varepsilon = 0.25 \times 10^5$ $M^{-1}.cm^{-1}$), λ_{max} 633 nm ($\varepsilon = 0.11 \times 10^5$ $M^{-1}.cm^{-1}$), λ_{max} 692 nm ($\varepsilon = 0.11 \times 10^5$ $M^{-1}.cm^{-1}$). IR (KBr, cm^{-1}): 3070 (w, CH_{aryl}), 1536 (s, C=O), 1261 (s, CF_3). ^1H NMR (400 MHz, CD_3CN): δ (ppm) = 8.43 (s, 8 H, $H_{bipyridine}$), 7.69 (d, 8 H, $H_{bipyridine}$), 7.17 (s, 8 H, H_q), 5.69 (d, 8 H, H_{cym}), 5.48 (d, 8 H, H_{cym}), 2.83 (sept, 4 H, C*H*$(CH_3)_2$), 2.16 (s, 12 H, CH_3), 1.37 (d, 24 H, CH(C*H*$_3)_2$). $^{13}C(^1H)$ NMR (100 MHz, CD_3CN): δ (ppm) = 171.9 (CO), 153.9 ($CH_{bipyridine}$), 145.8 ($C_{bipyridine}$), 138.4 (CH_q), 123.9 ($CH_{bipyridine}$), 114.8 (C_q), 104.7 (C_{cym}), 100.5 (C_{cym}), 85.2 (CH_{cym}), 84.0 (CH_{cym}), 31.5 (*C*H$(CH_3)_2$), 23.1 (CH(*C*$H_3)_2$), 17.3 (CH_3). Anal. calc. for $C_{84}H_{80}F_{12}N_4O_{20}Ru_4S_4$ (2226.0): C 45.32, H 3.62, N 2.52; Found: C 44.82, H 3.48, N 2.42.

R_{17}: Yield 192 mg (77 %): UV-vis (1.0×10^{-5} M, $(CH_3)_2CO$): λ_{max} 312 nm ($\varepsilon = 3.58 \times 10^5$ $M^{-1}\cdot cm^{-1}$), λ_{max} 418 nm ($\varepsilon = 0.39 \times 10^5$ $M^{-1}\cdot cm^{-1}$), λ_{max} 608 nm ($\varepsilon = 0.16 \times 10^5$ $M^{-1}\cdot cm^{-1}$), λ_{max} 658 nm ($\varepsilon = 0.18 \times 10^5$ $M^{-1}\cdot cm^{-1}$). IR (KBr, cm^{-1}): 3069 (w, CH_{aryl}), 1539 (s, C=O), 1260 (s, CF_3). ^1H NMR (400 MHz, CD_3CN): δ (ppm) = 8.62 (m, 4 H, $H_q + H_{q'}$), 8.46 (d, 8 H, H_α), 7.93

(m, 4 H, $H_{q\,+\,Hq'}$), 7.60 (d, 8 H, H_β), 7.21 (s, 2 H, H_q), 7.20 (s, 2 H, $H_{q'}$), 5.78 (d, 4 H, H_{cym}), 5.73 (d, 4 H, H_{cym}), 5.56 (m, 8 H, H_{cym}), 2.85 (sept, 4 H, C*H*$(CH_3)_2$), 2.11 (s, 12 H, CH_3), 1.30 (d, 24 H, CH(C*H*$_3)_2$). $^{13}C(^1H)$ NMR (100 MHz, CD_3CN): δ (ppm) = 171.2 (CO), 170.3 (CO), 153.8 (CH_α), 145.7 (C_{bipy}), 138.7 (CH_q), 134.4 (CH_q), 134.0 (C_q), 133.9 (C_q), 128.3 (CH_q), 123.9 (CH_β), 104.6 (C_{cym}), 100.5 (C_{cym}), 85.2 (CH_{cym}), 84.9 (CH_{cym}), 83.7 (CH_{cym}), 83.7 (CH_{cym}), 31.4 (*C*H$(CH_3)_2$), 22.5 (CH(*C*$H_3)_2$), 17.6 (CH_3). Anal. calc. for $C_{92}H_{84}F_{12}N_4O_{20}Ru_4S_4$ (2325.55): C 47.52, H 3.61, N 2.41; Found: C 45.48, H 3.27, N 2.21.

R_{18}: Yield 211 mg (81 %): UV-vis (1.0×10^{-5} M, $(CH_3)_2CO$): λ_{max} 312 nm ($\varepsilon = 3.58 \times 10^5$ $M^{-1}\cdot cm^{-1}$), λ_{max} 384 nm ($\varepsilon = 0.34 \times 10^5$ $M^{-1}\cdot cm^{-1}$), λ_{max} 533 nm ($\varepsilon = 0.14 \times 10^5$ $M^{-1}\cdot cm^{-1}$), λ_{max} 573 nm ($\varepsilon = 0.19 \times 10^5$ $M^{-1}\cdot cm^{-1}$), λ_{max} 618 nm ($\varepsilon = 0.20 \times 10^5$ $M^{-1}\cdot cm^{-1}$). IR (KBr, cm^{-1}): 3071 (w, CH_{aryl}), 1543 (s, C=O), 1262 (s, CF_3). ^1H NMR (400 MHz, CD_3CN): δ (ppm) = 8.69 (d, 8 H, H_q), 7.93 (d, 8 H, H_α), 7.57 (d, 8 H, H_β), 7.52 (d, 8 H, H_q), 5.85 (d, 8 H, H_{cym}), 5.63 (d, 8 H, H_{cym}), 2.88 (sept, 4 H, C*H*$(CH_3)_2$), 2.16 (s, 12 H, CH_3), 1.37 (d, 24 H, CH(C*H*$_3)_2$). $^{13}C(^1H)$ NMR (100 MHz, CD_3CN): δ (ppm) = 170.0 (CO), 153.7 (CH_α), 134.5 (C_{bipy}), 134.0 (CH_q), 128.2 (CH_β), 123.9 (CH_q), 108.0 (C_q), 104.7 (C_{cym}), 100.7 (C_{cym}), 85.1 (CH_{cym}), 83.5 (CH_{cym}), 31.4 (*C*H$(CH_3)_2$), 22.4 (CH(*C*$H_3)_2$), 17.8 (CH_3). Anal. calc. for $C_{100}H_{88}F_{12}N_4O_{20}Ru_4S_4$ (2425.64): C 49.52, H 3.63, N 2.31; Found: C 51.20, H 3.75, N 2.80.

R_{19}: Yield 178 mg (73 %): UV-vis (1.0×10^{-5} M, $(CH_3)_2CO$): λ_{max} 314 nm ($\varepsilon = 3.76 \times 10^5$ $M^{-1}.cm^{-1}$), λ_{max} 438 nm ($\varepsilon = 0.33 \times 10^5$ $M^{-1}.cm^{-1}$), λ_{max} 608 nm ($\varepsilon = 0.14 \times 10^5$ $M^{-1}.cm^{-1}$), λ_{max} 650 nm ($\varepsilon = 0.13 \times 10^5$ $M^{-1}.cm^{-1}$), 713 nm ($\varepsilon = 0.13 \times 10^5$ $M^{-1}.cm^{-1}$). IR (KBr, cm^{-1}): 3067 (w, CH_{aryl}), 1537 (s, C=O), 1272 (s, CF_3). ^1H NMR (400 MHz, CD_3CN): δ (ppm) = 8.28 (d, 8 H, $H_{pyridine}$), 7.45 (d, 8 H, $H_{pyridine}$), 7.31 (s, 4 H, $H_{C=C}$), 7.15 (s, 8 H, H_q), 5.66 (d, 8 H, H_{cym}), 5.46 (d, 8 H, H_{cym}), 2.79 (sept, 4 H, C*H*$(CH_3)_2$), 2.17 (s, 12 H, CH_3), 1.29 (d, 24 H, CH(C*H*$_3)_2$). $^{13}C(^1H)$ NMR (100 MHz, CD_3CN): δ (ppm) = 171.8 (CO), 153.2 ($CH_{pyridine}$), 146.9 ($C_{pyridine}$), 138.3 (CH_q), 132.1 ($C_{ethylene}$), 124.2 ($CH_{pyridine}$), 112.3 (C_q), 104.5 (C_{cym}), 100.2 (C_{cym}), 85.1 (CH_{cym}), 84.0 (CH_{cym}), 31.4 (*C*H$(CH_3)_2$), 22.3 (CH(*C*$H_3)_2$), 17.3 (CH_3). Anal. calc. for $C_{88}H_{84}F_{12}N_4O_{20}Ru_4S_4$ (2278.0): C 46.40, H 3.72, N 2.46; Found: C 45.59, H 3.32, N 2.60.

R_{20}: Yield 189 mg (74 %): UV-vis (1.0×10^{-5} M, $(CH_3)_2CO$): λ_{max} 313 nm ($\varepsilon = 3.75 \times 10^5$ $M^{-1}\cdot cm^{-1}$), λ_{max} 416 nm ($\varepsilon = 0.35 \times 10^5$ $M^{-1}\cdot cm^{-1}$), λ_{max} 608 nm ($\varepsilon = 0.14 \times 10^5$ $M^{-1}\cdot cm^{-1}$), λ_{max} 658 nm ($\varepsilon = 0.16 \times 10^5$ $M^{-1}\cdot cm^{-1}$). IR (KBr, cm^{-1}): 3068 (w, CH_{aryl}), 1538 (s, C=O), 1260 (s, CF_3). ^1H NMR (400 MHz, CD_3CN): δ (ppm) = 8.63 (m, 4 H, $H_{q\,+\,Hq'}$), 8.33 (d, 8 H, H_α), 7.92 (m, 4 H, $H_{q\,+\,Hq'}$), 7.38 (d, 8 H, H_β), 7.23 (s, 4 H, $H_{C=C}$), 7.18 (s, 2 H, H_q), 7.17 (s, 2 H, $H_{q'}$),

5.76 (d, 4 H, H_{cym}), 5.69 (d, 4 H, H_{cym}), 5.53 (d, 4 H, H_{cym}), 5.51 (d, 4 H, H_{cym}), 2.85 (sept, 4 H, C*H*$(CH_3)_2$), 2.11 (s, 12 H, CH_3), 1.29 (d, 24 H, CH(C*H*$_3)_2$). $^{13}C(^1H)$ NMR (100 MHz, CD_3CN): δ (ppm) = 171.3 (CO), 170.4 (CO), 153.1 (CH_α), 146.8 ($C_{ethylene}$), 138.6 (CH_q), 134.2 (CH_q), 134.1 (C_q), 132.0 (C_q), 128.3 (CH_q), 128.2 (CH=CH), 124.1 (CH_β), 110.6 (CF_3), 104.5 (C_{cym}), 100.3 (C_{cym}), 85.1 (CH_{cym}), 84.8 (CH_{cym}), 83.8 (CH_{cym}), 83.7 (CH_{cym}), 31.4 (*C*H$(CH_3)_2$), 22.5 (CH(*C*H$_3)_2$), 17.6 (CH_3). Anal. calc. for $C_{96}H_{88}F_{12}N_4O_{20}Ru_4S_4$ (2377.61): C 48.50, H 3.70, N 2.35; Found: C 46.87, H 3.96, N 2.62.

R_{21}: Yield 199 mg (75 %): UV-vis (1.0×10^{-5} M, $(CH_3)_2CO$): λ_{max} 315 nm ($\varepsilon = 3.84 \times 10^5$ $M^{-1}\cdot cm^{-1}$), λ_{max} 382 nm ($\varepsilon = 0.46 \times 10^5$ $M^{-1}\cdot cm^{-1}$), λ_{max} 531 nm ($\varepsilon = 0.12 \times 10^5$ $M^{-1}\cdot cm^{-1}$), λ_{max} 570 nm ($\varepsilon = 0.20 \times 10^5$ $M^{-1}\cdot cm^{-1}$), λ_{max} 618 nm ($\varepsilon = 0.24 \times 10^5$ $M^{-1}\cdot cm^{-1}$). IR (KBr, cm^{-1}): 3070 (w, CH_{aryl}), 1543 (s, C=O), 1259 (s, CF_3). ^1H NMR (400 MHz, CD_3CN): δ (ppm) = 8.69 (d, 8 H, H_q), 8.37 (d, 8 H, H_α), 7.92 (d, 8 H, H_q), 7.30 (d, 8 H, H_β), 7.14 (s, 4 H, $H_{C=C}$), 5.81 (d, 8 H, H_{cym}), 5.60 (d, 8 H, H_{cym}), 2.90 (sept, 4 H, $CH(CH_3)_2$), 2.13 (s, 12 H, CH_3), 1.28 (d, 24 H, $CH(CH_3)_2$). $^{13}C(^1H)$ NMR (100 MHz, CD_3CN): δ (ppm) = 170.4 (CO), 153.0 (CH_α), 146.8 ($C_{ethylene}$), 134.6 (CH_q), 133.9 (C_q), 133.8 (C_q), 131.9 (CH_q), 128.1 (CH=CH), 124.1 (CH_β), 100.4 (C_{cym}), 84.9 (CH_{cym}), 83.5 (CH_{cym}), 31.4 (*C*H$(CH_3)_2$), 22.5 (CH(*C*H$_3)_2$), 17.9 (CH_3). Anal. calc. for $C_{104}H_{92}F_{12}N_4O_{20}Ru_4S_4$ (2477.69): C 50.41, H 3.71, N 2.26; Found: C 48.22, H 3.51, N 2.38.

General procedure for metalla-rectangles **R_{23}** – **R_{31}**: $AgCF_3SO_3$ (149.0 mg, 0.58 mmol) is added to a suspension of $[(\eta^6\text{-}p\text{-cym})_2Ru_2(OO\cap OO)Cl_2]$ (*OO*∩*OO* = oxa (**R_{23}**, **R_{30}**; 190.1 mg), oxo (**R_{24}**, **R_{31}**; 202.6 mg), ox (**R_{25}**; 182.6 mg), dobq (**R_{26}**; 196.9 mg), donq (**R_{27}**; 211.4 mg), doaq (**R_{28}**; 225.9 mg), dotq (**R_{29}**; 240.4 mg); 0.29 mmol) in methanol (100 mL) at 60 °C and stirred for 12 h, followed by filtration to remove AgCl. Then, 1,2-bis(4-pyridyl)ethylene (**R_{23}**, **R_{24}**; 52.8 mg, 0.29 mmol) or 1,2-bis(4-pyridyl)ethane (**R_{25}** – **R_{31}**; 53.4 mg, 0.29 mmol) is added to the filtrate. The solution is stirred at 60 °C for 24 h. The solvent is removed and the residue extracted with dichloromethane. The filtrate is concentrated to about 2 mL and diethyl ether is added. The precipitate is washed with diethyl ether (3 × 50 mL) and pentane (3 × 50 mL) and dried *in vacuo* to give the corresponding product as powder.

R_{23}: Yield 200 mg (65 %). UV-vis (1.0×10^{-5} M, CH_2Cl_2): λ_{max} 269 nm ($\varepsilon = 3.15 \times 10^5$ $M^{-1}\cdot cm^{-1}$), λ_{max} 340 nm ($\varepsilon = 0.61 \times 10^5$ $M^{-1}\cdot cm^{-1}$). IR (KBr, cm^{-1}): 3070 (m, CH_{ar}), 1616 (s, C=O), 1256 (s, CF_3). ^1H NMR (400 MHz, CD_3CN): δ (ppm) = 7.95 (m, 8 H, H_α), 7.53 (m, 8 H, H_β), 7.40 (s, 4 H, $H_{C=C}$), 5.80 (m, 8 H, H_{cym}), 5.30 (m, 8 H, H_{cym}), 3.51 (s, 12 H, CH_3), 2.75

(m, 4 H, C*H*$(CH_3)_2$), 1.96 (s, 12 H, CH_3), 1.30 (m, 24 H, CH(C*H*$_3)_2$). $^{13}C(^1H)$ NMR (100 MHz, CD_3CN): δ (ppm) = 170.6 (CO), 152.8 (CH_α), 145.8 (C_{pyr}), 132.0 (HC=CH), 123.4 (CH_β), 102.4 (C_{cym}), 99.7 (C_{cym}), 86.5 (CH_{cym}), 84.5 (CH_{cym}), 81.7 (CH_{cym}), 78.4 (CH_{cym}), 37.9 (CH_3), 31.0 (*C*H$(CH_3)_2$), 21.6 (CH(*C*H$_3)_2$), 16.9 (CH_3). Anal. calc. for $C_{76}H_{88}F_{12}N_8O_{16}Ru_4S_4$ (2130.1): C 42.85, H 4.16, N 5.26; Found: C 42.76, H 4.30, N 5.18.

R_{24}: Yield 208 mg (65 %). UV-vis (1.0×10^{-5} M, CH_2Cl_2): λ_{max} 265 nm ($\varepsilon = 3.00 \times 10^5$ $M^{-1}\cdot cm^{-1}$), λ_{max} 331 nm ($\varepsilon = 0.51 \times 10^5$ $M^{-1}\cdot cm^{-1}$). IR (KBr, cm^{-1}): 3077 (m, CH_{ar}), 1712 (s, C=N), 1612 (s, C=O), 1259 (s, CF_3). ^1H NMR (400 MHz, CD_3CN): δ (ppm) = 7.95 (m, 8 H, H_α), 7.53 (m, 8 H, H_β), 7.40 (s, 4 H, $H_{C=C}$), 5.80 (m, 8 H, H_{cym}), 5.30 (m, 8 H, H_{cym}), 3.51 (s, 12 H, CH_3), 2.75 (m, 4 H, C*H*$(CH_3)_2$), 1.96 (s, 12 H, CH_3), 1.30 (m, 24 H, CH(C*H*$_3)_2$). $^{13}C(^1H)$ NMR (100 MHz, CD_3CN): δ (ppm) = 178.9 (CO), 162.4 (CN), 154.6 (CH_α), 146.1 (C_{pyr}), 132.1 (HC=CH), 124.0 (CH_β), 106.0 (C_{cym}), 99.4 (C_{cym}), 83.9 (CH_{cym}), 83.7 (CH_{cym}), 83.6 (CH_{cym}), 80.7 (CH_{cym}), 30.9 (*C*H$(CH_3)_2$), 21.5 (CH(*C*H$_3)_2$), 17.0 (CH_3). Anal. calc. for $C_{76}H_{78}F_{12}N_{10}O_{20}Ru_4S_4$ (2212.0): C 41.27, H 3.55, N 6.33; Found: C 41.20, H 3.66, N 6.22.

R_{25}: Yield 205 mg (68 %). UV-vis (1.0×10^{-5} M, CH_2Cl_2): λ_{max} 267 nm ($\varepsilon = 2.89 \times 10^5$ $M^{-1}\cdot cm^{-1}$). IR (KBr, cm^{-1}): 3070 (m, CH_{ar}), 1533 (s, C=O), 1259 (s, CF_3). ^1H NMR (400 MHz, CD_3CN): δ (ppm) = 7.74 (d, 8 H, H_α), 7.00 (d, 8 H, H_β), 5.82 (d, 8 H, H_{cym}), 5.69 (d, 8 H, H_{cym}), 3.25 (s, 8 H, H_{bpa}), 2.80 (sept, 4 H, C*H*$(CH_3)_2$), 2.15 (s, 12 H, CH_3), 1.30 (d, 24 H, CH(C*H*$_3)_2$). $^{13}C(^1H)$ NMR (100 MHz, CD_3CN): δ (ppm) = 173.0 (CO), 151.8 (CH_α), 145.2 (C_{pyr}), 127.3 (CH_β), 100.2 (C_{cym}), 98.7 (C_{cym}), 84.9 (CH_{cym}), 83.7 (CH_{cym}), 33.0 (CH_{bpa}), 32.2 (*C*H$(CH_3)_2$), 22.7 (CH(*C*H$_3)_2$), 19.2 (CH_3). Anal. calc. for $C_{72}H_{80}F_{12}N_4O_{20}Ru_4S_4$ (2081.9): C 41.54, H 3.87, N 2.69; Found: C 41.45, H 4.03, N 2.65.

R_{26}: Yield 259 mg (82 %). UV-vis (1.0×10^{-5} M, CH_2Cl_2): λ_{max} 265 nm ($\varepsilon = 3.01 \times 10^5$ $M^{-1}\cdot cm^{-1}$), λ_{max} 317 nm ($\varepsilon = 0.46 \times 10^5$ $M^{-1}\cdot cm^{-1}$), λ_{max} 510 nm ($\varepsilon = 0.43 \times 10^5$ $M^{-1}\cdot cm^{-1}$). IR (KBr, cm^{-1}): 3068 (m, CH_{ar}), 1530 (s, C=O), 1260 (s, CF_3). ^1H NMR (400 MHz, CD_3CN) : δ (ppm) = 7.78 (d, 8 H, H_α), 7.13 (d, 8 H, H_β), 5.92 (d, 8 H, H_{cym}), 5.86 (d, 8 H, H_{cym}), 5.48 (s, 4 H, H_q), 3.26 (s, 8 H, H_{bpa}), 2.85 (sept, 4 H, C*H*$(CH_3)_2$), 2.10 (s, 12 H, CH_3), 1.30 (d, 24 H, CH(C*H*$_3)_2$). $^{13}C(^1H)$ NMR (100 MHz, CD_3CN): δ (ppm) = 171.4 (CO), 153.2 (CH_α), 150.7 (C_{pyr}), 130.1 (CH_β), 114.6 (CH_q), 108.2 (C_q), 102.1 (C_{cym}), 99.8 (C_{cym}), 84.2 (CH_{cym}), 84.0 (CH_{cym}), 29.3 (CH_{bpa}), 30.0 (*C*H$(CH_3)_2$), 20.9 (CH(*C*H$_3)_2$), 17.4 (CH_3). Anal. calc. for $C_{80}H_{84}F_{12}N_4O_{20}Ru_4S_4$ (2182.1): C 44.03, H 3.88, N 2.57; Found: C 43.92, H 4.00, N 2.50.

R_{27}: Yield 248 mg (75 %). UV-vis (1.0×10^{-5} M, CH_2Cl_2): λ_{max} 266 nm ($\varepsilon = 2.99 \times 10^5$ $M^{-1}\cdot cm^{-1}$), λ_{max} 327 nm ($\varepsilon = 0.30 \times 10^5$ $M^{-1}\cdot cm^{-1}$), λ_{max} 454 nm ($\varepsilon = 0.22 \times 10^5$ $M^{-1}\cdot cm^{-1}$), λ_{max} 720 nm ($\varepsilon = 0.08 \times 10^5$ $M^{-1}\cdot cm^{-1}$). IR (KBr, cm^{-1}): 3070 (m, CH_{ar}), 1529 (s, C=O), 1259 (s, CF_3). ^{1}H NMR (400 MHz, CD_3CN) : δ (ppm) = 7.94 (d, 8 H, H_α), 7.03 (d, 8 H, H_β), 6.96 (s, 8 H, H_q), 5.66 (d, 8 H, H_{cym}), 5.44 (d, 8 H, H_{cym}), 3.21 (s, 8 H, H_{bpa}), 2.82 (sept, 4 H, C*H*$(CH_3)_2$), 2.10 (s, 12 H, CH_3), 1.30 (d, 24 H, CH(C*H*$_3)_2$). ^{13}C(^{1}H) NMR (100 MHz, CD_3CN): δ (ppm) = 170.3 (CO), 152.9 (CH_α), 151.9 (C_{pyr}), 137.2 (CH_β), 125.8 (CH_q), 111.3 (C_q), 103.4 (C_{cym}), 99.0 (C_{cym}), 83.7 (CH_{cym}), 82.8 (CH_{cym}), 31.1 (CH_{bpa}), 30.6 (*C*H$(CH_3)_2$), 21.4 (CH(*C*H$_3)_2$), 16.5 (CH_3). Anal. calc. for $C_{88}H_{88}F_{12}N_4O_{20}Ru_4S_4$ (2282.2): C 46.31, H 3.89, N 2.45; Found: C 46.16, H 3.99, N 2.39.

R_{28}: Yield 266 mg (77 %). UV-vis (1.0×10^{-5} M, CH_2Cl_2): λ_{max} 264 nm ($\varepsilon = 3.01 \times 10^5$ $M^{-1}\cdot cm^{-1}$), λ_{max} 324 nm ($\varepsilon = 0.32 \times 10^5$ $M^{-1}\cdot cm^{-1}$), λ_{max} 417 nm ($\varepsilon = 0.25 \times 10^5$ $M^{-1}\cdot cm^{-1}$), λ_{max} 683 nm ($\varepsilon = 0.13 \times 10^5$ $M^{-1}\cdot cm^{-1}$). IR (KBr, cm^{-1}): 3070 (m, CH_{ar}), 1528 (s, C=O), 1260 (s, CF_3). ^{1}H NMR (400 MHz, CD_3CN) : δ (ppm) = 8.46 (d, 8 H, H_α), 8.01 (d, 8 H, H_β), 7.90 (m, 4 H, H_q), 7.06 (s, 4 H, H_q), 5.78 (d, 4 H, H_{cym}), 5.73 (d, 4 H, H_{cym}), 5.54 (d, 4 H, H_{cym}), 5.50 (d, 4 H, H_{cym}), 3.21 (s, 8 H, H_{bpa}), 2.92 (sept, 4 H, C*H*$(CH_3)_2$), 2.11 (s, 12 H, CH_3), 1.34 (d, 12 H, CH(C*H*$_3)_2$), 1.30 (d, 12 H, CH(C*H*$_3)_2$). ^{13}C(^{1}H) NMR (100 MHz, CD_3CN): δ (ppm) = 171.5 (CO), 170.7 (CO), 155.4 (CH_α), 151.9 (C_{pyr}), 139.9 (**C**H_q), 138.3 (CH_β), 136.6 (**C**H_q), 134.3 (C_q), 132.0 (C_q), 128.2 (CH_q), 104.7 (C_{cym}), 100.3 (C_{cym}), 85.4 (CH_{cym}), 84.8 (CH_{cym}), 83.9 (CH_{cym}), 82.0 (CH_{cym}), 29.2 (CH_{bpa}), 31.2 (*C*H$(CH_3)_2$), 21.2 (CH(*C*H$_3)_2$), 21.0 (CH(*C*H$_3)_2$), 17.0 (CH_3). Anal. calc. for $C_{96}H_{92}F_{12}N_4O_{20}Ru_4S_4$ (2382.3): C 48.40; H 3.89; N 2.35; Found: C 48.22; H 4.001; N, 2.30.

R_{29}: Yield 255 mg (71 %). UV-vis (1.0×10^{-5} M, CH_2Cl_2): λ_{max} 267 nm ($\varepsilon = 3.07 \times 10^5$ $M^{-1}\cdot cm^{-1}$), λ_{max} 327 nm ($\varepsilon = 0.44 \times 10^5$ $M^{-1}\cdot cm^{-1}$), λ_{max} 379 nm ($\varepsilon = 0.38 \times 10^5$ $M^{-1}\cdot cm^{-1}$), λ_{max} 409 nm ($\varepsilon = 0.29 \times 10^5$ $M^{-1}\cdot cm^{-1}$), λ_{max} 588 nm ($\varepsilon = 0.16 \times 10^5$ $M^{-1}\cdot cm^{-1}$), λ_{max} 636 nm ($\varepsilon = 0.19 \times 10^5$ $M^{-1}\cdot cm^{-1}$). IR (KBr, cm^{-1}): 3068 (m, CH_{ar}), 1532 (s, C=O), 1260 (s, CF_3). ^{1}H NMR (400 MHz, CD_3CN) : δ (ppm) = 8.53 (d, 8 H, H_α), 7.97 (d, 8 H, H_q), 7.89 (d, 8 H, H_β), 6.88 (d, 8 H, H_q), 5.85 (d, 8 H, H_{cym}), 5.61 (d, 8 H, H_{cym}), 3.33 (s, 8 H, H_{bpa}), 3.00 (sept, 4 H, C*H*$(CH_3)_2$), 2.12 (s, 12 H, CH_3), 1.37 (d, 24 H, CH(C*H*$_3)_2$). ^{13}C(^{1}H) NMR (100 MHz, CD_3CN): δ (ppm) = 170.4 (CO), 153.1 (CH_α), 152.5 (C_{pyr}), 139.1 (CH_β), 134.7 (CH_q), 133.6 (C_q), 133.5 (C_q), 132.4 (CH_q), 100.2 (C_{cym}), 96.0 (C_{cym}), 84.7 (CH_{cym}), 83.9 (CH_{cym}), 32.3

(CH_{bpa}), 31.3 ($CH(CH_3)_2$), 19.8 ($CH(CH_3)_2$), 17.0 (CH_3). Anal. calc. for $C_{104}H_{96}F_{12}N_4O_{20}Ru_4S_4$ (2482.4): C 50.32, H 3.90, N 2.26; Found: C 50.11, H 3.97, N 2.20.

R_{30}: Yield 191 mg (62 %). UV-vis (1.0×10^{-5} M, CH_2Cl_2): λ_{max} 727 nm ($\varepsilon = 3.08 \times 10^5$ $M^{-1} \cdot cm^{-1}$), λ_{max} 342 nm ($\varepsilon = 0.65 \times 10^5$ $M^{-1} \cdot cm^{-1}$). IR (KBr, cm^{-1}): 3073 (m, CH_{ar}), 1620 (s, C=O), 1259 (s, CF_3). ^{1}H NMR (400 MHz, CD_3CN): δ (ppm) = 7.89 (d, 4 H, H_α), 7.67 (d, 4 H, H_α), 7.09 (d, 4 H, H_β), 6.84 (d, 4 H, H_β), 5.81 (d, 4 H, H_{cym}), 5.73 (d, 4 H, H_{cym}), 5.45 (d, 4 H, H_{cym}), 5.31 (d, 4 H, H_{cym}), 3.36 (s, 12 H, CH_3), 2.70 (sept, 4 H, $CH(CH_3)_2$), 2.28 (br, 8 H, H_{bpa}), 1.81 (s, 12 H, CH_3), 1.78 (d, 12 H, $CH(CH_3)_2$), 1.22 (d, 12 H, $CH(CH_3)_2$). $^{13}C(^1H)$ NMR (100 MHz, CD_3CN): δ (ppm) = 170.1 (CO), 153.8 (CH_α), 153.5 (CH_α), 152.8 (C_{pyr}), 150.6 (C_{pyr}), 129.1 (CH_β), 128.0 (CH_β), 103.5 (C_{cym}), 99.8 (C_{cym}), 86.7 (CH_{cym}), 84.7 (CH_{cym}), 82.6 (CH_{cym}), 79.3 (CH_{cym}), 38.5 (CH_3), 36.0 (CH_{bpa}), 22.5 ($CH(CH_3)_2$), 22.4 ($CH(CH_3)_2$), 18.1 (CH_3). Anal. calc. for $C_{76}H_{92}F_{12}N_8O_{16}Ru_4S_4$ (2134.1): C 42.77, H 4.35, N 5.25; Found: C 42.68, H 4.48, N 5.16.

R_{31}: Yield 251 mg (78 %). UV-vis (1.0×10^{-5} M, CH_2Cl_2): λ_{max} 269 nm ($\varepsilon = 2.81 \times 10^5$ $M^{-1} \cdot cm^{-1}$), λ_{max} 374 nm ($\varepsilon = 0.20 \times 10^5$ $M^{-1} \cdot cm^{-1}$). IR (KBr, cm^{-1}): 3077 (m, CH_{ar}), 1709 (s, C=N), 1594 (s, C=O), 1260 (s, CF_3). ^{1}H NMR (400 MHz, CD_3CN): δ (ppm) = 9.98 (s, 2 H, NH), 8.02 (m, 4 H, H_α), 7.42 (m, 4 H, H_α), 7.06 (m, 4 H, H_β), 6.92 (m, 4 H, H_β), 6.02 (m, 8 H, H_{cym}), 5.90 (m, 4 H, H_{cym}), 5.80 (m, 4 H, H_{cym}), 3.24 (s, 8 H, H_{bpa}), 2.73 (m, 4 H, $CH(CH_3)_2$), 2.09 (s, 12 H, CH_3), 1.23 (m, 12 H, $CH(CH_3)_2$), 1.15 (m, 12 H, $CH(CH_3)_2$). $^{13}C(^1H)$ NMR (100 MHz, CD_3CN): δ (ppm) = 178.9 (CO), 162.4 (CN), 154.6 (CH_α), 146.2 (C_{pyr}), 124.1 (CH_β), 106.1 (C_{cym}), 99.3 (C_{cym}), 84.0 (CH_{cym}), 83.8 (CH_{cym}), 83.7 (CH_{cym}), 83.6 (CH_{cym}), 30.9 ($CH(CH_3)_2$), 21.5 ($CH(CH_3)_2$), 17.1 (CH_3). Anal. calc. for $C_{76}H_{82}F_{12}N_{10}O_{20}Ru_4S_4$ (2216.0): C 41.19, H 3.73, N 6.32; Found: C 41.15, H 3.87, N 6.23.

Procedure for metalla-rectangle **R_{32}**: A solution of metalla-rectangle **R_{22}** (100 mg, 0.05 mmol) in methanol (10 mL) is stirred close to the Hg lamp (180 W) for 60 h. The solvent is removed ant the powder is washed with dichloromethane to give **R_{32}**.

R_{32}: Yield 83 mg (83 %). UV-vis (1.0×10^{-5} M, CH_3OH): λ_{max} 266 nm ($\varepsilon = 3.4 \times 10^5$ $M^{-1} \cdot cm^{-1}$). IR (KBr, cm^{-1}): 3077 (m, CH_{ar}), 1628 (s, C=O), 1262 (s, CF_3). ^{1}H NMR (400 MHz, CD_3OD): δ (ppm) = 8.05 (d, 4 H, H_{pyr}), 7.94 (d, 4 H, H_{pyr}), 7.55 (dd, 4 H, H_{pyr}), 7.21 (dd, 4 H, H_{pyr}), 5.97 (d, 8 H, H_{cym}), 5.79 (d, 8 H, H_{cym}), 4.99 (s, 4 H, CH-CH), 2.84 (sept, 4 H, $CH(CH_3)_2$), 2.20 (s, 12 H, CH_3), 1.35 (d, 24 H, $CH(CH_3)_2$). $^{13}C(^1H)$ NMR (100 MHz,

CD_3OD): 171.9 (CO), 154.3 (CH_{pyr}), 153.5 (CH_{pyr}), 152.9 (C_{pyr}),128.9 (CH_{pyr}), 125.6 (CH_{pyr}), 103.9 (C_{cym}), 98.6 (C_{cym}), 83.2 (CH_{cym}), 82.8 (CH_{cym}), 44.9 (CH-CH), 32.5 ($CH(CH_3)_2$), 22.5 ($CH(CH_3)_2$), 18.0 (CH_3).

6.2.3 Arene Ruthenium Metalla-Prisms $P_2 - P_4$

General procedure for metalla-prisms **$P_2 - P_4$**: A mixture of $[(\eta^6\text{-}p\text{-cym})_2Ru_2(OO\cap OO)Cl_2]$ ($OO\cap OO$ = donq 46.6 mg, doaq 50.0 mg, dotq 53.3 mg; 0.064 mmol), $AgCF_3SO_3$ (33.0 mg, 0.128 mmol) and tpt (13.4 mg, 0.043 mmol) in MeOH (20 mL) is heated under reflux for 24h, and then filtered. The solvent is removed and the dark residue is dissolved in CH_2Cl_2 (3 mL) and diethyl ether is added to precipitate a dark green solid. The solid is filtered and dried under vacuum.

P_2: Yield 60 mg (80 %). UV-vis (1.0×10^{-5} M, $(CH_3)_2CO$): λ_{max} 308 nm ($\varepsilon = 3.93 \times 10^5$ $M^{-1}\cdot cm^{-1}$), λ_{max} 437 nm ($\varepsilon = 0.53 \times 10^5$ $M^{-1}\cdot cm^{-1}$), λ_{max} 643 nm ($\varepsilon = 0.18 \times 10^5$ $M^{-1}\cdot cm^{-1}$), λ_{max} 700 nm ($\varepsilon = 0.19 \times 10^5$ $M^{-1}\cdot cm^{-1}$). IR (KBr, cm^{-1}): 3064 (w, CH_{aryl}), 1536 (s, C=O), 1259 (s, CF_3). ^1H NMR (400 MHz, CD_3CN): δ (ppm) = 8.58 (d, 12 H, H_{pyr}), 8.47 (d, 12 H, H'_{pyr}), 7.22 (s, 12 H, H_q), 5.73 (d, 12 H, H_{cym}), 5.52 (d, 12 H, H_{cym}), 2.85 (sept, 6 H, $CH(CH_3)_2$), 2.10 (d, 18 H, CH_3), 1.33 (d, 36 H, $CH(CH_3)_2$). $^{13}C(^1H)$ NMR (100 MHz, CD_3CN): δ (ppm) = 171.8 (CO), 170.7 (C_{tpt}), 154.3 (CH_{pyr}), 145.2 (C_{tpt}), 138.4 (CH_q), 125.0 (CH'_{pyr}), 112.5 (C_q), 104.9 (C_{cym}), 100.5 (C_{cym}), 85.2 (CH_{cym}), 84.2 (CH_{cym}), 31.5 ($CH(CH_3)_2$), 23.1 ($CH(CH_3)_2$), 22.3 ($CH(CH_3)_2$), 17.3 (CH_3). Anal. calc. for $C_{132}H_{120}F_{18}N_{12}O_{30}Ru_6S_6$ (3495.2): C 45.32, H 3.43, N 4.81; Found: C 45.10, H 3.44, N 4.65.

P_3: Yield 59 mg (76%). UV-Vis (1.0×10^{-5} M, (CH_2Cl_2)): λ_{max} 372 nm ($\varepsilon = 4.30 \times 10^5$ $M^{-1}\cdot cm^{-1}$), λ_{max} 401 nm ($\varepsilon = 4.01 \times 10^5$ $M^{-1}\cdot cm^{-1}$), λ_{max} 552 nm ($\varepsilon = 1.33 \times 10^5$ $M^{-1}\cdot cm^{-1}$), λ_{max} 601 nm ($\varepsilon = 1.91 \times 10^5$ $M^{-1}\cdot cm^{-1}$). IR (KBr, cm^{-1}): 3065 (w, CH_{aryl}), 1539 (s, C=O), 1261 (s, CF_3). ^1H NMR (400 MHz, CD_3CN): δ = 8.70 (m, 3 H, H_{bq}), 8.66 (m, 3 H, H_{bq}), 8.61 (dd, 6 H, H_α), 8.59 (dd, 6 H, H_α), 8.38 (dd, 6 H, H_β), 8.35 (dd, 6 H, H_β), 7.99 (m, 3 H, H_{cq}), 7.95 (m, 3 H, H_{cq}), 7.27 (d, 3 H, H_{aq}), 7.23 (d, 3 H, H_{aq}), 5.81 (m, 6 H, H_{cym}), 5.75 (m, 6 H, H_{cym}), 5.58 (m, 12 H, H_{cym}), 2.89 (sept, 6 H, $CH(CH_3)_2$), 2.12 (m, 18 H, CH_3), 1.31 (m, 36 H, $CH(CH_3)_2$) ppm. $^{13}C(^1H)$ NMR (100 MHz, CD_3CN): δ = 171.5 (CO), 170.6 (C_{tpt}), 170.5 (CO), 154.2 (CH_α), 145.1 (C_{tpt}), 138.7 (CH_{aq}), 134.4 (CH_{cq}), 134.0 (C_q), 128.3 (CH_{bq}), 124.9 (CH_β), 110.7 (C_q), 104.8 (C_{cym}), 100.6 (C_{cym}), 85.3 (CH_{cym}), 85.0 (CH_{cym}), 83.9 (CH_{cym}), 83.8 (CH_{cym}), 31.4

(*C*H(CH$_3$)$_2$), 22.5 (CH(*C*H$_3$)$_2$), 22.3 (CH(*C*H$_3$)$_2$), 17.6 (CH$_3$) ppm. Anal. calc. for $C_{144}H_{126}F_{18}N_{12}O_{30}Ru_6S_6$ (3645.5): C 47.44, H 3.48, N 4.61; Found C 47.51, H 3.60, N 4.63.

P$_4$: Yield 62 mg (77%). UV-Vis (1.0×10^{-5} M, (CH_2Cl_2)): λ_{max} 370 nm ($\varepsilon = 4.20 \times 10^5$ $M^{-1}\cdot cm^{-1}$), λ_{max} 398 nm ($\varepsilon = 3.42 \times 10^5$ $M^{-1}\cdot cm^{-1}$), λ_{max} 558 nm ($\varepsilon = 1.06 \times 10^5$ $M^{-1}\cdot cm^{-1}$), λ_{max} 602 nm ($\varepsilon = 1.91 \times 10^5$ $M^{-1}.cm^{-1}$). IR (KBr, cm^{-1}): 3070 (w, CH_{aryl}), 1540 (s, C=O), 1260 (s, CF_3) cm^{-1}. ^{1}H NMR (400 MHz, CD_3CN): δ = 8.74 (br, 12 H, H_{bq}), 8.62 (br, 12 H, H_α), 8.27 (br, 12 H, H_β), 7.97 (br, 12 H, H_{cq}), 5.88 (d, 12 H, H_{cym}), 5.66 (d, 12 H, H_{cym}), 2.93 (sept, 6 H, C*H*(CH$_3$)$_2$), 2.13 (s, 18 H, CH$_3$), 1.30 (d, 36 H, CH(C*H*$_3$)$_2$) ppm. ^{13}C(^{1}H) NMR (100 MHz, CD_3CN): δ = 170.5 (C_{tpt}), 170.0 (CO), 154.1 (CH_α), 145.0 (C_{tpt}), 134.6 (C_q), 134.1 (CH_{cq}), 128.2 (CH_{bq}), 124.9 (CH_β), 108.1 (C_q), 104.9 (C_{cym}), 100.7 (C_{cym}), 85.1 (CH_{cym}), 83.6 (CH_{cym}), 31.5 (*C*H(CH$_3$)$_2$), 22.5 (CH(*C*H$_3$)$_2$), 17.8 (CH$_3$) ppm. Anal. calc. for $C_{156}H_{132}F_{18}N_{12}O_{30}Ru_6S_6$ (3795.6): C 49.36, H 3.51, N 4.43; Found C 49.88, H 3.70, N 4.44.

6.2.4 Host-Guest and Carceplex Systems [guest⊂P][CF_3SO_3]$_6$ (P = P$_2$ – P$_4$)

General procedure for [guest⊂**P$_2$**][CF_3SO_3]$_6$ – [guest⊂**P$_4$**][CF_3SO_3]$_6$: [(η^6-*p*-cym)$_2$Ru$_2$(*OO*∩*OO*)Cl$_2$] (*OO*∩*OO* = donq 46.6 mg, doaq 50.0 mg, dotq 53.0 mg; 0.064 mmol), and $AgCF_3SO_3$ (33.0 mg, 0.128 mmol) in MeOH (20 mL), tpt (13.4 mg, 0.043 mmol) and guest molecule (0.023 mmol) is added. The mixture is stirred at reflux for 24h, and then filtered. The solvent is removed and the dark residue is dissolved in CH_2Cl_2 (3 mL). Diethyl ether is added to precipitate a dark green solid. The solid is filtered and dried under vacuum.

[phenanthrene⊂**P$_2$**][CF_3SO_3]$_6$: Yield 65 mg (83%). UV-vis (1.0×10^{-5} M, $(CH_3)_2CO$): λ_{max} = 348 nm (4.2×10^5 $M^{-1}\cdot cm^{-1}$), 383 nm (4.3×10^5 $M^{-1}\cdot cm^{-1}$), 550 nm (1.6×10^4 $M^{-1}\cdot cm^{-1}$), 612 nm (3.2×10^4 $M^{-1}\cdot cm^{-1}$). IR (KBr, cm^{-1}): 3070 (w, CH_{aryl}), 1532 (s, C=O), 1260 (s, CF_3) cm^{-1}. ^{1}H NMR (400 MHz, CD_3CN): δ = 8.58 (d, 12 H, H_α), 8.08 (m, 12 H, H_β), 7.48 (s, 12 H, H_q), 6.70 (br, 2 H, $H_{phenanthrene}$), 5.95 (d, 12 H, H_{cym}), 5.80 (br, 2 H, $H_{phenanthrene}$), 5.60 (d, 12 H, H_{cym}), 5.59 (br, 2 H, $H_{phenanthrene}$), 5.10 (br, 2 H, $H_{phenanthrene}$), 4.58 (br, 2 H, $H_{phenanthrene}$), 2.91 (sept, 6 H, C*H*(CH$_3$)$_2$), 1.99 (s, 18 H, CH$_3$), 1.28 (d, 36 H, CH(C*H*$_3$)$_2$) ppm. ^{13}C(^{1}H) NMR (100 MHz, CD_3CN): δ = 171.0 (CO), 153.1 (CH_α), 132.3 (C_q), 127.9 (CH_q), 120.2 (CH_β), 104.1 (C_q), 103.2 (C_{cym}), 99.9 (C_{cym}), 84.2 (CH_{cym}), 83.9 (CH_{cym}), 30.0 (*C*H(CH$_3$)$_2$), 21.9 (CH(*C*H$_3$)$_2$), 17.3 (CH$_3$) ppm. Anal. calc. for $C_{146}H_{130}F_{18}N_{12}O_{30}Ru_6S_6$ (3673.5): C 47.74, H 3.57, N 4.58; Found C 47.68, H 3.62, N 3.61.

[pyrene⊂**P$_2$**][CF_3SO_3]$_6$: Yield 65 mg (83 %). UV-vis (1.0×10^{-5} M, $(CH_3)_2CO$): λ_{max} 308 nm ($\varepsilon = 3.92 \times 10^5$ $M^{-1}\cdot cm^{-1}$), λ_{max} 334 nm ($\varepsilon = 1.21\times 10^5$ $M^{-1}\cdot cm^{-1}$), λ_{max} 437 nm ($\varepsilon = 0.47 \times 10^5$ $M^{-1}\cdot cm^{-1}$), λ_{max} 643 nm ($\varepsilon = 0.16 \times 10^5$ $M^{-1}\cdot cm^{-1}$), λ_{max} 700 nm ($\varepsilon = 0.16 \times 10^5$ $M^{-1}\cdot cm^{-1}$). IR (KBr, cm^{-1}): 3062 (w, CH_{aryl}), 1537 (s, C=O), 1260 (s, CF_3), 713 (w, C=C). ^{1}H NMR (400 MHz, CD_3CN): δ (ppm) = 8.41 (d, 12 H, H_{pyr}), 7.81 (m, 12 H, H'_{pyr}), 7.44 (s, 12 H, H_q), 6.61 (m, 4 H, H_{pyrene}), 6.14 (m, 4 H, H_{pyrene}), 5.69 (d, 12 H, H_{cym}), 5.47 (d, 12 H, H_{cym}), 5.20 (m, 2 H, H_{pyrene}), 2.83 (sept, 6 H, C*H*$(CH_3)_2$), 2.09 (d, 18 H, CH_3), 1.32 (d, 36 H, CH(C*H*$_3)_2$). ^{13}C(^{1}H) NMR (100 MHz, CD_3CN): δ (ppm) = 171.8 (CO), 170.7 (C_{tpt}), 154.3 (CH_{pyr}), 145.2 (C_{tpt}), 138.4 (CH_q), 130.0 (C_{pyrene}), 127.5 (CH_{pyrene}), 126.1 (CH_{pyrene}), 125.5 (C_{pyrene}), 125.0 (CH'_{pyr}), 112.5 (C_q), 104.9 (C_{cym}), 100.5 (C_{cym}), 85.2 (CH_{cym}), 84.2 (CH_{cym}), 31.5 (C*H*$(CH_3)_2$), 23.1 (CH(C*H*$_3)_2$), 22.3 (CH(C*H*$_3)_2$), 17.3 (CH_3). Anal. calc. for $C_{148}H_{130}F_{18}N_{12}O_{30}Ru_6S_6$ (3697.5): C 48.04, H 3.52, N 4.54; Found: C 48.10, H 3.55, N 4.50.

[triphenylene⊂**P$_2$**][CF_3SO_3]$_6$: Yield 68 mg (86 %). UV-vis (1.0×10^{-5} M, $(CH_3)_2CO$): λ_{max} 308 nm ($\varepsilon = 3.92 \times 10^5$ $M^{-1}\cdot cm^{-1}$), λ_{max} 437 nm ($\varepsilon = 0.51 \times 10^5$ $M^{-1}\cdot cm^{-1}$), λ_{max} 643 nm ($\varepsilon = 0.16 \times 10^5$ $M^{-1}\cdot cm^{-1}$), λ_{max} 700 nm ($\varepsilon = 0.17 \times 10^5$ $M^{-1}\cdot cm^{-1}$). IR (KBr, cm^{-1}): 3064 (w, CH_{aryl}), 1536 (s, C=O), 1258 (s, CF_3). ^{1}H NMR (400 MHz, CD_3CN): δ (ppm) = 8.36 (d, 12H, H_{pyr}), 7.82 (d, 12 H, H'_{pyr}), 7.45 (s, 12 H, H_q), 7.29 (m, 6 H, $H_{triphenylene}$), 5.70 (d, 12 H, H_{cym}), 5.48 (d, 12 H, H_{cym}), 4.66 (m, 6 H, $H_{triphenylene}$), 2.83 (sept, 6 H, C*H*$(CH_3)_2$), 2.04 (d, 18 H, CH_3), 1.31 (d, 36 H, CH(C*H*$_3)_2$). ^{13}C(^{1}H) NMR (100 MHz, CD_3CN): δ (ppm) = 170.9 (CO), 167.8 (C_{tpt}), 152.2 (CH_{pyr}), 143.1 (C_{tpt}), 137.8 (CH_q), 128.0 ($C_{triphenylene}$), 125.8 ($CH_{triphenylene}$), 123.7 (CH'_{pyr}), 122.5 ($CH_{triphenylene}$), 111.4 (C_q), 103.9 (C_{cym}), 99.8 (C_{cym}), 84.5 (CH_{cym}), 83.2 (CH_{cym}), 30.5 (*C*H$(CH_3)_2$), 21.5 (CH(*C*H$_3)_2$), 16.4 (CH_3). Anal. calc. for $C_{150}H_{132}F_{18}N_{12}O_{30}Ru_6S_6$: C 48.35, H 3.54, N 4.51; Found: C 48.10, H 3.52, N 4.45.

[coronene⊂**P$_2$**][CF_3SO_3]$_6$: Yield 65 mg (81%). UV-vis (1.0×10^{-5} M, $(CH_3)_2CO$): λ_{max} = 301 nm (4.1×10^5 $M^{-1}\cdot cm^{-1}$), 340 nm (3.2×10^5 $M^{-1}\cdot cm^{-1}$), 370 nm (5.8×10^4 $M^{-1}\cdot cm^{-1}$), 622 nm (3.1×10^4 $M^{-1}\cdot cm^{-1}$). IR (KBr, cm^{-1}): 3071 (w, CH_{aryl}), 1540 (s, C=O), 1260 (s, CF_3) cm^{-1}. ^{1}H NMR (400 MHz, CD_3CN): δ = 8.42 (d, 12 H, H_α), 8.02 (d, 12 H, H_β), 7.42 (s, 12 H, H_q), 6.21 (s, 12 H, $H_{coronene}$), 5.80 (d, 12 H, H_{cym}), 5.65 (d, 12 H, H_{cym}), 2.90 (sept, 6 H, C*H*$(CH_3)_2$), 2.00 (s, 18 H, CH_3), 1.32 (d, 36 H, CH(C*H*$_3)_2$) ppm. ^{13}C(^{1}H) NMR (100 MHz, CD_3CN): δ = 170.2 (CO), 158.0 (C_{tpt}), 151.1 (CH_α), 141.4 (C_{tpt}), 132.4 (CH_q), 127.0 ($C_{coronene}$), 124.4 ($CH_{coronene}$), 120.5 (CH_β), 120.2 ($C_{coronene}$), 106.1 (C_q), 104.2 (C_{cym}), 100.7 (C_{cym}), 85.3

(CH_{cym}), 84.9 (CH_{cym}), 30.1 ($CH(CH_3)_2$), 21.9 ($CH(CH_3)_2$), 17.2 (CH_3) ppm. Anal. calc. for $C_{156}H_{132}F_{18}N_{12}O_{30}Ru_6S_6$ (3795.5): C 49.36, H 3.51, N 4.43; Found C 49.91, H 3.62, N 4.22.

[$Pd(acac)_2$⊂**P₂**][CF_3SO_3]$_6$: Yield 64 mg (80 %). UV-vis (1.0×10^{-5} M, $(CH_3)_2CO$): λ_{max} 308 nm ($\varepsilon = 3.91 \times 10^5$ $M^{-1}.cm^{-1}$), λ_{max} 437 nm ($\varepsilon = 0.50 \times 10^5$ $M^{-1}\cdot cm^{-1}$), λ_{max} 643 nm ($\varepsilon = 0.16 \times 10^5$ $M^{-1}\cdot cm^{-1}$), λ_{max} 700 nm ($\varepsilon = 0.17 \times 10^5$ $M^{-1}\cdot cm^{-1}$). IR (KBr, cm^{-1}): 3063 (w, CH_{aryl}), 1533 (s, C=O), 1262 (s, CF_3), 689 (w, $Pd(acac)_2$). ^{1}H NMR (400 MHz, CD_3CN): δ (ppm) = 8.58 (d, 12 H, H_{pyr}), 8.36 (d, 12 H, H'_{pyr}), 7.28 (s, 12 H, H_q), 5.73 (d, 12 H, H_{cym}), 5.53 (d, 12 H, H_{cym}), 3.40 (m, 2 H, CH_{acac}), 2.85 (sept, 6 H, $CH(CH_3)_2$), 2.10 (d, 18 H, CH_3), 1.32 (d, 36 H, $CH(CH_3)_2$), 0.02 (m, 12 H, CH_{3acac}). $^{13}C(^1H)$ NMR (100 MHz, CD_3CN): δ (ppm) = 171.8 (CO), 170.7 (C_{tpt}), 154.3 (CH_{pyr}), 145.2 (C_{tpt}), 138.4 (CH_q), 125.0 (CH'_{pyr}), 112.5 (C_q), 104.9 (C_{cym}), 102.0 (CH_{acac}), 100.5 (C_{cym}), 85.2 (CH_{cym}), 84.2 (CH_{cym}), 31.5 ($CH(CH_3)_2$), 23.1 ($CH(CH_3)_2$), 22.3 ($CH(CH_3)_2$), 17.3 (CH_3), 15.6 (CH_{3acac}). Anal. calc. for $C_{142}H_{134}F_{18}N_{12}O_{34}PdRu_6S_6$ (3799.8): C 44.88, H 3.45, N 4.42; Found: C 44.99, H 3.42, N 4.55.

[pyrene-X⊂**P₂**][CF_3SO_3]$_6$: Yield 149 mg (83 %). UV-vis (1.0×10^{-5} M, CH_2Cl_2): λ_{max} = 308 nm ($\varepsilon = 3.88 \times 10^5$ $M^{-1}\cdot cm^{-1}$), 377 nm ($\varepsilon = 0.47\times 10^5$ $M^{-1}\cdot cm^{-1}$), 563 nm ($\varepsilon = 0.24 \times 10^5$ $M^{-1}\cdot cm^{-1}$), 613 nm ($\varepsilon = 0.17 \times 10^5$ $M^{-1}\cdot cm^{-1}$). IR (KBr, cm^{-1}): 3060 (w, CH_{aryl}), 1536 (s, C=O), 1500 (m, C=C), 1260 (s, CF_3) cm^{-1}. ^{1}H NMR (400 MHz, CD_3CN): δ = 8.40 (d, 12 H, H_α), 7.78 (m, 12 H, H_β), 7.47 (s, 12 H, H_q), 7.25 (m, 1 H, H_{pyr}), 7.08 (m, 1 H, H_{pyr}), 6.12 (m, 1 H, H_{pyr}), 5.82 (m, 1 H, H_{pyr}), 8.75 (m, 1 H, H_{pyr}), 5.69 (d, 12 H, H_{cym}), 5.44 (d, 12 H, H_{cym}), 5.22 (m, 1 H, H_{pyr}), 4.92 (m, 1 H, H_{pyr}), 4.81 (m, 1 H, H_{pyr}), 4.75 (m, 1 H, H_{pyr}), 2.80 (sept, 6 H, $CH(CH_3)_2$), 2.07 (s, 18 H, CH_3), 1.32 (d, 36 H, $CH(CH_3)_2$) ppm. $^{13}C(^1H)$ NMR (100 MHz, CD_3CN): δ = 171.2 (CO), 170.5 (C_{tpt}), 155.1 (CH_α), 144.3 (C_{tpt}), 139.9 (CH_q), 130.8 (C_{pyr}), 128.6 (CH_{pyr}), 127.8 (CH_{pyr}), 126.6 (C_{pyr}), 126.2 (CH_β), 115.5 (C_q), 104.8 (C_{cym}), 100.4 (C_{cym}), 85.1 (CH_{cym}), 84.6 (CH_{cym}), 31.4 ($CH(CH_3)_2$), 23.0 ($CH(CH_3)_2$), 22.1 ($CH(CH_3)_2$), 17.3 (CH_3) ppm. Anal. calc. for $C_{151}H_{129}Cl_2F_{18}N_{15}O_{30}Ru_6S_6$ (3845.4): C 47.16, H 3.38, N 5.46; Found: C 47.08, H 3.46, N 5.42.

[pyrene-G_0⊂**P₂**][CF_3SO_3]$_6$: Yield 116 mg (85 %). UV-vis (1.0×10^{-5} M, CH_2Cl_2): λ_{max} = 272 nm ($\varepsilon = 1.27 \times 10^5$ $M^{-1}\cdot cm^{-1}$), 329 nm ($\varepsilon = 0.39 \times 10^5$ $M^{-1}\cdot cm^{-1}$), 345 nm ($\varepsilon = 0.91 \times 10^5$ $M^{-1}\cdot cm^{-1}$), 444 nm ($\varepsilon = 0.43 \times 10^5$ $M^{-1}\cdot cm^{-1}$), 638 nm ($\varepsilon = 0.11 \times 10^5$ $M^{-1}\cdot cm^{-1}$), 696 nm ($\varepsilon = 0.12 \times 10^5$ $M^{-1}\cdot cm^{-1}$). IR (KBr): ν = 3060 (w, CH_{aryl}), 2228 (s, CN), 1730 (s, C=O), 1536 (s,

C=O), 1500 (m, C=C), 1260 (s, CF_3) cm^{-1}. ^1H NMR (400 MHz, CD_2Cl_2): δ = 8.40 (d, 12 H, H_α), 8.13 (d, 2 H, H_{arom}), 7.78 (m, 12 H, H_β), 7.76 (d, 2 H, H_{arom}), 7.72 (d, 2 H, H_{arom}), 7.67 (d, 2 H, H_{arom}), 7.47 (s, 12 H, H_q), 7.33 (d, 2 H, H_{arom}), 7.25 (m, 1 H, H_{pyr}), 7.08 (m, 1 H, H_{pyr}), 6.99 (d, 2 H, H_{arom}), 6.12 (m, 1 H, H_{pyr}), 5.82 (m, 1 H, H_{pyr}), 5.75 (m, 1 H, H_{pyr}), 5.71 (d, 12 H, H_{cym}), 5.44 (d, 12 H, H_{cym}), 5.22 (m, 1 H, H_{pyr}), 4.92 (m, 1 H, H_{pyr}), 4.81 (m, 1 H, H_{pyr}), 4.75 (m, 1 H, H_{pyr}), 4.22 (t, 2 H, CO_2CH_2), 4.08 (t, 2 H, CH_2O), 3.03 (m, 2 H, $C_{pyr}CH_2$), 2.93 (sept, 6 H, $CH(CH_3)_2$), 2.52 (t, 2 H, CH_2CO_2), 2.07 (s, 18 H, CH_3), 1.90 (m, 2 H, $C_{pyr}CH_2CH_2$), 1.90 (m, 2 H, CH_2CH_2O), 1.71 (m, 2 H, $CO_2CH_2CH_2$), 1.44 (m, 2 H, $CH_2CH_2CH_2O$), 1.32 (d, 36 H, $CH(CH_3)_2$), 1.30 (m, 10 H, H_{aliph}) ppm. $^{13}C(^1H)$ NMR (100 MHz, CD_2Cl_2): δ = 173.7 ($CH_2CO_2CH_2$), 171.2 (*C*O), 170.5 (C_{tpt}), 165.2 (CO_2C_{arom}), 164.1 (OC_{arom}), 155.1 (CH_α), 152.3 (CO_2C_{arom}), 145.0 ($C_{arom}C_{arom}$), 144.3 (C_{tpt}), 139.9 (CH_q), 137.2 ($C_{arom}C_{arom}$), 136.2 ($C_{pyr}CH_2$), 133.1 (*C*H), 132.5 (*C*H), 131.8 (C_{pyr}), 131.3 (C_{pyr}), 130.8 (C_{pyr}), 130.3 (C_{pyr}), 129.1 (C_{pyr}), 128.7 (*C*H), 128.6 (CH_{pyr}), 128.0 (*C*H), 127.8 (CH_{pyr} and CH_{pyr}), 127.6 (CH_{pyr}), 127.5 (CH_{pyr}), 127.4 (CH_{pyr}), 126.6 (C_{pyr}), 126.2 (CH_β), 126.1 (CH_{pyr}), 125.2 (C_{pyr}), 125.0 (C_{pyr}, CH_{pyr}, and CH_{pyr}), 124.9 (CH_{pyr}), 123.7 (CH_{pyr}), 122.6 (*C*H), 121.6 ($C_{arom}CO_2$), 119.1 (*C*N), 115.5 (C_q), 114.6 (*C*H), 111.4 ($C_{arom}CN$), 104.8 (C_{cym}), 100.4 (C_{cym}), 85.1 (CH_{cym}), 84.6 (CH_{cym}), 68.9 (CH_2O), 64.5 (CO_2CH_2), 34.2 (CH_2CO_2), 33.0 ($C_{pyr}CH_2$), 31.4 ($CH(CH_3)_2$), 29.7 (CH_2), 29.6 (CH_2 and CH_2), 29.4 (CH_2), 29.1 (CH_2CH_2O), 27.2 ($C_{pyr}CH_2CH_2$), 26.3 ($CH_2CH_2CH_2O$ and $CO_2CH_2CH_2CH_2$), 23.0 ($CH(CH_3)_2$), 22.1 ($CH(CH_3)_2$), 17.3 (CH_3) ppm. Anal. calc. for $C_{182}H_{167}F_{18}N_{13}O_{35}Ru_6S_6$ (4237.1): C 51.59, H 3.97, N 4.30; Found: C 50.84, H 3.93, N 4.22.

[pyrene-G_1⊂**P_2**][CF_3SO_3]$_6$: Yield 134 mg (81 %). UV-vis (1.0×10^{-5} M, CH_2Cl_2): λ_{max} = 270 nm ($\varepsilon = 1.29 \times 10^5$ $M^{-1}\cdot cm^{-1}$), 330 nm ($\varepsilon = 0.40 \times 10^5$ $M^{-1}\cdot cm^{-1}$), 343 nm ($\varepsilon = 0.88 \times 10^5$ $M^{-1}\cdot cm^{-1}$), 445 nm ($\varepsilon = 0.45 \times 10^5$ $M^{-1}\cdot cm^{-1}$), 640 nm ($\varepsilon = 0.12 \times 10^5$ $M^{-1}\cdot cm^{-1}$), 696 nm ($\varepsilon = 0.12 \times 10^5$ $M^{-1}\cdot cm^{-1}$). IR (KBr): ν = 3060 (w, CH_{aryl}), 2229 (s, CN), 1733 (s, C=O), 1536 (s, C=O), 1500 (m, C=C), 1260 (s, CF_3) cm^{-1}. ^1H NMR (400 MHz, CD_2Cl_2): δ = 8.50 (t, 1 H, H_{arom}), 8.38 (m, 12 H, H_α), 8.11 (d, 4 H, H_{arom}), 7.91 (d, 2 H, H_{arom}), 7.79 (m, 12 H, H_β), 7.76 (d, 4 H, H_{arom}), 7.71 (d, 4 H, H_{arom}), 7.60 (m, 4 H, H_{arom}), 7.45 (br, 12 H, H_q), 7.32 (m, 4 H, H_{arom}), 7.30 (m, 1 H, H_{pyr}), 7.12 (m, 1 H, H_{pyr}), 6.98 (d, 4 H, H_{arom}), 6.15 (m, 1 H, H_{pyr}), 5.80 (m, 1 H, H_{pyr}), 5.73 (d, 12 H, H_{cym}), 5.72 (m, 1 H, H_{pyr}), 5.48 (d, 12 H, H_{cym}), 5.20 (m, 1 H, H_{pyr}), 4.87 (m, 1 H, H_{pyr}), 4.82 (m, 1 H, H_{pyr}), 4.75 (m, 1 H, H_{pyr}), 4.04 (m, 4 H, CO_2CH_2), 4.00 (m, 4 H, CH_2O), 3.05 (m, 2 H, $C_{pyr}CH_2$), 2.81 (m, 6 H, $CH(CH_3)_2$), 2.53 (m, 2 H, CH_2CO_2), 2.28 (m, 2 H, $C_{pyr}CH_2CH_2$), 2.05 (s, 18 H, CH_3), 1.69 (m, 8 H, $CO_2CH_2CH_2$ and

C*H*$_2$CH$_2$O), 1.45 (m, 8 H, CO$_2$CH$_2$CH$_2$C*H*$_2$ and C*H*$_2$CH$_2$CH$_2$O), 1.32 (m, 16 H, H$_{aliph}$), 1.28 (m, 36 H, CH(C*H*$_3$)$_2$) ppm. ^{13}C(^{1}H) NMR (100 MHz, CD$_2$Cl$_2$): δ = 171.9 (C$_{arom}$*C*O$_2$CH$_2$), 170.6 (*C*O), 170.4 (*C*$_{tpt}$), 165.1 (CH$_2$*C*O$_2$C$_{arom}$), 165.0 (C$_{arom}$*C*O$_2$C$_{arom}$), 163.8 (O*C*$_{arom}$), 155.1 (*C*H$_α$), 151.0 (C$_{arom}$CO$_2$*C*$_{arom}$ and CH$_2$CO$_2$*C*$_{arom}$), 145.0 (C$_{arom}$*C*$_{arom}$), 144.2 (*C*$_{tpt}$), 139.9 (*C*H$_q$), 137.1 (*C*$_{arom}$C$_{arom}$), 132.8 (*C*H), 132.7 (*C*$_{arom}$CO$_2$CH$_2$), 132.6 (*C*H), 131.5 (*C*$_{pyr}$), 131.4 (*C*$_{pyr}$), 130.7 (*C*$_{pyr}$), 130.4 (*C*$_{pyr}$), 129.8 (*C*$_{pyr}$), 128.5 (*C*H$_{pyr}$ and *C*H), 128.1 (*C*H), 128.0 (*C*H), 127.8 (*C*H$_{pyr}$, *C*H$_{pyr}$, *C*H$_{pyr}$, and *C*H$_{pyr}$), 127.7 (*C*H), 127.2 (*C*H$_{pyr}$), 126.6 (*C*$_{pyr}$), 126.5 (*C*H$_{pyr}$), 126.4 (*C*H$_{pyr}$), 126.1 (*C*H$_β$), 125.3 (*C*H$_{pyr}$), 124.8 (*C*H$_{pyr}$), 123.2 (*C*H$_{pyr}$), 122.6 (*C*H), 121.0 (*C*$_{arom}$CO$_2$C$_{arom}$), 119.1 (*C*N), 115.5 (*C*$_q$), 114.8 (*C*H), 111.5 (*C*$_{arom}$CN), 104.6 (*C*$_{cym}$), 100.2 (*C*$_{cym}$), 84.5 (*C*H$_{cym}$), 84.4 (*C*H$_{cym}$), 68.9 (*C*H$_2$O), 66.2 (CO$_2$*C*H$_2$), 34.2 (*C*H$_2$CO$_2$), 31.4 (*C*H(CH$_3$)$_2$), 30.2 (C$_{pyr}$*C*H$_2$), 27.2 (*C*H$_2$), 26.8 (*C*H$_2$), 26.7 (*C*H$_2$), 26.6 (*C*H$_2$), 26.5 (*C*H$_2$), 26.1 (*C*H$_2$CH$_2$O), 25.8 (C$_{pyr}$CH$_2$*C*H$_2$), 25.2 (*C*H$_2$CH$_2$CH$_2$O), 25.0 (CO$_2$CH$_2$CH$_2$*C*H$_2$), 23.0 (CH(*C*H$_3$)$_2$), 19.8 (CH(*C*H$_3$)$_2$), 17.1 (*C*H$_3$) ppm. Anal. calc. for C$_{220}$H$_{202}$F$_{18}$N$_{14}$O$_{42}$Ru$_6$S$_6$ (4854.8): C 54.43, H 4.19, N 4.04; Found: C 53.74, H 4.12, N 3.96.

[pyrene-G$_2$⊂**P$_2$**][CF$_3$SO$_3$]$_6$: Yield 182 mg (77 %). UV-vis (1.0 × 10^{-5} M, CH$_2$Cl$_2$): λ$_{max}$ = 270 nm (ε = 1.25 × 10^5 M^{-1}·cm^{-1}), 330 nm (ε = 0.42 × 10^5 M^{-1}·cm^{-1}), 343 nm (ε = 0.88 × 10^5 M^{-1}·cm^{-1}), 442 nm (ε = 0.45 × 10^5 M^{-1}·cm^{-1}), 640 nm (ε = 0.11 × 10^5 M^{-1}·cm^{-1}), 696 nm (ε = 0.12 × 10^5 M^{-1}·cm^{-1}). IR (KBr): *ν* = 3060 (w, CH$_{aryl}$), 2225 (s, CN), 1732 (s, C=O), 1536 (s, C=O), 1500 (m, C=C), 1260 (s, CF$_3$) cm^{-1}. ^{1}H NMR (400 MHz, CD$_2$Cl$_2$): δ = 8.91 (m, 1 H, H$_{arom}$), 8.59 (t, 2 H, H$_{arom}$), 8.37 (d, 2 H, H$_{arom}$), 8.36 (m, 12 H, H$_α$), 8.12 (d, 10 H, H$_{arom}$), 8.11 (d, 4 H, H$_{arom}$), 7.79 (m, 12 H, H$_β$), 7.75 (d, 8 H, H$_{arom}$), 7.69 (d, 8 H, H$_{arom}$), 7.66 (d, 8 H, H$_{arom}$), 7.45 (s, 12 H, H$_q$), 7.29 (d, 8 H, H$_{arom}$), 7.14 (m, 1 H, H$_{pyr}$), 7.05 (m, 1 H, H$_{pyr}$), 6.97 (d, 10 H, H$_{arom}$), 6.11 (m, 1 H, H$_{pyr}$), 5.81 (m, 1 H, H$_{pyr}$), 5.74 (m, 1 H, H$_{pyr}$), 5.68 (d, 12 H, H$_{cym}$), 5.41 (d, 12 H, H$_{cym}$), 5.20 (m, 1 H, H$_{pyr}$), 4.91 (m, 1 H, H$_{pyr}$), 4.75 (m, 1 H, H$_{pyr}$), 4.72 (m, 1 H, H$_{pyr}$), 4.05 (m, 8 H, CO$_2$CH$_2$), 4.02 (m, 2 H, CO$_2$CH$_2$), 3.92 (m, 8 H, CH$_2$O), 3.88 (m, 2 H, CH$_2$O), 3.12 (m, 2 H, C$_{pyr}$CH$_2$), 2.81 (m, 6 H, C*H*(CH$_3$)$_2$), 2.09 (s, 18 H, CH$_3$), 2.05 (m, 2 H, C*H*$_2$CO$_2$CH$_2$), 1.99 (m, 2H, C$_{pyr}$CH$_2$C*H*$_2$), 1.74 (m, 18 H, C*H*$_2$CH$_2$O and CO$_2$CH$_2$C*H*$_2$), 1.59 (m, 2 H, CO$_2$CH$_2$C*H*$_2$), 1.45 (m, 18 H, C*H*$_2$CH$_2$CH$_2$O and CO$_2$CH$_2$CH$_2$C*H*$_2$), 1.30 (m, 42 H, CO$_2$CH$_2$CH$_2$C*H*$_2$ and H$_{aliph}$), 1.29 (m, 36 H, CH(C*H*$_3$)$_2$) ppm. ^{13}C(^{1}H) NMR (100 MHz, CD$_2$Cl$_2$): δ = 173.0 (CH$_2$*C*O$_2$CH$_2$), 171.3 (*C*O), 170.4 (*C*$_{tpt}$), 165.1 (C$_{arom}$*C*O$_2$CH$_2$), 165.0 (C$_{arom}$*C*O$_2$C$_{arom}$), 164.7 (C$_{arom}$*C*O$_2$C$_{arom}$), 164.5 (O*C*$_{arom}$), 164.1 (O*C*$_{arom}$), 163.2 (C$_{arom}$*C*O$_2$C$_{arom}$), 155.0 (*C*H$_α$), 152.1 (CO$_2$*C*$_{arom}$), 152.0 (CO$_2$*C*$_{arom}$), 151.0 (CO$_2$*C*$_{arom}$), 144.3 (*C*$_{tpt}$), 139.9 (*C*H$_q$), 134.1 (*C*$_{pyr}$CH$_2$), 132.9 (*C*H), 132.1 (*C*H), 131.5(*C*H),

131.2 ($C_{arom}CO_2$), 130.6 (C_{pyr}), 129.3 (*C*H), 128.7 (*C*H), 128.6 (C_{pyr}), 128.5 (*C*H), 128.1 (*C*H), 127.8 (C_{pyr}), 127.6 (*C*H), 126.8 (C_{pyr}), 126.6 (C_{pyr}), 126.4 (CH_{pyr}), 126.3 (CH_{pyr}), 126.2 (CH_{β}), 125.8 (CH_{pyr}), 125.3 (C_{pyr}), 124.9 (C_{pyr}), 124.3 (C_{pyr}), 124.2 (CH_{pyr}), 124.1 (CH_{pyr}), 123.2 (CH_{pyr}), 122.3 (*C*H), 121.6 ($C_{arom}CO_2$), 120.5 ($C_{arom}CO_2$), 119.2 (*C*N), 114.8 (C_q), 114.6 (*C*H), 114.5 (*C*H), 111.1 ($C_{arom}CN$), 104.8 (C_{cym}), 100.1 (C_{cym}), 85.1 (CH_{cym}), 84.8 (CH_{cym}), 68.7 (CH_2O and CH_2O), 66.3 ($C_{arom}CO_2CH_2$), 64.5 ($CH_2CO_2CH_2$), 34.2 ($C_{pyr}CH_2CH_2CH_2$), 31.4 ($CH(CH_3)_2$), 30.2 ($C_{pyr}CH_2$), 29.2 (CH_2), 28.9 (CH_2), 28.5 (CH_2), 28.4 (CH_2), 28.2 (CH_2), 27.7 (CH_2), 27.5 (CH_2 and CH_2), 27.1 (CH_2CH_2O), 26.8 (CH_2CH_2O), 26.4 ($C_{pyr}CH_2CH_2$), 26.2 ($CH_2CH_2CH_2O$), 25.3 ($CH_2CH_2CH_2O$ and $CO_2CH_2CH_2CH_2$), 23.0 ($CH(CH_3)_2$), 22.1 ($CH(CH_3)_2$), 17.3 (CH_3) ppm. Anal. calc. for $C_{313}H_{296}F_{18}N_{16}O_{59}Ru_6S_6$ (6366.5): C 59.05, H 4.69, N 3.52; Found: C 58.47, H 4.64, N 3.47.

[phenanthrene⊂**P$_3$**][CF_3SO_3]$_6$: Yield 68 mg (84%). UV-vis (1.0×10^{-5} M, $(CH_3)_2CO$): λ_{max} 373 nm ($\varepsilon = 4.01 \times 10^5$ $M^{-1}.cm^{-1}$), λ_{max} 399 nm ($\varepsilon = 3.83 \times 10^5$ $M^{-1}\cdot cm^{-1}$), λ_{max} 554 nm ($\varepsilon = 0.13 \times 10^5$ $M^{-1}\cdot cm^{-1}$), λ_{max} 601 nm ($\varepsilon = 0.18 \times 10^5$ $M^{-1}\cdot cm^{-1}$). IR (KBr, cm^{-1}): 3068 (w, CH_{aryl}), 1539 (s, C=O), 1262 (s, CF_3) cm^{-1}. ^{1}H NMR (400 MHz, CD_3CN): δ = 8.74 (m, 3 H, H_{bq}), 8.70 (m, 3 H, H_{bq}), 8.56 (dd, 6 H, H_{α}), 8.53 (dd, 6 H, H_{α}), 8.19 (m, 12 H, H_{β}), 8.02 (m, 6 H, H_{cq}), 7.41 (m, 2 H, $H_{phenanthrene}$), 7.33 (d, 3 H, H_{aq}), 7.29 (d, 3 H, H_{aq}), 6.91 (d, 2 H, $H_{phenanthrene}$), 5.81 (m, 6 H, H_{cym}), 5.75 (m, 6 H, H_{cym}), 5.63 (m, 2 H, $H_{phenanthrene}$), 5.57 (m, 12 H, H_{cym}), 5.20 (m, 2 H, $H_{phenanthrene}$), 4.50 (dd, 2 H, $H_{phenanthrene}$), 2.89 (sept, 6 H, C*H*$(CH_3)_2$), 2.11 (m, 18 H, CH_3), 1.32 (m, 36 H, CH(C*H*$_3)_2$) ppm. ^{13}C(^{1}H) NMR (100 MHz, CD_3CN): δ = 171.5 (CO), 170.6 (CO), 170.3 (C_{tpt}), 154.0 (CH_{α}), 153.9 (CH_{α}), 145.0 (C_{tpt}), 138.8 (CH_{aq}), 134.5 (CH_{cq}), 134.1 (C_q), 128.4 (CH_{bq}), 124.8 (CH_{β}), 110.6 (C_q), 104.8 (C_{cym}), 100.7 (C_{cym}), 85.3 (CH_{cym}), 85.0 (CH_{cym}), 83.9 (CH_{cym}), 83.8 (CH_{cym}), 31.5 ($CH(CH_3)_2$), 22.5 ($CH(CH_3)_2$), 22.3 ($CH(CH_3)_2$), 17.6 (CH_3) ppm. Anal. calc. for $C_{158}H_{136}F_{18}N_{12}O_{30}Ru_6S_6$ (3823.7): C 49.63, H 3.59, N 4.40; Found C 49.77, H 3.72, N 4.45.

[pyrene⊂**P$_3$**][CF_3SO_3]$_6$: Yield: 68 mg (83%). UV-vis (1.0×10^{-5} M, $(CH_3)_2CO$): λ_{max} = 321 (7.1×10^4 $M^{-1}\cdot cm^{-1}$), 337 (6.9×10^4 $M^{-1}\cdot cm^{-1}$), 374 (4.3×10^4 $M^{-1}\cdot cm^{-1}$), 402 (4.1×10^4 $M^{-1}\cdot cm^{-1}$), 649 (2.3×10^4 $M^{-1}\cdot cm^{-1}$) nm. IR (KBr, cm^{-1}): 3064 (w, CH_{aryl}), 1539 (s, C=O), 1260 (s, CF_3) cm^{-1}. ^{1}H NMR (400 MHz, CD_3CN): δ = 8.79 (m, 6 H, H_{bq}), 8.48 (m, 12 H, H_{α}), 8.10 (m, 6 H, H_{cq}), 7.95 (m, 12 H, H_{β}), 7.42 (m, 6 H, H_{aq}), 6.16 (m, 4 H, H_{pyrene}), 5.81 (m, 6 H, H_{cym}), 5.75 (m, 6 H, H_{cym}), 5.65 (br, 2 H, H_{pyrene}), 5.56 (m, 12H, H_{cym}), 5.00 (m, 4 H, H_{pyrene}), 2.89 (sept, 6 H, C*H*$(CH_3)_2$), 2.09 (m, 18 H, CH_3), 1.32 (m, 36 H, CH(C*H*$_3)_2$) ppm. ^{13}C(^{1}H)

NMR (100 MHz, CD_3CN): δ = 171.5 (*C*O), 170.7 (*C*O), 169.9 (C_{tpt}), 153.7 (CH_{α}), 144.3 (C_{tpt}), 139.0 (CH_{aq}), 134.7 (CH_{cq}), 134.2 (C_q), 129.9 (CH_{pyrene}), 128.4 (CH_{bq}), 127.1 (CH_{pyrene}), 125.1 (CH_{pyrene}), 124.5 (CH_{β}), 110.7 (C_q), 104.8 (C_{cym}), 100.7 (C_{cym}), 85.2 (CH_{cym}), 83.8 (CH_{cym}), 31.4 ($CH(CH_3)_2$), 22.4 ($CH(CH_3)_2$), 17.6 (CH_3) ppm. Anal. calc. for $C_{160}H_{136}F_{18}N_{12}O_{30}Ru_6S_6$ (3847.7): C 49.95, H 3.56, N 4.37; Found C 49.98, H 3.74, N 4.42.

[triphenylene⊂**P$_3$**][CF_3SO_3]$_6$: Yield: 72 mg (84%). UV-vis (1.0×10^{-5} M, $(CH_3)_2CO$): λ_{max} = 380 nm (3.8×10^4 $M^{-1}\cdot cm^{-1}$), 415 nm (4.0×10^4 $M^{-1}\cdot cm^{-1}$), 550 nm (0.9×10^4 $M^{-1}\cdot cm^{-1}$), 612 nm (1.5×10^4 $M^{-1}\cdot cm^{-1}$), 659 nm (1.9×10^4 $M^{-1}\cdot cm^{-1}$). IR (KBr, cm^{-1}): 3060 (w, CH_{aryl}), 1539 (s, C=O), 1260 (s, CF_3) cm^{-1}. ^{1}H NMR (400 MHz, CD_3CN): *δ* = 8.82 (m, 6 H, H_{bq}), 8.38 (dd, 6 H, H_{α}), 8.29 (dd, 6 H, H_{α}), 8.28 (m, 6 H, H_{cq}), 7.71 (s, 3 H, H_{aq}), 7.69 (d, 3 H, H_{aq}), 6.92 (dd, 6 H, H_{β}), 6.79 (dd, 6 H, H_{β}), 6.58 (m, 6 H, $H_{triphenylene}$), 5.78 (m, 6 H, H_{cym}), 5.74 (m, 6 H, H_{cym}), 5.63 (m, 12 H, H_{cym}), 4.44 (m, 6 H, $H_{triphenylene}$), 2.88 (sept, 6 H, C*H*$(CH_3)_2$), 2.04 (m, 18 H, CH_3), 1.29 (m, 36 H, CH(C*H*$_3)_2$) ppm. ^{13}C(^{1}H) NMR (100 MHz, CD_3CN): δ = 171.3 (*C*O), 171.1 (*C*O), 166.0 (C_{tpt}), 152.0 (CH_{α}), 142.4 (C_{tpt}), 138.5 (CH_{aq}), 134.6 (CH_{cq}), 132.2 (C_q), 128.4 ($C_{triphenylene}$), 128.1 (CH_{bq}), 127.1 ($CH_{triphenylene}$), 122.4 ($CH_{triphenylene}$), 120.2 (CH_{β}), 108.9 (C_q), 103.2 (C_{cym}), 100.1 (C_{cym}), 86.4 (CH_{cym}), 86.1 (CH_{cym}), 83.0 (CH_{cym}), 82.9 (CH_{cym}), 30.4 ($CH(CH_3)_2$), 21.6 ($CH(CH_3)_2$), 21.4 ($CH(CH_3)_2$), 16.9 (CH_3) ppm. Anal. calc. for $C_{162}H_{138}F_{18}N_{12}O_{30}Ru_6S_6$ (3873.8): C 50.23, H 3.59, N 4.34; found C 50.45, H 3.73, N 4.43.

[coronene⊂**P$_3$**][CF_3SO_3]$_6$: Yield: 72 mg (86%). UV-vis (1.0×10^{-5} M, $(CH_3)_2CO$): λ_{max} = 385 nm (3.9×10^4 $M^{-1}\cdot cm^{-1}$), 409 nm (3.9×10^4 $M^{-1}\cdot cm^{-1}$), 555 nm (0.8×10^4 $M^{-1}\cdot cm^{-1}$), 609 nm (1.5×10^4 $M^{-1}\cdot cm^{-1}$), 654 nm (1.8×10^4 $M^{-1}\cdot cm^{-1}$). IR (KBr, cm^{-1}): 3062 (w, CH_{aryl}), 1539 (s, C=O), 1261 (s, CF_3) cm^{-1}. ^{1}H NMR (400 MHz, CD_3CN): *δ* = 8.95 (m, 6 H, H_{bq}), 8.35 (dd, 6 H, H_{α}), 8.30 (dd, 6 H, H_{α}), 8.29 (m, 6 H, H_{cq}), 7.70 (s, 3 H, H_{aq}), 7.67 (d, 3 H, H_{aq}), 6.86 (dd, 6 H, H_{β}), 6.77 (dd, 6 H, H_{β}), 6.59 (s, 12 H, $H_{coronene}$), 5.80 (m, 6 H, H_{cym}), 5.71 (m, 6 H, H_{cym}), 5.53 (m, 12 H, H_{cym}), 2.88 (sept, 6 H, C*H*$(CH_3)_2$), 2.05 (m, 18 H, CH_3), 1.31 (m, 36 H, CH(C*H*$_3)_2$) ppm. ^{13}C(^{1}H) NMR (100 MHz, CD_3CN): δ = 170.2 (*C*O), 170.1 (*C*O), 166.1 (C_{tpt}), 152.2 (CH_{α}), 142.0 (C_{tpt}), 138.4 (CH_{aq}), 134.1 (CH_{cq}), 133.3 (C_q), 127.8 (CH_{bq}), 127.2 ($C_{coronene}$), 125.2 ($CH_{coronene}$), 122.6 (CH_{β}), 120.4 ($C_{coronene}$), 109.7 (C_q), 103.9 (C_{cym}), 99.8 (C_{cym}), 84.5 (CH_{cym}), 84.1 (CH_{cym}), 83.0 (CH_{cym}), 82.9 (CH_{cym}), 30.6 ($CH(CH_3)_2$), 21.6 ($CH(CH_3)_2$), 21.4 ($CH(CH_3)_2$), 16.7 (CH_3) ppm. Anal. calc. for $C_{168}H_{138}F_{18}N_{12}O_{30}Ru_6S_6$ (3945.8): C 51.09, H 3.62, N 4.25; Found C 51.14, H 3.53, N 4.26.

[Pd(acac)$_2$⊂**P$_3$**][CF_3SO_3]$_6$: Yield 147 mg (80 %). UV-vis (1.0×10^{-5} M, CH_2Cl_2): λ_{max} = 308 nm ($\varepsilon = 3.95 \times 10^5$ $M^{-1}\cdot cm^{-1}$), 371 nm ($\varepsilon = 0.66 \times 10^5$ $M^{-1}\cdot cm^{-1}$), 447 nm ($\varepsilon = 0.50 \times 10^5$ $M^{-1}\cdot cm^{-1}$), 648 nm ($\varepsilon = 0.22 \times 10^5$ $M^{-1}\cdot cm^{-1}$). IR (KBr, cm^{-1}): 3060 (w, CH_{aryl}), 1536 (s, C=O), 1260 (s, CF_3) cm^{-1}. ^{1}H NMR (400 MHz, CD_3CN): δ = 8.81 (m, 6 H, H_q), 8.64 (m, 12 H, H_α), 8.15 (m, 6 H, H_q), 8.05 (m, 12 H, H_β), 7.42 (m, 6 H, H_q), 5.81 (d, 12 H, H_{cym}), 5.63 (d, 12 H, H_{cym}), 3.49 (m, 2 H, CH_{acac}), 2.81 (sept, 6 H, C*H*$(CH_3)_2$), 2.11 (s, 18 H, CH_3), 1.30 (d, 36 H, CH(C*H*$_3)_2$), 0.02 (m, 12 H, CH_{3acac}) ppm. ^{13}C(^{1}H) NMR (100 MHz, CD_3CN): δ = 171.5 (CO), 170.5 (CO), 169.9 (C_{tpt}), 157.9 (CH_α), 144.8 (C_{tpt}), 139.8 (CH_q), 134.7 (CH_q), 129.6 (CH_q), 124.9 (CH_β), 110.7 (C_q), 103.8 (C_{cym}), 102.0 (CH_{acac}), 101.2 (C_{cym}), 89.7 (CH_{cym}), 88.6 (CH_{cym}), 85.2 (CH_{cym}), 84.7 (CH_{cym}), 31.4 (*C*H$(CH_3)_2$), 22.5 (CH(*C*H$_3)_2$), 22.1 (CH(*C*H$_3)_2$), 17.6 (CH_3), 15.5 (CH_{3acac}) ppm. Anal. calc. for $C_{154}H_{140}F_{18}N_{12}O_{34}PdRu_6S_6$ (3950.0): C 46.83, H 3.57, N 4.26; found: C 46.31, H 3.54, N 4.15.

[pyrene-X⊂**P$_3$**][CF_3SO_3]$_6$: Yield 146 mg (78 %). UV-vis (1.0×10^{-5} M, CH_2Cl_2): λ_{max} = 308 nm ($\varepsilon = 3.79 \times 10^5$ $M^{-1}\cdot cm^{-1}$), 442 nm ($\varepsilon = 0.36 \times 10^5$ $M^{-1}\cdot cm^{-1}$), 659 nm ($\varepsilon = 0.18 \times 10^5$ $M^{-1}\cdot cm^{-1}$). IR (KBr, cm^{-1}): *ν* = 3060 (w, CH_{aryl}), 1536 (s, C=O), 1500 (m, C=C), 1260 (s, CF_3) cm^{-1}. ^{1}H NMR (400 MHz, CD_3CN): δ = 8.78 (m, 6 H, H_q), 8.60 (m, 12 H, H_α), 8.09 (m, 6 H, H_q), 8.01 (m, 12 H, H_β), 7.96 (m, 1 H, H_{pyr}), 7.71 (m, 1 H, H_{pyr}), 7.40 (m, 6 H, H_q), 7.21 (m, 1 H, H_{pyr}), 7.01 (m, 1 H, H_{pyr}), 5.98 (m, 1 H, H_{pyr}), 5.81 (d, 12 H, H_{cym}), 5.62 (d, 12 H, H_{cym}), 5.52 (m, 1 H, H_{pyr}), 5.09 (m, 1 H, H_{pyr}), 4.96 (m, 1 H, H_{pyr}), 4.75 (m, 1 H, H_{pyr}), 2.80 (sept, 6 H, C*H*$(CH_3)_2$), 2.10 (s, 18 H, CH_3), 1.29 (d, 36 H, CH(C*H*$_3)_2$) ppm. ^{13}C(^{1}H) NMR (100 MHz, CD_3CN): δ = 170.5 (CO), 170.2 (CO), 169.8 (C_{tpt}), 156.7 (CH_α), 142.4 (C_{tpt}), 141.0 (CH_q), 135.6 (CH_q), 130.2 (CH_q), 129.7 (C_{pyr}), 128.2 (CH_{pyr}), 126.8 (CH_{pyr}), 126.2 (C_{pyr}), 125.9 (CH_β), 109.1 (C_q), 104.9 (C_{cym}), 101.1 (C_{cym}), 88.6 (CH_{cym}), 87.8 (CH_{cym}), 86.1 (CH_{cym}), 85.9 (CH_{cym}), 32.2 ($CH(CH_3)_2$), 22.9 ($CH(CH_3)_2$), 22.7 ($CH(CH_3)_2$), 17.0 (CH_3) ppm. Anal. calc. for $C_{163}H_{135}Cl_2F_{18}N_{15}O_{30}Ru_6S_6$ (3995.6): C 49.00, H 3.41, N 5.26; Found: C 48.91, H 3.48, N 5.22.

[phenanthrene⊂**P$_4$**][CF_3SO_3]$_6$: Yield 70 mg (83%). UV-vis (1.0×10^{-5} M, $(CH_3)_2CO$): λ_{max} = 354 nm (6.3×10^4 $M^{-1}\cdot cm^{-1}$), 368 nm (6.2×10^4 $M^{-1}\cdot cm^{-1}$), 523 nm (1.7×10^4 $M^{-1}\cdot cm^{-1}$), 563 nm (2.7×10^4 $M^{-1}\cdot cm^{-1}$), 607 nm (3.4×10^4 $M^{-1}\cdot cm^{-1}$). IR (KBr, cm^{-1}): 3070 (w, CH_{aryl}), 1544 (s, C=O), 1259 (s, CF_3) cm^{-1}. ^{1}H NMR (400 MHz, CD_3CN): *δ* = 8.78 (dd, 12 H, H_{bq}), 8.54 (d, 12 H, H_α), 8.01 (m, 24 H, H_β and H_{cq}), 6.73 (br, 2 H, $H_{phenanthrene}$), 5.87 (d, 12 H, H_{cym}), 5.75 (br, 2 H, $H_{phenanthrene}$), 5.63 (d, 12 H, H_{cym}), 5.56 (br, 2 H, $H_{phenanthrene}$), 5.16 (br, 2 H,

$H_{phenanthrene}$), 4.63 (br, 2 H, $H_{phenanthrene}$), 2.93 (sept, 6 H, C*H*$(CH_3)_2$), 2.11 (s, 18 H, CH_3), 1.30 (d, 36 H, CH(C*H*$_3)_2$) ppm. $^{13}C(^1H)$ NMR (100 MHz, CD_3CN): δ = 168.7 (CO), 152.5 (CH_α), 133.3 (C_q), 132.9 (CH_{cq}), 127.0 (CH_{bq}), 123.4 (CH_β), 106.7 (C_q), 103.5 (C_{cym}), 99.4 (C_{cym}), 83.9 (CH_{cym}), 82.3 (CH_{cym}), 30.1 (*C*H$(CH_3)_2$), 21.2 (CH(*C*H$_3)_2$), 16.5 (CH_3) ppm. Anal. calc. for $C_{170}H_{142}F_{18}N_{12}O_{30}Ru_6S_6$ (3973.8): C 51.33, H 3.70, N 4.22; Found C 51.38, H 3.60, N 4.23.

[pyrene⊂**P$_4$**][CF_3SO_3]$_6$: Yield 75 mg (84%). UV-vis (1.0×10^{-5} M, $(CH_3)_2CO$): λ_{max} = 350 nm (6.1×10^4 $M^{-1}\cdot cm^{-1}$), 362 nm (6.2×10^4 $M^{-1}\cdot cm^{-1}$), 522 nm (1.6×10^4 $M^{-1}\cdot cm^{-1}$), 565 nm (2.6×10^4 $M^{-1}\cdot cm^{-1}$), 609 nm (3.6×10^4 $M^{-1}\cdot cm^{-1}$). IR (KBr, cm^{-1}): 3070 (w, CH_{aryl}), 1540 (s, C=O), 1260 (s, CF_3) cm^{-1}. ^1H NMR (400 MHz, CD_3CN): *δ* = 8.80 (dd, 12H, H_{bq}), 8.50 (d, 12H, H_α), 8.01 (m, 24H, H_β and H_{cq}), 6.14 (m, 4H, H_{pyrene}), 5.90 (d, 12H, H_{cym}), 5.70 (br, 2H, H_{pyrene}), 5.60 (d, 12H, H_{cym}), 5.05 (m, 4H, H_{pyrene}), 2.94 (sept, 6H, C*H*$(CH_3)_2$), 2.10 (s, 18H, CH_3), 1.29 (d, 36H, CH(C*H*$_3)_2$) ppm. $^{13}C(^1H)$ NMR (100 MHz, CD_3CN): δ = 170.1 (*C*O), 152.4 (*C*H_α), 133.1 (*C*$_q$), 132.6 (*C*H_{cq}), 129.7 (*C*H_{pyrene}), 127.4 (*C*H_{pyrene}), 127.0 (*C*H_{bq}), 125.3 (*C*H_{pyrene}), 123.0 (*C*H_β), 106.8 (*C*$_q$), 103.4 (*C*$_{cym}$), 99.2 (*C*$_{cym}$), 83.6 (*C*H_{cym}), 82.1 (*C*H_{cym}), 29.9 (*C*H$(CH_3)_2$), 19.2 (H(*C*H$_3)_2$) 16.8 (*C*H_3) ppm. Anal. calc. for $C_{172}H_{142}F_{18}N_{12}O_{30}Ru_6S_6$ (3997.8): C 51.67, H 3.68, N 4.20; Found C 51.96, H 3.90, N 4.28.

[triphenylene⊂**P$_4$**][CF_3SO_3]$_6$: Yield 75 mg (87%). UV-vis (1.0×10^{-5} M, $(CH_3)_2CO$): λ_{max} = 351 nm (6.3×10^4 $M^{-1}\cdot cm^{-1}$), 368 nm (6.1×10^4 $M^{-1}\cdot cm^{-1}$), 526 nm (1.5×10^4 $M^{-1}\cdot cm^{-1}$), 564 nm (2.5×10^4 $M^{-1}\cdot cm^{-1}$), 608 nm (3.3×10^4 $M^{-1}\cdot cm^{-1}$). IR (KBr, cm^{-1}): 3069 (w, CH_{aryl}), 1543 (s, C=O), 1259 (s, CF_3) cm^{-1}. ^1H NMR (400 MHz, CD_3CN): δ = 8.86 (m, 12 H, H_{bq}), 8.42 (d, 12 H, H_α), 8.12 (m, 12 H, H_{cq}), 7.58 (d, 12 H, H_β), 6.58 (m, 6 H, $H_{triphenylene}$), 5.87 (d, 12 H, H_{cym}), 5.61 (d, 12 H, H_{cym}), 4.41 (m, 6 H, $H_{triphenylene}$), 2.92 (sept, 6 H, C*H*$(CH_3)_2$), 2.06 (s, 18 H, CH_3), 1.29 (d, 36 H, CH(C*H*$_3)_2$) ppm. $^{13}C(^1H)$ NMR (100 MHz, CD_3CN): δ = 170.2 (CO), 168.6 (C_{tpt}), 153.0 (CH_α), 143.9 (C_{tpt}), 134.6 (CH_{cq}), 134.4 (C_q), 128.5 ($C_{triphenylene}$), 128.5 (CH_{bq}), 126.4 ($CH_{triphenylene}$), 124.4 (CH_β), 122.9 ($CH_{triphenylene}$), 107.8 (C_q), 104.8 (C_{cym}), 100.8 (C_{cym}), 85.3 (CH_{cym}), 83.5 (CH_{cym}), 31.5 (*C*H$(CH_3)_2$), 22.5 (CH(*C*H$_3)_2$), 17.8 (CH_3) ppm. Anal. calc. for $C_{174}H_{144}F_{18}N_{12}O_{30}Ru_6S_6$ (4023.9): C 51.94, H 3.61, N 4.23; Found C 51.92, H 3.71, N 4.18.

[coronene⊂**P$_4$**][CF_3SO_3]$_6$: Yield 71 mg (81%). UV-vis (1.0×10^{-5} M, $(CH_3)_2CO$): λ_{max} = 305 nm (17.2×10^4 $M^{-1}\cdot cm^{-1}$), 343 nm (8.7×10^4 $M^{-1}\cdot cm^{-1}$), 372 nm (5.8×10^4 $M^{-1}\cdot cm^{-1}$), 568 nm

(2.3×10^4 $M^{-1}\cdot cm^{-1}$), 611 nm (3.0×10^4 $M^{-1}\cdot cm^{-1}$). IR (KBr, cm^{-1}): 3064 (w, CH_{aryl}), 1544 (s, C=O), 1261 (s, CF_3) cm^{-1}. ^1H NMR (400 MHz, CD_3CN): δ = 8.99 (dd, 12 H, H_{bq}), 8.36 (d, 12 H, H_α), 8.27 (dd, 12 H, H_{cq}), 6.71 (d, 12 H, H_β), 6.23 (s, 12 H, $H_{coronene}$), 5.86 (d, 12 H, H_{cym}), 5.60 (d, 12 H, H_{cym}), 2.93 (sept, 6 H, C*H*$(CH_3)_2$), 2.05 (s, 18 H, CH_3), 1.31 (d, 36 H, CH(C*H*$_3)_2$) ppm. $^{13}C(^1H)$ NMR (100 MHz, CD_3CN): δ = 169.9 (CO), 166.0 (C_{tpt}), 152.1 (CH_α), 141.8 (C_{tpt}), 133.9 (C_q), 133.8 (CH_{cq}), 127.7 (CH_{bq}), 127.0 ($C_{coronene}$), 124.9 ($CH_{coronene}$), 122.5 (CH_β), 120.2 ($C_{coronene}$), 107.1 (C_q), 104.0 (C_{cym}), 99.8 (C_{cym}), 84.2 (CH_{cym}), 82.7 (CH_{cym}), 30.6 (*C*H$(CH_3)_2$), 21.6 (CH(*C*H$_3)_2$), 16.9 (CH_3) ppm. Anal. calc. for $C_{180}H_{144}F_{18}N_{12}O_{30}Ru_6S_6$ (4095.9): C 52.78, H 3.54, N 4.10; Found C 52.91, H 3.72, N 4.12.

[Pd(acac)$_2$⊂**P$_4$**][CF_3SO_3]$_6$: Yield 157 mg (82 %). UV-vis (1.0×10^{-5} M, CH_2Cl_2): λ_{max} = 308 nm ($\varepsilon = 3.90 \times 10^5$ $M^{-1}\cdot cm^{-1}$), 380 nm ($\varepsilon = 0.56 \times 10^5$ $M^{-1}\cdot cm^{-1}$), 607 nm ($\varepsilon = 0.20 \times 10^5$ $M^{-1}\cdot cm^{-1}$), 655 nm ($\varepsilon = 0.22 \times 10^5$ $M^{-1}\cdot cm^{-1}$). IR (KBr, cm^{-1}): 3060 (w, CH_{aryl}), 1536 (s, C=O), 1260 (s, CF_3) cm^{-1}. ^1H NMR (400 MHz, CD_3CN): δ = 8.80 (dd, 12 H, H_q), 8.51 (d, 12 H, H_α), 8.02 (m, 24 H, H_q + H_β), 5.90 (d, 12 H, H_{cym}), 5.60 (d, 12 H, H_{cym}), 3.51 (m, 2 H, CH_{acac}), 2.79 (sept, 6 H, C**H**$(CH_3)_2$), 2.10 (s, 18 H, CH_3), 1.30 (d, 36 H, CH(C**H**$_3)_2$), 0.02 (m, 12 H, CH_{3acac}) ppm. $^{13}C(^1H)$ NMR (100 MHz, CD_3CN): δ = 170.0 (CO), 165.7 (C_{tpt}), 152.2 (CH_α), 141.3 (C_{tpt}), 133.1 (C_q), 132.6 (CH_q), 127.0 (CH_q), 123.2 (CH_β), 106.5 (C_q), 103.4 (C_{cym}), 102.2 (CH_{acac}), 101.1 (C_{cym}), 85.2 (CH_{cym}), 85.1 (CH_{cym}), 84.8 (CH_{cym}), 84.6 (CH_{cym}), 31.2 ($CH(CH_3)_2$), 22.1 ($CH(CH_3)_2$), 22.0 ($CH(CH_3)_2$), 17.9 (CH_3), 15.8 (CH_{3acac}) ppm. Anal. calc. for $C_{166}H_{146}F_{18}N_{12}O_{34}PdRu_6S_6$ (4100.2): C 48.63, H 3.59, N 4.10; Found: C 47.92, H 3.57, N 4.02.

[pyrene-X⊂**P$_4$**][CF_3SO_3]$_6$: Yield 155 mg (80 %). UV-vis (1.0×10^{-5} M, CH_2Cl_2): λ_{max} = 308 nm ($\varepsilon = 3.60 \times 10^5$ $M^{-1}\cdot cm^{-1}$), 390 nm ($\varepsilon = 0.23 \times 10^5$ $M^{-1}\cdot cm^{-1}$), 607 nm ($\varepsilon = 0.14 \times 10^5$ $M^{-1}\cdot cm^{-1}$), 658 nm ($\varepsilon = 0.13 \times 10^5$ $M^{-1}\cdot cm^{-1}$). IR (KBr, cm^{-1}): 3060 (w, CH_{aryl}), 1536 (s, C=O), 1500 (m, C=C), 1260 (s, CF_3) cm^{-1}. ^1H NMR (400 MHz, CD_3CN): δ = 8.90 (m, 12 H, H_α), 8.84 (m, 12 H, H_β), 8.11 (m, 12 H, H_q), 7.90 (m, 1 H, H_{pyr}), 7.75 (m, 1 H, H_{pyr}), 7.22 (m, 12 H, H_q), 7.18 (m, 1 H, H_{pyr}), 7.09 (m, 1 H, H_{pyr}), 6.31 (m, 1 H, H_{pyr}), 5.88 (d, 12 H, H_{cym}), 5.61 (d, 12 H, H_{cym}), 5.35 (m, 1 H, H_{pyr}), 5.18 (m, 1 H, H_{pyr}), 4.88 (m, 1 H, H_{pyr}), 4.71 (m, 1 H, H_{pyr}), 2.80 (sept, 6 H, C*H*$(CH_3)_2$), 2.09 (s, 18 H, CH_3), 1.32 (d, 36 H, CH(C*H*$_3)_2$) ppm. $^{13}C(^1H)$ NMR (100 MHz, CD_3CN): δ = 171.1 (CO), 166.9 (C_{tpt}), 151.3 (CH_α), 140.2 (C_{tpt}), 133.1 (C_q), 132.8 (CH_q), 131.2 (C_{pyr}), 128.9 (CH_{pyr}), 128.2 (CH_{pyr}), 127.4 (C_{pyr}), 126.9 (CH_q), 124.3 (CH_β), 105.5 (C_q), 104.8 (C_{cym}), 100.9 (C_{cym}), 85.4 (CH_{cym}), 85.3 (CH_{cym}), 85.1

(CH_{cym}), 84.9 (CH_{cym}), 31.0 ($CH(CH_3)_2$), 22.2 ($CH(CH_3)_2$), 20.9 ($CH(CH_3)_2$), 18.1 (CH_3) ppm. Anal. calc. for $C_{175}H_{141}Cl_2F_{18}N_{15}O_{30}Ru_6S_6$ (4145.8): C 50.70, H 3.43, N 5.07; Found: C 49.97, H 3.41, N 4.97.

6.2.5 Arene Ruthenium Metalla-Cubes $Q_2 - Q_{14}$

General procedure for [**Q₂** − **Q₁₀**][CF_3SO_3]$_8$: A mixture of Ag(CF_3SO_3) (165 mg, 0.64 mmol) and [Ru_2(arene)$_2$(*OO*∩*OO*)$_2Cl_2$] (0.32 mmol; **Q₂** and **Q₃**: *p*-cym, ox, 201 mg; **Q₄** − **Q₆**: *p*-cym, dobq, 218 mg; **Q₇**: indane, dobq, 207 mg; **Q₈**: nonylbenzene, dobq, 262 mg; **Q₉** and **Q₁₀**: toluene, dobq, 185 mg) in methanol (30 mL) is stirred at room temperature for 3 h, then filtered. To the red filtrate, the corresponding porphyrin (0.16 mmol; **Q₄**, **Q₇**, **Q₈**, and **Q₉**: tpp-2H, 99 mg; **Q₂** and **Q₅**: tpp-Ni, 108 mg; **Q₃**, **Q₁₀** and **Q₆**: tpp-Zn, 106 mg) is added. The solution is refluxed for 48 h, and the solvent removed under vacuum. The residue is dissolved in acetonitrile (3 mL), and diethyl ether is added to precipitate the purple or black solid.

Q₂: Yield 305 mg (79 %). UV-vis (1.0×10^{-5} M, (CH_2Cl_2)): λ_{max} 416 nm ($\varepsilon = 4.09 \times 10^5$ $M^{-1}\cdot cm^{-1}$), λ_{max} 542 nm ($\varepsilon = 0.47 \times 10^5$ $M^{-1}\cdot cm^{-1}$). IR (KBr, cm^{-1}): 3069 (w, CH_{aryl}), 1521 (s, C=O), 1258 (s, CF_3). ^{1}H NMR (400 MHz, CD_3CN): δ (ppm) = 9.25 (d, 8 H, H_{pyr}), 9.18 (d, 8 H, H'$_\alpha$), 8.92 (d, 8 H, H_β), 8.17 (d, 8 H, H_α), 8.10 (d, 8 H, H'$_{pyr}$), 7.91 (d, 8 H, H'$_\beta$), 6.15 (m, 16 H, H_{cym}), 5.97 (m, 16 H, H_{cym}), 3.05 (sept, 6 H, C*H*(CH_3)$_2$), 2.45 (s, 12 H, CH_3), 1.49 (d, 24 H, CH(C*H*$_3$)$_2$). ^{13}C(^{1}H) NMR (100 MHz, CD_3CN): δ (ppm) = 172.3 (CO), 153.7 (CH'$_\alpha$), 151.2 (CH_α), 149.4 ($C_{pyridyl}$), 140.1 (C_{pyr}), 139.9 (C_{pyr}), 133.5 (CH'$_\beta$), 133.1 (CH_β), 130.0 (CH'$_{pyr}$), 129.6 (CH'$_{pyr}$), 104.2 (C_{cym}), 101.3 (C_{cym}), 84.2 (CH_{cym}), 83.8 (CH_{cym}), 83.0 (CH_{cym}), 82.6 (CH_{cym}), 32.0 ($CH(CH_3)_2$), 21.8 ($CH(CH_3)_2$), 21.2 ($CH(CH_3)_2$), 17.5 (CH_3). ESI-MS: m/z 1045.0 [**Q₂** + (CF_3SO_3)$_4$]$^{4+}$. Anal. calc. for $C_{176}H_{160}F_{24}N_{16}Ni_2O_{40}Ru_8S_8$ (4777.7): C 44.24, H 3.37, N 4.69; Found: C 44.01, H 3.29, N 4.34.

Q₃: Yield: 298 mg (78 %). UV-vis (1.0×10^{-5} M, (CH_2Cl_2)): λ_{max} 416 nm ($\varepsilon = 4.12 \times 10^5$ $M^{-1}\cdot cm^{-1}$), λ_{max} 510 nm ($\varepsilon = 0.53 \times 10^5$ $M^{-1}\cdot cm^{-1}$). IR (KBr, cm^{-1}): 3072 (w, CH_{aryl}), 1520 (s, C=O), 1257 (s, CF_3). ^{1}H NMR (400 MHz, CD_3CN): δ(ppm) = 9.28 (d, 8 H, H_{pyr}), 9.22 (d, 8 H, H'$_\alpha$), 8.97 (m, 16 H, H_α), 8.15 (d, 8 H, H_β), 8.10 (d, 8 H, H'$_{pyr}$), 7.97 (d, 8 H, H'$_\beta$), 6.15 (m, 24 H, H_{cym}), 5.96 (m, 8 H, H_{cym}), 3.13 (sept, 8 H, C*H*(CH_3)$_2$), 2.36 (s, 24 H, CH_3), 1.60 (m, 48 H, CH(C*H*$_3$)$_2$). ^{13}C(^{1}H) NMR (100 MHz, CD_3CN): δ(ppm) = 171.2 (CO), 153.7 (CH'$_\alpha$), 153.1 (CH_α), 147.2 (CH'$_\beta$), 147.0 (CH_β), 133.0 (C_{pyr}), 132.9 (C_{pyr}), 114.6 (CCH(CH_3)$_2$), 101.8

(CH_q), 97.6 (CCH_3), 83.9 (CH_{cym}), 82.7 (CH_{cym}), 81.8 (CH_{cym}), 31.3 ($CH(CH_3)_2$), 21.9 ($CH(CH_3)_2$), 21.4 ($CH(CH_3)_2$), 17.6 (CH_3). ESI-MS: m/z 1048.7 [**Q$_3$** + $(CF_3SO_3)_4$]$^{4+}$ and 1448.0 [**Q$_3$** + $(CF_3SO_3)_5$]$^{3+}$. Anal. calc. for $C_{176}H_{160}F_{24}N_{16}O_{40}Ru_8S_8Zn_2$ (4791): C 44.12, H 3.37, N 4.68; Found C 43.82, H 3.19, N 4.68.

Q$_4$: Yield 287 mg (74 %). UV-vis (1.0×10^{-5} M, $(CH_3)_2CO$): λ_{max} 257 nm ($\varepsilon = 4.32 \times 10^5$ M^{-1}·cm^{-1}), λ_{max} 312 nm ($\varepsilon = 0.43 \times 10^5$ M^{-1}·cm^{-1}), λ_{max} 411 nm ($\varepsilon = 0.41 \times 10^5$ M^{-1}·cm^{-1}), λ_{max} 514 nm ($\varepsilon = 0.08 \times 10^5$ M^{-1}·cm^{-1}), λ_{max} 654 nm ($\varepsilon = 0.01 \times 10^5$ M^{-1}·cm^{-1}). IR (KBr, cm^{-1}): 3450 (m, NH), 3070 (w, CH_{aryl}), 1520 (s, C=O), 1260 (s, CF_3). ^{1}H NMR (400 MHz, CD_3CN): δ (ppm) = 8.89 (d, 8 H, H_{pyr}), 8.81 (d, 8 H, H′$_\alpha$), 8.59 (m, 16 H, H_α + H_β), 8.30 (d, 8 H, H′$_{pyr}$), 7.45 (d, 8 H, H′$_\beta$), 6.20 (m, 16 H, H_{cym}), 6.17 (s, 8 H, H_q), 6.03 (m, 16 H, H_{cym}), 3.13 (sept, 8 H, C*H*$(CH_3)_2$), 2.43 (s, 24 H, CH_3), 1.54 (m, 48 H, CH(C*H*$_3)_2$), -6.96 (s, 4 H, NH). ^{13}C(^{1}H) NMR (100 MHz, CD_3CN): δ (ppm) = 184.1 (CO), 183.6 (CO), 152.4 (CH'$_\alpha$), 151.2 (CH_α), 133.0 (CH'$_\beta$), 131.5 (CH_β), 122.8 (C_{pyr}), 119.6 (C_{pyr}), 101.9 (CH_q), 104.1 ($CCH(CH_3)_2$), 98.8 (CCH_3), 83.8 (CH_{cym}), 83.3 (CH_{cym}), 82.3 (CH_{cym}), 82.2 (CH_{cym}), 31.3 ($CH(CH_3)_2$), 21.5 ($CH(CH_3)_2$), 21.9 ($CH(CH_3)_2$), 17.5 (CH_3). ESI-MS: m/z 1067.3 [**Q$_4$** + $(CF_3SO_3)_4$]$^{4+}$; 1472.5 [**Q$_4$** + $(CF_3SO_3)_5$]$^{3+}$. Anal. calc. for $C_{192}H_{172}F_{24}N_{16}O_{40}Ru_8S_8$ (4864.5): C 47.41, H 3.56, N 4.61; Found: C 46.87, H 3.11, N 4.43.

Q$_5$: Yield 311 mg (78 %). UV-vis (1.0×10^{-5} M, (CH_2Cl_2)): λ_{max} 409 nm ($\varepsilon = 3.45 \times 10^5$ M^{-1}·cm^{-1}), λ_{max} 533 nm ($\varepsilon = 0.58 \times 10^5$ M^{-1}·cm^{-1}). IR (KBr, cm^{-1}): 3068 (m, CH_{aryl}), 1520 (s, C=O), 1258 (s, CF_3). ^{1}H NMR (400 MHz, CD_3CN): δ (ppm) = 8.80 (d, 8 H, H_{pyr}), 8.77 (d, 8 H, H'$_\alpha$), 8.44 (d, 8 H, H_β), 8.32 (d, 8 H, H_α), 8.14 (d, 8 H, H'$_{pyr}$), 7.39 (d, 8 H, H'$_\beta$), 6.19 (d, 8 H, H_{cym}), 6.15 (d, 8 H, H_{cym}), 6.11 (s, 8 H, H_q), 6.01 (d, 8 H, H_{cym}), 5.98 (d, 8 H, H_{cym}), 3.10 (sept, 8 H, $CH(CH_3)_2$), 2.42 (m, 48 H, $CH(CH_3)_2$), 1.52 (s, 24 H, CH_3). ^{13}C(^{1}H) NMR (100 MHz, CD_3CN): δ (ppm) = 184.1 (CO), 183.6 (CO), 152.5 (CH'$_\alpha$), 150.6 (CH_α), 150.5 ($C_{pyridyl}$), 141.1 (C_{pyr}), 140.8 (C_{pyr}), 132.5 (CH'$_\beta$), 132.0 (CH_β), 131.2 (CH'$_{pyr}$), 130.6 (CH'$_{pyr}$), 104.0 (C_{cym}), 101.9 (C_{cym}), 98.6 (CH_q), 83.8 (CH_{cym}), 83.2 (CH_{cym}), 82.5 (CH_{cym}), 82.3 (CH_{cym}), 31.4 ($CH(CH_3)_2$), 21.9 ($CH(CH_3)_2$), 21.4 ($CH(CH_3)_2$), 17.5 (CH_3). ESI-MS: m/z 1095.5 [**Q$_5$** + $(CF_3SO_3)_4$]$^{4+}$, 1510.3 [**Q$_5$** + $(CF_3SO_3)_5$]$^{3+}$. Anal. calc. for $C_{192}H_{168}F_{24}N_{16}Ni_2O_{40}Ru_8S_8$ (4977.9): C 46.33, H 3.40, N 4.50; Found: C 46.08, H 3.28, N 4.41.

Q$_6$: Yield 301 mg (76 %). UV-vis (1.0×10^{-5} M, (CH_2Cl_2)): λ_{max} 418 nm ($\varepsilon = 4.28 \times 10^5$ M^{-1}·cm^{-1}), λ_{max} 506 nm ($\varepsilon = 0.44 \times 10^5$ M^{-1}·cm^{-1}). IR (KBr, cm^{-1}): 3068 (w, CH_{aryl}), 1521 (s,

C=O), 1257 (s, CF_3). ^{1}H NMR (400 MHz, CD_3CN): δ (ppm) = 8.83 (d, 8 H, H_{pyr}), 8.75 (d, 8 H, H'_{α}), 8.63 (d, 8 H, H_{β}), 8.51 (d, 8 H, H_{α}), 8.20 (d, 8 H, H'_{pyr}), 7.41 (d, 8 H, H'_{β}), 6.20 (m, 16 H, H_{cym}), 6.18 (s, 8 H, H_q), 6.04 (d, 8 H, H_{cym}), 5.97 (d, 8 H, H_{cym}), 3.12 (sept, 8 H, C*H*$(CH_3)_2$), 2.42 (m, 48 H, CH(C*H*$_3)_2$), 1.54 (s, 24 H, C*H*$_3$). ^{13}C(^{1}H) NMR (100 MHz, CD_3CN): δ (ppm) = 185.2 (CO) and 184.8 (CO), 154.0 (CH'_{α}), 152.8 (CH_{α}), 150.9 ($C_{pyridyl}$), 148.2 and 147.7 ($C_{pyrrole}$), 134.6 (CH'_{β}), 133.0 (CH_{β}), 132.8 (CH'_{pyr}), 132.5 (CH_{pyr}), 105.0 and 99.9 (C_{cym}), 102.9 (CH_q), 84.9, 84.5, 83.4 and 82.9 (CH_{cym}), 32.4 ($CH(CH_3)_2$), 22.9 and 22.5 ($CH(CH_3)_2$), 18.6 (CH_3). ESI-MS: m/z 1099.3 [**Q$_6$** + $(CF_3SO_3)_4$]$^{4+}$ and 1515.4 [**Q$_6$** + $(CF_3SO_3)_5$]$^{3+}$. Anal. calc. for $C_{192}H_{168}F_{24}N_{16}O_{40}Ru_8S_8Zn_2$ (4993.3): C 46.18, H 3.43, N 4.49; found: C 46.08, H 3.42, N 4.47.

Q$_7$: Yield 315 mg (83 %). UV-vis (1.0×10^{-5} M, (CH_2Cl_2)): λ_{max} 413 nm ($\varepsilon = 3.49 \times 10^5$ $M^{-1}\cdot cm^{-1}$), λ_{max} 519 nm ($\varepsilon = 0.54 \times 10^5$ $M^{-1}\cdot cm^{-1}$). IR (KBr, cm^{-1}): 3450 (m, NH), 3070 (w, CH_{aryl}), 1528 (s, C=O), 1260 (s, CF_3). ^{1}H NMR (400 MHz, CD_3CN): δ (ppm) = 8.99 (m, 8 H, H_{pyr}), 8.90 (d, 8 H, H'_{α}), 8.82 (m, 16 H, H_{β} + H_{α}), 8.29 (m, 8 H, H'_{pyr}), 7.43 (d, 8 H, H'_{β}), 6.33 (d, 8 H, H_{indane}), 6.25 (d, 8 H, H_{indane}), 6.15 (s, 8 H, H_q), 6.08 (t, 8 H, H_{indane}), 6.02 (t, 8 H, H_{indane}), 3.06 (m, 16 H, $CH_{2indane}$), 2.95 (m, 8 H, $CH_{2indane}$), -6.96 (s, 4 H, NH). ^{13}C(^{1}H) NMR (100 MHz, CD_3CN): δ (ppm) = 184.9 (CO), 184.8 (CO), 153.5 (CH'_{α}), 152.2 (CH_{α}), 151.7 ($C_{pyridyl}$), 133.7 (C_{pyr}), 133.5 (C_{pyr}), 132.5 (CH'_{β}), 132.0 (CH_{β}), 127.0 (CH'_{pyr}), 126.9 (CH'_{pyr}), 105.1 (C_{indane}), 104.8 (C_{indane}), 102.9 (CH_q), 83.2 (CH_{indane}), 83.0 (CH_{indane}), 82.8 (CH_{indane}), 82.7 (CH_{indane}), 30.7 ($CH_{2indane}$), 23.5 ($CH_{2indane}$). ESI-MS: m/z 1035.5 [**Q$_7$** + $(CF_3SO_3)_4$]$^{4+}$. Anal. calc. for $C_{184}H_{140}F_{24}N_{16}O_{40}Ru_8S_8$ (4736.2): C 46.66, H 2.98, N 4.73; Found: C 46.44, H 2.92, N, 4.58.

Q$_8$: Yield 337 mg (78 %). UV-vis (1.0×10^{-5} M, (CH_2Cl_2)): λ_{max} 412 nm ($\varepsilon = 4.05 \times 10^5$ $M^{-1}\cdot cm^{-1}$), λ_{max} 522 nm ($\varepsilon = 0.69 \times 10^5$ $M^{-1}\cdot cm^{-1}$). IR (KBr, cm^{-1}): 3450 (m, NH), 3070 (w, CH_{aryl}), 1528 (s, C=O), 1260 (s, CF_3). ^{1}H NMR (400 MHz, CD_3CN): δ (ppm) = 8.90 (d, 8 H, H_{pyr}), 8.84 (d, 8 H, H'_{α}), 8.63 (m, 16 H, H_{β} + H_{α}), 8.30 (d, 8 H, H'_{pyr}), 7.42 (d, 8 H, H'_{β}), 6.33 (dd, 16 H, H_{phenyl}), 6.25 (s, 8 H, H_q), 6.15 (t, 8 H, H_{phenyl}), 6.09 (dd, 8 H, H_{phenyl}), 6.02 (d, 8 H, H_{phenyl}), 2.77 (t, 16 H, CH_2), 1.52 (m, 16 H, CH_2), 1.33 (m, 96 H, CH_2), 0.89 (m, 24 H, CH_3), -6.96 (s, 4 H, NH). ^{13}C(^{1}H) NMR (100 MHz, CD_3CN): δ (ppm) = 185.2 (CO), 184.8 (CO), 153.5 (CH'_{α}), 152.5 (CH_{α}), 152.2 ($C_{pyridyl}$), 132.9 (C_{pyr}), 132.7 (C_{pyr}), 132.6 (CH'_{β}), 129.3 (CH_{β}), 129.2 (CH'_{pyr}), 123.8 (CH'_{pyr}), 108.5 (C_q), 102.8 (CH_q), 90.1 (C_{phenyl}), 89.8 (C_{phenyl}), 80.4 (CH_{phenyl}), 79.9 (CH_{phenyl}), 78.4 (CH_{phenyl}), 33.8 (CH_2), 32.6 (CH_2), 30.2 (CH_2), 30.0

(CH_2), 29.9 (CH_2), 23.4 (CH_2), 14.4 (CH_3). ESI-MS: m/z 1207.8 [**Q$_8$** + $(CF_3SO_3)_4$]$^{4+}$. Anal. calc. for $C_{232}H_{252}F_{24}N_{16}O_{40}Ru_8S_8$ (5425.6): C 51.36, H 4.68, N 4.13; Found: C 51.10, H 4.61, N 4.02.

Q$_9$: Yield: 300 mg (83 %). UV-vis (1.0×10^{-5} M, $(CH_3)_2CO$): λ_{max} 257 nm ($\varepsilon = 3.90 \times 10^5$ M$^{-1}\cdot$cm^{-1}), λ_{max} 314 nm ($\varepsilon = 0.43 \times 10^5$ M$^{-1}\cdot$cm^{-1}), λ_{max} 410 nm ($\varepsilon = 0.42 \times 10^5$ M$^{-1}\cdot$cm^{-1}), λ_{max} 515 nm ($\varepsilon = 0.08 \times 10^5$ M$^{-1}\cdot$cm^{-1}), λ_{max} 655 nm ($\varepsilon = 0.01 \times 10^5$ M$^{-1}\cdot$cm^{-1}). IR (KBr, cm^{-1}): 3470 (m, NH), 3075 (w, CH_{aryl}), 1520 (s, C=O), 1260 (s, CF_3). ^{1}H NMR (400 MHz, CD_3CN): δ (ppm) = 8.87 (m, 16 H, H_{pyr} + H′$_\alpha$), 8.69 (m, 16 H, H_α + H_β), 8.32 (m, 8 H, H′$_{pyr}$), 7.45 (d, 8 H, H′$_\beta$), 6.35 (m, 16 H, H_q + H_{tol}), 6.14 (m, 16 H, H_{tol}), 5.97 (m, 16 H, H_{tol}), 2.48 (s, 24 H, CH_3), -6.94 (s, 4 H, NH). ^{13}C(^{1}H) NMR (100 MHz, CD_3CN): δ (ppm) = 184.3 (CO), 183.9 (CO), 152.6 (CH'$_\alpha$), 151.1 (CH_α), 132.6 (CH'$_\beta$), 131.5 (CH_β), 123.0 (C_{pyr}), 120.1 (C_{pyr}), 101.8 (CH_q), 89.4 (CCH_3), 79.7 (CH_{tol}), 79.1 (CH_{tol}), 76.7 (CH_{tol}), 18.2 (CH_3). ESI-MS: m/z 983.0 [**Q$_9$** + $(CF_3SO_3)_4$]$^{4+}$; 1359.3 [**Q$_9$** + $(CF_3SO_3)_5$]$^{3+}$. Anal. calc. for $C_{168}H_{124}F_{24}Ru_8N_{16}O_{40}S_8$ (4527.9): C 44.52, H 2.74, N 4.95; Found: C 43.98, H 2.33, N 4.65.

Q$_{10}$: Yield 219 mg (86 %). UV-vis (1.0×10^{-5} M, (CH_2Cl_2)): λ_{max} 420 nm ($\varepsilon = 4.02 \times 10^5$ M$^{-1}\cdot$cm^{-1}), λ_{max} 515 nm ($\varepsilon = 0.35 \times 10^5$ M$^{-1}\cdot$cm^{-1}). IR (KBr, cm^{-1}): 3070 (w, CH_{aryl}), 1518 (s, C=O), 1258 (s, CF_3). ^{1}H NMR (400 MHz, CD_3CN): δ (ppm) = 8.85 (d, 8 H, H_{pyr}), 8.72 (d, 8 H, H'$_\alpha$), 8.64 (d, 8 H, H_β), 8.48 (d, 8 H, H_α), 8.17 (d, 8 H, H'$_{pyr}$), 7.42 (d, 8 H, H'$_\beta$), 6.22 (m, 16 H, H_{tol}), 6.18 (s, 8 H, H_q), 6.09 (d, 8 H, H_{tol}), 5.99 (d, 8 H, H_{tol}), 2.47 (s, 24 H, CH_3). ^{13}C(^{1}H) NMR (100 MHz, CD_3CN): δ (ppm) = 184.5 (CO), 184.0 (CO), 153.0 (CH'$_\alpha$), 152.0 (CH_α), 150.6 ($C_{pyridyl}$), 147.2 ($C_{pyrrole}$), 146.9 ($C_{pyrrole}$), 133.3 (CH'$_\beta$), 131.9 (CH_β), 131.7 (CH_{pyr}), 131.6 (CH'$_{pyr}$), 104.4 (C_{tol}), 89.6 (CCH_3), 89.5, 79.8 and 79.3 (CH_{tol}), 76.9 (CH_q), 18.8 (CH_3). ESI-MS: m/z 1014.7 [**Q$_{10}$** + $(CF_3SO_3)_4$]$^{4+}$ and 1402.6 [**Q$_{10}$** + $(CF_3SO_3)_5$]$^{3+}$. Anal. calc. for $C_{168}H_{120}F_{24}Ru_8N_{16}O_{40}S_8Zn_2$ (4654.7): C 43.31, H 2.56, N 4.81; Found: C 42.48, H 2.53, N 4.72.

General procedure for **Q$_{11}$** – **Q$_{14}$**: A mixture of arene ruthenium dinuclear complexes **C$_0$** (**Q$_{11}$**: 57 mg, 0.09 mmol; **Q$_{13}$**: 85 mg, 0.13 mmol) or C_1 (**Q$_{12}$**: 61 mg, 0.09 mmol; **Q$_{14}$**: 92 mg, 0.13 mmol), $AgCF_3SO_3$ (**Q$_{11}$**, **Q$_{12}$**: 46 mg, 0.18 mmol; **Q$_{13}$**, **Q$_{14}$**: 69 mg, 0.27 mmol) and the corresponding porphyrin panels 5,15-bis(4-pyridyl)-10,20-diphenylporphyrin (**Q$_{11}$**, **Q$_{12}$**: 55 mg, 0.09 mmol) or 5,10,15-tris(4-pyridyl)-20-phenylporphyrin (**Q$_{13}$**, **Q$_{14}$**: 56 mg, 0.09 mmol) is stirred at 60°C for 24 hours and then the solution is filtered to remove silver chloride. The

solvent is removed under vacuum and the residue is taken up in dichloromethane (3 mL) and diethyl ether added to precipitate the products as red solids.

Q_{11}: Yield 75 mg (85%). UV-vis (1.0×10^{-5} M, ($(CH_3)_2CO$)): λ_{max} 411 nm ($\varepsilon = 3.27 \times 10^5$ $M^{-1}\cdot cm^{-1}$), 515 nm ($\varepsilon = 0.47 \times 10^5$ $M^{-1}\cdot cm^{-1}$), 550 nm ($\varepsilon = 0.30 \times 10^5$ $M^{-1}\cdot cm^{-1}$), 589 nm ($\varepsilon = 0.16 \times 10^5$ $M^{-1}\cdot cm^{-1}$), 649 nm ($\varepsilon = 0.12 \times 10^5$ $M^{-1}\cdot cm^{-1}$). IR (KBr, cm^{-1}): 3436 (m, NH), 3070 (w, CH_{aryl}), 1523 (s, C=O), 1258 (s, CF_3). ^{1}H NMR (400 MHz, CD_3CN): δ (ppm) = - 4.25 (br, 4 H, NH), 1.58 (d, 24 H, $CH(CH_3)_2$), 2.40 (s, 12 H, CH_3), 3.13 (sept, 4 H, $CH(CH_3)_2$), 6.04 (m, 8 H, H_{cym}), 6.18 (m, 8 H, H_{cym}), 7.25 (br, 7 H, H_{phenyl}), 8.17 (m, 4 H, H_{pyr}), 8.35 (m, 3 H, H_{phenyl}), 8.48 (m, 4 H, H_{pyr}), 8.55 (d, 4 H, H_β), 8.90 (d, 4 H, H_α). $^{13}C(^1H)$ NMR (100 MHz, CD_3CN): δ (ppm) = 18.4 (CH_3), 22.7 ($CH(CH_3)_2$), 32.2 ($CH(CH_3)_2$), 83.1 (CH_{cym}), 84.9 (CH_{cym}), 98.5 (CCH_3), 103.6 ($CCH(CH_3)_2$), 115.5 (C_{pyr}), 132.1 (CH_{phenyl}), 132.4 (CH_{phenyl}), 133.0 (CH_β), 133.4 (CH_β), 142.7 (C_{phenyl}), 142.8 (C_{phenyl}), 151.1 (CH_α), 153.3 (CH_α), 171.9 (CO). ESI-MS: m/z 833.5 $[\mathbf{Q_{11}} + CF_3SO_3]^{3+}$, 587.9 $[\mathbf{Q_{11}}]^{4+}$. Anal. calc. for $C_{132}H_{112}N_{12}F_{12}O_{20}S_4Ru_4$ (2946.9): C 53.73, H 3.80, N 5.70; Found C 54.07, H 3.95, N 5.98.

Q_{12}: Yield 79 mg (86%). UV-vis (1.0×10^{-5} M, ($(CH_3)_2CO$)): λ_{max} 413 nm ($\varepsilon = 2.3 \times 10^5$ $M^{-1}\cdot cm^{-1}$), 521 nm ($\varepsilon = 0.23 \times 10^5$ $M^{-1}\cdot cm^{-1}$), 560 nm ($\varepsilon = 0.16 \times 10^5$ $M^{-1}\cdot cm^{-1}$), 599 nm ($\varepsilon = 0.11 \times 10^5$ $M^{-1}\cdot cm^{-1}$), 654 nm ($\varepsilon = 0.11 \times 10^5$ $M^{-1}\cdot cm^{-1}$). IR (KBr, cm^{-1}): 3446 (m, NH), 3066 (w, CH_{aryl}), 1631 (s, C=O), 1259 (s, CF_3). ^{1}H NMR (400 MHz, CD_3CN): δ (ppm) = - 3.50 (br, 4 H, NH), 1.55 (d, 24 H, $CH(CH_3)_2$), 2.39 (s, 12 H, CH_3), 3.07 (sept, 4 H, $CH(CH_3)_2$), 5.92 (d, 8 H, H_{cym}), 6.10 (s, 4 H, H_q), 6.13 (d, 8 H, H_{cym}), 7.25 (br, 7 H, H_{phenyl}), 8.10 (m, 4 H, H_{pyr}), 8.35 (m, 3 H, H_{phenyl}), 8.42 (m, 4 H, H_{pyr}), 8.58 (d, 4 H, H_β), 8.75 (d, 4 H, H_α). $^{13}C(^1H)$ NMR (100 MHz, CD_3CN): δ (ppm) = 18.5 (CH_3), 22.6 ($CH(CH_3)_2$), 32.3 ($CH(CH_3)_2$), 83.2 (CH_{cym}), 84.8 (CH_{cym}), 98.4 (CCH_3), 103.7 ($CCH(CH_3)_2$), 115.6 (C_{pyr}), 125.7 (CH_{phenyl}), 132.8 (CH_{phenyl}), 132.9 (CH_{phenyl}), 133.0 (CH_β), 133.1 (CH_β), 141.3 (C_{phenyl}), 141.4 (C_{phenyl}), 151.0 (CH_α), 153.3 (CH_α), 171.8 (CO). ESI-MS: m/z 866.8 $[\mathbf{Q_{12}} + CF_3SO_3]^{3+}$, 612.8 $[\mathbf{Q_{12}}]^{4+}$. Anal. calc. for $C_{140}H_{116}N_{12}F_{12}O_{20}S_4Ru_4$ (3047.0): C 55.12, H 3.80, N 5.51; Found: C 55.38, H 3.63, N 4.92.

Q_{13}: Yield 97 mg (85%). UV-vis (1.0×10^{-5} M, ($(CH_3)_2CO$)): λ_{max} 410 nm ($\varepsilon = 3.4 \times 10^5$ $M^{-1}\cdot cm^{-1}$), 522 nm ($\varepsilon = 0.23 \times 10^5$ $M^{-1}\cdot cm^{-1}$), 565 nm ($\varepsilon = 0.16 \times 10^5$ $M^{-1}\cdot cm^{-1}$), 602 nm ($\varepsilon = 0.12 \times 10^5$ $M^{-1}\cdot cm^{-1}$), 656 nm ($\varepsilon = 0.10 \times 10^5$ $M^{-1}\cdot cm^{-1}$). IR (KBr, cm^{-1}): 3467 (m, NH), 3069 (w, CH_{aryl}), 1631 (s, C=O), 1258 (s, CF_3). ^{1}H NMR (400 MHz, CD_3CN): δ (ppm) = - 6.94 (s, 4 H, NH), 1.54 (m, 36 H, $CH(CH_3)_2$), 2.42 (s, 18 H, CH_3), 3.14 (m, 6 H, $CH(CH_3)_2$), 6.22 to

6.26 (m, 12 H, H_{cym}), 6.36 to 6.42 (m, 12 H, H_{cym}), 7.32 (m, 1 H, H_{β}), 7.39 (m, 2 H, H_{phenyl}), 7.65 (m, 2 H, H_{phenyl}), 7.90 (m, 3 H, H_{pyr}), 7.99 (m, 4 H, H_{phenyl}), 8.10 (m, 2 H, H_{pyr}), 8.26 (m, 1 H, H_{α}), 8. 30 (m, 1 H, H_{phenyl}), 8.38 (d, 1 H, H_{β}), 8.40 (m, 1 H, H_{α}), 8.55 (m, 1 H, H_{α}), 8.78 (m, 1 H, H_{α}), 8.86 (m, 3 H, H_{pyr}), 8.95 (m, 1 H, H_{pyr}), 9.20 (m, 1 H, H_{pyr}), 9.42 (d, 1 H, H_{α}), 7.60 to 9.40 (br, 6 H, H_{pyr}, 1 H, H_{phenyl}, 7 H, H_{α}, 10 H, H_{β}). $^{13}C(^{1}H)$ NMR (100 MHz, CD_3CN): δ (ppm) = 19.1 (CH_3), 19.2 (CH_3), 19.2 (CH_3), 22.1 ($CH(\mathit{C}H_3)_2$), 22.5 ($CH(\mathit{C}H_3)_2$), 22.6 ($CH(\mathit{C}H_3)_2$), 32.0 ($\mathit{C}H(CH_3)_2$), 32.2 ($\mathit{C}H(CH_3)_2$), 32.2 ($\mathit{C}H(CH_3)_2$), 85.5 (CH_{cym}), 88.3 (CH_{cym}), 99.6 ($\mathit{C}CH_3$), 121.0 (C_{pyr}), 125.1 (CH_{phenyl}), 125.2 (CH_{phenyl}), 127.1 (CH_{β}), 128.5 (CH_{phenyl}), 128.7 (CH_{phenyl}), 128.9 (CH_{phenyl}), 129.7 (CH_{phenyl}), 142.2 (C_{phenyl}), 153.2 (CH_{α}), 153.3 (CH_{α}), 184.4 (CO), 184.5 (CO). ESI-MS: m/z 1119.8 [**Q$_{13}$** + $CF_3SO_3]^{3+}$, 802.3 [**Q$_{13}$** + $(CF_3SO_3)_2]^{4+}$. Anal. calc. for $C_{154}H_{136}N_{14}F_{18}O_{30}S_6Ru_6$ (3803.6): C 48.63, H 3.60, N 5.15; Found: C 48.27, H 3.29, N 5.02.

Q$_{14}$: Yield 98 mg (82%). UV-vis (1.0×10^{-5} M, ($(CH_3)_2CO$)): λ_{max} 409 nm ($\varepsilon = 3.6 \times 10^5$ $M^{-1}\cdot cm^{-1}$), 517 nm ($\varepsilon = 0.60 \times 10^5$ $M^{-1}\cdot cm^{-1}$), 560 nm ($\varepsilon = 0.14 \times 10^5$ $M^{-1}\cdot cm^{-1}$), 654 nm ($\varepsilon = 0.15 \times 10^5$ $M^{-1}\cdot cm^{-1}$). IR (KBr, cm^{-1}): 3434 (m, NH), 3059 (w, CH_{aryl}), 1522 (s, C=O), 1258 (s, CF_3). ^{1}H NMR (400 MHz, CD_3CN): δ (ppm) = - 6.96 (s, 2 H, NH), - 6.76 (m, 2 H, NH), 1.52 (m, 36 H, $CH(C\mathit{H}_3)_2$), 2.45 (m, 18 H, CH_3), 3.15 (m, 6 H, $C\mathit{H}(CH_3)_2$), 5.80 to 6.30 (m, 24 H, H_{cym}), 6.13 (s, 1 H, H_q), 6.14 (s, 1 H, H_q), 6.15 (s, 1 H, H_q), 6.16 (s, 1 H, H_q), 6.17 (s, 1 H, H_q), 6.18 (s, 1 H, H_q), 6.75 (m, 1 H, H_{pyr}), 7.12 (m, 1 H, H_{pyr}), 7.18 (m, 1 H, H_{β}), 7.32 (m, 1 H, H_{β}), 7.35 (m, 2 H, H_{phenyl}), 7.50 (m, 6 H, H_{β}), 7.65 (m, 2 H, H_{phenyl}), 7.78 (m, 4 H, H_{β}), 7.85 (m, 3 H, H_{pyr}), 7.98 (m, 4 H, H_{phenyl}), 8.05 (m, 1 H, H_{phenyl}), 8.10 (m, 2 H, H_{pyr}), 8.18 (m, 5 H, H_{pyr}), 8.22 (m, 1 H, H_{α}), 8.26 (m, 1 H, H_{α}), 8. 30 (m, 1 H, H_{phenyl}), 8.35 (m, 1 H, H_{α}), 8.42 (m, 1 H, H_{α}), 8.58 (m, 1 H, H_{α}), 8.60 (m, 1 H, H_{α}), 8.62 (m, 1 H, H_{α}), 8.70 (m, 1 H, H_{α}), 8.76 (m, 1 H, H_{α}), 8.77 (m, 1 H, H_{α}), 8.82 (m, 1 H, H_{α}), 8.85 (m, 3 H, H_{pyr}), 8.95 (m, 1 H, H_{α}), 9.00 (m, 1 H, H_{pyr}). $^{3}C(^{1}H)$ NMR (100 MHz, CD_3CN): δ (ppm) = 18.5 (CH_3), 18.5 (CH_3), 18.5 (CH_3), 18.6 (CH_3), 18.6 (CH_3), 18.7 (CH_3), 22.2 ($CH(\mathit{C}H_3)_2$), 22.5 ($CH(\mathit{C}H_3)_2$), 22.5 ($CH(\mathit{C}H_3)_2$), 22.5 ($CH(\mathit{C}H_3)_2$), 22.6 ($CH(\mathit{C}H_3)_2$), 22.6 ($CH(\mathit{C}H_3)_2$), 22.7 ($CH(\mathit{C}H_3)_2$), 22.8 ($CH(\mathit{C}H_3)_2$), 22.8 ($CH(\mathit{C}H_3)_2$), 22.9 ($CH(\mathit{C}H_3)_2$), 22.9 ($CH(\mathit{C}H_3)_2$), 22.9 ($CH(\mathit{C}H_3)_2$), 32.4 ($\mathit{C}H(CH_3)_2$), 32.4 ($\mathit{C}H(CH_3)_2$), 32.4 ($\mathit{C}H(CH_3)_2$), 32.4 ($\mathit{C}H(CH_3)_2$), 32.5 ($\mathit{C}H(CH_3)_2$), 32.5 ($\mathit{C}H(CH_3)_2$), 82.8 (CH_{cym}), 82.9 (CH_{cym}), 82.9 (CH_{cym}), 83.1 (CH_{cym}), 83.2 (CH_{cym}), 83.3 (CH_{cym}), 83.5 (CH_{cym}), 83.8 (CH_{cym}), 83.9 (CH_{cym}), 83.9 (CH_{cym}), 84.0 ($CH_{\mathit{p}\text{-}cym}$), 84.0 ($CH_{\mathit{p}\text{-}cym}$), 84.2 ($CH_{cym}$), 84.3 ($CH_{cym}$), 84.3 ($CH_{cym}$), 84.4 ($CH_{cym}$), 84.4 ($CH_{cym}$), 84.8 ($CH_{cym}$), 84.9 ($CH_{cym}$), 85.0 ($CH_{cym}$), 85.1 ($CH_{cym}$), 85.1 ($CH_{cym}$), 85.1 ($CH_{cym}$), 85.1 ($CH_{cym}$), 99.6

(*C*CH_3), 99.6 (*C*CH_3), 99.7 (*C*CH_3), 99.8 (*C*CH_3), 99.8 (*C*CH_3), 99.8 (*C*CH_3), 102.6 (CH_q), 102.8 (CH_q), 102.9 (CH_q), 103.0 (CH_q), 103.0 (CH_q), 103.1 (CH_q), 104.6 (*C*$CH(CH_3)_2$), 104.7 (*C*$CH(CH_3)_2$), 104.7 (*C*$CH(CH_3)_2$), 105.0 (*C*$CH(CH_3)_2$), 105.1 (*C*$CH(CH_3)_2$), 105.2 (*C*$CH(CH_3)_2$), (*C*$CH(CH_3)_2$), 122.1 (C_{pyr}), 122.4 (C_{pyr}), 122.6 (C_{pyr}), 122.9 (C_{pyr}), 125.4 (CH_{phenyl}), 125.5 (CH_{phenyl}), 127.0 (CH_β), 127.2 (CH_β), 127.9 (CH_β), 128.3 (CH_β), 128.6 (CH_{phenyl}), 128.6 (CH_{phenyl}), 128.6 (CH_{phenyl}), 128.7 (CH_{phenyl}), 129.4 (CH_β), 129.7 (CH_{phenyl}), 129.8 (CH_{phenyl}), 129.9 (CH_β), 131.9 (CH_β), 132.0 (CH_β), 132.4 (CH_{phenyl}), 132.4 (CH_{phenyl}), 132.5 (CH_β), 133.4 (CH_β), 135.5 (CH_β), 136.0 (CH_β), 141.3 (C_{phenyl}), 141.8 (C_{phenyl}), 150.2 (CH_α), 150.7 (CH_α), 150.9 (CH_α), 151.4 (CH_α), 151.6 (CH_α), 151.8 (CH_α), 152.1 (CH_α), 152.4 (CH_α), 152.8 (CH_α), 152.9 (CH_α), 153.3 (CH_α), 153.5 (CH_α), 184.4 (CO), 184.5 (CO), 184.6 (CO), 184.6 (CO), 184.7 (CO), 184.7 (CO). ESI-MS: m/z 1169.5 [$\mathbf{Q_{14}}$ + CF_3SO_3]$^{3+}$, 839.9 [$\mathbf{Q_{14}}$ + CF_3SO_3]$^{3+}$. Anal. calc. for $C_{166}H_{142}N_{14}F_{18}O_{30}S_6Ru_6$ (3953.8): C 50.42, H 3.62, N 4.96; Found: C 50.27, H 3.23, N 4.52.

Chapter 7: References

1. N. V. Pitchkov, *Platinum Met. Rev.* **1996**, *40*, 181-188.
2. N. N. Greenwood and A. Earnshaw, *Chemistry of the elements*. Pergamon: Oxford, **1984**; 1242-1289.
3. D. D. Pathak, A. T. Hutton, J. Hyde, A. Walkden and C. White, *J. Organomet. Chem.* **2000**, *606*, 188-196.
4. C. Li, W. K. Leong and Z. Zhong, *J. Organomet. Chem.* **2009**, *694*, 2315-2318.
5. M. I. Bruce, *Comprehensive Organometallic Chemistry II*. E. W. Abel; F. G. A. Stone; G. Wilkinson; Pergamon: Oxford, **1995**; Vol. 7, 291-298.
6. (a) P. B. Arockiam, C. Fischmeister, C. Bruneau and P. H. Dixneuf, *Angew. Chem. Int. Ed.* **2010**, *49*, 6629-6632; (b) C. Bruneau and P. H. Dixneuf, *Acc. Chem. Res.* **1999**, *32*, 311-323; (c) C. V.-L. Bray, S. Derien and P. H. Dixneuf, *C. R. Chim.* **2010**, *13*, 293-303.
7. IUPAC, *Compendium of Chemical Terminology, 2nd ed.*; A. Wilkinson; A. D. McNaught; Blackwell Scientific Publications: Oxford, **1997**; 1318-1319.
8. W. D. Harman and P. A. Lay, *Recent Advances in Osmium Chemistry*. A. G. Sykes; Academic Press, Inc: San Diego, **1991**; Vol. 37, 201-237.
9. D. Astruc, *Chimie organométallique*. EDP Sciences: Les Ulis, **2000**; 31-54.
10. W. D. Harman, *Chem. Rev.* **1997**, *97*, 1953-1978.
11. B. Therrien, *Coord. Chem. Rev.* **2009**, *253*, 493-519.
12. G. Winkhaus and H. Singer, *J. Organomet. Chem.* **1967**, *7*, 487-491.
13. R. A. Zelonka and M. C. Baird, *Can. J. Chem.* **1972**, *50*, 3063-3072.
14. J. W. Kang, K. Moseley and P. M. Maitlis, *J. Am. Chem. Soc.* **1969**, *91*, 5970-5977.
15. M. A. Bennett and A. K. Smith, *J. Chem. Soc., Dalton Trans.* **1974**, 233-241.
16. M. A. Bennett, T. N. Huang, T. W. Matheson and A. K. Smith, *Inorg. Synth.* **1982**, *21*, 74-76.
17. (a) B. Therrien, T. R. Ward, M. Pilkington, C. Hoffmann, F. Gilardoni and J. Weber, *Organometallics* **1998**, *17*, 330-337; (b) P. Pinto, G. Marconi, F. W. Heinemann and U. Zenneck, *Organometallics* **2004**, *23*, 374-380.
18. P. S. Engel, R. L. Allgren, W.-K. Chae, R. A. Leckonby and N. A. Marron, *J. Org. Chem.* **1979**, *44*, 4233-4239.
19. B. Therrien and G. Süss-Fink, *Inorg. Chim. Acta* **2006**, *359*, 4350-4354.
20. J.-M. Lehn, *Science* **1993**, *260*, 1762-1763.
21. J.-P Sauvage and M. W. Hosseini, *Comprehensive Supramolecular Chemistry*. J. L. Atwood; J. E. D. Davies; D. D. MacNicol; F. Vögtle; Pergamon: Oxford, **1996**; Vol. 9, 507-528.
22. J. S. Lindsey, *New J. Chem.* **1991**, *15*, 153-180.
23. J. D. Watson and F. H. C. Crick, *Nature* **1953**, *171*, 737-738.

24. J.-M. Lehn, *Angew. Chem.* **1988**, *100*, 91-116.
25. J.-M. Lehn, *Angew. Chem. Int. Ed. Engl.* **1990**, *29*, 1304-1319.
26. D. Amabilino and J. F. Stoddart, *New Scientist* **1994**, *141*, 25-29.
27. D. S. Lawrence, T. Jiang and M. Levett, *Chem. Rev.* **1995**, *95*, 2229-2260.
28. G. R. Desiraju, *The Crystal as a Supramolecular Entity*. Wiley: Chichester, **1996**; 1-325.
29. B. Donnio, S. Buathong, I. Bury and D. Guillon, *Chem. Soc. Rev.* **2007**, *36*, 1495-1513.
30. S. Khalid, P. J. Bond, J. Holyoake, R. W. Hawtin and M. S. P. Sansom, *J. R. Soc. Interface* **2008**, *5*, S241-S250.
31. E. Joselevich, *Nano Res.* **2009**, *2*, 743-754.
32. B. H. Northrop, H.-B. Yang and P. J. Stang, *Chem. Commun.* **2008**, 5896-5908.
33. S. Leininger, B. Olenyuk and P. J. Stang, *Chem. Rev.* **2000**, *100*, 853-907.
34. M. Fujita, M.Tominaga, A. Hori and B. Therrien, *Acc. Chem. Res.* **2005**, *38*, 369-378.
35. S. R. Seidel and P. J. Stang, *Acc. Chem. Res.* **2002**, *35*, 972-983.
36. D. L. Caulder and K. N. Raymond, *Acc. Chem. Res.* **1999**, *32*, 975-982.
37. B. J. Holliday and C. A. Mirkin, *Angew. Chem. Int. Ed.* **2001**, *40*, 2022-2043.
38. M. Fujita and M. Yoshizawa, *Modern Supramolecular Chemistry: Strategies for Macrocycle Synthesis*. P. S. F. Diederich, R. R. Tykwinski,; Wiley-VCH: Verlag, **2008**; 277-309.
39. D. J. Cram and J. M. Cram, *Acc. Chem. Res.* **1978**, *11*, 8-14.
40. D. J. Cram and J. M. Cram, *Science* **1974**, *183*, 803-809.
41. C. J. Pedersen, *J. Am. Chem. Soc.* **1967**, *89*, 7017-7036.
42. J. R. Moran, S. Karbach and D. J. Cram, *J. Am. Chem. Soc.* **1982**, *104*, 5826-5828.
43. C. D. Gutsche, *Calixarenes, An Introduction*. The Royal Society of Chemistry Publishing: Cambridge, **2008**; 1-24.
44. D. J. Cram, *Science* **1983**, *219*, 1177-1183.
45. R. G. Harvey, *Polycyclic Aromatic Hydrocarbons*. Wiley-VCH: New York, **1997**; 96-111.
46. E. Clar, *The Aromatic Sextet*. J. Wiley & Sons: Chichester, **1972**; 57-77.
47. J. R. Platt, *J. Chem. Phys.* **1954**, *22*, 1448-1455.
48. M. Randić, *Chem. Phys. Lett.* **1976**, *38*, 68-70.
49. M. Randić, *Chem. Rev.* **2003**, *103*, 3449-3605.
50. D. P. Lydon, P. Li, A. C. Benniston, W. McFarlane, R. W. Harrington and W. Clegg, *Eur. J. Org. Chem.* **2007**, 1653-1658.
51. J. B. Birks, *Photophysics of Aromatic Molecules*. Wiley-Interscience: London, **1970**; 1-100.
52. E. A. Mangle and M. R. Topp, *J. Phys. Chem* **1986**, *90*, 802-807.
53. K. M. Matkovich, L. M. Thorne, M. O. Wolf, T. C. S. Pace, C. Bohne and B. O. Patrick, *Inorg. Chem.* **2006**, *45*, 4610-4618.
54. T. Shyamala, S. Sankararaman and A. K. Mishra, *Chem. Phys.* **2006**, *330*, 467-477.

55. S. M. Borisov and O. S. Wolfbeis, *Chem. Rev.* **2008**, *108*, 423-461.
56. S. Ugur, O. Yargi and O. Pekcan, *Polym. Compos.* **2010**, *31*, 77-82.
57. D. Dumas, V. Latger, M.-L. Viriot, W. Blondel and J.-F. Stoltz, *Clin. Hemorheol. Micro.* **1999**, *21*, 255-261.
58. (a) E. G. Mik, J. Stap, M. Sinaaseppel, J. F. Beek, J. A. Aten, T. G. van Leeuwen and C. Ince, *Nat. Methods* **2006**, *3*, 939-945; (b) T. C. O'Riordan, K. Fitzgerald, G. V. Ponomarev, J. Mackrill, J. Hynes and C. Taylor, *Am. J. Physiol. Regul. Integr. Comp. Physiol.* **2007**, *292*, 1613-1620.
59. A. W. Maverick, S. C. Buckingham, Q. Yao, J. R. Bradbury and G. G. Stanley, *J. Am. Chem. Soc.* **1986**, *108*, 7430-7431.
60. M. Fujita, J. Yazaki and K. Ogura, *J. Am. Chem. Soc.* **1990**, *112*, 5645-5647.
61. M. Fujita, D. Ogura, M. Miyazawa, H. Oka, K. Yamaguchi and K. Ogura, *Nature* **1995**, *378*, 469-471.
62. T. Beissel, R. E. Powers and K. N. Raymond, *Angew. Chem. Int. Ed.* **1996**, *35*, 1084-1086.
63. (a) R. V. Slone, K. D. Benkstein, S. Bélanger, J. T. Hupp, I. A. Guzei and A. L. Rheingold, *Coord. Chem. Rev.* **1998**, *171*, 221-243; (b) R. V. Slone, D. I. Yoon, R. M. Calhoun and J. T. Hupp, *J. Am. Chem. Soc.* **1995**, *117*, 11813-11814.
64. (a) B. H. Northrop, Y.-R. Zheng, K.-W. Chi and P. J. Stang, *Acc. Chem. Res.* **2009**, *42*, 1554-1563; (b) P. J. Stang, *Chem. Eur. J.* **1998**, *4*, 19-27.
65. B. Therrien, *Eur. J. Inorg. Chem.* **2009**, 2445-2453.
66. K. Severin, *Chem. Commun.* **2006**, 3859-3867.
67. (a) S. Korn and W. S. Sheldrick, *J. Chem. Soc., Dalton Trans.* **1997**, 2191-2199; (b) S. Korn and W. S. Sheldrick, *Inorg. Chim. Acta* **1997**, *254*, 85-91; (c) P. Annen, S. Schildberg and W. S. Sheldrick, *Inorg. Chim. Acta* **2000**, *307*, 115-124.
68. (a) H. Piotrowski, K. Polborn, G. Hilt and K. Severin, *J. Am. Chem. Soc.* **2001**, *123*, 2699-2700; (b) H. Piotrowski, G. Hilt, A. Schulz, P. Mayer, K. Polborn and K. Severin, *Chem. Eur. J.* **2001**, *7*, 3196-3208; (c) S. Mirtschin, A. Slabon-Turski, R. Scopelliti, A. H. Velders and K. Severin, *J. Am. Chem. Soc.* **2010**, *132*, 14004-14005.
69. (a) R. H. Fish and G. Jaouen, *Organometallics* **2003**, *22*, 2166-2177; (b) R. H. Fish, *Coord. Chem. Rev.* **1999**, *185-186*, 569-584; (c) S. Ogo, S. Nakamura, H. Chen, K. Isobe, Y. Watanabe and R. H. Fish, *J. Org. Chem.* **1998**, *63*, 7151-7156; (d) H. Chen, S. Ogo and R. H. Fish, *J. Am. Chem. Soc.* **1996**, *118*, 4993-5001.
70. K. K. Klausmeyer, T. B. Rauchfuss and S. R. Wilson, *Angew. Chem. Int. Ed.* **1998**, *37*, 1694-1696.

71. (a) K. Yamanari, R. Ito, S. Yamamoto, T. Konno, A. Fuyuhiro, M. Kobayashi and R. Arakawa, *Dalton Trans.* **2003**, 380-386; (b) K. Yamanari, S. Yamamoto, R. Ito, Y. Kushi, A. Fuyuhiro, N. Kubota, T. Fukuo and R. Arakawa, *Angew. Chem. Int. Ed.* **2001**, *40*, 2268-2271.
72. B. Therrien, G. Süss-Fink, P. Govindaswamy, A. K. Renfrew and P. J. Dyson, *Angew. Chem. Int. Ed.* **2008**, *47*, 3773-3776.
73. J. Mattsson, P. Govindaswamy, J. Furrer, Y. Sei, K. Yamaguchi, G. Süss-Fink and B. Therrien, *Organometallics* **2008**, *27*, 4346-4356.
74. Z. Huaizhi and N. Yuantao, *Gold Bulletin* **2001**, *34*, 24-29.
75. J. R. Glauber, *La teinture de l'or ou le véritable or potable*. Thomas Jolly: **1659**; 1-22.
76. P. Charlier, J. Poupon, I. Huynh-Charlier, J.-F. Saliege, D. Favier, C. Keyser and B. Ludes, *BMJ* **2009**, *339*, 1402-1403.
77. L. Pearce and W. H. Brown, *J. Pharmacol.* **1917**, *9*, 354-355.
78. B. Rosenberg, L. van Camp and T. Krigas, *Nature* **1965**, *205*, 698-699.
79. B. Rosenberg, *Cancer* **1985**, *53*, 2303-2314.
80. R. C. Todd and S. J. Lippard, *Metallomics* **2009**, *1*, 280-291.
81. J. Reedijk, *Proc. Nat. Acad. Sci. U.S.A.* **2003**, *100*, 3611-3616.
82. N. Farrell, *Coord. Chem. Rev.* **2002**, *232*, 1-4.
83. B. Lippert, *Coord. Chem. Rev.* **1999**, *182*, 263-295.
84. Y. Chen, Z. Guo and P. J. Sadler, *Cisplatin* **1999**, 293-318.
85. J. M. Rademaker-Lakhai, C. Mirjam, P. Dick, R. W. Sparidans, P. Baas, J. H. Beijnen, N. van Zandwijk and J. H. M. Schellens, *Anti-cancer drugs* **2005**, *16*, 1029-1036.
86. C. J. Jones and J. R. Thornback, *Medicinal Applications of Coordination Chemistry*. RSC Publishing: Cambridge, **2007**; 1-14.
87. M. J. Clarke, *Metal Complexes in Cancer Chemotherapy*. B. K. Keppler; J. Wiley & Sons: Chichester, **1993**; 152-156.
88. G. Sava, *Metal Compounds in Cancer Therapy*. S. P. Fricker; Chapman & Hall: London, **1994**; Vol. 1, 65-91.
89. J. C. Dabrowiak, *Metals in Medicine*. J. Wiley & Sons: Chichester, **2009**; 149-212.
90. (a) A. Bergamo and G. Sava, *Dalton Trans.* **2007**, 1267-1272; (b) C. G. Hartinger, M. A. Jakupec, S. Zorbas-Seifried, M. Groessl, A. Egger, W. Berger, H. Zorbas, P. J. Dyson and B. K. Keppler, *Chem. Biodiversity* **2008**, *5*, 2140-2155.
91. G. Sava, S. Pacor, A. Bergamo, M. Cocchietto, G. Mestroni and E. Alessio, *Chem. Biol. Interact.* **1995**, *95*, 109-126.
92. A. V. Vargiu, A. Robertazzi, A. Magistrato, P. Ruggerone and P. Carloni, *J. Phys. Chem. B* **2008**, *112*, 4401-4409.

93. E. Reisner, V. B. Arion, B. K. Keppler and A. J. L. Pombeiro, *Inorg. Chim. Acta* **2008**, *361*, 1569-1583.

94. M. Brindell, D. Piotrowska, A. A. Shoukry, G. Stochel and R. Eldik, *J. Biol. Inorg. Chem.* **2007**, *12*, 809-818.

95. (a) W. H. Ang and P. J. Dyson, *Eur. J. Inorg. Chem.* **2006**, 4003-4018; (b) P. J. Dyson, *Chimia* **2007**, *61*, 698-703; (c) A. Renfrew, *Chimia* **2009**, *63*, 217-219; (d) C. S. Allardyce, P. J. Dyson, D. J. Ellis and S. L. Heath, *Chem. Commun.* **2001**, 1396-1397.

96. (a) A. F. A. Peacock and P. J. Sadler, *Chem.-Asian J.* **2008**, *3*, 1890-1899; (b) S. J. Dougan and P. J. Sadler, *Chimia* **2007**, *61*, 704-715; (c) Y. K. Yan, M. Melchart, A. Habtemariam and P. J. Sadler, *Chem. Commun.* **2005**, 4764-4776; (d) R. E. Morris, R. E. Aird, P. d. S. Murdoch, H. Chen, J. Cummings, N. D. Hughes, S. Pearsons, A. Parkin, G. Boyd, D. I. Jodrell and P. J. Sadler, *J. Med. Chem.* **2001**, *44*, 3616-3621.

97. F. Wang, H. Chen, S. Parsons, I. D. H. Oswald, J. E. Davidson and P. J. Sadler, *Chem. Eur. J.* **2003**, 5810-5820.

98. P. J. Dyson and G. Sava, *Dalton Trans.* **2006**, 1929-1933.

99. C. Scolaro, C. G. Hartinger, C. S. Allardyce, B. K. Keppler and P. J. Dyson, *J. Inorg. Biochem.* **2008**, *102*, 1743-1748.

100. H. Chen, J. A. Parkinson, R. E. Morris and P. J. Sadler, *J. Am. Chem. Soc.* **2003**, *125*, 173-186.

101. C. A. Lipinski, F. Lombardo, B. W. Dominy and P. J. Feeney, *Adv. Drug Delivery Rev.* **1997**, *23*, 3-25.

102. Y. Matsumura and H. Maeda, *Cancer Res.* **1986**, *46*, 6387-6392.

103. (a) K. Iwai, H. Maeda and T. Konno, *Cancer Res.* **1984**, *44*, 2115-2121; (b) K. Iwai, H. Maeda, T. Konno, Y. Matsumura, R. Yamashita, K. Yamasaki, S. Hirayama and Y. Miyauchi, *Anticancer Res.* **1987**, *7*, 321-328; (c) T. Konno, H. Maeda, K. Iwai, S. Maki, S. Tashiro, M. Uchida and Y. Miyauchi, *Cancer* **1984**, *54*, 2367-2374; (d) S. Maki, T. Konno and H. Maeda, *Cancer* **1985**, *56*, 751-757; (e) T. Konno, H. Maeda, K. Iwai, S. Tashiro, S. Maki, T. Morinaga, M. Mochinaga, T. Hiraoka and I. Yokoyama, *Eur. J. Cancer Clin. Oncol.* **1983**, *19*, 1053-1065.

104. H. Maeda, *Advan. Enzyme Regul.* **2001**, *41*, 189-207.

105. J. Fang, H. Nakamura and A. K. Iyer, *J. Drug. Targeting* **2007**, *15*, 475-486.

106. M. Yokoyama, T. Okano, Y. Sakurai and K. Kataoka, *J. Controlled Release* **1994**, *32*, 269-277.

107. R. Duncan, *Adv. Drug Delivery Rev.* **2009**, *61*, 1131-1148.

108. S. Zalipsky, M. Saad, R. Kiwan, E. Ber, N. Yu and T. Minko, *J. Drug. Targeting* **2007**, *15*, 518-530.

109. M. Zhao, M. Yang, H. Ma, X. Li, X. Tan, S. Li, Z. Yang and R. M. Hoffman, *Cancer Res.* **2006**, *66*, 7647-7652.

110. J. Mattsson, P. Govindaswamy, A. K. Renfrew, P. J. Dyson, P. Štěpnička, G. Süss-Fink and B. Therrien, *Organometallics* **2009**, *28*, 4350-4357.

111. Y.-F. Han, W.-G. Jia, Y.-J. Lin and G.-X. Jin, *Organometallics* **2008**, *27*, 5002-5008.

112. F. Linares, M. A. Galindo, S. Galli, M. A. Romero, J. A. R. Navarro and E. Barea, *Inorg. Chem.* **2009**, *48*, 7413-7420.

113. P. Govindaswamy, G. Süss-Fink and B. Therrien, *Organometallics* **2007**, *26*, 915-924.

114. P. Govindaswamy, D. Linder, J. Lacour, G. Süss-Fink and B. Therrien, *Chem. Commun.* **2006**, 4691-4693.

115. J. Mattsson, O. Zava, A. K. Renfrew, Y. Sei, K. Yamaguchi, P. J. Dyson and B. Therrien, *Dalton Trans.* **2010**, *39*, 8248-8255.

116. O. Zava, J. Mattsson, B. Therrien and P. J. Dyson, *Chem. Eur. J.* **2010**, *16*, 1428-1431.

117. (a) A. K. Holzer, K. Katano, L. W. Klomp and S. B. Howell, *Clin. Cancer Res.* **2004**, *10*, 6744-6749; (b) G. V. Kalayda, C. H. Wagner, I. Buss, J. Reedijk and U. Jaehde, *BMC Cancer* **2008**, *8*, 175-187.

118. M. D. Hall, M. Okabe, D. W. Shen, X. J. Liang and M. M. Gottesman, *Annu. Rev. Pharmacol. Toxicol.* **2008**, *48*, 495-535.

119. P. D. Dobson and D. B. Kell, *Nat. Rev. Drug Discovery* **2008**, *7*, 205-220.

120. H. Yan, G. Süss-Fink, A. Neels and H. Stoeckli-Evans, *J. Chem. Soc., Dalton Trans.* **1997**, 4345-4350.

121. W.-Z. Zhang, Y.-F. Han, Y.-J. Lin and G.-X. Jin, *Dalton Trans.* **2009**, 8426-8431.

122. Y.-F. Han, H. Li and G.-X. Jin, *Chem. Commun.* **2010**, *46*, 6879-6890.

123. F. Linares, E. Q. Procopio, M. A. Galindo, M. A. Romero, J. A. R. Navarro and E. Barea, *Cryst. Eng. Comm.* **2010**, *12*, 2343-2346.

124. Y.-F. Han, W.-G. Jia, Y.-J. Lin and G.-X. Jin, *Angew. Chem. Int. Ed.* **2009**, *48*, 6234-6238.

125. (a) J. Moussa, M. N. Rager, L. M. Chamoreau, L. Ricard and H. Amouri, *Organometallics* **2009**, *28*, 397-404; (b) J.-P. Taquet, O. Siri, P. Braunstein and R. Welter, *Inorg. Chem.* **2004**, *43*, 6944-6953.

126. A. B. P. Lever and S. I. Gorelsky, *Coord. Chem. Rev.* **2000**, *208*, 153-167.

127. S. Berger, P. Hertl and A. Rieker, *Chem. Quinonoid Compd.* **1988**, 29-86.

128. S. M. Carter, A. Sia, M. J. Shaw and A. F. Heyduk, *J. Am. Chem. Soc.* **2008**, *130*, 5838-5839.

129. (a) A. Dei, D. Gatteschi and L. Pardi, *Inorg. Chem.* **1990**, *29*, 1442-1444; (b) M. R. Churchill, K. M. Keil, F. V. Bright, S. Pandey, G. A. Baker and J. B. Keister, *Inorg. Chem.* **2000**, *39*, 5807-5816.

130. S. Ghumaan, S. Mukherjee, S. Kar, D. Roy, S. M. Mobin, R. B. Sunoj and G. K. Lahiri, *Eur. J. Inorg. Chem.* **2006**, 4426-4441.
131. F. Kühlwein, K. Polborn and W. Z. Beck, *Anorg. Allg. Chem.* **1997**, *623*, 1931-1944.
132. D. H. Wu, A. Chen and C. S. Johnson, *J. Magn. Reson. A.* **1995**, *115*, 123-126.
133. (a) Y. Kikuchi, Y. Kato, Y. Tanaka, H. Toi and Y. Aoyama, *J. Am. Chem. Soc.* **1991**, *113*, 1349-1354; (b) L. Fielding, *Tetrahedron* **2000**, *56*, 6151-6170.
134. M. J. Hynes, *J. Chem. Soc., Dalton Trans.* **1993**, 311-312.
135. C. Chotimarkorn, N. R, H. Ushio, T. Ohshima and S. Matsunaga, *Biochem. Biophys. Res. Commun.* **2005**, *338*, 1222-1228.
136. A. Morandeira, A. Fuerstenberg and E. Vauthey, *J. Phys. Chem. A* **2004**, *108*, 8190-8200.
137. C.Wu, Y. Zheng, C. Szymanski and J. McNeill, *J. Phys. Chem. C* **2008**, *112*, 1772-1781.
138. N. Bouquin, V. L. Malinovskii and R. Häner, *Chem. Commun.* **2008**, 1974-1976.
139. N. P. E. Barry, J. Furrer and B. Therrien, *Helv. Chim. Acta* **2010**, *93*, 1313-1328.
140. N. P. E. Barry, J. Furrer, J. Freudenreich, G. Süss-Fink and B. Therrien, *Eur. J. Inorg. Chem.* **2010**, 725-728.
141. J. Kostova, *Curr. Med. Chem.* **2006**, *13*, 1085-1107.
142. G. Süss-Fink, *Dalton Trans.* **2010**, *39*, 1673-1688.
143. A. Pitto-Barry, N. P. E. Barry, O. Zava, R. Deschenaux and B. Therrien, *submitted.*
144. W. Sun, H. Zhu and P. M. Barron, *Chem. Mater.* **2006**, *18*, 2602-2610.
145. I. Mathew, Y. Li, Z. Li and W. Sun, *Dalton Trans.* **2010**, *39*, 11201-11209.
146. J. Freudenreich, J. Furrer, G. Süss-Fink and B. Therrien, *Organometallics* **2011**, 10.1021/om100920v.
147. K.-I. Yamashita, K.-I. Sato, M. Kawano and M. Fujita, *New J. Chem.* **2009**, *33*, 264-270.
148. J. Ruiz, J. Lorenzo, C. Vicente, G. Lopez, J. L. d. Luzuriaga, M. Monge, F. X. Aviles, D. Bautista, V. Moreno and A. Laguna, *Inorg. Chem.* **2008**, *47*, 6990-7001.
149. D. Braga and F. Grepioni, *Angew. Chem., Int. Ed.* **2004**, *43*, 4002-4011.
150. L. R. MacGillivray, G. S. Papaefstathiou, T. Friščić, T. D. Hamilton, D.-K. Bučar, Q. Chu, D. B. Varshney and I. G. Georgiev, *Acc. Chem. Res.* **2008**, *41*, 280-291.
151. W.-Z. Zhang, Y.-F. Han, Y.-J. Lin and G.-X. Jin, *Organometallics* **2010**, *29*, 2842-2849.
152. M. Nagarathinam and J. J. Vittal, *Angew. Chem. Int. Ed.* **2006**, *45*, 4337-4341.
153. Q. Chu, D. C. Swenson and L. R. MacGillivray, *Angew. Chem. Int. Ed.* **2005**, *44*, 3569-3572.
154. D. M. Bassani, V. Darcos, S. Mahony and J.-P. Desvergne, *J. Am. Chem. Soc.* **2000**, *122*, 8795-8796.
155. Y.-F. Han, Y.-J. Lin, W.-G. Jia, G.-L. Wang and G.-X. Jin, *Chem. Commun.* **2008**, 1807-1809.
156. L. Hwang and A. J. Shaka, *J. Magn. Reson.* **1998**, *135*, 280-287.
157. D. H. Johnston and D. F. Shriver, *Inorg. Chem.* **1993**, *32* 1045-1047.

158. T. Katsumoto, *Bull. Chem. Soc. J.* **1960**, *33* 1376-1379.

159. C. J. Kuehl, S. D. Huang and P. J. Stang, *J. Am. Chem. Soc.* **2001**, *123*, 9634-9641.

160. J. Vansant, S. Toppet, G. Smets, J. P. Declercq, G. Germain and M. V. Meerssche, *J. Org. Chem.* **1980**, *45* 1565-1573.

161. N. P. E. Barry and B. Therrien, *Inorg. Chem. Commun.* **2009**, *12*, 465-468.

162. C. A. Schalley and J. Rebek-Jr, *Stimulating Concepts in Chemistry*. W. Wiley-VCH; **2000**; 199-200.

163. C. J. Kuehl, Y. K. Kryschenko, U. Radhakrishnan, S. R. Seidel, S. D. Huang and P. J. Stang, *Proc. Natl. Acad. Sci. U.S.A.* **2002**, *99*, 4932-4936.

164. T. Kusukawa and M. Fujita, *Angew. Chem., Int. Ed.* **1998**, *37*, 3142-3144.

165. (a) J. Lacour, C. Ginglinger, C. Grivet and G. Bernardinelli, *Angew. Chem. Int. Ed. Engl.* **1997**, *36*, 608-609; (b) F. Favarger, C. Goujon-Ginglinger, D. Monchaud and J. Lacour, *J. Org. Chem.* **2004**, *69*, 8521-8524.

166. (a) P. Govindaswamy, D. Linder, J. Lacour, G. Süss-Fink and B. Therrien, *Dalton Trans.* **2007**, 4457-4463; (b) B. Therrien and G. Süss-Fink, *Chimia* **2008**, *62*, 514-518.

167. N. P. E. Barry and B. Therrien, *Eur. J. Inorg. Chem.* **2009**, 4695-4700.

168. J. Freudenreich, N. P. E. Barry, G. Süss-Fink and B. Therrien, *Eur. J. Inorg. Chem.* **2010**, 2400-2405.

169. (a) W. M. Nau, *Nat. Chem.* **2010**, *2*, 248-250; (b) K. K. Cotí, M. E. Belowich, M. Liong, M. W. Ambrogio, Y. A. Lau, H. A. Khatib, J. I. Zink, N. M. Khashab and J. F. Stoddart, *Nanoscale* **2009**, *1*, 16-39; (c) G. Wenz, *Clin. Drug Invest.* **2000**, *19*, 21-25.

170. (a) M. Vallet-Regí, F. Balas and D. Arcos, *Angew. Chem. Int. Ed.* **2007**, *46*, 7548-7558; (b) E. Gabano, M. Ravera and D. Osella, *Curr. Med. Chem.* **2009**, *16*, 4544-4580.

171. (a) S. H. v. Rijt and P. J. Sadler, *Drug Discovery Today* **2009**, *14*, 1089-1097; (b) C. Sanchez-Cano and M. J. Hannon, *Dalton Trans.* **2009**, 10702-10711.

172. (a) T. Boulikas and M. Vougiouka, *Oncol. Rep.* **2003**, *10*, 1663-1682; (b) K. S. Lovejoy and S. J. Lippard, *Dalton Trans.* **2009**, 10651-10659.

173. N. W. S. Kam, T. C. Jessop, P. A. Wender and H. Dai, *J. Am. Chem. Soc.* **2004**, *126*, 6850-6851.

174. Z. Yang, X. Wang, H. Diao, J. Zhang, H. Li, H. Sun and Z. Guo, *Chem. Commun.* **2007**, 3453-3455.

175. (a) A. M. Krause-Heuer, N. J. Wheate, M. J. Tilby, D. G. Pearson, C. J. Ottley and J. R. Aldrich-Wright, *Inorg. Chem.* **2008**, *47*, 6880-6888; (b) N. J. Wheate, A. I. Day, R. J. Blanch, A. P. Arnold, C. Cullinane and J. G. Collins, *Chem. Commun.* **2004**, 1424-1425.

176. (a) J. M. Rademaker-Lakhai, C. Terret, S. B. Howell, C. M. Baud, R. F. d. Boer, D. Pluim, J. H. Beijnen, J. H. M. Schellens and J. P. Droz, *Clin. Cancer Res.* **2004**, *10*, 3386-3395; (b) M.

Campone, J. M. Rademaker-Lakhai, J. Bennouna, S. B. Howell, D. P. Nowotnik, J. H. Beijnen and J. H. M. Schellens, *Cancer Chemother. Pharmacol.* **2007**, *60*, 523-533; (c) P. Govender, N. C. Antonels, J. Mattsson, A. K. Renfrew, P. J. Dyson, J. R. Moss, B. Therrien and G. S. Smith, *J. Organomet. Chem.* **2009**, *694*, 3470-3476.

177. P. Govindaswamy, J. Furrer, G. Süss-Fink and B. Therrien, *Z. Anorg. Allg. Chem.* **2008**, *634*, 1349-1352.
178. *Hyperchem Computational Chemistry Software Package Version 7.5, Hypercube Inc.,Gainesville, Florida* **2003**.
179. (a) R. Kjeken, S. A. Mousavi, A. Brech, G. Griffiths and T. Berg, *Biochem. J.* **2001**, *357*, 497-503; (b) S. Falcone, E. Cocucci, P. Podini, T. Kirchhausen, E. Clementi and J. Meldolesi, *J. Cell Sci.* **2006**, *119*, 4758-4769.
180. C. A. Puckett and J. K. Barton, *J. Am. Chem. Soc.* **2009**, *131*, 8738-8739.
181. W. I. Lencer, P. Weyer, A. S. Verkman, D. A. Ausiello and D. Brown, *Am. J. Physiol.* **1990**, *258*, C309-C317.
182. N. P. E. Barry, O. Zava, P. J. Dyson and B. Therrien, *Chem. Eur. J.* **2011**, *submitted*.
183. D. Astruc, E. Boisselier and C. Ornelas, *Chem. Rev.* **2010**, *110*, 1857-1959.
184. A. W. Bosman, H. M. Janssen and E. W. Meijer, *Chem. Rev.* **1999**, *99*, 1665-1688.
185. G. R. Newkome, Z. Yao, G. R. Baker and V. K. Gupta, *J. Org. Chem.* **1985**, *50*, 2003-2004.
186. D. A. Tomalia, *Prog. Polym. Sci.* **2005**, *30*, 294-324.
187. C. J. Hawker and J. M. J. Frechet, *J. Am. Chem. Soc.* **1990**, *112*, 7638-7647.
188. (a) S. Campidelli, P. Bourgun, B. Guintchin, J. Furrer, H. Stoeckli-Evans, I. M. Saez, J. W. Goodby and R. Deschenaux, *J. Am. Chem. Soc.* **2010**, *132*, 3574-3581; (b) V. Percec, M. Peterca, Y. Tsuda, B. M. Rosen, S. Uchida, M. R. Imam, G. Ungar and P. A. Heiney, *Chem. Eur. J.* **2009**, *15*, 8994-9004.
189. G. R. Newkome, E. He and C. N. Moorefield, *Chem. Rev.* **1999**, *99*, 1689-1746.
190. M. A. Mintzer and M. W. Grinstaff, *Chem. Soc. Rev.* **2011**, *40*, 173-190.
191. C. Z. Chen, N. C. Beck-Tan, P. Dhurjati, T. K. v. Dyk, R. A. LaRossa and S. L. Cooper, *Biomacromolecules* **2000**, *1*, 473-480.
192. A. Pérez-Anes, G. Spataro, Y. Coppel, C. Moog, M. Blanzat, C.-O. Turrin, A.-M. Caminade, I. Rico-Lattes and J.-P. Majoral, *Org. Biomol. Chem.* **2009**, *7*, 3491-3498.
193. R. G. Denkewalter, J. Kolc and W. J. Lukasavage, *US Pat. 4289872* **1981**.
194. E. Buhleier, W. Wehner and F. Vögtle, *Synthesis* **1978**, *2*, 155-158.
195. H. Ihre, A. Hult and E. Söderlind, *J. Am. Chem. Soc.* **1996**, *118*, 6388-6395.
196. M. E. Fox, F. C. Szoka and J. M. J. Fréchet, *Acc. Chem. Res.* **2009**, *42*, 1141-1151.
197. A. Pitto-Barry, N. P. E. Barry, O. Zava, R. Deschenaux, P. J. Dyson and B. Therrien, *Chem. Eur. J.* **2011**, *17*, 1966-1971.

198. B. Dardel, D. Guillon, B. Heinrich and R. Deschenaux, *J. Mater. Chem.* **2001**, *11*, 2814-2831.

199. M. K. Dymond and G. S. Attard, *Langmiur* **2008**, *24*, 11743-11751

200. Y. Tsukube, H. Furuta, A. Odani, Y. Takeda, Y. Kudo, Y. Inoue, Y. Liu, H. Sakamoto and K. Kimura, *Comprehensive Supramolecular Chemistry*. J. L. Atwood; J. E. D. Davies; D. D. Macnicol; F. Vögtle; Pergamon Press: Oxford, **1996**; 425-482.

201. K. A. Connors, *Binding Constants*. Wiley: New York, **1987**; 141-187.

202. (a) R. Duncan and L. Izzo, *Adv. Drug Delivery Rev.* **2005**, *57*, 2215-2237; (b) A. Samad, I. Alam and K. Saxena, *Curr. Pharm. Des.* **2009**, *6*, 835-850; (c) K. Jaina, P. Kesharwania, U. Guptaa and N. K. Jain, *Int. J. Pharm.* **2010**, *394*, 122-142; (d) J. LaRoque, D. J. Bharali and S. A. Mousa, *Mol. Biotechmol.* **2009**, *42*, 358-366; (e) M. Labieniec, O. Ulicna, O. Vancova, J. Kucharska, T. Gabryelak and C. Watala, *Cell Biol. Int.* **2010**, *34*, 89-97; (f) S. Svenson, *Eur. J. Pharm. Biopharm.* **2009**, *71*, 445-462.

203. A. Warnecke, I. Fichtner, D. Garmann, U. Jaehde and F. Kratz, *Bioconjugate Chem.* **2004**, *15*, 1349-1359.

204. (a) M. Gras, B. Therrien, G. Süss-Fink, A. Casini, F. Edafe and P. J. Dyson, *J. Organomet. Chem.* **2010**, *695*, 1119-1125; (b) M. Groessl, Y. O. Tsybin, C. G. Hartinger, B. K. Keppler and P. J. Dyson, *J. Biol. Inorg. Chem.* **2010**, *15*, 677-688; (c) W. Hu, Q. Luo, X. Ma, K. Wu, J. Liu, Y. Chen, S. Xiong, J. Wang, P. J. Sadler and F. Wang, *Chem. Eur. J.* **2009**, *15*, 6586-6594.

205. (a) Y.-F. Han, Y.-J. Lin, L.-H. Weng, H. Berke and G.-X. Jin, *Chem. Commun.* **2008**, 350-352; (b) N. P. E. Barry, P. Govindaswamy, J. Furrer, G. Süss-Fink and B. Therrien, *Inorg. Chem. Commun.* **2008**, *11*, 1300-1303.

206. N. P. E. Barry, M. Austeri, J. Lacour and B. Therrien, *Organometallics* **2009**, *28*, 4894-4897.

207. (a) L. J. Prins, R. Hulst, P. Timmerman and D. N. Reinhoudt, *Chem. Eur. J.* **2002**, *8*, 2288-2301; (b) S. Hiraoka, T. Harano, T. Tanaka, M. Shiro and M. Shionoya, *Angew. Chem. Int. Ed.* **2003**, *42*, 5182-5185; (c) S. Hiraoka, E. Okuno, T. Tanaka, M. Shiro, M. Shionoya and J. A. Chem., *J. Am. Chem. Soc.* **2008**, *130*, 9089-9098.

208. F. Ricchelli, *J. Photochem. Photobiol., B* **1995**, *29*, 109-118.

209. N. P. E. Barry, O. Zava, P. J. Dyson and B. Therrien, *Aust. J. Chem.* **2010**, *63*, 1529-1537.

210. *"The Nobel Prize in Physiology or Medicine 2009". Nobelprize.org*.

211. M. Gellert, M. N. Lipsett, D. R. Davies, Proc. Natl. Acad. Sci. USA. and 1962, 2013, *Proc. Natl. Acad. Sci. USA* **1962**, *48*, 2013-2018.

212. S. Neidle and S. Balasubramanian, *Quadruplex Nucleic Acids*. RSC Publishing: Cambridge, **2006**;

213. E. H. Blackburn, *Angew. Chem. Int. Ed.* **2010**, *49*, 7405-7421.

214. G. N. Parkinson, M. P. H. Lee and S. Neidle, *Nature* **2002**, *417*, 876-880.

215. (a) J. L. Huppert, *Biochimie* **2008**, *90*, 1140-1148; (b) J. L. Huppert and S. Balasubramanian, **2007**, *35*, 406-413.
216. A. D. Cian, L. Lacroix, C. Douarre, N. Temime-Smaali, C. Trentesaux, J. F. Riou and J. L. Mergny, *Biochimie* **2008**, *90*, 131-155.
217. L. H. Hurley, *Nat. Rev. Cancer* **2002**, *2*, 188-200.
218. D. Monchaud and M. P. Teulade-Fichou, *Org. Biomol. Chem.* **2008**, *6*, 627-636.
219. A. Arola-Arnal, J. Benet-Buchholz, S. Neidle and R. Vilar, *Inorg. Chem.* **2008**, *47*, 11910-11919.
220. R. Kieltyka, P. Englebienne, J. Fakhoury, C. Autexier, N. Moitessier and H. F. Sleiman, *J. Am. Chem. Soc.* **2008**, *130*, 10040-10041.
221. R. T. Wheelhouse, D. Sun, H. Han, F. X. Han and L. H. Hurley, *J. Am. Chem. Soc.* **1998**, *120*, 3261-3262.
222. D. P. N. Goncalves, R. Rodriguez, S. Balasubramanian and J. K. M. Sanders, *Chem. Commun.* **2006**, 4685-4687.
223. R. Kieltyka, P. Englebienne, J. Fakhoury, C. Autexier, N. Moitessier and H. F. Sleiman, *J. Am. Chem. Soc.* **2008**, *130*, 10040-10041.
224. D. Monchaud, C. Allain, H. Bertrand, N. Smargiasso, F. Rosu, V. Gabelica, A. D. Cian, J. L. Mergny and M. P. Teulade-Fichou, *Biochimie* **2008**, *90*, 1207-1223.
225. N. P. E. Barry, N. H. A. Karim, R. Vilar and B. Therrien, *Dalton Trans.* **2009**, 10717-10719.
226. L. L. Gladkov and K. N. Solovyov, *Spectrochim. Acta.* **1986**, *42A*, 1-10.
227. X.-Y. Li, R. S. Czernuszewicz, J. R. Kincaid, P. Stein and T. G. Spiro, *J. Phys. Chem.* **1990**, *94*, 47-61.
228. B. Vitorge, S. Bieri, M. Humam, P. Christen, K. Hostettmann, O. Muñoz, S. Loss and D. Jeannerat, *Chem. Commun.* **2009**, 950-952.
229. A. V. Klein and T. W. Hambley, *Chem. Rev.* **2009**, *109*, 4911-4920.
230. M. G. Mendoza-Ferri, C. G. Hartinger, A. A. Nazarov, R. E. Eichinger, M. A. Jakupec, K. Severin and B. K. Keppler, *Organometallics* **2009**, *28*, 6260-6265.
231. N. P. E. Barry, O. Zava, J. Furrer, P. J. Dyson and B. Therrien, *Dalton Trans.* **2010**, *39*, 5272-5277.
232. J. Freudenreich, N. P. E. Barry, F. Schmitt and B. Therrien, *in preparation*.
233. S. H. vanRiijt, H. Kostrhunova, V. Brabec and P. J. Sadler, *Bioconjugate Chem.* **2011**, *22*, 218-226.
234. N. P. E. Barry, F. Edafe, P. J. Dyson and B. Therrien, *Dalton Trans.* **2010**, *39*, 2816-2820.
235. H. L. Anderson, S. Anderson and J. K. M. Sanders, *J. Chem. Soc. Perkin Trans. 1* **1995**, 2231-2245.

236. J. Mattsson and B. Therrien, *Acta Crystallogr., Sect. E: Struct. Rep. Online* **2007**, *E63*, Sm2757/1-Sm2757/7.

237. L. Vieille-Petit, B. Therrien and G. Süss-Fink, *Acta Crystallogr., Sect. E: Struct. Rep. Online* **2002**, *E58*, m656-m657.

238. J. Furrer, *J. Nat. Prod.* **2009**, *74*, 1437-1441.

Abbreviations

cyclopentadienyl: Cp
pentamethylcyclopentadienyl: Cp*
isopropyl group: Pr^i
International Union of Pure and Applied Chemistry: IUPAC
methyl group: Me
para-cymene: *p*-cym
hexamethylbenzene: hmb
deoxyribonucleic acid: DNA
polycyclic aromatic hydrocarbon: PAHs
4,4'-bipyridine: bpy
3,5-bis(pyridin-4-yl)-benzene: bpb
2,4,6-tri(pyridin-4-yl)-1,3,5-triazine: tpt
5,10,15,20-tetra(pyridin-4-yl)porphyrin: tpp-2H
2,5-dihydroxy-1,4-benzoquinone: dhbq-H_2
2,5-dichloro-1,4-benzoquinone: dClbq-H_2
oxalato: ox
2,5-dioxydo-1,4-benzoquinonato: dobq
2,5-dichlorido-1,4-benzoquinonato: dClobq
acetylacetonato: acac
reactive oxygen species: ROS
cis-diamminedichloroplatinum(II): cisplatin
Food and Drug Administration: FDA
imidazolium-*trans*-dimethylsulfoxide-imidazole-tetrachlororuthenate: NAMI-A
imidazolium-*trans*-bis(1H-indazole)-tetrachlororuthenate: KP1019
1,3,5-triaza-7-phosphaadamantane: pta
ethane-1,2-diamine: en
enhanced permeability and retention: EPR
drug concentration necessary for 50% inhibition of cell viability: IC_{50}
pyrazine: pyr
1,2-bis(4-pyridyl)ethylene: bpe
5,8-dihydroxy-1,4-naphthoquinone: dhnq-H_2
5,8-dihydroxy-1,4-anthraquinone: dhaq-H_2

6,11-dihydroxy-5,12-naphthacenedione: dhtq-H_2
5,8-dioxydo-1,4-naphthoquinonato: donq
5,8-dioxydo-1,4-anthraquinonato: doaq
6,11-dioxydo-5,12-naphthacenedionato: dotq
oxamide: oxa
oxonico: oxo
1,2-bis(4-pyridyl)ethane: bpa
metal-to-ligand charge transfer: MLCT
intra-ligand charge transfer: ILCT
tris(tetrachlorobenzenediolato)-phosphate(V): trisphat
inductively coupled plasma mass spectroscopy: ICP-MS
N,*N*'-dicyclohexylcarbodiimide: dcc
4-(dimethylamino)pyrimidium para-toluenesulfonate: dpts
standard deviation: SD
5,10,15,20-tetra(4-pyridyl)porphyrin-M(II): (M = Ni (tpp-Ni), Zn (tpp-Zn))
electrospray mass spectrometry: ESI-MS
fluorescence intercalation displacement: FID
thiazole orange: TO
5,15-bis(4-pyridyl)-10,20-diphenylporphyrin: bpp
5,10,15-tris(4-pyridyl)-20-phenylporphyrin: tpp
Resistance Factor: RF

List of Structures

Metalla-Clips

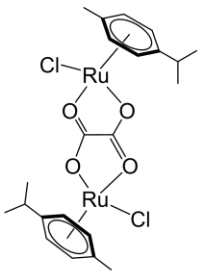

C_0

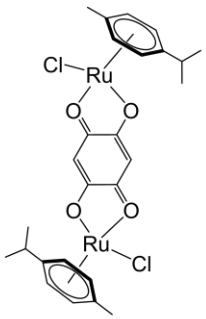

C_1

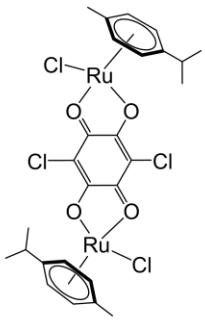

C_2

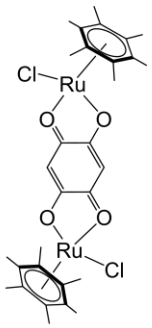

C_3

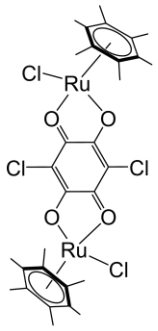

C_4

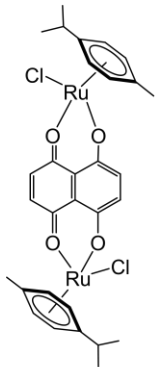

C_5

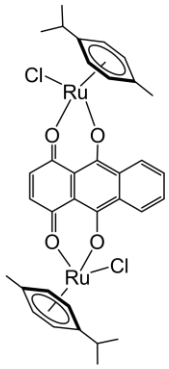

C_6

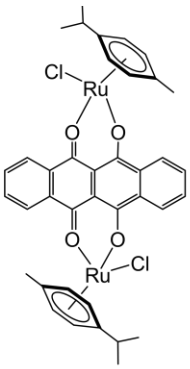

C_7

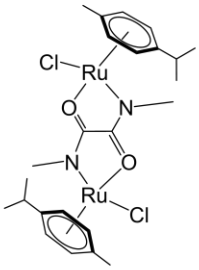

C_8

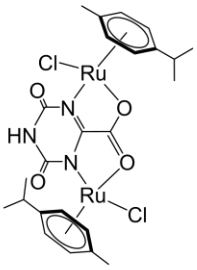

C_9

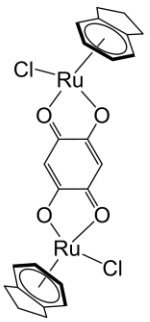

C_{10}

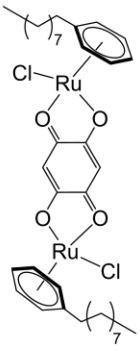

C_{11}

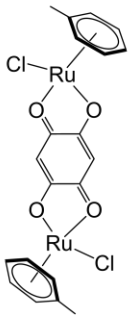

C_{12}

Metalla-Rectangles

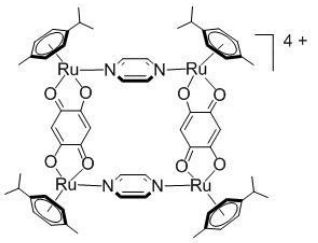

R_1

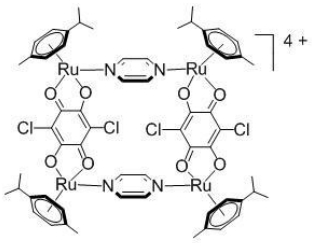

R_2

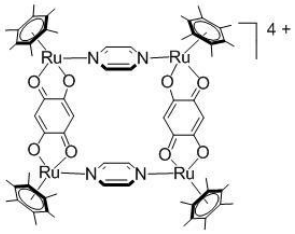

R_3

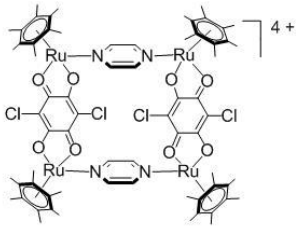

R_4

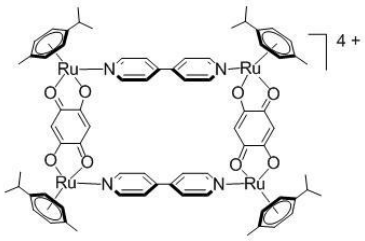

R_5

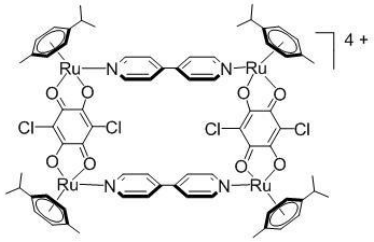

R_6

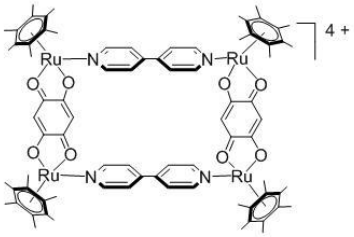

R_7

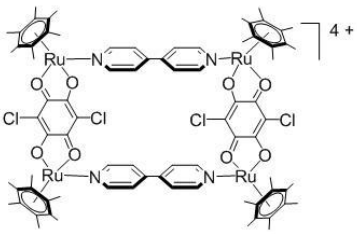

R_8

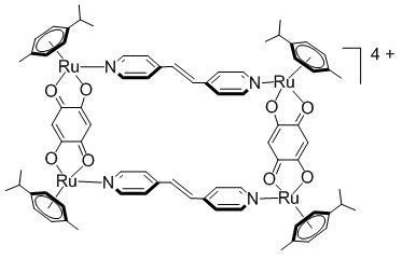

R_9

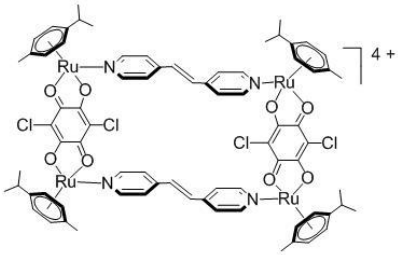

R_{10}

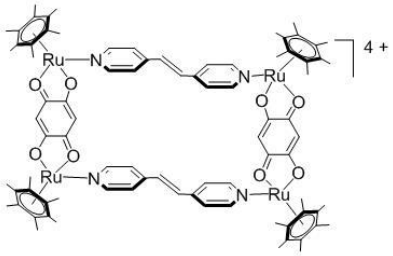

R_{11}

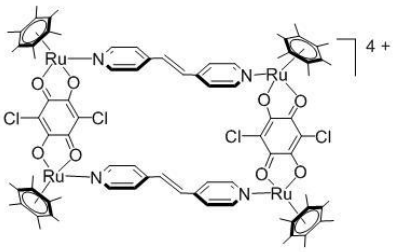

R_{12}

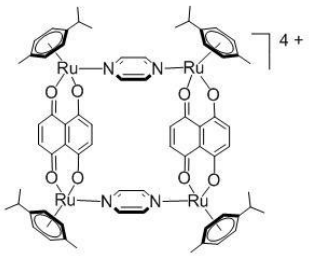

R_{13}

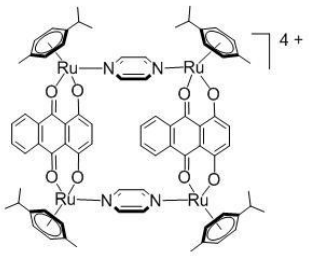

R_{14}

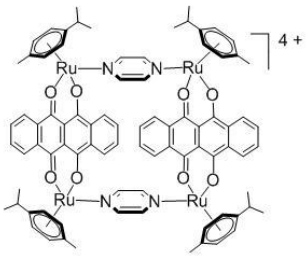

R_{15}

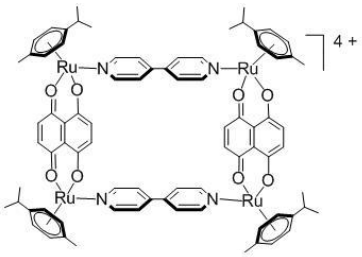

R_{16}

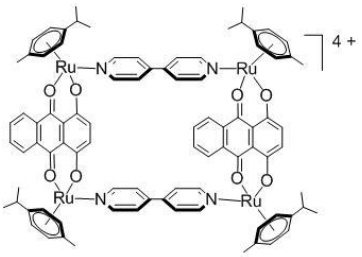

R_{17}

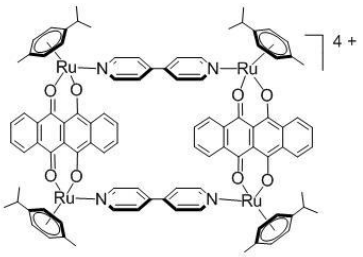

R_{18}

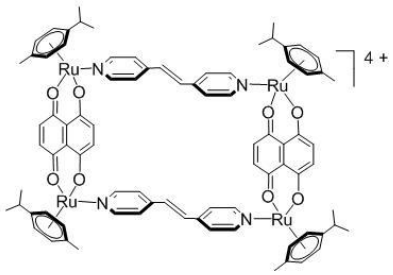

R_{19}

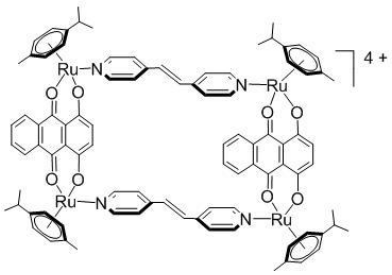

R_{20}

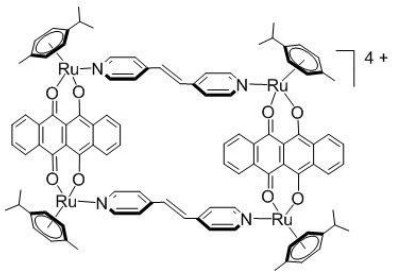

R_{21}

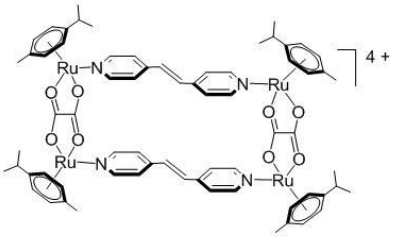

R_{22}

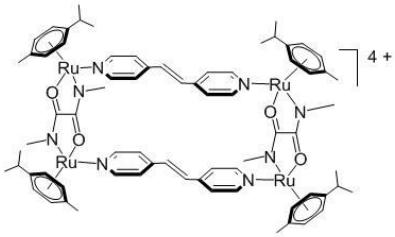

R_{23}

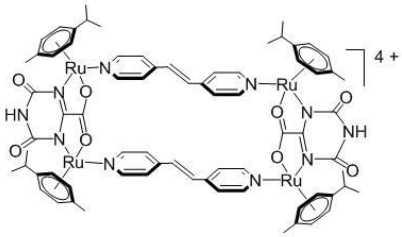

R_{24}

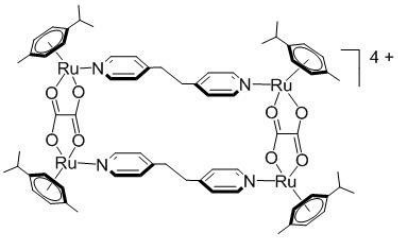

R_{25}

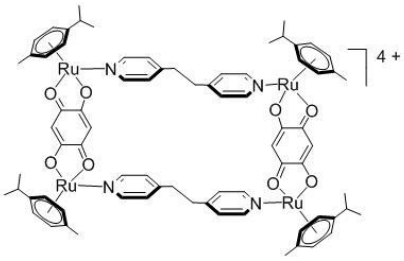

R_{26}

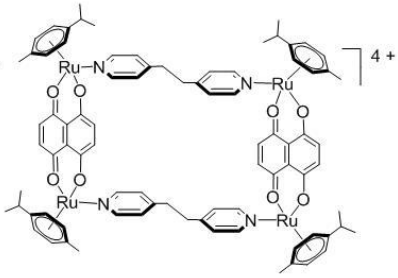

R_{27}

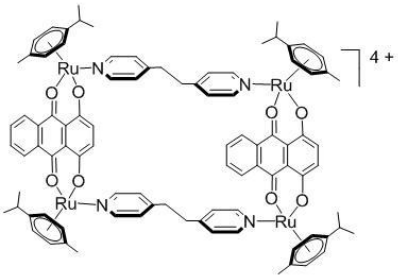

R_{28}

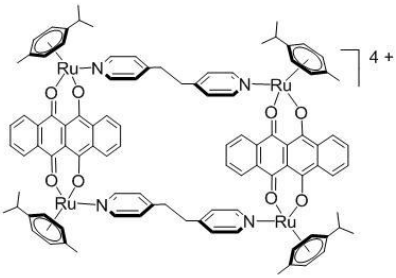

R_{29}

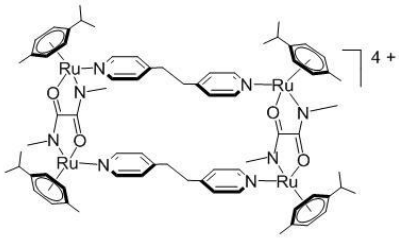

R_{30}

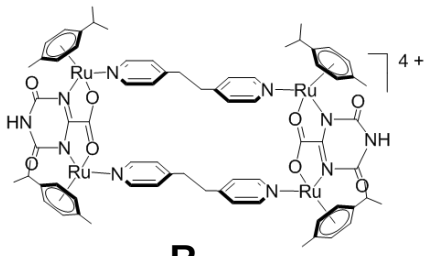

R_{31}

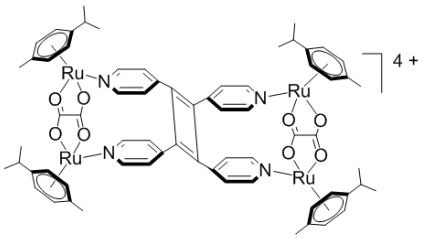

R_{32}

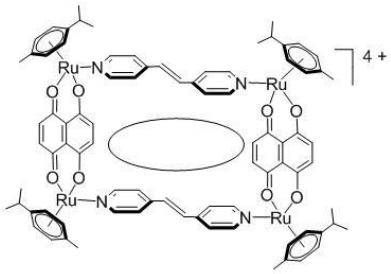

[guest⊂**R_{19}**]$^{4+}$

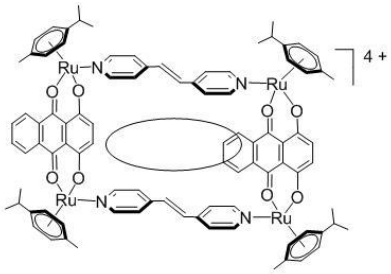

[guest⊂**R_{20}**]$^{4+}$

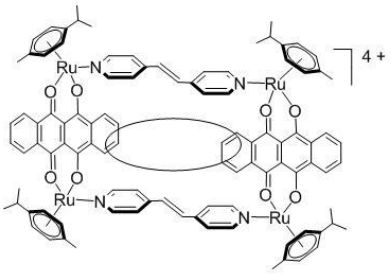

[guest⊂**R_{21}**]$^{4+}$

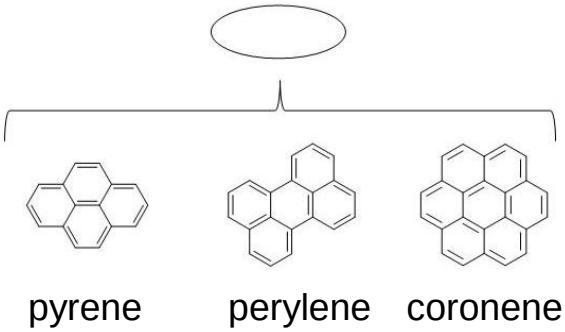

pyrene perylene coronene

Metalla-Prisms

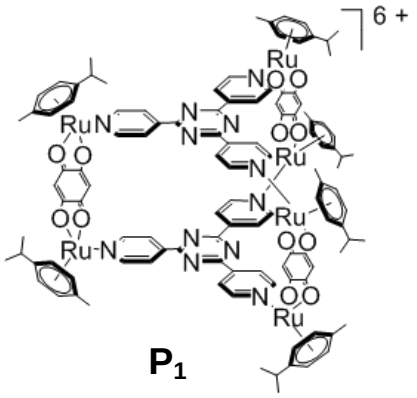

P_1

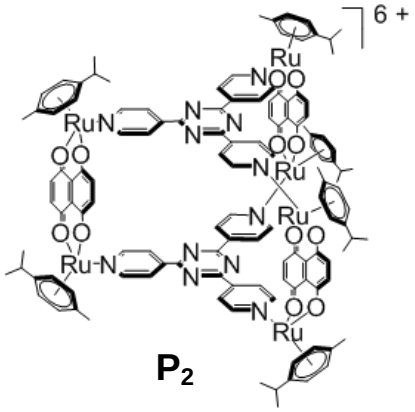

P_2

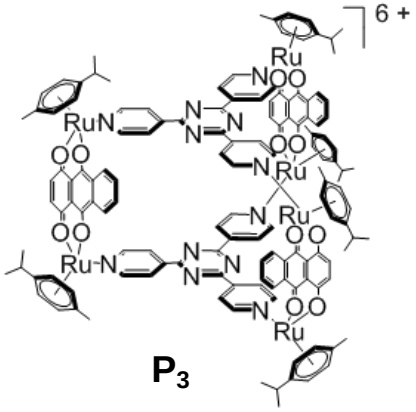

P_3

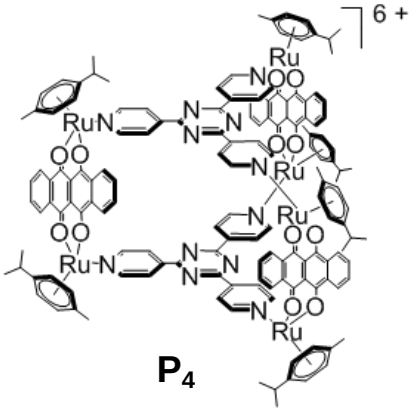

P_4

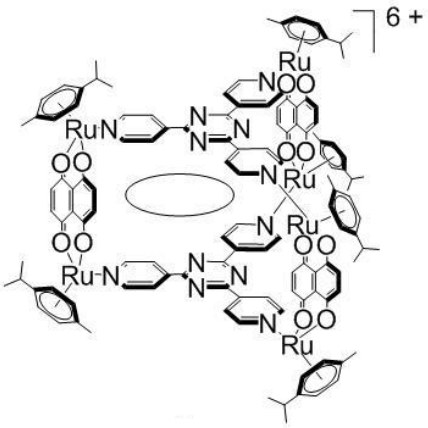

[guest⊂**P$_2$**]$^{6+}$

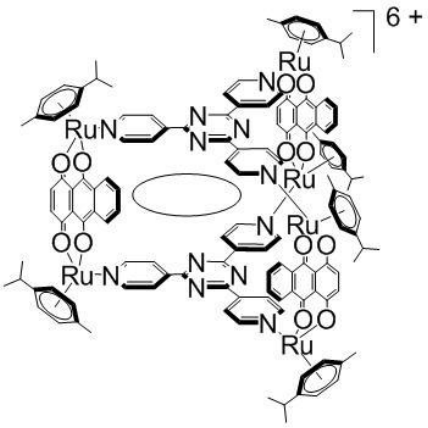

[guest⊂**P$_3$**]$^{6+}$

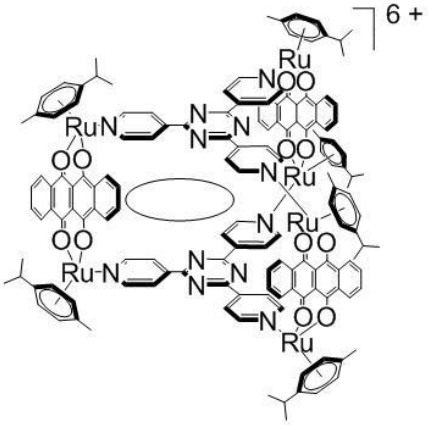

[guest⊂**P$_4$**]$^{6+}$

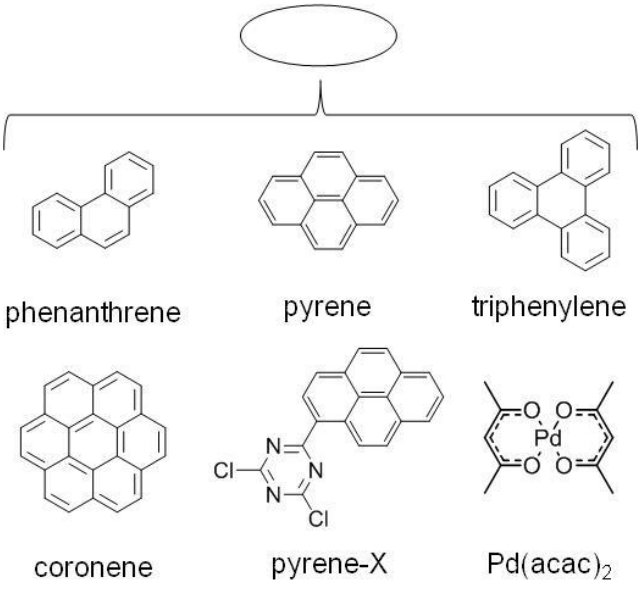

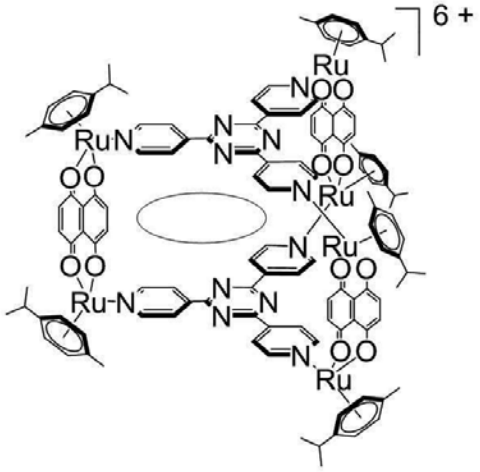

[pyrene-G⊂**P₂**]$^{2+}$ (G = G_0 – G_2)

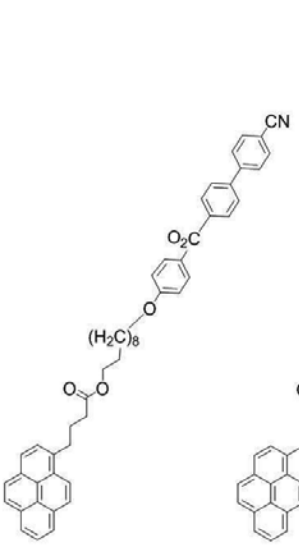

pyrene-G_0

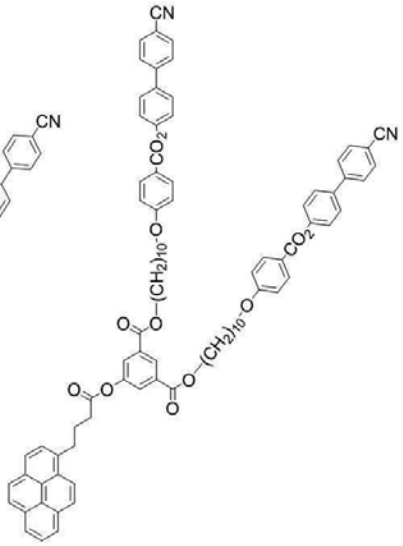

pyrene-G_1

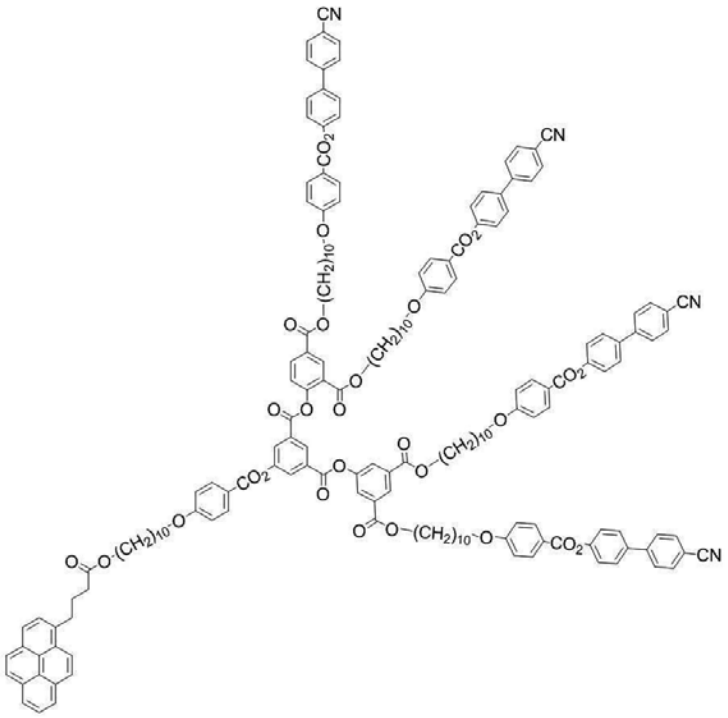

pyrene-G_2

Metalla-Cubes

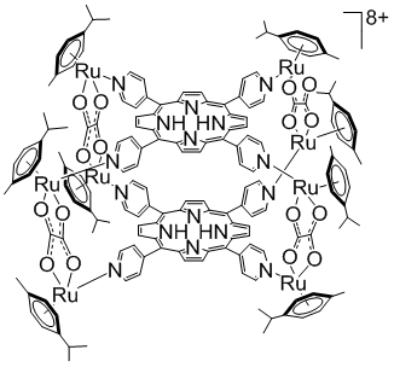

Q_1

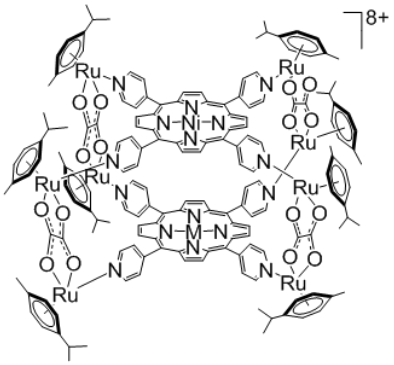

Q_2

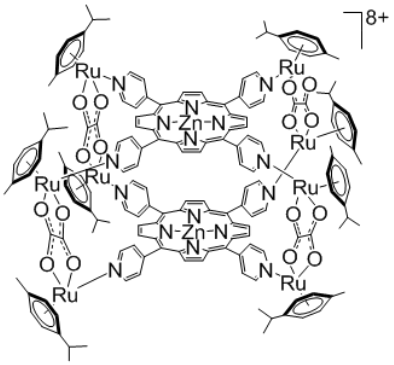

Q_3

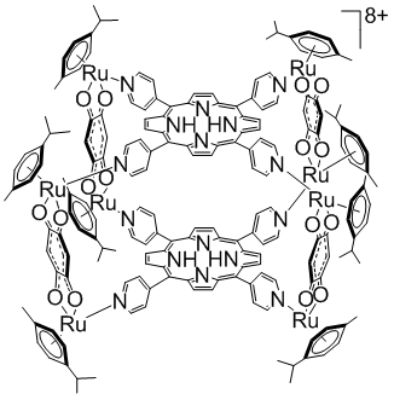

Q_4

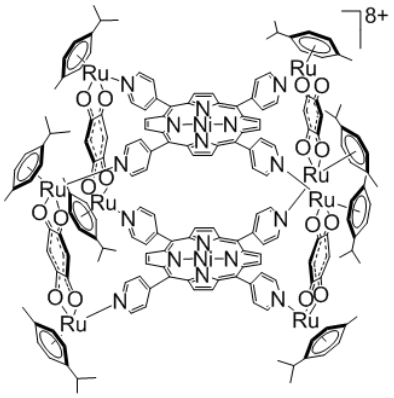

Q_5

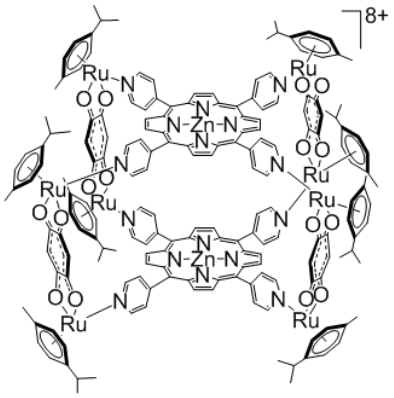

Q_6

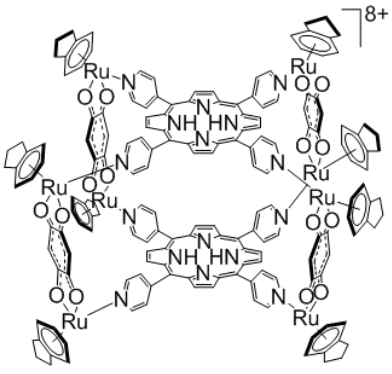

Q_7

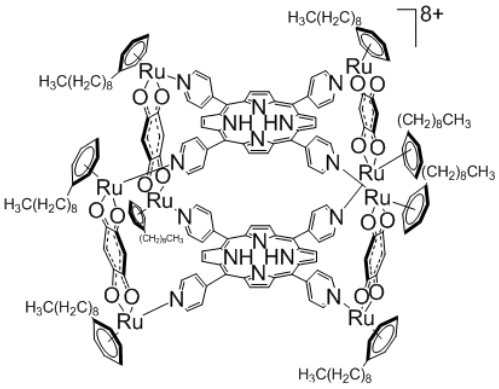

Q_8

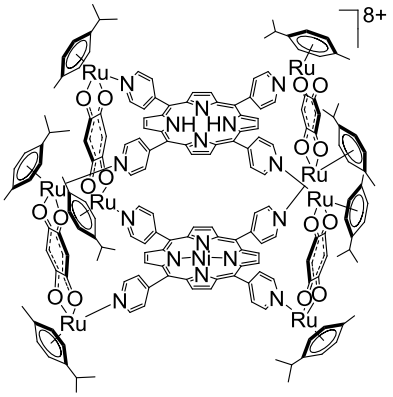

Q_9

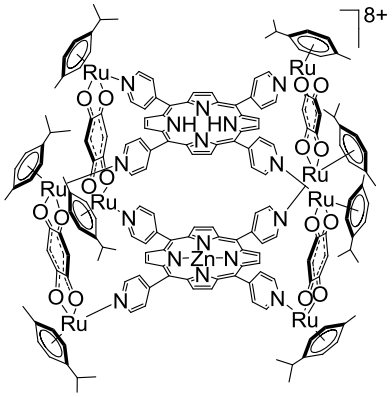

Q_{10}

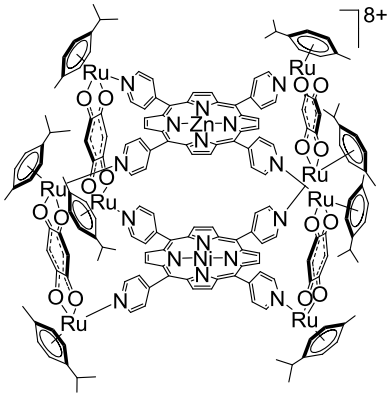

Q_{11}

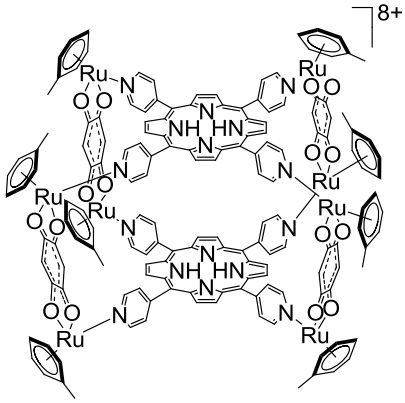

Q_{12}

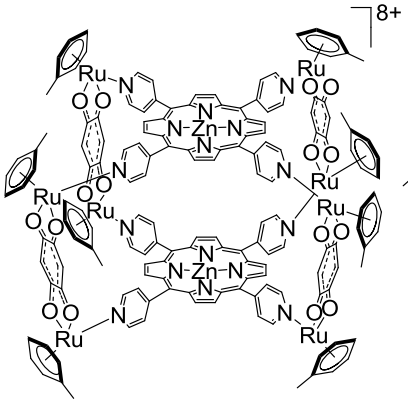

Q_{13}

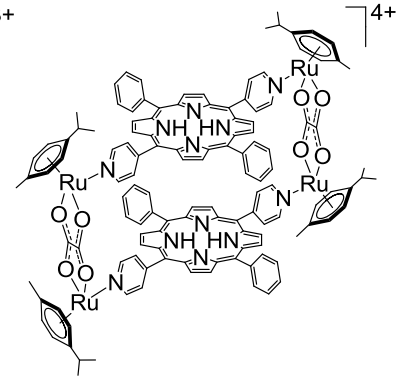

Q_{14}

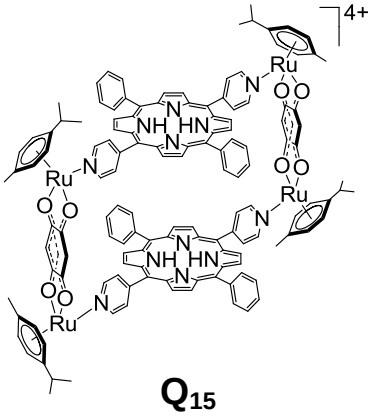

Q_{15}

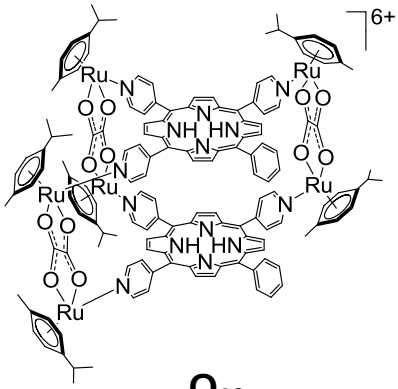

Q_{16}

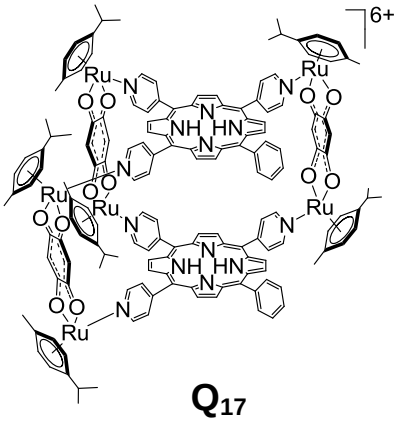

Q_{17}

Tables of Figures, Schemes and Tables

List of Publications

1. Organometallic boxes built from 5,10,15,20-tetra(4-pyridyl)porphyrin panels and hydroxyquinonato-bridged diruthenium clips, N. P. E. Barry, P. Govindaswamy, J. Furrer, G. Süss-Fink, B. Therrien, *Inorganic Chemistry Communications*, **2008**, *11*, 1300-1303.

2. Photochemical [2 + 2] cycloaddition of the olefinic double bonds in the supramolecular rectangle $[Ru_4(p\text{-cymene})_4(oxalato)_2(4,4'\text{-bipyridylethylene})_2]^{4+}$, N. P. E. Barry, B. Therrien, *Inorganic Chemistry Communications*, **2009**, *12*, 465-468.

3. Highly efficient NMR enantiodiscrimination of chiral octanuclear metalla-boxes in polar solvent, N. P. E. Barry, M. Austeri, J. Lacour, B. Therrien, *Organometallics*, **2009**, *28*, 4894-4897.

4. Host-guest chemistry in the hexanuclear arene ruthenium metalla-prismatic cage $[Ru_6(p\text{-cymene})_6(tpt)_2(dhnq)_3]^{6+}$, N. P. E. Barry, B. Therrien, *European Journal of Inorganic Chemistry*, **2009**, 4695-4700.

5. Interactions of ruthenium coordination cubes with DNA, N. P. E. Barry, N. H. Abd Karim, R. Vilar, B. Therrien, *Dalton Transactions*, **2009**, 10717-10719.

6. Designing the host-guest properties of tetranuclear arene ruthenium metalla-rectangles to accommodate a pyrene molecule, N. P. E. Barry, J. Furrer, J. Freudenreich, G. Süss-Fink, B. Therrien, *European Journal of Inorganic Chemistry*, **2010**, 725-728.

7. Anticancer activity of osmium metalla-rectangles, N. P. E. Barry, F. Edafe, P. J. Dyson, B. Therrien, *Dalton Transactions*, **2010**, *39*, 2816-2820.

8. Permanent encapsulation or host-guest behavior of aromatic molecules in hexanuclear arene ruthenium prisms, J. Freudenreich, N. P. E. Barry, G. Süss-Fink, B. Therrien, *European Journal of Inorganic Chemistry*, **2010**, 2400-2405.

9. Anticancer activity of opened arene ruthenium metalla-assemblies, N. P. E. Barry, O. Zava, J. Furrer, P. J. Dyson, B. Therrien, *Dalton Transactions*, **2010**, *39*, 5272-5277.

10. In- and out-of-cavity interactions by modulating the size of ruthenium metalla-rectangles, N. P. E. Barry, J. Furrer, B. Therrien, *Helvetica Chimica Acta*, **2010**, *93*, 1313-1328.

11. Synthesis, Characterisation and Anticancer Activity of Porphyrin Containing Organometallic Cubes, N. P. E. Barry, O. Zava, P. J. Dyson, B. Therrien, *Australian Journal of Chemistry*, **2010**, *63*, 1529-1537.

12. Double Targeting of Tumours with Pyrenyl-Modified Dendrimers Encapsulated in an Arene-Ruthenium Metalla-Prism, A. Pitto-Barry, N. P. E. Barry, O. Zava, R. Deschenaux, P. J. Dyson, B. Therrien, *Chemistry A European Journal*, **2011**, *17*, 1966-1971.

13. $Ru_2(CO)_4(OOCR)_2L_2$ sawhorse-type complexes containing axial 5-(4-pyridyl)-10,15,20-triphenylporphyrin ligands, M. Gras, N. P. E. Barry, B. Therrien, G. Süss-Fink, *Inorganica Chimica Acta*, **2011**, in the press, *doi:10.1016/j.ica.2011.03.012*.

14. Encapsulation of pyrene-functionalised poly(benzyl ether) dendrons into an arene ruthenium metalla-prism, A. Pitto-Barry, N. P. E. Barry, O. Zava, R. Deschenaux, B. Therrien, *Chemistry An Asian Journal*, **2011**, in the press, *doi : 10.1002/asia.201100136*.

15. Drug Delivery Metalla-Cages: Excellent Correlation between Drug Release and Portal Size, N. P. E. Barry, O. Zava, P. J. Dyson, B. Therrien, *Chemistry A European Journal*, submitted.

16. Anticancer activity of tetra-cationic arene ruthenium metalla-cycles, N. P. E. Barry, F. Edafe, B. Therrien, *Dalton Transactions*, submitted.

17. Pyrene, the guest of honour, N. P. E. Barry, B. Therrien, in preparation.

Since the development of supramolecular chemistry in the 1980s more and more discrete molecular objects have been synthesised. In this research area metals play a key role. Indeed, the coordination-driven self-assembly allows a directional-bonding approach that organises the different building blocks into supramolecular objects according to the coordination modes of the transition metal. Therefore, the versatility of metalla-cages and their application potential raised an increasing interest for this chemistry.

On the other hand, ever since the clinical success of cisplatin as an antitumour drug, transition metals have raised considerable expectations for the treatment of cancer. So far, mononuclear arene ruthenium complexes are of central interest due to established cytotoxicity towards cancer cells and low general toxicity.

The aim of this thesis was to combine the assembling properties of arene ruthenium complexes in supramolecular chemistry with their antiproliferative activity. Thus, different metalla-cages were synthesised, the permanent or reversible hosting ability of which was studied by various spectroscopic methods with different guest molecules. The antiproliferative behaviour of the resulting systems was established *in vitro* towards different cancer cell lines.